Methane Emissions in UK: Deciphering Regional Sources with Mobile Measurements and Isotopic Characterisation

Giulia Zazzeri

Royal Holloway, University of London

A thesis submitted for the degree of Doctor in Philosophy

August 2015

ABSTRACT

UK national inventories suggest that methane emissions for waste, gas transmission and coal mining sectors have decreased since 1990. Inventories are compiled from statistical databases multiplied by pre-defined emission factors. This “bottom-up” approach may produce precise but highly inaccurate estimates, since databases might be incomplete and emission factors poorly established.

Methane stable isotope analysis, coupled with mole fraction measurement, has been used to link isotopic signature to methane emissions from the leading methane sources in UK, such as landfills, gas leaks, sewage works and coal mines, and verify the consistency of UK emission inventories. A mobile Picarro G2301 CRDS analyser was installed in a vehicle, together with an anemometer and a Hemisphere GPS receiver, to measure atmospheric methane mole fractions and their relative location. When methane plumes were located and intercepted, air samples were collected for $\delta^{13}C\text{-}CH_4$ isotopic analysis by CF-GC-IRMS (Continuous Flow-Gas Chromatography-Isotopic Ratio Mass Spectroscopy). The bulk signature of the methane plume into the atmosphere from the whole source area was obtained by Keeling plot analysis, and a $\delta^{13}C\text{-}CH_4$ signature, with the relative uncertainty, allocated to each methane source investigated. The averaged $\delta^{13}C\text{-}CH_4$ signature measured for landfill sites around the London region was -58 ±3 ‰, whereas the $\delta^{13}C\text{-}CH_4$ signature for gas leaks was fairly constant at -36 ±2 ‰.

Diurnal studies were carried out in central London and Egham, measuring the methane isotopic composition and mole fractions of air samples collected over a 24 hours period. The mean $\delta^{13}C\text{-}CH_4$ source signature recorded in central London was -40.2 ±2.6 (2SD) ‰, revealing the primacy of fossil CH_4 emissions in the CH_4 budget.

From the isotopic characterisation of methane sources, the contribution to the methane budget and the local distribution of methane sources given in inventories could be validated.

ACKNOWLEDGEMENTS

Firstly, I would like to thank my supervisors, Professor Euan Nisbet, Dr. Dave Lowry and Dr. Rebecca Fisher for their continuous support, for having trusted me, despite my initial insecurity.

"You're a scientist, and being lost is the key for the most important insights, so being lost is good". Professor Nisbet always found the right words to encourage me. The patience of Dr. Dave Lowry has been terrific and I am extremely grateful to him for his accuracy and constancy in guiding me during the entire project. Dr. Rebecca Fisher's insights have been fundamental for this research and she represents for me a source of inspiration, as she is able to manage both family and career with great passion.

My sincere thanks also go to Mathias Lanoisellé and Dr. James France, for having taught me the use of all the instrumentation in the laboratory and helped me in most of the surveys carried out for this project, Dr. Kevin Clemitshaw for his precious advice, Eldert Advokaat for collection of samples in Utrecht and Rotterdam, Rebecca Brownlow for helping me with lab work and Aliah Alshalan, for the fantastic time spent together in Kuwait. I would like to acknowledge Professor Sue Grimmond and Alex Bjorkegren for provision of data I required for the interpretation of my results.

I wish to thank all my colleagues at the Earth Science Department at Royal Holloway and my friends in Egham, who accompanied me in this challenging but exciting journey. A particular thanks goes to my housemates and those friends who support me even from far away.

This research was funded by the Department of Earth Sciences and by the University of London with provision of a Crossland scholarship.

Finally, I would like to thank my parents, my brother Flavio, my sister in law Alessandra and my little nephew Massimo, who cheered me up through difficult times. My mum deserves more than a special thanks, she deserves my entire gratitude for all the wisdom that she constantly instills in me.

CONTENTS

LIST OF TABLES

LIST OF FIGURES

1

INTRODUCTION TO GLOBAL METHANE

1.1 Methane and its Quantification

The interaction between atmospheric composition and the climate system occurs primarily through perturbations of the radiation budget. One of the most important radiative effects is exerted by greenhouse gases, which absorb the outgoing thermal radiative fluxes emitted by the surface and reradiate it, thus increasing the atmospheric temperature. Chemically active compounds can either be formed in the atmosphere – e.g. ozone - or emitted into the atmosphere from anthropogenic and natural sources – e.g. CH_4 and CO_2. It is well known that CH_4, as one of the main greenhouse gases, together with H_2O, CO_2 and O_3, influences the thermal structure of the atmosphere.

The methane abundance is driven by the balance between a large number of surface sources and its removal through chemical oxidation processes, and it can be estimated by systematic observations from the worldwide distributed measurement network. Direct atmospheric measurements are involved in a “top-down” assessment of the methane emissions budget, whereas in a “bottom-up” approach local statistics (i.e. fuel consumption, number of cows) multiplied by predefined emissions factors are used. Emissions estimates resulting from these two different methods can disagree by factor of two or more (Weiss et al., 2008; Levin et al., 2010), and therefore the different emissions scenarios need to be reconciled by validating bottom-up estimates through enhanced measurement techniques and a well-branched data collection network.

Substantial effort is needed to quantify individual methane sources, challenged by the high variability of methane emissions at both regional and global scale. Analysis of stable isotopes has opened new perspectives on the investigation of methane sources, as it allows them to be carefully distinguished and offers a bottom-up approach for their estimate. A detailed overview of methane $\delta^{13}C$ signatures is offered in this thesis, with a focus on the development of a new procedure to isotopically characterise methane plumes from source areas. New isotopic values will be assigned to the leading methane sources in the UK in order to identify the main drivers of the methane budget in SE England and verify the consistency of UK emission inventories.

Constraints placed on the methane budget by isotopic analysis can potentially help in finding more effective regulation strategies and in defining more accurate future scenarios of methane emissions.

1.2 Methane Sources

Both natural and anthropogenic sources contribute to the global methane budget, recently projected at 554 ±56 Tg CH_4 yr^{-1}(Prather et al., 2012). Much attention has been focused on anthropogenic emissions, as during the past century humans have substantially added an important amount of greenhouse gases and very likely affected the global temperature and the related climate changes (IPCC, 2013). However, methane natural sources have also changed over time, strongly contributing to variations in the atmospheric methane growth rate. By looking at the historic record of methane mole fractions derived from ice core samples (Figure 1.1), it follows that atmospheric methane mixing ratio remained relatively stable for at least 800 years, and an increase from the pre-industrial value of approximately 700 ppb has been observed. Nevertheless, the methane budget is subjected to large uncertainties, and a better knowledge of both sources and sink processes is strictly required.

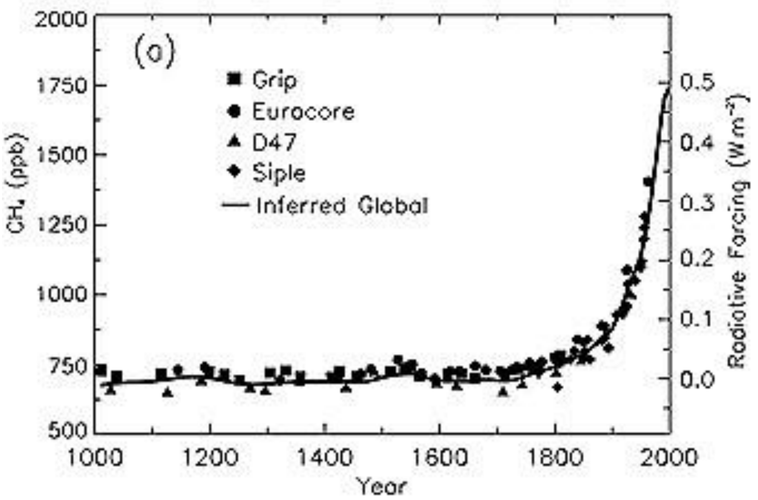

Figure 1.1 Change in CH_4 abundance (mole fraction, in ppb = 10^{-9}) determined from ice cores, firn, and whole air samples plotted for the last 1,000 years. Data sets are as follows: Grip, (Blunier et al., 1995) and (Chappellaz et al., 1997); Eurocore,(Blunier et al., 1995); D47, (Chappellaz et al., 1997); Siple, (Stauffer et al., 1985) (1985); Global (inferred from Antarctic and Greenland ice cores, firn air, and modern measurements), (Etheridge et al., 1998) and (Dlugokencky et al., 1998). Radiative forcing, approximated by a linear scale since the pre-industrial era, is plotted on the right axis.

Global methane emissions calculated using a bottom-up approach are summarised in Table 1.1. These values are much higher than the ones estimated with a top-down approach (see (Kirschke et al., 2013)).

Natural Sources	**Tg/yr of CH_4**	**Reference**
Wetlands	177-284	(Hodson et al., 2011), (Ringeval et al., 2011), (Spahni et al., 2011)
Hydrates	2-9	(U.S. EPA, 2010), (Dickens, 2003), (Shakhova et al., 2010b)
Wildfires	1-5	(Denman, 2008), (U.S. EPA, 2010), (Van Der Werf et al., 2010)
Anthropogenic sources		
Enteric fermentation and manure	87-94	(European Commission Joint Research Centre/Netherlands Environmental Assessment Agency, 2011), (Dentener et al., 2005), (U.S. EPA, 2011)
Rice paddies	33-40	Yan et al. 2009
Landfills and waste	67-90	(European Commission Joint Research Centre/Netherlands Environmental Assessment Agency, 2011), (Dentener et al., 2005), (U.S. EPA, 2011)
Biomass Burning	32-39	(Chen and Prinn, 2006)
Natural Gas and Oil	63 ±9	(Bousquet et al., 2006)
Coal	47 ±10	(Bousquet et al., 2006)
Sinks		
OH	509-764	(Young et al., 2013)
Soil	9-47	(Spahni et al., 2011); (Ito and Inatomi, 2012)
Tropospheric Chlorine	13-37	(Allan et al., 2007)

Table 1.1 Summary of bottom-up estimates of global methane emissions in Tg/yr from natural and anthropogenic sources and methane sinks for the period 2000-2009. Source: (Kirschke et al., 2013).

1.2.1 Anthropogenic Sources

A description of anthropogenic methane sources divided by sectors is provided in the following sections.

1.2.1.1 Agricultural Sector

The agricultural sector represents the most important one in terms of methane emissions from anthropogenic sources, contributing more than 50% to the overall anthropogenic methane emissions (Karakurt et al., 2012).

Domesticated ruminants such as cattle, sheep and goats account for the majority of methane emissions in this sector by producing methane as a by-product of fermentation in their rumens. Among the livestock, the cattle population contributes 73 % of the ruminant emissions (Johnson and Johnson, 1995). These emissions vary with respect to the demand pressure and the global trend of meat and dairy consumption. In 1990, China, Brazil, India, the U.S. and Russia accounted for 43 % of global methane from enteric fermentation (U.S. EPA, 2006). The overall meat production is expected to increase by 22 % from 2005 to 2030 (U.S. EPA, 2013), mainly due to the transition from a pasture system towards a commercialized production in developing countries.

Methane emissions from manure management tend to be smaller than enteric emissions, but are significant where manure is handled in liquid-based systems (IPCC, 2007). The amount of methane from manure management depends on the storage type, the temperature for storage and the composition of manure, directly related to the animal types and diet.

Flooded rice fields are a big methane source, providing the anoxic, carbon-rich conditions for high rates of microbial methanogenesis (Conrad, 1993). Since the total global rice consumption is expected to grow, cultivations in China, India, Thailand, Indonesia, Vietnam, and Myanmar will likely increase in the next years (U.S. EPA, 2013). However this increase might be partially offset by the improvement of agricultural practices.

1.2.1.2 Energy Sector

The energy sector is the second largest contributor to global emissions of non-CO_2 emissions (U.S. EPA, 2013) and it includes four main sources: natural gas and oil systems, coal mining activities, stationary and mobile combustion, biomass combustion.

Fugitive emissions from natural gas and oil systems are the largest source of methane from this sector, followed by fugitive emissions from coal mining and biomass consumption. Methane emissions from the energy sector in the most recent years are driven by a shift from coal to natural gas in several regions and by the growth in energy consumption in the developing countries. Methane, being the principal component of natural gas, is emitted from natural gas production, processing, transmission and distribution, from leaks and venting gas during operation or maintenance (U.S. EPA, 2013). Currently, in Russia and several Eastern European countries gas and oil facilities are improving in order to prevent fugitive emissions.

Large deposits of methane can remain trapped within or next to the coal seam during the coalification process, until it is released by mining operations or natural erosion and faulting-defaulting of coal strata. Methane is diluted and emitted through ventilation shafts in underground coal mines, whereas it is directly emitted to atmosphere in surface coal mining. The amount of methane released is affected by coal rank (carbon content of the coal) and permeability, depth of seam and geologic parameters (Karakurt et al., 2012). All these variables are explained in detail in Chapter 5.2. Aydin et al. (2011) suggested that the gradual reduction in fossil fuel emission towards the end of the twentieth century contributed to the overall decline in methane growth rate in that period (see Chapter 1.6). However in China, coal production has increased very rapidly over the last 8 years, which is thought to be one of the main reasons why global methane is rising again (U.S. EPA, 2013).

Methane is also released by incomplete combustion of biomass, including woodlands, peatlands, savannah and agricultural waste. Emissions are dependent on fire temperature and biomass composition. For instance, due to the relatively high water content and low oxygen availability, burning of peat and agricultural waste tend to generate higher methane emissions (U.S. EPA, 2013). The estimate of methane from biomass burning is highly uncertain, mainly because most fires are triggered in developing countries, and individual farmers do not keep records of the amount burned (Andreae, 1991).

Vehicle combustion is also a source of methane, although direct emissions of CH_4 from vehicles are often neglected in the overall climate impact of the transport sector (Myhre et al., 2011), and it is strictly dependant on the methane content of the fuel and the combustion efficiency (U.S. EPA, 2013). Improvements in the combustion engines are expected to reduce methane emissions from the transportation sector, despite the increasing demand of automobiles in countries such as China and India.

1.2.1.3 Waste Sector

Methane sources in the waste sector include landfilling of solid waste (58%) and wastewater treatment (35%) (U.S. EPA, 2013).

Landfills have been estimated to release worldwide between 35 and 69 Tg/year of methane to the atmosphere (Bogner at al., 2007). The biogas generated in landfill sites contains methane (55–60 vol %), carbon dioxide (40–45 vol %), and numerous trace compounds, as a result of complex reactions involved in the anaerobic degradation of the organic fraction of solid wastes (Bogner and Spokas, 1993). The methane that is initially produced within the landfill migrates towards the aerobic zone in the top-soil, and it is partially oxidised to carbon dioxide by methanotrophs. Methane oxidation rates depend on the methane residence time in the cover, O_2 diffusion from the atmosphere, as well as on the soil moisture, temperature and all the variables that affect the microbial process in soil (Molins et al., 2008). The landfilled waste volume, the content of organic waste fractions and the degradability of these fractions, as well as the waste age and environmental parameters (i.e. temperature, moisture content, nutrients, inhibiting compounds) are all crucial factors in the methane production (Scheutz et al., 2009). The methanogenesis persists until most of the organic matter is decomposed, which can take several decades, contributing to methane emissions for long time period. In order to reduce the biogas release into the atmosphere, an extraction system is diffusely implemented and the gas extracted can be used as a local source of renewable energy.

Recent studies demonstrate that substantial methane emissions derive from sewage treatment plants, most of which are expected from leaks in the anaerobic digestion of the sludge (Daelman et al., 2012). Although most developed countries manage the municipal waste-water using aerobic wastewater treatments, in areas without wastewater infrastructures, anaerobic systems such as latrines, open sewers or lagoons prevail. Untreated and uncollected wastewater contributes significantly to methane emissions, especially in countries such as China, India and Indonesia, where increasing volumes of wastewater due to the population growth do not undergo advanced treatment (U.S. EPA, 2013). Methane emissions from urban sewage works are covered in more detail in Chapter 5.4.

1.2.2 Natural Methane Sources

Major natural sources include wetlands, forest fires triggered by lightning and releases from onshore and offshore geological sources.

Wetlands, transitional areas at the interface between upland, terrestrial environments and the aquatic system, represent the major natural source of global atmospheric methane. They are concentrated in tropical regions, particularly coastal swamps and seasonally flooded areas, and at high latitudes, where frozen soil curtails water drainage (U.S. EPA, 2013). The anaerobic environment established by the presence of water sustains distinctive communities of methane producing archea (methanogens) and methane consuming bacteria (methanotrophs), whose balance drives the methane emissions rate. Methanogenic archea are found to be extremely sensitive to temperature variations, so that small changes in temperature are likely to affect methane production (Christensen et al., 2003). Wetlands emissions are estimated to total between 100 and 231 Tg per year (Denman et al., 2007). The large uncertainty affecting these estimates stems from the inter-annual fluctuations in wetland extent and from the high vulnerability of wetlands to temperature variations (Bousquet et al., 2006a). The positive feedback between global warming and wetland emissions is clearly observed in the Arctic, where increasing temperatures enhance the water supply from melting ice and thus the extent of wetlands and their relative emissions (Dlugokencky et al., 2011). Higher Arctic temperatures are expected to increase high-latitude emissions, whereas tropical wetland areas are likely diminishing by the rapid land use change (Isaksen et al., 2009).

Currently there is big concern regarding methane emissions from hydrates, due to the enormous size of the reservoirs. Methane clathrates (hydrates) are non-stoichiometric solid structures composed of cages of water molecules surrounding methane molecules, formed either at temperatures less than 0°C (continental sedimentary rocks in polar region), or under higher temperatures (≈2°C) in ocean depths typically greater than 500 metres. Hydrate deposits are commonly contained in ocean sediments along continental margins (Kvenvolden, 2002), and can dissociate with an increase in water temperature and changes in ocean circulation (Kennett et al., 2000), as well as through earthquakes and landslides. Reservoirs of gas hydrates frequently outgas and emit methane fluxes to the seafloor, but mostly the methane does not reach the atmosphere because it is oxidised within the sediments or dissolved into the water column (U.S. EPA, 2013). The shallow deposits of hydrates in the Arctic are expected to be the most susceptible to the warming of the surface (Nisbet, 2002; Westbrook et al., 2009; Shakhova et al., 2010a), as they can be quickly destabilised with the thawing of permafrost and therefore constitute a positive feedback to global warming.

Different studies estimated methane emissions from wildfires between 2 and 5 Tg CH_4 yr^{-1} (Denman, 2008; Van Der Werf et al., 2010), but emissions remain poorly constrained because of the high spatial and temporal variability in fire activity. Natural fires mainly occur in the mid to high latitude temperate-boreal ecosystems, where the climate is warmer and there is a dry period sufficiently long to allow vegetation to dry (Levine, 1999). The composition and the extent of the biomass burned control the methane emissions rate. Satellites have proven to be useful in determining the spatial and temporal distribution of fires (Dwyer et al., 2000), but do not discriminate natural wildfires from the human initiated ones. Thus emissions estimates still rely on the assumption that roughly 10 % of the global biomass burning is natural (Levine, 1999).

Living vegetation has been recently suggested as another natural source of methane by Keppler et al. (Keppler et al., 2006), even though many contentions arose from this study (Nisbet et al., 2009), and plants are generally excluded from the global methane budget (U.S. EPA, 2013).

1.3 Methane Chemistry and Sinks

The oxidation mediated by hydroxyl radicals is the primary sink of methane, accounting for around 90 % of the CH_4 loss in the atmosphere (Ehhalt and Heidt, 1973). The rest of the CH_4 sink is due to the uptake of CH_4 by soil, removal in the stratosphere by reaction with OH, Cl, ($O\ ^1D$), and by reaction with atomic chlorine in the marine boundary layer.

The reaction of methane with hydroxyls is occurring mostly in the troposphere (Levy, 1971):

$$CH_4 + OH \rightarrow H_2O + CH_3 \tag{1.1}$$

Hydroxyl radicals are mainly formed by the photo dissociation of ozone and by reaction with water vapour:

$$O_3 + h\nu\ (\lambda<340\ \text{nm}) \rightarrow O\ (^1D) + O_2 \tag{1.2}$$

$$O(^1D) + H_2O \rightarrow 2OH \tag{1.3}$$

where $O(^1D)$ are excited state oxygen atoms. Therefore hydroxyl production is enhanced during summer and in the tropical lower and middle troposphere, as a result of high levels of water vapour and high incident UV radiation. The lifetime of OH is less than 1 sec (Hobbs, 2000), as it is used up in reactions with CO, CH_4 and NMVOCs (Naik et al., 2013). Reaction 1.4 shows the OH consumption by oxidation of CO (in reaction 1.5 M is a non-reacting species that can take up the energy released in the reaction).

$$CO + OH \rightarrow CO_2 + H \tag{1.4}$$

$H + O_2 + (M) \rightarrow HO_2 + (M)$

1.5

In a NO_x-rich environment OH is partially supplied as by-product in the CH_4 oxidation sequence, through the reaction of hydroperoxyl radicals (HO_2) with NO (1.9) (Crutzen, 1973):

$CH_4 + OH\ (+ O_2) \rightarrow CH_3O_2 + H_2O$

1.6

$CH_3O_2 + NO \rightarrow CH_3O + NO_2$

1.7

$CH_3O + O_2 \rightarrow CH_2O + HO_2$

1.8

$HO_2 + NO \rightarrow NO_2 + OH$

1.9

NO_2 can subsequently photolyse and form O_3, the main precursor of hydroxyls:

$2NO_2 + h\nu\ (\lambda > 420\ nm) \rightarrow 2NO + 2O$

1.10

$2O_2 + 2O\ (+M) \rightarrow 2O_3\ (+M)$

1.11

Further breakdown of formaldehyde (CH_2O in reaction 1.8) additionally yields O_3 and OH by producing hydroperoxyl radicals (HO_2), which in turn are a key species for the secondary production of OH (Lelieveld et al., 1998):

$CH_2O + h\nu \rightarrow H + HCO$

1.12

$H + O_2 + (M) \rightarrow HO_2 + (M)$

1.13

The secondary production of OH via NO_x occurs especially at higher latitudes, where NO_x and ozone concentrations are generally higher, and solar radiation and water vapour are less abundant (Lelieveld et al., 2002).

Conversely, at low levels of NO_x in the atmosphere, hydroxyls are preferentially reformed by the removal of O_3:

$$O_3 + HO_2 \rightarrow 2O_2 + OH$$

1.14

Overall, tropospheric OH concentrations are the result of a balance between OH sources (tropospheric ozone, water vapour and NO_x for the secondary OH production) and sinks (methane, CO, NMVOCs), where temperature modulates the reaction rates and the amount of tropospheric water vapour (Naik et al., 2013). As hydroxyls represent the primary sink of methane, methane mole fractions and lifetime are expected to be strongly influenced by changes in the OH distribution (Stevenson et al., 2005). A larger abundance of OH, due to higher temperature and thus higher vapour content in the atmosphere, will increase methane oxidation. On the other hand, enhanced CH_4 emissions will intensify the OH loss, leading to a slowing in the methane removal and a longer atmospheric methane lifetime. This is estimated to be 9.8 ±1.6 years (Voulgarakis et al., 2013), although it is highly uncertain value resulting from a large variety of models (Prather et al., 2012).

Well-aerated upland soils, such as rural forests, act as a net sink for atmospheric CH_4, whereas wet soils, such as wetlands, are sources of methane (see Chapter 1.2.2). Under aerobic conditions, methane is mineralized to CO_2 by methanotrophic bacteria. More than a half of the produced CH_4 is oxidized by microbes in the soil before being emitted into the atmosphere (Reeburgh, 2003). However, the methane uptake has been reduced by human activities, by converting natural forests and grasslands to agricultural and urban land (Smith et al., 2000). In highly urbanised environments such as London the role of soil in the methane uptake is strongly reduced.

The reaction with atomic chlorine in the marine boundary layer represents another methane sink, albeit very small, which leads to the formation of HCl (Platt et al., 2004) (reaction 1.15).

$$CH_4 + Cl \rightarrow CH_3 + HCl \quad \textbf{1.15}$$

In urban environments the uptake of methane is mainly driven by the rate of reaction with hydroxyl radicals, whose chemistry involves production and loss processes very complex and difficult to quantify (Teixeira et al., 2009).

1.4 Methane Climate Forcing and Global Warming Potential

In the IPCC report (2007) the concept of Radiative Forcing (RF) is defined as:

> *'A measure of how the energy balance of the Earth-atmosphere system is influenced when factors that affect climate are altered. The word radiative arises because these factors change the balance between incoming solar radiation and outgoing infrared radiation within the Earth's atmosphere. This radiative balance controls the Earth's surface temperature. The term forcing is used to indicate that Earth's radiative balance is being pushed away from its normal state.'*

Radiative Forcing is usually quantified as the 'rate of energy change per unit area of the globe as measured at the top of the atmosphere', and it is expressed in W m^{-2}. A positive RF means that the energy of the earth-atmosphere system will eventually increase, leading to a warming of the system. The global mean equilibrium temperature response at surface (ΔT_s) is related to RF through a linear relation $\Delta T_s = \lambda RF$, where λ is the climate sensitivity parameter (Ramaswamy et al., 2001).

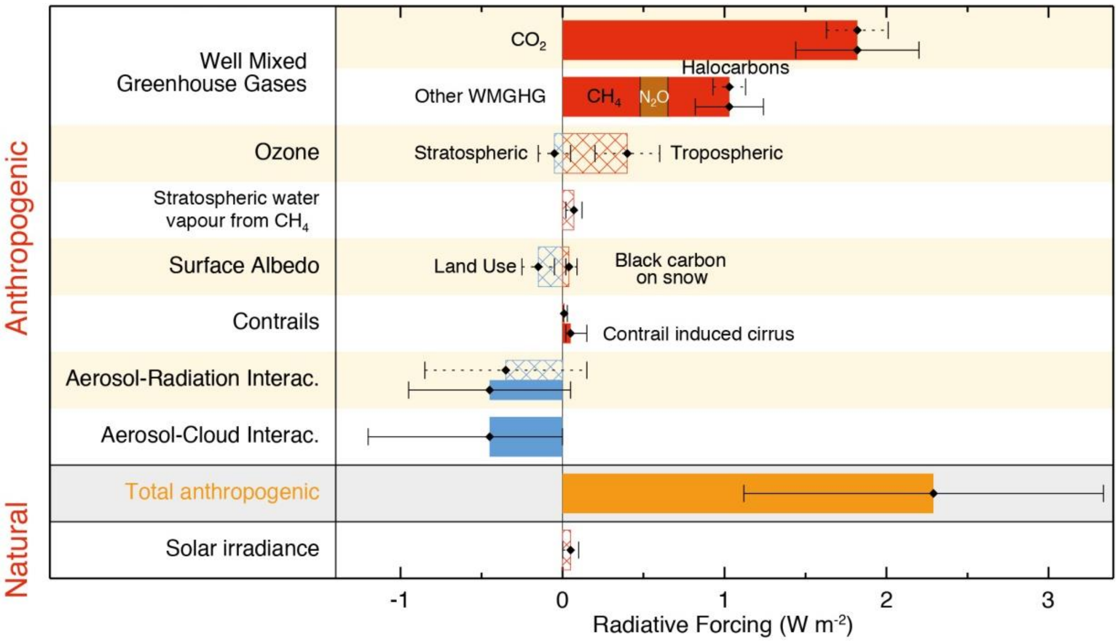

Figure 1.2 Radiative forcing of climate between 1750 and 2011 (IPCC, 2013).

RF values have been assessed by simple radiative-convective models, considering the climate response to the change in solar insolation, and allow a first comparison between anthropogenic and natural drivers of climate change (Shindell et al., 2009).

The pre-industrial global mixing ratio for methane in 1750, based on ice core records of methane (722 +/- 25 ppb according to IPCC), was used as reference level for the RF calculation.

Measurements from AGAGE[1] and NOAA GMD[2] networks provide an average mixing ratio of 1803 ±2 ppb in 2011. The increase in methane burden gives a RF of + 0.48 W/m^2, ranking CH_4 as the second highest RF of the LLGHG$_S$ (Long Life Greenhouse Gases) after CO_2 (1.82 W/m^2) (IPCC 2013). Climate-chemistry interactions with the atmosphere and the related feedbacks must be included in

---

[1] The ALE/GAGE/AGAGE stations are coastal or mountain sites around the world chosen primarily to provide accurate measurements of trace gases whose lifetimes are long compared to global atmospheric circulation times. http://agage.eas.gatech.edu/stations.htm

[2] The NOAA ESRL/GMD tall tower network and the data from the NOAA ESRL GMD surface flasks sampling network provide regionally representative measurements of carbon dioxide (CO_2), CH_4 and related gases in the continental boundary layer. http://www.esrl.noaa.gov/gmd/ccgg/towers/ http://www.esrl.noaa.gov/gmd/ccgg/flask.html

the quantification of RF. For instance, methane emissions are estimated to account for most of the increase in global tropospheric ozone (Shindell et al., 2005), which in turn enhances the greenhouse effect. This additional contribution to the energy balance leads to a higher RF value for methane.

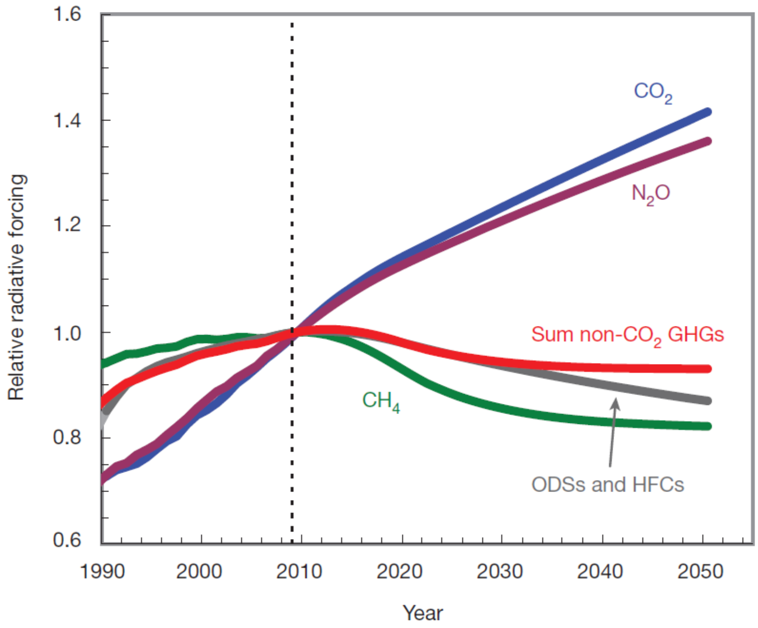

Figure 1.3 Relative changes in radiative forcing from 25% drop in emissions GHGs included in the Kyoto Protocol. The RF is expressed as a fraction of the forcing in 2009. Past forcings are based on measured mixing ratios. Future forcings are calculated assuming a 25% decline in 2008 emissions, phased in linearly between 2009 and 2020; emissions are kept at 2020 rates thereafter. Projections presume constant natural emissions and losses, and thus do not include the potentially significant changes in natural emissions or non-OH losses (Montzka et al., 2011).

Figure 1.3 illustrates a modelled response of all non-CO_2 GHGs to a 25 % reduction in anthropogenic emissions as a function of their different lifetimes. According to this emissions cut, the RF of these gases would peak throughout the next decade (Montzka et al., 2011), but the increase in RF from longer-lived GHGs could be offset by CH_4 emissions on a rather short time scale, due to the relatively short life-time of methane and its proximity to the steady state.

Impacts of different GHGs are usually compared using the GWP (Global Warming Potential) parameter, which represents the *time-integrated RF due to a pulse emission of a given component, relative to a pulse emission of an equal mass of CO_2* (IPCC, 2013). The Absolute Global Warming Potential (AGWP) is calculated by integrating the RF due to emission pulses over a chosen time horizon; for example, 20 and 100 years (vertical lines in Figure 1.4).

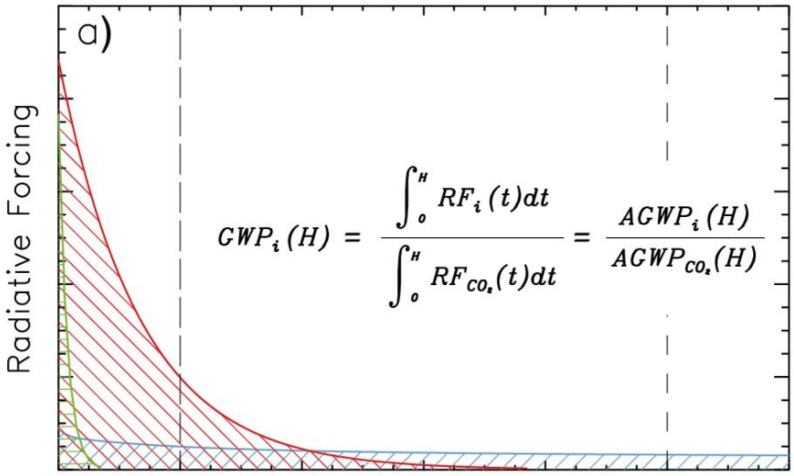

Figure 1.4 GWP calculation. The GWP is the ratio of AGWP for component i over AGWP for the reference gas CO_2. The blue-hatched field represents the integrated RF from a pulse of CO_2, while the green and red fields represent example gases with 1.5 and 13 years lifetimes, respectively (IPCC, 2013).

Multiplying emissions amount by 100 years GWPs allows the estimation of the CO_2-equivalent emissions, so that CH_4 fluxes are converted into units directly comparable with CO_2. The IPCC provides the following definition:

‘*CO_2 equivalent emission is the amount of CO_2 emission that would cause the same time-integrated radiative forcing, over a given time horizon, as an emitted amount of a long-lived GHG as a mixture of GHGs.*’

Usually a 100-year time horizon GWP value is used (e.g. 28 for methane). A reduction of 1 tonne of CH_4 would amount to a reduction of 28 tonnes CO_2-eq.

By expressing emissions on a CO_2-equivalent scale, the impact of specific mitigation targets on climate can be estimated, framing the worldwide climate policy scheme. The concept of GWP is therefore the most widely used parameter to compare GHGs influence on future climate and it is also adopted in the Kyoto Protocol. However, this parameter is not immune from limitations, as it includes only physical properties and it is very dependent on emission timing and location. The 100 yrs time horizon conventionally chosen, over which the mean radiative forcing is calculated, strongly reduces the influence of species that are short-lived relative to CO_2 (Shindell et al., 2009) and it undervalues the importance of methane as greenhouse gas.

1.5 The Kyoto Protocol and the Cost of Reducing CH_4

Emissions reduction is a major challenge and developed countries started pursuing it after the drafting of the Kyoto Protocol in December 1997, which mandates nations to reduce or limit their emissions of the six main GHGs (CO_2-Carbon dioxide, CH_4-Methane, N_2O-Nitrous oxide, PFCs-Perfluorocarbons, HFCs-Hydrofluorocarbons, SF_6-Sulphur hexafluoride.). This international treaty, formally entered into force on 16 February 2005, bound industrialized countries and those in transition to a market economy, as they are largely responsible for the current level of GHGs emissions in the atmosphere; no binding targets or timetables for developing countries were decided.

The reduction or limitation targets imposed defined the amount of GHGs that the countries were allowed to emit in the ‘commitment period’ of 2008-2012. Signatory countries needed to take action in their own country to reduce emissions, but they could also engage in emission trading to meet their target through the Carbon Credit market. In fact, the Kyoto Protocol gave GHGs a carbon credit, a value equivalent to one tonne of CO_2. If a company had emissions over its allowance, it could purchase carbon credits, whereas those companies able to stay under this allowance could receive credits.

A second commitment period was proposed in 2012, known as the Doha Amendment, but New Zealand, Japan, Russia, Canada and United States did not commit themselves to meet the new targets.

1.6 Global Methane and Anomalies in the Methane Global Growth Rate

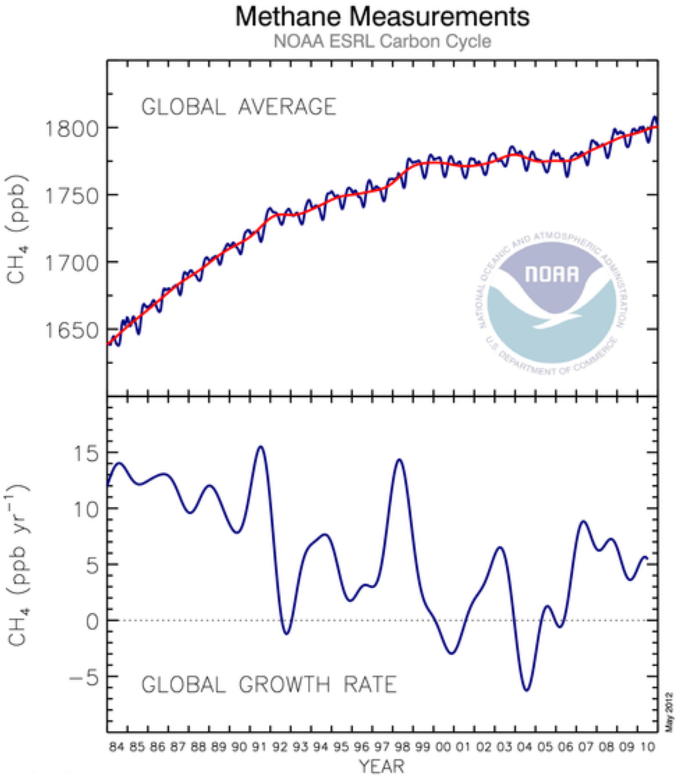

Figure 1.5 Global atmospheric methane mixing ration (blue line) determined using measurements from the Carbon Cycle cooperative air sampling network. The red line represents the long-term trend. Bottom: global average growth rate for methane. Source: http://www.esrl.noaa.gov/gmd/

After a steady increase of atmospheric methane in the 1980's and a stabilisation of the global levels between 1999 and 2006, methane concentrations have risen again (Nisbet et al., 2014). A large scientific debate is weaved around the latest increase in methane mixing ratio and the weakening of the global growth rate after the early 1990s, believed to be only temporary (Bousquet et al., 2011) and mainly ascribed to a gradual reduction in fossil fuel emissions. The breakup of the Soviet Union in 1991, with the associated decline in the production of coal, oil and natural gas, has been considered one of the key events.

The methane growth rate in Figure 1.5 shows a high inter-annual variability, including occasional anomalies likely caused by remarkable perturbations, such as the eruption of Mount Pinatubo in 1991 (Bousquet et al., 2006b) and an exceptional El Nino during the 1997-1998 period. The eruption of Mount Pinatubo injected a considerable amount of aerosols into the atmosphere, strongly altering photochemical reactions. A reduced production of hydroxyl radicals inhibited the removal of methane, which nonetheless was offset by a general cooling of the Northern Hemisphere, associated with a reduction in methane emissions from wetlands. A faster growth of methane concentrations was attributed to the widespread increase in temperature and dryness during El Nino in 1997, which caused many wildfires in the tropical zone. The following large emissions of carbon monoxide and the concomitant decrease in hydroxyl radicals concentration led to an overall increase in the methane mixing ratio (Chen and Prinn, 2006).

After a stagnation period at the beginning of the 21st century, a new positive anomaly stood out in 2002-2003, ascribed to the increase in the emissions from biomass burning, predominantly in South Asia and in boreal regions of Siberia (van der Werf et al., 2003).

Atmospheric methane growth rate has started to increase again after 2006, but the reasons are still not certain, given the limited understanding of the driving factors in the global methane budget. Atmospheric observations can constrain at global levels both emissions estimates and the chemical sink of methane (Kirschke et al., 2013), providing insights into the main causes of the renewed methane growth. Rising emissions from human activities, such as coal mining in China and the natural gas exploitation in Russia and in United States, might justify the increase in methane mixing ratio. However, measurements of $\delta^{13}C\text{-}CH_4$ suggest a trend towards more ^{13}C depleted emissions (see Chapter 2.5.3), implying enhanced methane emissions from wetlands as a result of greater than usual rainfall in the tropics and very warm temperatures observed at polar northern latitude (Dlugokencky et al., 2011; Nisbet et al., 2014).

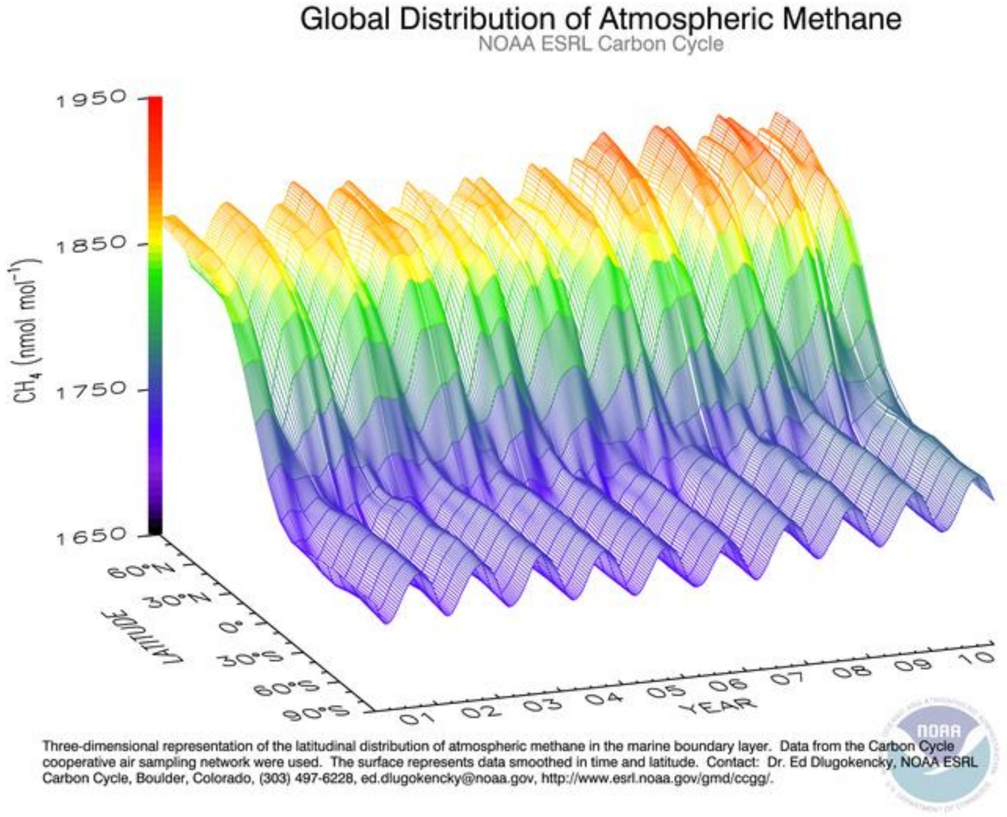

Global Distribution of Atmospheric Methane
NOAA ESRL Carbon Cycle

Three-dimensional representation of the latitudinal distribution of atmospheric methane in the marine boundary layer. Data from the Carbon Cycle cooperative air sampling network were used. The surface represents data smoothed in time and latitude. Contact: Dr. Ed Dlugokencky, NOAA ESRL Carbon Cycle, Boulder, Colorado, (303) 497-6228, ed.dlugokencky@noaa.gov, http://www.esrl.noaa.gov/gmd/ccgg/.

Figure 1.6 Three dimensional representation of the latitudinal distribution of atmospheric methane in the boundary layer over a decadal period. Source: http://www.esrl.noaa.gov/gmd/ccgg/

Figure 1.6 shows the north-south methane concentration gradient, which is controlled by the spatial distribution of methane sources and sinks. Anthropogenic methane emissions from coal and gas industries, waste and agricultural sector predominantly occur in the northern mid-latitudes, and overtake emissions from tropical wetlands. At polar latitudes there is a rising concern that methane releases from the huge store of carbon in permafrost and from arctic hydrates might severely increase, and that this strong feedback may already be activated, affecting the global methane budget (Koven et al., 2011).

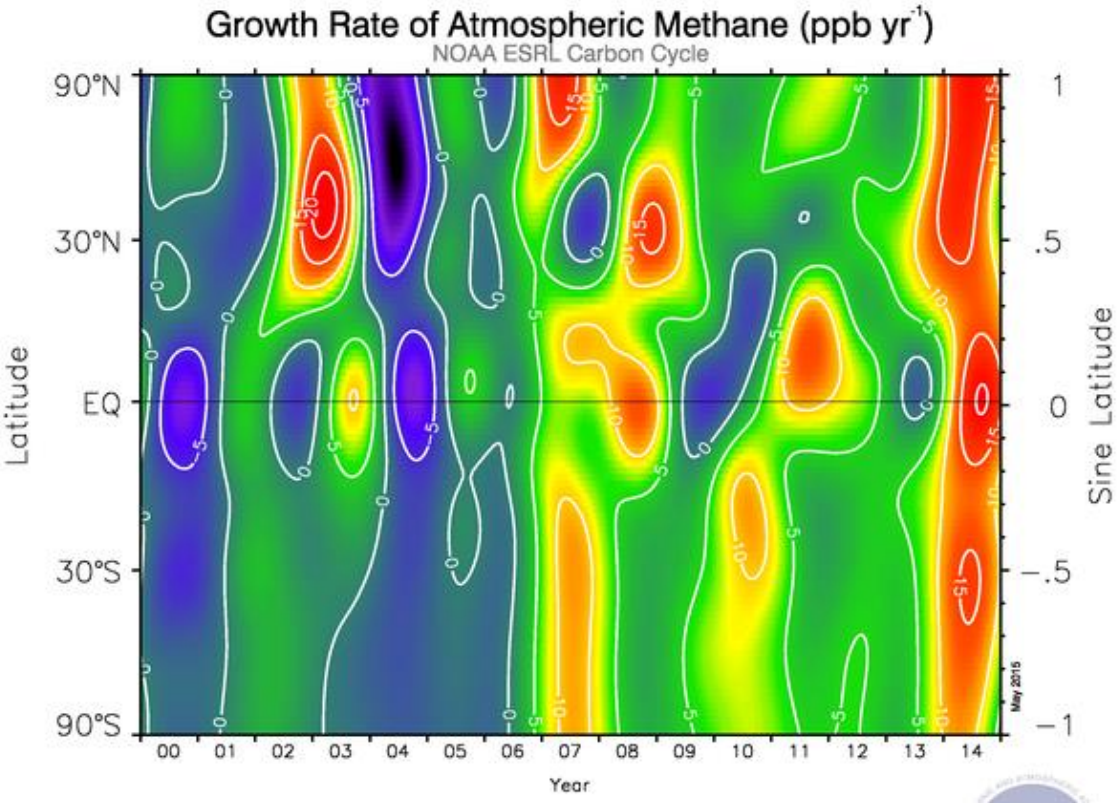

Figure 1.7 Contour map showing the temporal and spatial variation in the atmospheric increases in methane. The colder colours (green, blue, violet) represent periods of lower than average growth rates and the warmer colours (yellow, orange, red) represent periods of higher growth rates. Data from www.esrl.noaa.gov/gmd/ccgg/mbl/

Figure 1.7 shows the high inter-annual variability of the methane growth rate, whose fluctuations are thought to be critically influenced by the variability of wetlands emissions and atmospheric hydroxyl burden (Bergamaschi and Bousquet, 2008). The estimates for 2010-2011 infer a growth rate above global trend in the southern tropics, most likely driven by expanded wetlands areas (Nisbet et al., 2014). In 2014, the methane growth rate was high in all latitudes, and initial assessment of the mole fraction and isotopic records suggested increased emissions from both natural and anthropogenic sources (Nisbet et al., under review).

2

INTRODUCTION TO METHANE ISOTOPES

Development of widespread networks of CH_4 mole fraction and flux measurements has made it possible to refine the global methane budget (Kirschke et al., 2013), but the contribution of different sources to the overall atmospheric methane burden remains uncertain. The study of the isotopic composition of methane, correlated to its origin, provides a valuable constraint on the budget appraisal, allowing the partitioning of methane sources in a source mix and the estimation of their individual strength.

The isotopic composition of methane is expressed in terms of isotopic ratio, as parts per mil (‰). δ is the conventional notation relative to a standard for the isotopic signature and it is calculated from the following equation:

$$\delta=(R_A/R_{std}-1)\times 1000 \quad \textbf{2.1}$$

where R_A denotes the isotopic ratio in CO_2 derived by combustion of the methane sample (rare isotope/abundant isotope - e.g. $^{13}C/^{12}C$) and R_{std} is the corresponding ratio in the CO_2 reference gas, which is calibrated to the Vienna Peedee belemnite (V-PDB) scale for $\delta^{13}C$, using international standards.

Both methane production pathways and carbon isotope fractionation during methane oxidation affect the $\delta^{13}C$-CH_4 isotopic signature. Methane origin and uptake, together with the processes that determine the isotopic composition of atmospheric methane, are explained in the following paragraphs.

2.1 Methane Production Pathways

The production pathway accounts for the partitioning of the light (^{12}C) and heavy (^{13}C) isotopes of carbon, affecting the resulting $\delta^{13}C$ isotopic signature of methane, and it can be classified as either biogenic or abiogenic. Biogenic methane is usually derived from the anaerobic microbial fermentation of sedimentary organic matter and it is ^{13}C depleted compared to abiogenic methane, which is derived from abiological reactions, such as incomplete combustion or thermal modification of sedimentary organic matter (Quay et al., 1988). The latter normally occurs at great depth, where the increasing lithostatic pressure and concomitant rising temperatures applied to buried strata rich in organic matter result in their thermal maturation, breaking down the carbon bonds in the organic matter, and in the generation of methane (thermogenic methane).

For the biogenic methane formation the type of environment determines the preferential pathway of the microbial activity. In terrestrial environments the two main pathways are reduction of carbon dioxide with hydrogen 2.2 and the fermentation of acetate 2.3.

$$2CH_2O + 2H_2O \rightarrow 2CO_2 + 4H_2 \qquad CO_2 + 4H_2 \rightarrow CH_4 + 2H_2O \tag{2.2}$$

$$CH_3COOH \rightarrow CH_4 + CO_2 \tag{2.3}$$

These reactions are mediated by consortia of methanogens, which are fermentative archaea that metabolize only in absence of oxygen and other oxidants. In flooded basins and in sedimentary environments methanogenic archaea utilise the available acetate, mainly produced in the upper portion of peat or sediments by the degradation of organic matter (Whiticar, 1999). In sulphate-enriched environments, such as marine sediments, sulphate-reducing bacteria (SRB) effectively outcompete methanogens for carbon substrates, since sulphate respiration yields more energy than methane production. Once the SRB are inhibited by the exhaustion of the dissolved sulphate reservoir, methanogens start metabolizing the competitive substrates. Under these conditions the preferential pathway is carbonate reduction, because of the substantial bicarbonate pool which characterizes these environments (Oremland, 1988). Conversely, in fresh water, under anaerobic conditions, the fermentation of acetate is the prevailing metabolizing pathway, as methanogens do not have to compete with SRB for carbon substrates. Once these substrates are exhausted, methanogens start to reduce the dissolved carbonate. As a result, in marine system the preferential methane production pathway is CO_2 reduction, while in fresh water systems the acetate fermentation prevails. As methane is relatively insoluble in water, it migrates via 'ebullition' towards the water surface, where it is quickly consumed by methanotrophic bacteria communities (Chanton, 2005).

Different pathways lead to diverse $\delta^{13}C$-CH_4 isotopic signatures. Methane produced from acetate is indeed ^{13}C enriched relative to methane produced from

CO_2 reduction, ranging from -65 ‰ to -50 ‰ and -110 ‰ to -50 ‰ respectively (Levin et al., 1993; Waldron et al., 1998). Molecules with the lower isotopic mass ($^{12}CH_3COOH$) are generally favoured by methanogens, since they react and diffuse more easily than the isotopically heavier species. Therefore the resulting bacterial methane is ^{13}C depleted relative to the precursor substrate (Whiticar, 1999).

The fractionation factor is a further parameter that is used in the diagnosis of methane production pathway, since it tends to remain constant for one specific setting. The fractionation factor indicates the fractionation level of the organic substrates during methanogenesis and is defined as the ratio of the reaction rate constants for the two isotopes:

$$\alpha_c = {}^{13}k/{}^{12}k \tag{2.4}$$

where

$^{12}CO_2 \xrightarrow{^{12}k} {}^{12}CH_4$ and $^{13}CO_2 \xrightarrow{^{13}k} {}^{13}CH_4$.

Fractionation factors for methanogenesis via carbonate reduction (natural marine or saline environment) are distinctively higher than the corresponding α_c for methanogenesis via acetate fermentation (i.e. fresh water environment) (Whiticar, 1999).

2.2 Bacterial Methane Oxidation

Bacterial methane oxidation is carried out by methanotrophs and can be either aerobic or anaerobic (Whiticar, 1999). The aerobic consumption occurs in freshwater environments, usually at the boundary interface between the anoxic and oxic area, for instance within soils or in the superficial part of sediments in swamps and lakes. The anaerobic oxidation is mediated by at least two phylogenetically distinct groups of archaea, the ANME-1 and ANME-2, and it takes place especially in marine sediments, at the base of the sulphate reduction zone, where sulphate has been proposed to be the terminal electron acceptor for the anaerobic oxidation of methane (Valentine, 2002):

$$CH_4 + SO_4^{2-} \rightarrow HCO_3^- + HS^- + H_2O \tag{2.5}$$

The net production of carbonate in reaction 2.5 increases the alkalinity of the pore water, leading to the precipitation of calcium carbonate. Environmental factors such as temperature, CH_4 supply, sulphate supply, sediment organic content, sediment porosity and mineralogy all drive the anaerobic oxidation of methane (Valentine, 2002).

As methanotrophs preferentially remove the lighter isotopes, the residual CH_4 is ^{13}C and D enriched relative to the mean of the source input (Coleman et al., 1981). Coincidental shifts in $\delta^{13}C$ and δD are indeed symptomatic of bacterial oxidation (Levin et al., 1993). Figure 2.1 shows the systematic shifts in the isotopic composition of methane during both production and oxidation mechanisms.

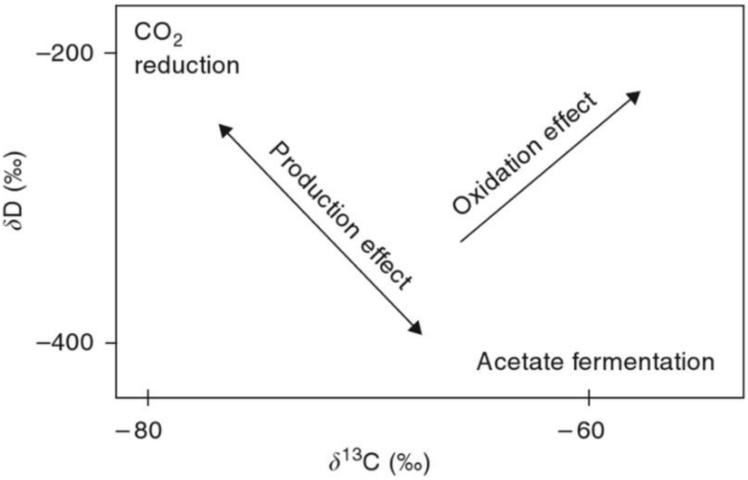

Figure 2.1 Scheme of variation in $\delta^{13}C$ and δD associated with methane production and oxidation mechanisms. Source: (Chanton et al., 2004).

As with methanogenesis, the bacterial oxidation of methane has an associated fractionation factor α ($\alpha_c = {^{13}k}/{^{12}k}$), where ^{n}k is the removal rate of $^{n}CH_4$ by the sink. This factor is typically less than 1, as the reaction rate constants are greater for $^{12}CH_4$ than for $^{13}CH_4$. Overall fractionation factors during methanogenesis are definitely larger than those related to methanotrophs, which seem to discriminate less between the lighter and heavier isotopes (Whiticar, 1999).

2.3 Methane Sinks and their Isotopic Fractionations (ε)

Methane removal processes also have isotopic fractionation effects, as $^{13}CH_4$ molecules typically react slower than the $^{12}CH_4$ molecules (Whiticar and Schaefer, 2007). A robust parameter used to weigh each sink is the kinetic isotopic effect ε, which refers to the departure from unity of the fractionation factor α, mentioned in Chapter 2.1, and usually expressed in ‰:

$$\varepsilon = \frac{^{12}K}{^{13}K} - 1$$

A ε value of -3.9 ‰ has been estimated by Sauressig et al. (2001b) for C isotope fractionation during methane oxidation via OH radicals. Allan et al. (2005) found that measurements at observation sites in Antarctica and New Zealand showed a generally larger ε value than the one expected considering only the hydroxyl radical sink. The methane oxidation exerted by the atomic chlorine in the marine boundary layer (MBL) might explain the divergence between the two ε values (Allan et al., 2007). Although the strength of this sink is not that relevant in the global methane budget, it is indeed characterized by a relatively high fractionation factor, estimated at -62.1 ±0.1 ‰ by Tyler et al. (2000).

Like for the MBL chlorine sink, fractionation factors for methane oxidation in the soil are relatively large (-22 ±4 ‰), taking into account the isotopic fractionation due to both diffusion of methane into the soil and to microbial activity (Tyler et al., 1994). Reactions of methane with OH, O (^{1}D) and Cl in the stratosphere are stratospheric sinks, all discriminating against $^{13}CH_4$. Lassey et al. (2007) assumed that the fractionation factor associated with these reactions is -3 ±3 ‰, whereas Brenninkmeijer et al. (1995) achieved from laboratory experiments a fractionation effect of -12 ‰. Methane that is not oxidised in the stratosphere is returned to the troposphere enriched in ^{13}C. The extent of the enrichment depends on the exposure of methane to oxidants in the stratosphere, such as anthropogenic chlorine in the lower stratosphere (McCarthy et al., 2001), whose burden has been augmented by the massive CFC (Chlorofluorocarbons) input in the atmosphere since the 1920's.

Sink	**ε_{sink} ‰**	**Reference**
OH	-3.9 ±0.4	(Saueressig et al., 2001a)
Chlorine	-62.1 ±0.1	(Tyler et al., 2000)
Stratosphere	≈-12	(Brenninkmeijer et al., 1995)
	-3 ±3	(Lassey et al., 2007)
	-22 ±4	(Tyler et al., 1994)
Soil	-17.3 ±1 (grassland)	(Snover and Quay, 2000)
	-18.1 ±0.4 (forest)	

Table 2.1 Published fractionation factors of methane sinks.

2.4 Carbon Isotopic Signatures of Methane Sources

Some methane sources can be effectively distinguished by measuring the stable isotopic composition of methane, since different source types are characterised by distinct isotopic signatures. More in detail, biogenic methane is ^{13}C depleted ($\delta^{13}C \approx -60$ ‰) relative to pyrogenic methane derived from incomplete combustion ($\delta^{13}C \approx -25$ ‰) and fossil methane of thermogenic origin, which is characterised by an intermediate ^{13}C value ($\delta^{13}C \approx -40$ ‰) (Lassey et al., 2011).

The variety of production pathways and local environmental conditions that discriminate for the methane formation process leads to a wide range of $\delta^{13}C\text{-}CH_4$ values.

2.4.1 Biogenic Sources

Methane originating from microbial metabolism is counted as the primary source of atmospheric methane (Cicerone and Oremland, 1988), including emissions from ruminants, rice paddies, wetlands, landfills and some hydrates.

$\delta^{13}C$ signatures of emissions from ruminants range between -71 ±4 and -55.6 ±1.4 ‰ (Bilek et al., 2001; Klevenhusen et al., 2010), and are highly controlled by the diet type. The change in the isotopic signature of the precursor substrate for methanogenesis can indeed affect the $\delta^{13}C$ of the methane produced.

Methane eructated by ruminants fed with a C_4[3] diet (maize) is found to be ^{13}C enriched compared to that emitted when ruminants are fed with a C_3 diet (Klevenhusen et al., 2010), as a result of C_4 plants being isotopically heavier than C_3 ones. Also the metabolism of the bacteria involved in the digestion seems to play an important role. Archaea found in the rumen are strictly anaerobic methanogens and can grow consuming either H_2 or formate, using electrons derived from H_2 (or formate) to reduce CO_2. A few species can produce methane via acetate fermentation, but the reduction of CO_2 is believed to be the preferred methane production pathway (Conrad, 2009).

The isotopic signatures assigned to wetland emissions average -59 ±8 ‰ according to Quay et al. (1988), whereas Bowes and Hornibrook (2006) suggested $\delta^{13}C$ values ranging from -70 to -90 ‰. The variability in the $\delta^{13}C$ values observed can be explained by the diverse isotopic composition of the parent organic matter undergoing decomposition and the degree of microbial oxidation of methane at the atmospheric interface (Tyler et al., 1994). The isotopic signature of organic matter depends primarily on the photosynthesis pathway - i.e. methane produced from the decay of C_4 plants is found to be ^{13}C enriched compared to methane produced from the decay of C_3 plants (Keppler et al., 2006; Vigano et al., 2009) - and on environmental parameters such as temperature and water level, which affect the microbial activity (Whiticar and Schaefer, 2007). Hornibrook et al. (1997) demonstrated a shift in the relative importance of methanogenic pathway with the temperate zone wetland depth, with associated change in the methane isotopic composition (see Chapter 2.1). In the deeper portion of peatland, where the substrates for acetate fermentation progressively decrease, the CO_2 reduction becomes the prevailing methanogenic pathway.

The isotopic composition of methane emissions from rice paddies is driven by the same equilibrium of methane production-oxidation characterising wetlands.

---

[3] C3 and C4 plants differ in the way to fix CO_2. C3 plants fix CO_2 via ribulose bisphosphate carboxylase and have $\delta^{13}C$ values that average about -25 ‰, while C4 and CAM plants, which fix CO_2 via P-enolpyruvate carboxylase, have average $\delta^{13}C$ values of about -13‰ (Sternberg et al., 1984).

Rice roots are actively involved in the methanogenesis as a site of a complex microbial community (Chidthaisong et al., 2002). The methane flux reaching the atmosphere is mitigated by the aerobic oxidation of methanotrophs, which takes place mostly in the rhizosphere (Conrad, 2009). Krüger et al. (2001) observed a methane isotopic signature ranging from -60 to -68 ‰, with lighter values preferentially towards the latter part of the growing season.

Landfills are sites of intense microbial activity. Consortia of anaerobic microorganisms break up the complex organic matter available in the landfill strata to produce acetate, CO_2, H_2 and organic acids. The large abundance of acetate supports the methane production through the acetate fermentation pathway. With the ageing of the landfill, the productivity of the organic matter decreases and methane is mainly produced via CO_2 reduction, characterized by lower $\delta^{13}C$ values (Hornibrook et al., 2000). The methane stream from the deep layers nourishes the methanotrophs within the topsoil cover layers, the aerobic region of the landfill. The bacterial oxidation leads to a ^{13}C enrichment of methane emissions (see Chapter 2.2), as Figure 2.2 shows. As oxidation is highly dependent on temperature, pH and moisture content, it exhibits certain seasonality, reaching the maximum value during summer months, when $\delta^{13}C$ values of the residual methane emitted to the atmosphere can approach -40 ‰ (Chanton and Liptay, 2000). Emissions to the atmosphere from landfills are therefore strictly related to the region and landfilling practices, which in turn affect the level of methane oxidation, the formation pathway and thus the isotopic composition. Methane $\delta^{13}C$ values observed in several studies span a range from -61 to -45 ‰ (Bergamaschi et al., 1998; Lowry et al., 2001).

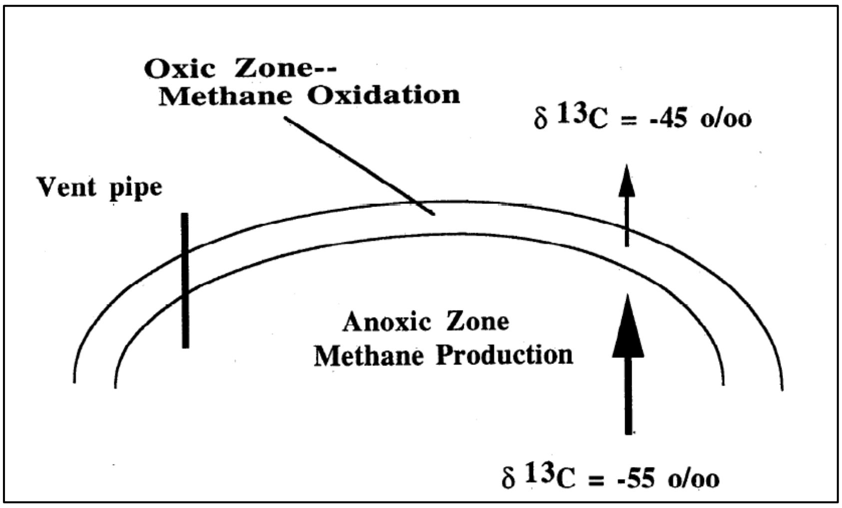

Figure 2.2 Conceptual model representing the use of isotopic measurements to quantify methane oxidation in landfill (Liptay et al., 1998).

Wastewater treatments include different methane sources, comprising the aerobic treatment of sewage and the anaerobic digestion of sludge. Methane emissions mainly derive from leaks in the anaerobic digesters of primary and secondary sludge (Daelman et al., 2012) and $\delta^{13}C$-CH_4 values agree with the isotopic composition of methane produced from acetate fermentation processes, ranging from -65 to -50 ‰ (see Chapter 2.1).

Methane Source	$\delta^{13}C$ (‰)	Reference
Ruminants	(C3 diet) -67.6 ±1.0	(Klevenhusen et al., 2010)
	(C4 diet) -55.6 ±1.4 to -57.5 ±1.0	(Klevenhusen et al., 2010)
Animal Waste	-49.3 to -46.0 ±1	(Klevenhusen et al., 2010)
Wetlands	-44 ±4 to – 88.8 ±5.0	(Quay et al., 1988) (Stevens and Engelkemeir, 1988) (Chanton et al., 1992) (Happell et al., 1993) (Tyler et al., 1994) (Happell et al., 1994) (Mikaloff Fletcher et al., 2004) (Bowes and Hornibrook, 2006)
Rice Paddies	-70 to -52	(Tyler et al., 1994; Krüger et al., 2001)
Landfills	-57.4 ±1.7 (Netherlands)	(Bergamaschi et al., 1998)
	-60.3 ±2.3 (Germany)	(Bergamaschi et al., 1998)
	-58.6 ±1.4 (Sweden)	(Börjesson et al., 2001)
	-50.8 to -52.6 (England)	(Lowry et al., 2001)
	-60.0 ±0.2 to -46.7 ±0.2 (France)	(Widory et al., 2012)
	-61	(Townsend-Small et al., 2012)
Wastewater	-54	(Levin et al., 1999)
	-47	(Townsend-Small et al., 2012)
Hydrates	– 42.2 to -74.7	(Milkov, 2005)

Table 2.2 Methane signatures of biogenic sources.

2.4.2 Thermogenic Methane Sources

Methane of thermogenic origin is generally enriched in ^{13}C compared with bacterial (biogenic) methane, ranging from -50 ‰ to -20 ‰ (Whiticar, 1999), and it becomes gradually even more heavier at high maturity stages . However, δ^{13}C values may overlap for different methane formation processes and the comparison of D and ^{13}C pairs is often used to discriminate methane of thermogenic and biogenic origin. Indeed, each methane type is characterised by systematic shifts in $\delta^{13}CH_4$ and δD-CH_4 values, as shown in the CD-diagram in Figure 2.3.

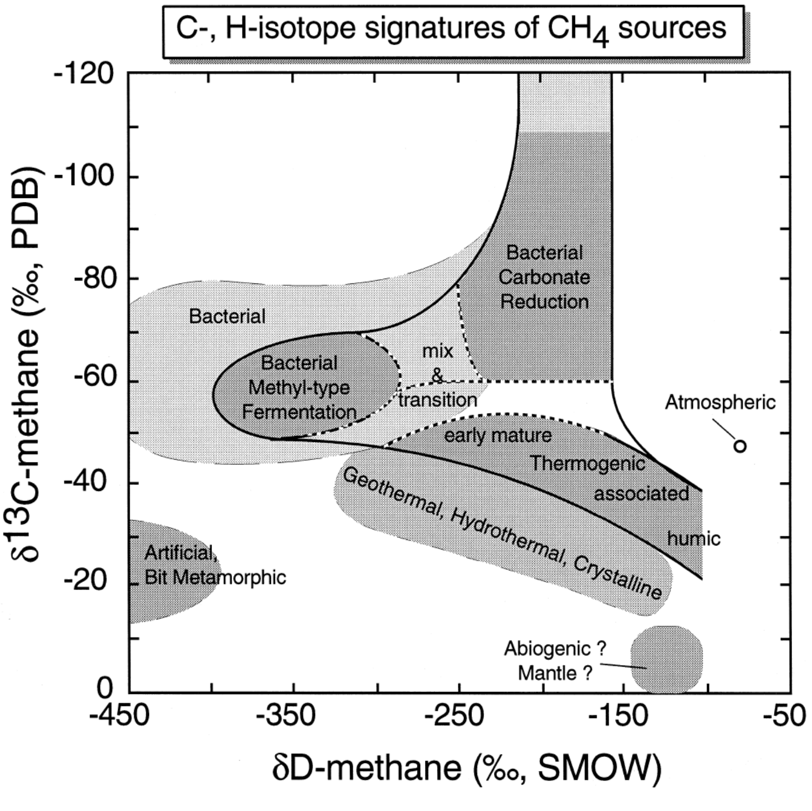

Figure 2.3 CD diagram for classification of bacteria and thermogenic natural gas by the combination of $\delta^{13}C$-CH_4 and δD-CH_4 signatures (Whiticar, 1999).

Thermogenic methane sources include most fossil fuels (i.e. coal and natural gas). Isotopic composition of methane emissions from both coal mining and leaks in the natural gas distribution network are discussed in detail in Chapter 5.2 and 5.3.1 respectively.

Methane Source	$\delta^{13}C$ (‰)	Reference
Natural gas	-34 ±3 (North Sea)	(Lokhorst, 1997)
	-50 ±3 (Siberia)	(Levin et al., 1999)
Coal Mines	-80 ‰ to -17 ‰	(Rice, 1993)

Table 2.3 Methane signatures of thermogenic sources.

2.4.3 Pyrogenic Methane Sources

Pyrogenic methane sources have a very distinctive isotopic signature, which makes methane emissions from incomplete combustion highly identifiable (Mikaloff Fletcher et al., 2004). Combustion leads to strongly ^{13}C enriched methane, and the variety of isotopic values is mainly associated with the type of fuel. Chanton et al. (2000) reported $\delta^{13}C$ values for biomass burning in a range of -26 to -30 ‰ for the C_3 forest fires and -16 to -20 ‰ for the C_4 grass fires (unpublished RHUL results, N. Rata and D. Lowry). They also observed substantial differences between the $\delta^{13}C$ emitted by smouldering and flaming fires. Flaming and hotter fires generally exhibit higher combustion efficiency and the methane released can be partially burnt; due to the preferential consumption of $^{12}CH_4$, the residual methane will be highly ^{13}C enriched. The portion of methane burnt could be considerable in a closed system such a wood stove or any engines. An efficient engine produces less methane and with a higher ^{13}C content than methane generated at lower combustion efficiencies. Methane emitted from newer automobiles were found to be ^{13}C enriched by more than 15 ‰ relatively to older ones, with $\delta^{13}C$ values of -9 ±0.3 ‰ (Nakagawa et al., 2005). Domestic boilers also can emit significant amounts of methane if not properly serviced, plus newer types release a pulse of methane before ignition. UK gas boilers have isotopic signatures for emitted methane of -25.3 ±0.8 ‰ (Fisher, 2006), typical of pyrogenic methane.

Methane Source	**$\delta^{13}C$ (‰)**	**Reference**
Biomass Burning	C3 forest -26 to -30	(Chanton and Liptay, 2000)
	C4 grass – 16 to -20	(unpublished results, N. Rata and D. Lowry)
Vehicles	-20.1 ±1.7 to -9 ±0.3	(Chanton et al., 2000; Nakagawa et al., 2005; Fisher, 2006)
Boiler	-25.3 ±0.8	(Fisher, 2006)

Table 2.4 Methane signatures of pyrogenic sources.

2.5 Global Methane

2.5.1 Global Methane Budget

According to a top-down approach, the change in the global methane budget can be estimated by the following equation:

$$\frac{d[CH_4]}{dt} = Q - \frac{[CH_4]}{\tau}$$

2.6

where Q is the sum of all methane sources, $[CH_4]$ is the global methane burden given by atmospheric methane mole fractions, and τ is the lifetime of the atmospheric CH_4. Isotopic measurements offer an additional constraint to the methane budget. The carbon isotopic ratio mass balance is given by the linear mixing equation:

$$\partial_q Q = \partial_{i1} Q_{i1} + \cdots + \partial_{in} Q_{in}$$

2.7

where δ_{ix} is the isotopic ratio associated to a specific methane source, δ_q is the flux weighted isotopic ratio and Q_{ix} are the source fluxes. The calculated atmospheric isotopic value δ_q is estimated taking into account both source and sink terms in the net carbon isotopic balance $\delta_q Q$ (Whiticar and Schaefer, 2007):

$$\partial_q = \frac{[\{\partial_{i1} Q_{i1} + \cdots + \partial_{in} Q_{in} \alpha \partial_a\}_{sources}]}{Q} - \varepsilon$$

2.8

In equation 2.8 ε refers to the combined isotope effect associated with all the sink processes (see Chapter 2.3). By comparison of the calculated δ_q with the measured atmospheric isotopic ratio, methane sources fluxes and sinks can be accommodated in the net methane balance, giving a powerful constraint in the attribution of the correct sources fluxes and $\delta^{13}C$ values.

The mean $\delta^{13}C$ of all global sources is -52.8 ‰, but the OH and soil sink fractionation factors result in a global atmospheric background seasonal cycle that varies between -47.8 and -46.8 ‰ (Levin et al., 2012).

2.5.2 Global Variation in the Atmospheric Isotopic Ratio

The study of atmospheric isotopic composition in the past can provide insights for the understanding of today's atmospheric methane trend. Changes of $\delta^{13}C$ signatures of methane sources and isotopic fractionation of sinks in the past, not necessarily associated with a corresponding change in the methane mole fractions, are thought to account for most of shifts in the isotopic composition of methane over the last millennia. The main changes comprise variations in the precursor material, in the methanogenic pathway, transports and sinks (Whiticar and Schaefer, 2007). Analysis of the $\delta^{13}C\text{-}CH_4$ in air trapped in Greenland ice cores over the last 2 millennia shows a depletion of 2 ‰ from 1000 to 1700 A.D., contextually to a small growth of methane concentration (~50 ppb), most likely driven by biogenic methane emissions (Ferretti et al., 2005). The ^{13}C excursions over the last two millennia are speculated to originate from increased pyrogenic methane emissions due to anthropogenic activities and / or a decrease in biogenic sources (Sapart et al., 2012).

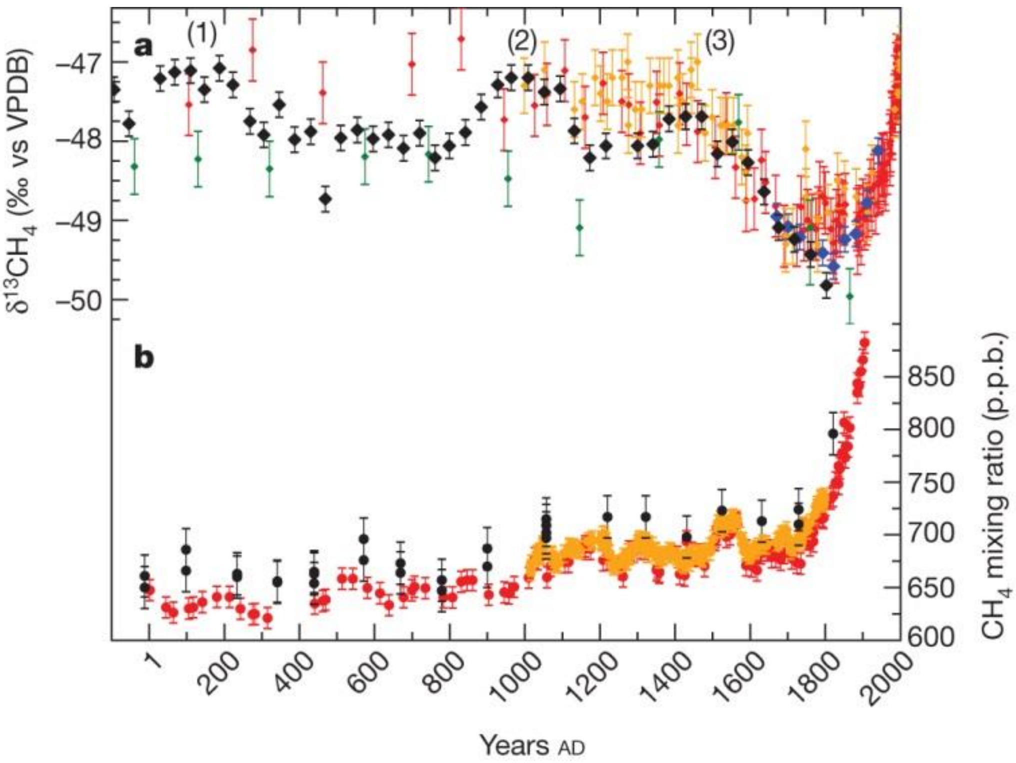

Figure 2.4 $\delta^{13}C$ measurements on air trapped in Greenland ice cores from NEEM (black diamonds) (Sapart et al., 2012); EUROCORE (blue diamonds) (Sapart et al., 2012); GISPII (green diamonds) (Sowers, 2010) and Antarctic ice cores from Law Dome (red diamonds) (Ferretti et al., 2005) and the WAIS divide (orange diamonds) (Mischler et al., 2009). (1), (2) and (3) correspond to the three excursions in the Northern Hemisphere $\delta^{13}C$ record. b, CH_4 mixing ratio records from Greenland (GRIP, black circles) (Blunier et al., 1995; Chappellaz et al., 1997), and Antarctica (Law Dome, red circles; WAIS, orange circles) (MacFarling Meure et al., 2006; Mitchell et al., 2011). Each data point represents one measurement. Error bars represent ±1σ, based on the reproducibility of the measurement systems. Source: (Sapart et al., 2012).

2.5.3 Spatial and Temporal Variation of Global Methane Sources

The spatial trend of global methane sources can be assessed through the study of north-south gradients in methane mole fractions and in methane isotopic composition. Miller et al. (2004) investigated the reasons behind this isotopic difference between hemispheres, suggesting the depletion of methane in ^{12}C by reaction with OH radicals, mainly in the tropics, and the prevalence of ^{13}C depleted methane sources in the North Hemisphere (NH) as the leading processes affecting the isotopic composition of methane. Furthermore, lower methane emissions and rapid atmospheric mixing lead to a substantial lack of $\delta^{13}C$ gradient in the SH.

Figure 2.5 shows measurements of the ^{13}C isotopic composition of atmospheric methane from 1978 to 1995, taken at various sites distributed around the globe.

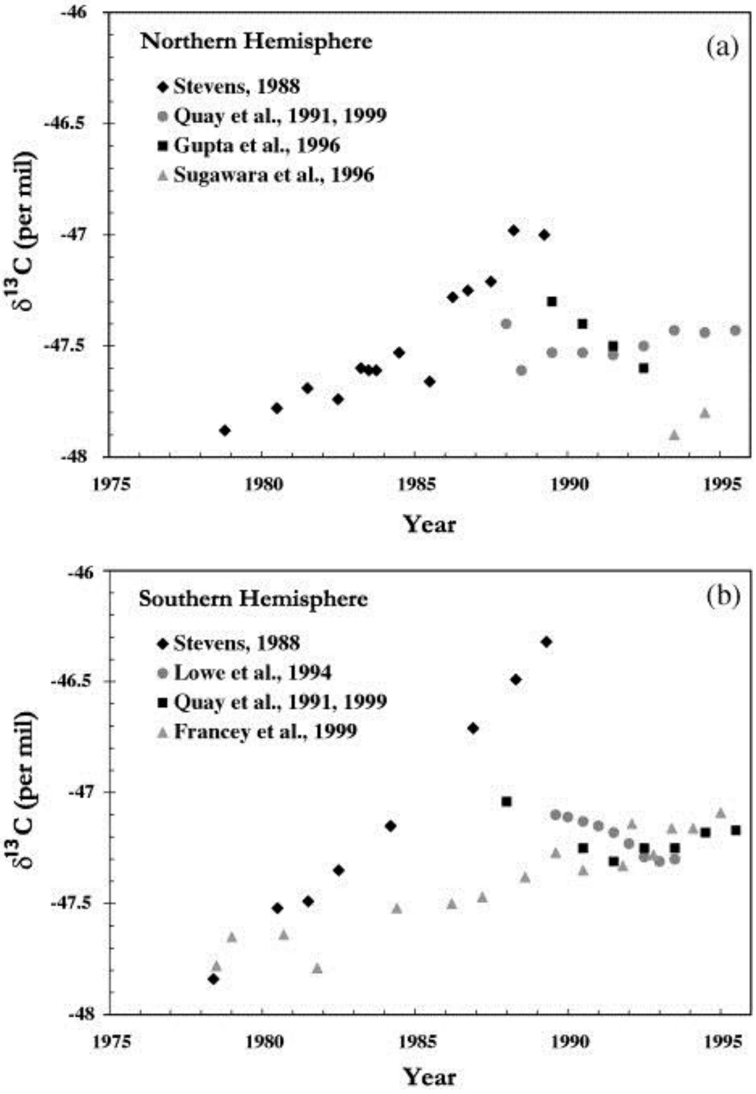

Figure 2.5 Measurements of the ^{13}C isotopic composition of atmospheric methane from 1978 to 1995. Hemispherically and annually averaged data were collected at a number of sites in (a) the Northern Hemisphere, and (b) the Southern Hemisphere (Stevens and Wahlen, 2000).

Lowe et al. (1994) reported a notable decrease in the annual mean $\delta^{13}C$ of ~0.2 ‰ in the SH, whereas in other studies this decrease in not evident. Quay et al (1999) revealed a clear spatial and temporal trend in the isotopic composition of methane and observed more ^{13}C enriched values by approximately 0.23 ‰ in the SH. This inter-hemispheric difference is interpreted by Quay et al. (1999) as the result of the atmospheric transport between hemispheres. An important portion of methane released in the NH (20-30 %) moves to the SH, following the global atmospheric circulation (Fung et al., 1991; Hein et al., 1997), so that changes in the isotopic composition and in the strength of methane sources in one hemisphere might be detected in the other one.

The Northern and Southern hemisphere exhibit also different seasonal variations in the methane isotopic composition. The larger seasonality in the NH and tropics is thought to be driven primarily by the high temporal variability of methane sources (Lassey et al., 2011). Towards the summer $\delta^{13}C\text{-}CH_4$ values start declining, as biogenic emissions from wetlands, associated with lower $\delta^{13}C\text{-}CH_4$ values, prevail during late summer and overtake the isotopic effect of the OH sink. The Extra Tropical Southern Hemisphere (ETSH) displays a greater spatial homogeneity, and seasonal cycles are mostly explained by in situ oxidation of CH_4 (Lassey et al., 1993). The overall seasonal cycle based on datasets from three different laboratories is shown in Figure 2.6 (a) (Levin et al., 2012).

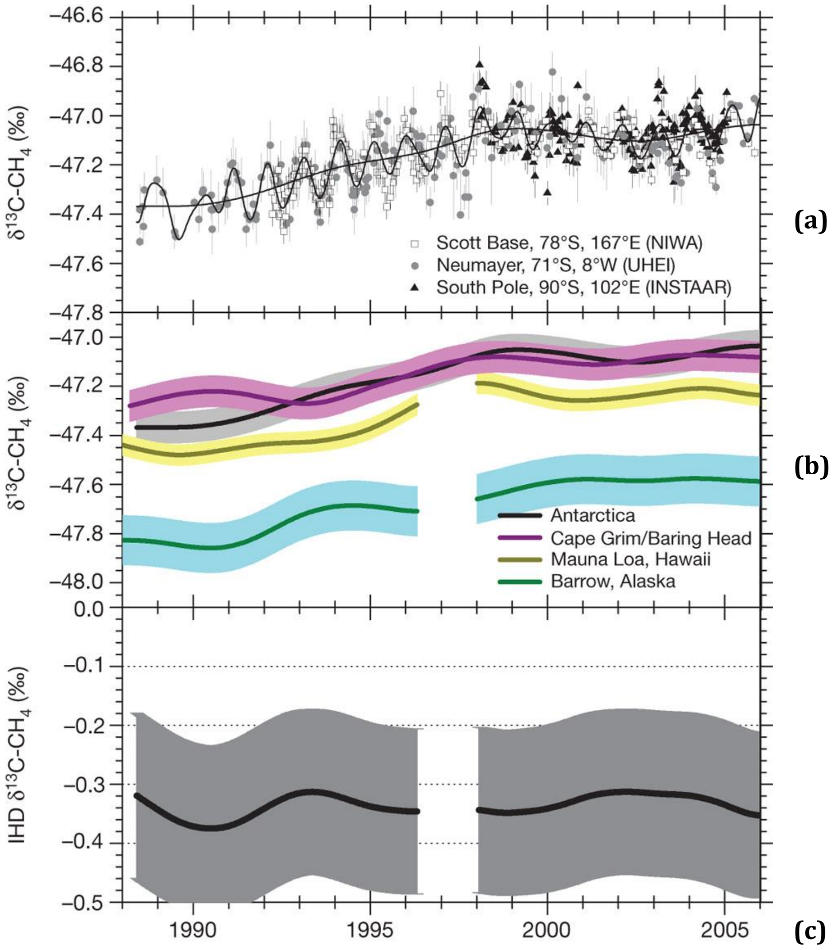

Figure 2.6 Long-term trends in atmospheric $^{13}CH_4$ (Levin et al., 2012).

2.6 Aim of this Research

As introduced in Chapter 1 and Chapter 2, the methane cycle and its drivers are continuously evolving, and a systematic record of methane isotopic composition and mole fractions would reduce the large uncertainties affecting the global and regional methane budget estimates. This research aims to isotopically characterise methane sources in the UK, with a focus on SE England, in order to define the contribution of each methane source to local emissions and validate UK inventories where it is possible. In order to achieve these goals a series of objectives were set and considered in the following 5 chapters.

UK methane emissions inventories at 1km^2 resolution have been assessed and emissions maps have been produced for the main areas of study, using ArcMap Software (Chapter 3).

A new methodology has been developed, based around the mobile deployment of a Picarro CRDS analyser for CH_4 and CO_2 mole fraction measurements (Chapter 4), to measure and sample methane plumes from sources (Zazzeri et al., 2015). This new procedure has been implemented around the hotspot sites highlighted by the inventory assessment in Chapter 3, allowing the isotopic characterisation of plumes and confirming their source. A detailed summary of the main source categories explored, the surveys carried out and the sites visited is provided in Chapter 5.

Diurnal measurements carried out at RHUL (Royal Holloway University of London) and in central London (King's College) to assess the isotopic signal of local methane emissions have permitted further understanding of the source mix in the London Region (Chapter 6), particularly a general verification of the latest inventories.

Finally, specific London Boroughs have been targeted for more detailed mobile assessment of methane emissions relative to inventories estimates (Chapter 7), providing an example of the use of isotopic analysis for verifying local inventories.

3

METHANE EMISSIONS INVENTORIES

3.1 Outline of IPCC Guidelines for Methane Emissions Inventories and their Uncertainties

Compliance with the IPCC Guidelines is strongly recommended for the assessment of national emission inventories. The 2006 guidelines indicate different methodologies for the emissions calculation, which are structured according to the level of accuracy required. The IPCC report (IPCC, 2006) defines "tier" as a level of methodological complexity: tier 1 represents the basic method and tier 2 and 3 are progressively more sophisticated, as they need more input data, but guarantee a higher accuracy. Each method includes equations developed on the basis of a bottom-up approach, using activity data multiplied by pre-established emission factors.

Emission: Factor x Activity

Activity data are mainly based on statistical surveys, which can introduce uncertainties if they do not rely on exhaustive investigations and if data acquired are not entirely dependable. Default emission factors are provided by the IPCC guidelines, but they may not reflect specific conditions associated with the target emissions within the reference country.

The overall uncertainty in the emissions estimate can be defined using standard statistical tests when the extent of the data sample is large enough. The recommendation is that uncertainties are calculated as ±2 standard deviations of the mean. However, as specific measured data are sporadically accessible, model based estimates may be performed. These tend to simplify methane production processes that are actually very complex and irregular (e.g. methane emissions from landfill sites), introducing further uncertainty. IPCC Guidelines provide default values of emissions uncertainties, but discrepancies in the natural and economic conditions between different countries do exert influence on the inventory estimate. Countries such as UK, USA, Netherlands, Norway and Austria have enhanced their inventory and uncertainty assessment, so that emission values are effectively comparable.

An outline of the methane estimation methods suggested by the 2006 IPCC report (IPCC, 2006) is presented in this chapter for each methane emission sector.

3.1.1 Stationary and Mobile Combustion

Methane emissions from combustion sources result from the incomplete combustion of fuel. Unlike CO_2 emissions, which can be properly estimated by applying a carbon content related emission factor to the fuel quantity consumed (U.S. EPA, 2008), CH_4 emissions are more complex to calculate. The emission rate depends specifically upon the characteristics of the fuel (e.g. the calorific value) and the combustion technology used, as well as the maintenance and operated practices followed. Technology-based emission factors, particularly if determined through direct measurements at stationary combustion sources, are suggested to be used rather than default ones, which may be too general and introduce further uncertainty in the estimate.

Emissions within the stationary combustion sector are assessed following this general IPCC equation:

$$Emissions = \sum (EF_{abc} \cdot FC_{abc})$$

3.1

where EF is the emission factor and FC the fuel consumption; *a* is the fuel type, *b* the sector activity and *c* the technology type. According to the Tier 3 approach, emission factors must be developed ad hoc, taking into account parameters such as combustion technology, fuel type, operating conditions etc. Fuel consumption is estimated from energy use statistics.

The mobile combustion category includes emissions from road transportation. Exhaust gases from road vehicles are often neglected in the global atmospheric budget of methane, but they become significant at more local scale, when large urban conurbations, such as London, are considered. According to the Tier 1 approach, methane emissions are calculated with the following equation:

$$Emissions = \sum (Fuel_a \cdot EF_a)$$

3.2

where EF_a is the emission factor (kg/TJ), $Fuel_a$ is the fuel consumed (TJ) (as represented by fuel sold) and the subscript a represents the fuel type (e.g. diesel, gasoline, natural gas, LPG). Higher Tiers recommend the use of an emission factor that takes into account the specific combustion and emission control technology characterising the vehicle, and include in the equation also vehicle distance travelled for a given mobile source activity. National statistic agencies should make available fuel combustion data, whose completeness plays a key role in the uncertainty estimate.

3.1.2 Coal Mining

Total methane emissions from coal mines include emissions coming from underground coal seams, which represent the largest methane source within the category, from surface mining and from post-mining activity.

In underground mines methane is mainly released into the atmosphere through wells that are drilled in order to vent the gas emitted from the coal formations into the surface and maintain a safe working environment. The degasification system can be also employed for methane recovery for energy use.

In surface mines methane emissions may occur as a result of the deterioration of the coal seam and they are usually less than emissions from underground mining. As these releases are not focused on defined locations but are distributed all over the mine, they are difficult to quantify and a routine procedure in their estimate has not been developed.

The Tier 1 IPCC general equation for calculating methane emissions from active coal mines is:

$$Emissions = CP \times EF \times UCF$$

3.3

where CP is the coal production (underground or surface coal production depending on the coal mine type), EF the emission factor (m^3/tonne) and UCF the units conversion factor (density of CH_4, which converts volume of CH_4 to mass of CH_4).

After closure coal mines continue emitting methane into the atmosphere through breakages in the coal seams or underground conduits (i.e. wells, vent pipes), until they are entirely flooded as a result of the groundwater inflow. The rate of methane released after the closure tends to decline over the year. Therefore the time elapsed since the mine was abandoned is critical in the emission estimate. The IPCC equation 3.4, used in the emissions assessment for abandoned mines, is applied for specific time intervals and the resulting emission estimates are then combined to calculate the total.

$$Emissions = ACM \times GCM \ \times EF \ \times CF \tag{3.4}$$

The term ACM represents the number of abandoned coal mines remaining unflooded. GCM is the fraction of gassy coal mines, EF the emission factor and CF the conversion factor. The emission factor, expressed in m^3/year, takes into account the mine's gassiness and is strictly related to the depth of the mine and the coal rank.

3.1.3 Natural Gas Leaks

Fugitive emissions from natural gas systems refer to emissions from equipment leaks, venting, flaring and accidental releases. Their quantification is one of the most difficult as, where emission sources are not intentional, flow rates and gas composition are not well characterised in all their variety, and direct measurements are not always available.

According to Tier 1 approach, the following equation describes emissions from a particular industry segment:

$$Emissions_{industry\ segment} = A_{industry\ segment} \cdot EF \tag{3.5}$$

where A is the activity value and the emission factor (EF) represents the emission per unit of activity. The choice of emission factors determines the level of accuracy of the emissions estimate. A higher Tier suggests an emission assessment at the individual facility by primary source type (e.g. venting, fugitive equipment leaks, accidental releases).

3.1.4 Enteric Fermentation

The methane emissions assessment within this category involves firstly a complete characterisation of livestock subcategories. Indeed, the main control on the rate of methane production is the type of digestive system. Ruminants, for instance, have a multi-chamber stomach, which enables an intensive microbial fermentation that leads to methane production. Dairy cows, defined by the IPCC report as “mature cows that are producing milk in commercial quantities for human consumption” should represent a subcategory, as they tend to produce more methane than the other ruminants.

Emission inventories are calculated multiplying the number of animals (P) by an emission factor (EF) for the specific livestock population (kg/head/year).

$$Emissions = EF \times P/(10^6\ kg/Gg) \tag{3.6}$$

The annual population, when official national statistics are not available or totally dependable, can be estimated using the Food and Agricultural Organisation (FAO) data. Emission factors are strictly related to the livestock diet, which has to be properly characterised if higher Tiers, and thus more accurate methodologies, are chosen for the emissions estimate. In fact, the extent of methane production is certainly affected by the feed intake type, which is in turn related to the growth rate and the animal size. The accuracy of the emissions estimate is positively linked to the level of detail of data collected.

3.1.5 Manure Management

Methane emissions from manure management mainly originate from confined areas where a large number of animals are managed –e.g. dairy farms- and thus anaerobic conditions suitable for methane production are established. If manure is stored and treated in a liquid system, methane production is further augmented.

According to the IPCC Tier 1 method, methane emissions are computed by multiplying animal population data (P) by a specific emission factor (EF) (kg x CH_4/head/yr):

$$Emissions = EF \times P/(10^6\, kg/Gg)$$

3.7

Default emission factors are provided by the IPCC guidelines and are used if a Tier 1 approach is adopted. However, uncertainty may be reduced if specific emission factors that reflect the manure management system of a country are used.

3.1.6 Solid Waste Disposal

The IPCC method used for the methane emissions estimate from landfill sites is based on a first order decay (FOD) model, which is widely considered as the process that approximates more truthfully the pattern of waste degradation over time. The key parameter of the model is the reaction constant k, which is proportional to the time ($t_{1/2}$) that DOC (Degradable Organic Carbon) in waste takes to decay to half its initial mass (k = ln $2/t_{1/2}$). This prediction model assumes that the methane generation potential depends only on the amount of decomposable DOC in the waste, and therefore it declines as the carbon material is gradually consumed. The methane originated is calculated from the fraction of DOC that each year is degraded. As the k value is based on the waste composition and moisture conditions of the site (e.g. slow decay is associated with dry sites and slowly degradable material), emissions estimate must be guided by specific studies of site conditions and waste composition. Historical data both on type of wastes and on management practices over a time frame of 3 to 5 half-lives must be available, in order to achieve the accuracy required by IPCC standards.

Total methane emissions are calculated according to the following IPCC equation:

$$Emissions = \left[\sum_{x} CH_4generated_{x,T} - R_T\right] \cdot (1 - OX_T)$$

3.8

where T is the inventory year, x the waste category or type/material, R_T the recovered CH_4 in year T, OX_T the oxidation factor in year T. Only the fraction of CH_4 that is not recovered will be subject to oxidation.

Critical parameters used in this estimation model are the oxidation factor and methane recovery. The amount of methane oxidised in the soil cover of wastes depends on the physical properties and moisture of the covering layers and it should be estimated directly on site, since methane can diffuse through fissures, escaping the oxidation process through the soil cover. Therefore, the use of default oxidation rates might result in an overestimation of the methane oxidised. The biogas produced in the landfill site can be recovered and combusted for energy use. In this case the greenhouse gases released from combustion should be reported under the "stationary combustion" sector.

The uncertainty in the methane emission estimates lies both in the selection of parameters chosen for the model and in the methodology itself. Each landfill site should be properly characterised, since parameters such as temperature, moisture conditions and waste composition vary widely even across the same site, and the use of averaged model input values would produce highly uncertain estimates. Furthermore, even though the FOD model is assumed to be the most valid, the system of chemical reactions involved in the decay of organic matter might be more complex and change over time.

3.1.7 Wastewater Treatment

Methane is generated in wastewater treatment by processes involving intense biological activity and concurrent absence of oxygen. The areas where these conditions occur are the influent lines, primary settling tanks, sludge holding tanks and sludge transfer lines (Czepiel et al., 1993). The temperature drives the microbial reactions and methane is likely to be produced above 15°C. However, methane originates primarily from the anaerobic digestion of the sludge and it is usually flared or recovered for energy. In this case it should be removed from the total methane emissions.

In the IPCC guidelines for estimating emissions from wastewater treatment, the activity data are represented by the total organic degradable material in the wastewater (TOW), which is a function of human population and BOD[4] generation per person.

$$Emissions = TOW \cdot EF - R$$

3.9

$$TOW = P \cdot BOD \cdot 0.001 \cdot I \cdot 365$$

3.10

In equation 3.10 P is the country population and I is the correction factor for additional industrial BOD discharged into sewers.

$$EF_j = B_0 \cdot MCF_j$$

3.11

The Emission factor EF for a wastewater treatment j is a function of the maximum methane producing potential of each waste type (B_0) and the weighted average of the methane conversion factor (MCF_j), which is the estimated fraction of BOD or COD[5] that will eventually deteriorate anaerobically.

---

[4] BOD is the Biochemical Oxygen Demand, the amount of dissolved oxygen in water consumed during 5 days of incubation at 20 °C.

[5] COD is the Chemical Oxygen Demand, which is the measure of all the organic compounds in water. It measures everything that can be oxidised chemically in water, whereas the BOD measures only the biological activity.

3.2 European Methane Emissions Inventories

Official greenhouse gas inventories for European countries are provided by the European Environment Agency (http://www.eea.europa.eu/data-and-maps). European methane emissions estimates show an overall reduction between 1990 and 2012, which is ascribed mainly to lower levels of coal mining and post mining activities, as well as lower emissions from disposal on land of biodegradable waste. The compliance with the EU Common Agriculture Policy, including a better management of manure and the introduction of "milk quotas" that led to higher milk production from less cattle, played also a key role in the methane emissions reduction (EEA, 2014).

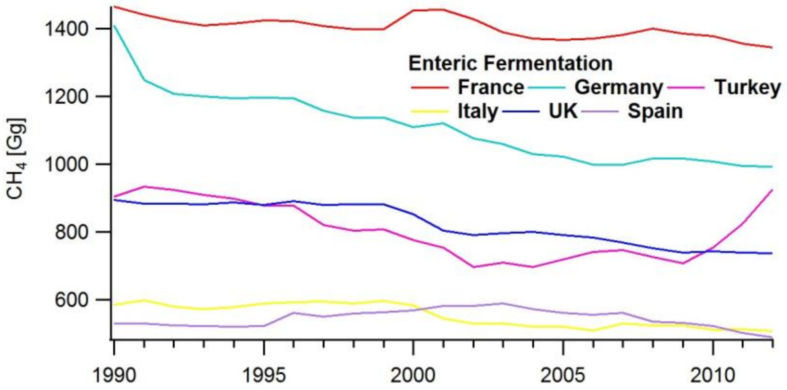

(a)

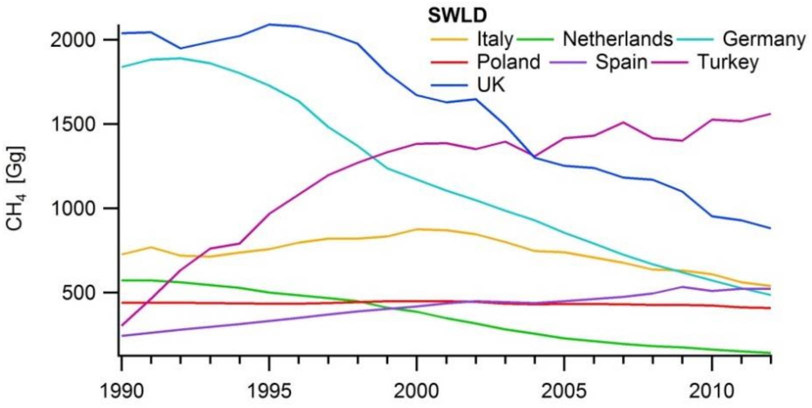

(b)

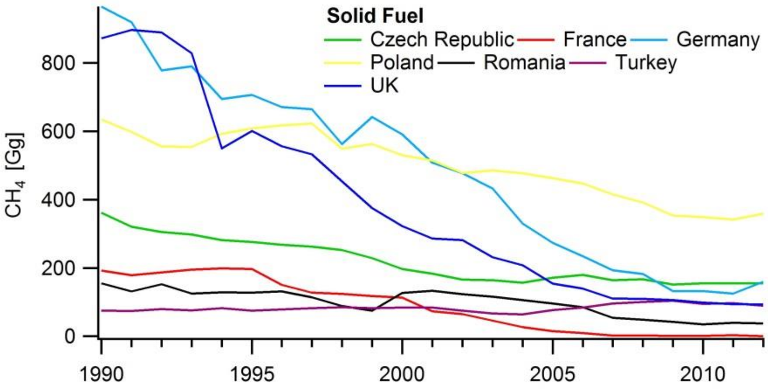

(c)

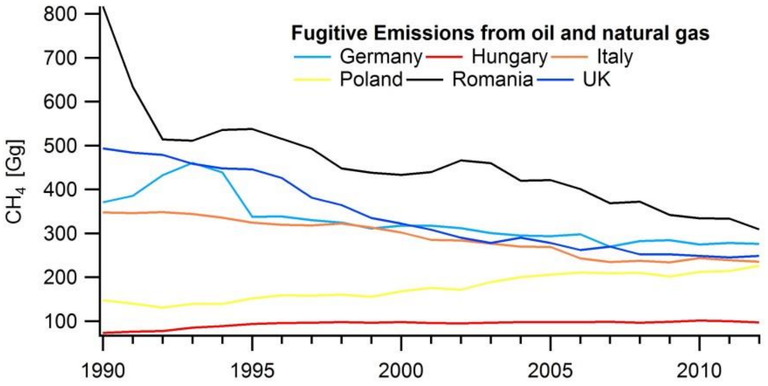

(d)

Figure 3.1 European methane emissions estimates of the most important sources (enteric fermentation-a, solid waste land disposal-b, solid fuel-c and fugitive emissions from oil and natural gas-d) from 1990 to 2012. Source: http://www.eea.europa.eu/data-and-maps

The waste treatment in the UK, Turkey, Germany and Italy still relies mostly on waste disposal in landfill sites, but a better management of landfills, especially in the UK and Germany, contributed to a significant abatement of emissions. Methane emissions from the solid fuel sector, including those from the coal exploitation, also sharply decrease in countries like Germany, Poland and UK. In the UK lower emissions are primarily the result of liberalising energy markets and the subsequent fuel switch from oil and coal to gas in electricity production (EEA, 2014). The change in coal industry in Russia and Eastern European coal producing countries during the 1990s, when the energy industry was restructured and many of the gassiest underground mines were closed, greatly slowed the coal production. Romania, UK, Germany and Italy contributed the most to methane emissions from the oil and natural gas sector throughout this period, through fugitive emissions from both exploitation activities and distribution system.

Methane emissions from enteric fermentation are persistently high in France, Germany, UK and Turkey.

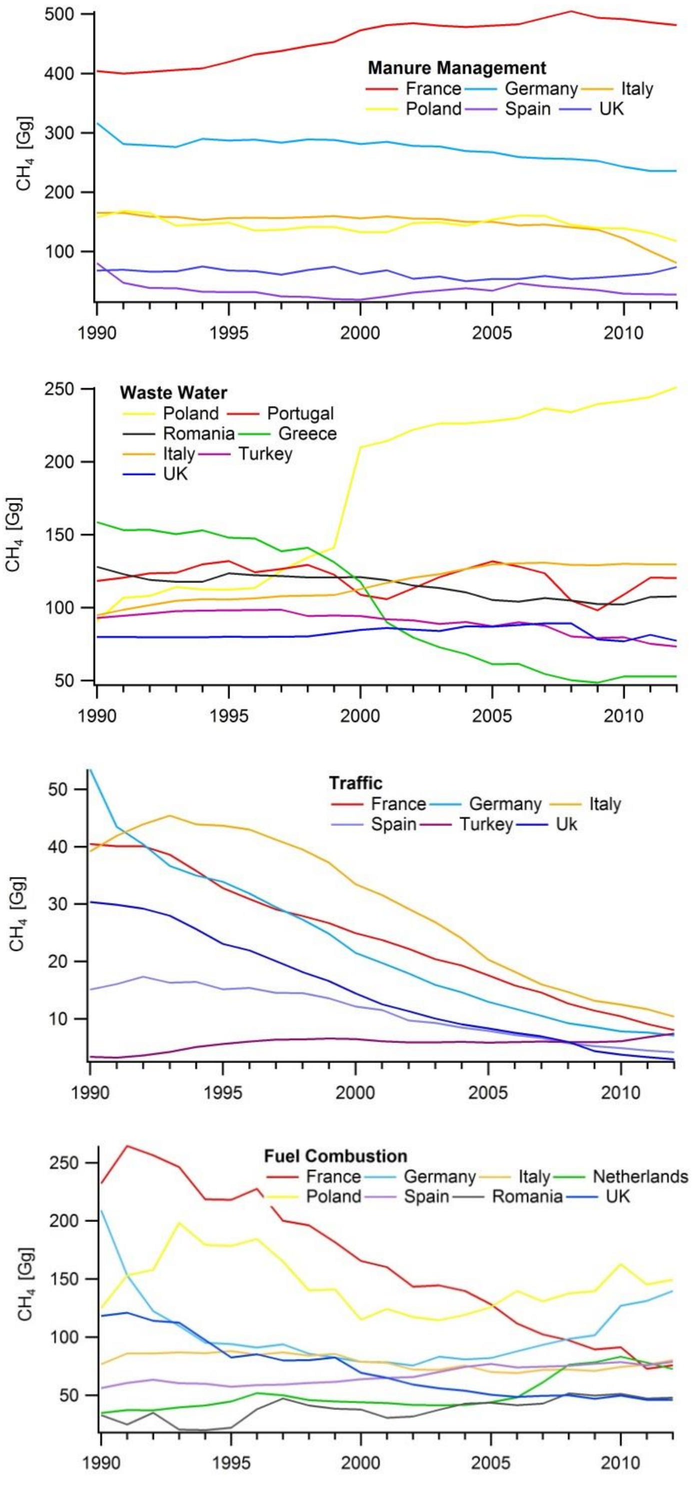

Figure 3.2 European methane emissions estimate of sources emitting less than 500 Gg from 1990 to 2012. Source: http://www.eea.europa.eu/data-and-maps

Changes in the agricultural management of organic manures partially explain the reduction in methane emissions from the agricultural sector, even though countries such as France and the UK did not significantly mitigate emissions. Methane emissions from wastewater treatment do not decrease across the time series and are conversely augmented in countries such as Poland and Italy. The improvement in energy efficiency as well as the decrease in primary energy intensity might explain the reduction of methane emissions from fuel combustion in France and the UK, but after 2000, countries such as Germany, Poland, and Italy show a positive trend, following an increasingly higher energy demand. Although total emissions from road transportation increased steadily between 1990 and 2007 and then decreased until 2012 (eea.europa.eu), methane emissions constantly declined thanks to the introduction of better engines across Europe.

3.3 National Atmospheric Emissions Inventories (NAEI)

Official methane inventories for the UK can be found in the National Atmospheric Emission Inventories (NAEI) website. An overall decline of methane emissions throughout the 1990-2012 period has been estimated for the main sectors.

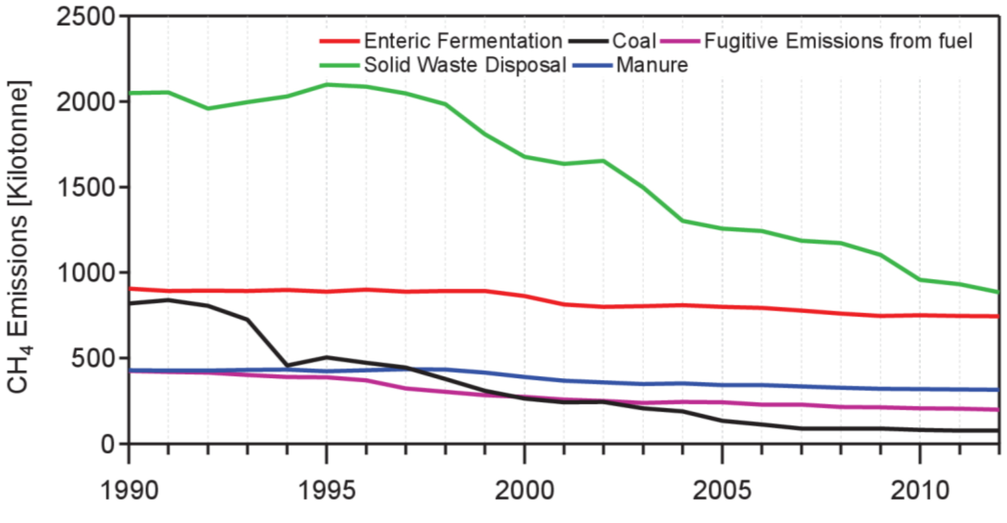

Figure 3.3 UK methane emissions trends of the most important methane sources from 1990 to 2012. Source: NAEI website.

Reduction in emissions from solid waste disposal, which is estimated to be the most important methane source sector, drove the overall reduction in the UK methane budget. The emissions decline is ascribed to stricter regulations in waste management and landfill gas recovery, which has become a common practice in the UK. Also the coal-mining sector contributed significantly to the decrease in the national methane emissions trend across the time series. Figure 3.3 highlights the collapse of methane emissions within the coal mining sector after 1993. The coal industry has been progressively impaired by the closure of most of the coal pits.

Enteric fermentation remains over the years the second most important methane source, accounting for 44% of total methane emissions in 2012, and it has undergone a small decrease only after the Foot-and-Mouth outbreak and massive cull of 2000. Inventories provide a parallel figure for emissions from manure management, which represents the third leading methane source in the UK.

Fugitive emissions from oil and natural gas activities have also declined since 1990, thanks to improved maintenance of the gas network, including the replacement of old metal pipes with plastic ones.

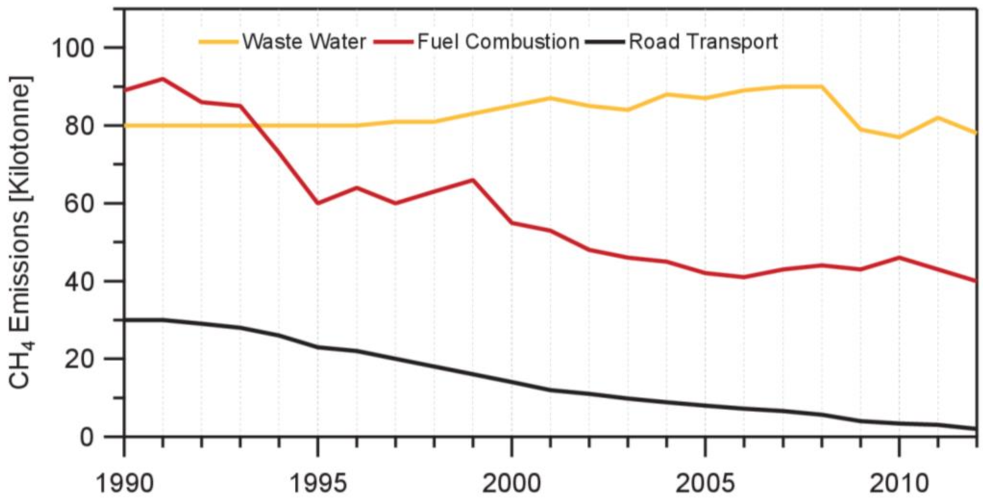

Figure 3.4 UK methane emissions trend for methane sources emitting less than 100 Kilotonnes per year, from 1990 to 2012.

Figure 3.4 shows UK methane emissions trends for minor methane sources. Unlike all the other sectors, the wastewater treatment (including domestic and industrial wastewater) has not undergone a significant reduction in methane emissions, as the improvement in the treatment process is compensated by the extension of sewage works and the intense organic load in wastewater due to the population growth. Conversely, methane emissions derived from fuel combustion have been cut off following a better quality of combustion technologies and operating conditions. The more effective combustion of newer engines and the introduction of catalytic converters in the UK in the early 1990s explain the decrease in methane emissions within the road transport sector.

3.4 Spatial Resolution of UK Methane Inventories

The National Atmospheric Emissions Inventory (NAEI) website makes available mapping datasets with estimates of the distribution of methane emissions at 1x1 km resolution for each UNECE sector (Table 3.1) and it is updated annually with some time delay.

UNECE sector code	Description
1	Combustion in energy production and transfer
2	Combustion in commercial, institutions, residential and agricultural sector
3	Combustion in industry
4	Production processes
5	Extraction/Distribution of fossil fuels
6	Solvent use
7	Road transport
8	Other transport and machinery
9	Waste treatment and disposal
10	Agricultural, forests and land use change
11	Other sources and sinks

Table 3.1 UNECE emissions sectors classification. The Agricultural sector comprises enteric fermentation together with the manure management.

Emission maps compiled within a GIS environment can be directly downloaded from the NAEI website. Figure 3.5 shows the 2012 methane map.

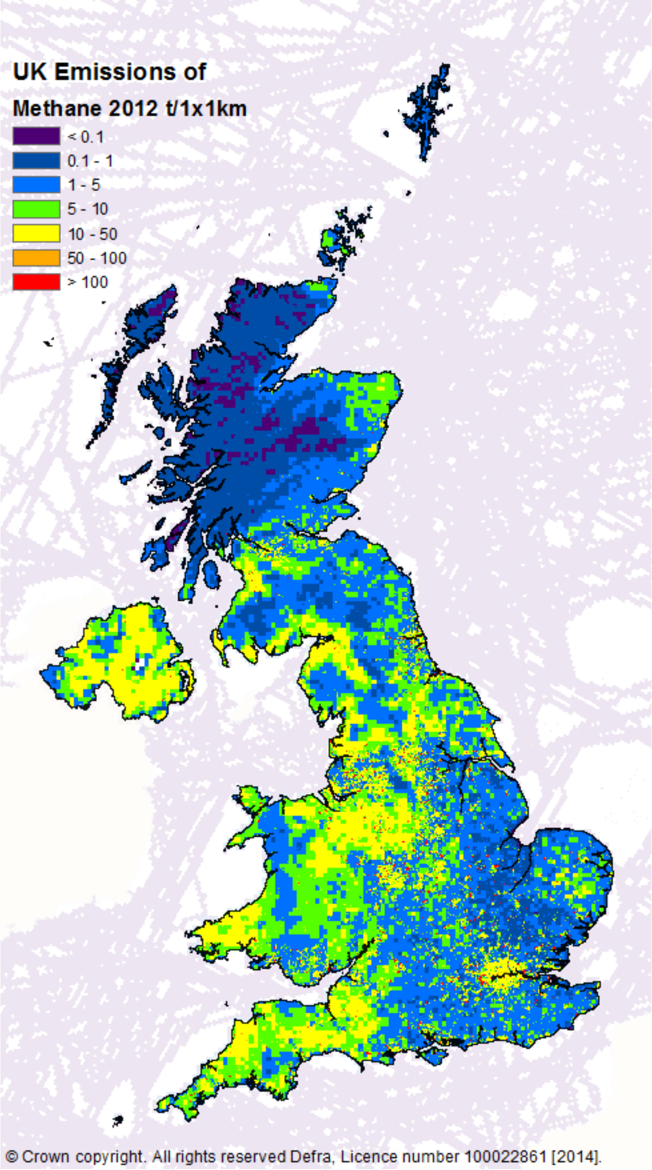

© Crown copyright. All rights reserved Defra, Licence number 100022861 [2014].

Figure 3.5 2012 UK methane land emissions inventory map. Source: NAEI website.

Using the 1 km^2 mapping dataset, customised maps can be built. Methane emissions for SE of England were mapped with the ArcMap software using 2009 and 2012 inventories (Figure 3.6). 2009 emission estimates were revised following the assessment of new emission factors, amendments in the estimation methodology and in the data quality. These developments led to a very different map of methane emissions for 2012, where methane hotspots (red squares) do not have the 5x5 km^2 resolution characterising the 2009 emission map, but are distributed on a more disaggregated spatial grid. Inventory uncertainties and spatial distribution are explained in Chapter 3.5 and 3.6.

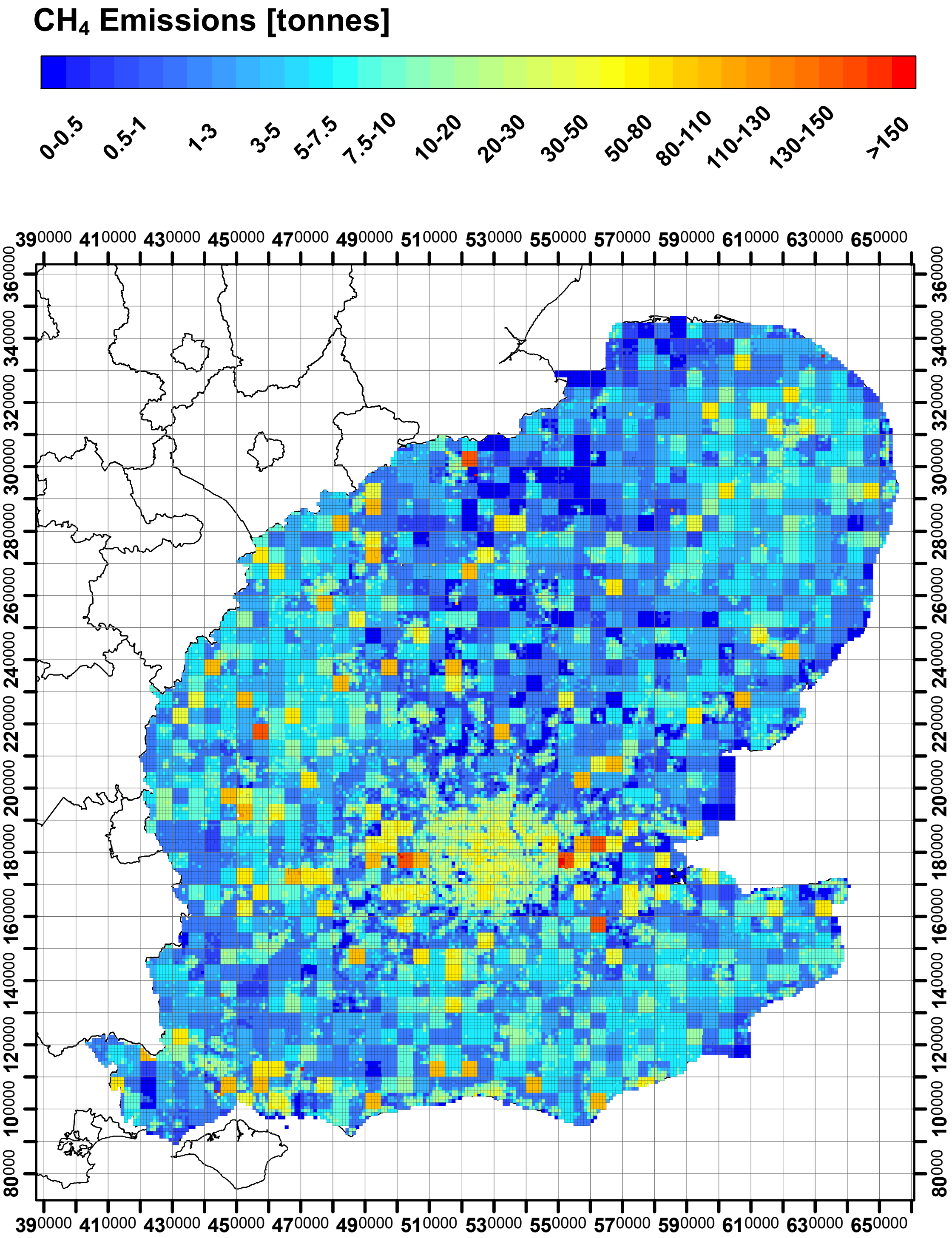
CH$_4$ Emissions [tonnes]
0-0.5
0.5-1
1-3
3-5
5-7.5
7.5-10
10-20
20-30
30-50
50-80
80-110
110-130
130-150
>150
390000
410000
430000
450000
470000
490000
510000
530000
550000
570000
590000
610000
630000
650000
80000
100000
120000
140000
160000
180000
200000
220000
240000
260000
280000
300000
320000
340000
360000

(a)

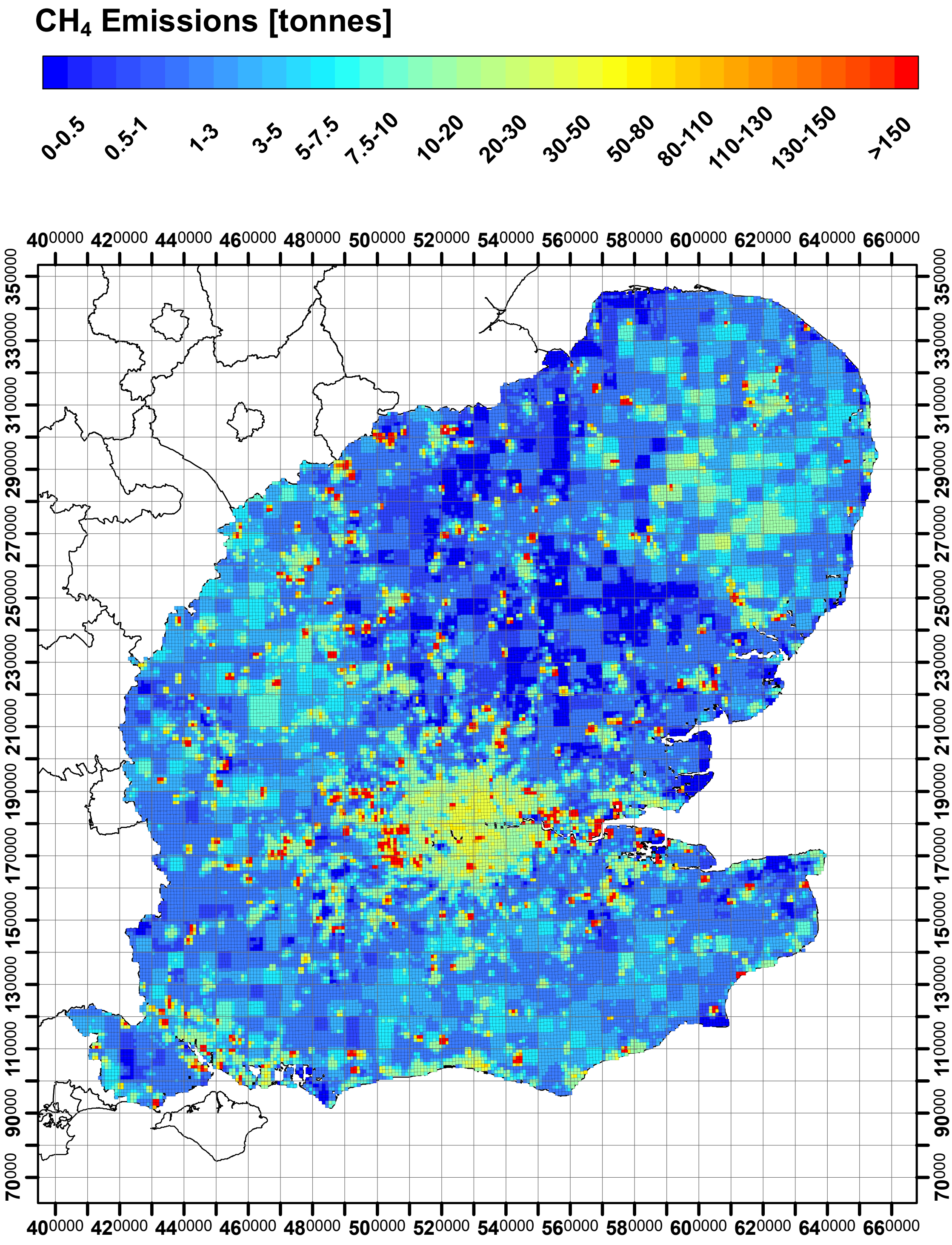

(b)

Figure 3.6 Emission map of SE England for 2009 (a) and 2012 (b) made by 1 Km^2 methane emissions data from NAEI website. The grid coordinates are displayed in the British National Coordinate System.

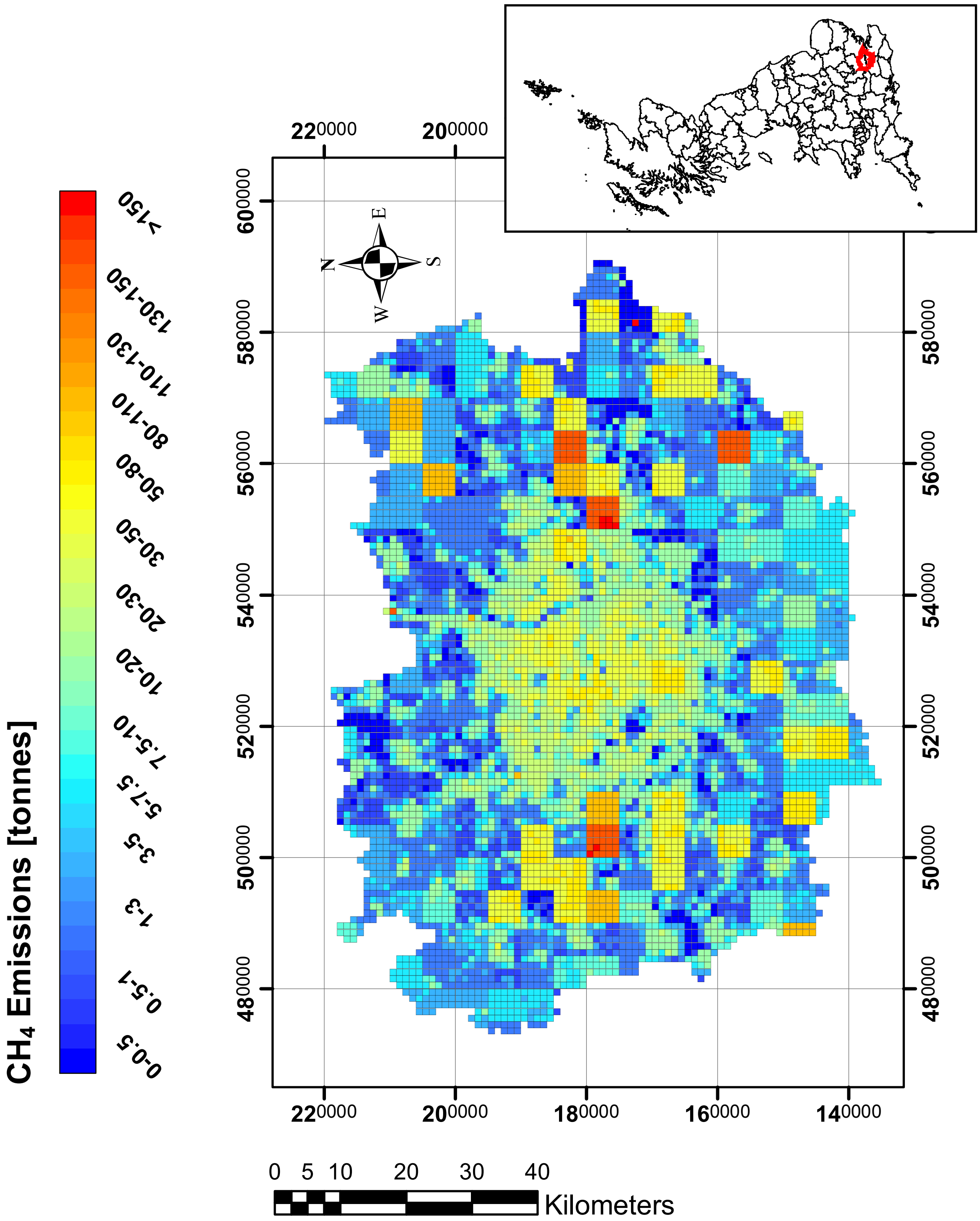

Figure 3.7 London Region emission map made by 1km^2 methane emission inventories for 2009.

A focus on 2009 emission inventories for the London Region (Figure 3.7) highlights the 5x5 km^2 emission areas, sited mainly outside and on the margins of the London conurbation, and all corresponding to landfill sites. With more than 8 million inhabitants, the London region represents approximately 6 % of total methane emissions in the UK.

As methane hotspots are spatially defined, the emission maps based on 2009 inventories, the only ones available when this project started, were used to focus measurement campaigns in order to verify the location of emitting areas (see Chapter 4). An independent verification through atmospheric measurements is strongly recommended because of the intrinsic uncertainty of the inventories provided by NAEI. These are modelled estimates calculated without an error assessment and therefore the level of accuracy of the emissions extent and location is not known. Emissions data are mostly developed using a bottom-up approach, as suggested by the IPCC Guidelines (see Chapter 3.1), aggregating local activity statistics (e.g. number of cows, volume of gas used, etc.) multiplied by an appropriate emission factor. Emission factors are generally defined by previous measurements carried out on a limited number of sources taken as representative of an emission sector, or based upon stoichiometric or empirical relationships between emissions and specific activities (Ioannis Tsagatakis, 2013). Standard emission factors provided by IPCC Guidelines might be uncertain and too unspecific.

High uncertainty may affect also activity values, which depend upon the data availability. Activity statistics are compiled from various official UK regulatory sources, e.g. the Institute of Grassland and Environmental Research (IGER) provides data on livestock numbers, whereas surrogate statistics of varying quality are used when emissions from diffuse emission sources are calculated (Ioannis Tsagatakis, 2013). Indeed, emission sources can be treated as ‘point’ or ‘area’ sources, a distinction that dictates the level of uncertainty, as explained in Chapter 3.7. A point source is characterised by a known location with a grid reference and it can be mapped directly. Its magnitude is estimated using data that are available from local authorities or the Environment Agency (EA). Conversely area sources are widely distributed, and both location and emission estimates are not well characterised. For each sector the method of allocating area sources varies and defines the quality of data.

When point sources are not regulated, emission estimates are generated using 'surrogate' activity data. For instance, individual large sources in the industrial and commercial sector are usually well characterised (point sources), whereas data of sources with small processes or emissions reported below the threshold may be missing and poorly updated, and need to be retrieved making assumptions (i.e. emissions for uncharacterised sites are calculated by assuming that these sites emit at the same rate as other sites whose emissions data are known) (Ioannis Tsagatakis, 2013). All the approaches undertaken to fill the gaps of data bring uncertainty in the emissions assessment.

3.5 Spatial Distribution of Emissions from the Industrial and Commercial, Domestic and Agricultural Sectors

Within the industrial and commercial fuel consumption sector, emissions from point sources (site-specific installations) represent a high percentage of the total. The residual emission, which is the portion of the national total emissions not released by point sources, is considered as an area source. This has to be spatially allocated using distribution maps based on employment statistics. Each distribution map gives the proportion of the UK's residual fuel consumption per sector to be allocated to each 1x1 km (Ioannis Tsagatakis, 2013).

For the spatial distribution of domestic sources, energy statistics and spatially-resolved databases obtained using OS (Ordinance Survey) code points were used to generate the gas spatial distribution for England. The allocation of solid and liquid fuels was based on the position of smoke control areas and the geographic distribution of gas availability.

Emissions from the agricultural sector were distributed using 1x1 km datasets for different livestock types and poultry, generated with data provided by the Department for Environment, Food and Rural Affairs (DEFRA).

3.6 Landfills and Sewage Works Emissions Sector: 5x5 km Resolution

In the calculation of methane emissions from landfills, two different source sectors are considered: landfill gas consumption for electricity generation and/or heating, and emissions from the landfill sites themselves. The first one is considered as a point source, whereas the second one is treated as an area source. When the landfill site locations are not available, population distribution data are taken into account to map the emissions. In this process the composition of landfilled material is assumed to be equal across the UK (Dragosits et al., 2013). Landfill locations and waste type data of different quality and completeness are available. Therefore, due to the inherent uncertainty, methane emissions inventories from NAEI in the waste sector were mapped at 5x5 km resolution for 2009 inventories, as distributing them on a 1 km^2 grid might yield unrealistic hotspots (Ioannis Tsagatakis, 2013). This process explains why some of the high emissions areas highlighted in 2009 emissions maps, which, according to the inventories, correspond to landfill sites and whose locations have been verified with measurement campaigns, do not coincide exactly with the areas where high methane emissions were actually detected.

Locations and magnitude of UK methane emissions from sewage works are estimated from data provided by the Environment Agency. EA sewage works records include only works larger than 10,000 population equivalents[6], and the rest of the population is assumed to be covered by small sewage works (Dragosits et al., 2013). Following this procedure, the methane emissions estimate may be highly uncertain. Furthermore, not all sewage works are registered and the spatial distribution of sources such as septic tanks in rural areas and land spreading of sewage sludge are difficult to define. Due to the high uncertainty of 2009 data, methane emissions from wastewater treatment have been distributed on a 5x5

---

[6] **Population equivalent** (**PE**) in waste-water treatment is the number expressing the ratio of the sum of the pollution load produced during 24 hours by industrial facilities and services to the individual pollution load in household sewage produced by one person in the same time.

km^2 scale. Subsequent upgrades of inventories resulted in a better resolution for 2012 emission maps.

3.7 Quality of NAEI Maps: Uncertainty on Methane Emissions

As explained in the NAEI website, the overall quality of NAEI emission maps for some of the major pollutants has been evaluated following two approaches: 1) considering the proportion of point and area sources of the pollutant; 2) allocating a quality rating to the emissions for each sector based upon the reliability of source data.

According to both these approaches the methane emission map turned out as the most uncertain (Ioannis Tsagatakis, 2013), since emissions are mostly produced from area sources that, as is mentioned in Chapter 3.4, are poorly characterised and thus difficult to allocate to a spatially resolved grid. Furthermore, methane data from landfills and sewage works are available at 5x5 km resolution and producing 1x1 km maps implies a loss in data quality. Methane emissions can be also very dispersed through small leaks in the natural gas network that cannot be accounted for, as they cannot be easily detected and quantified: location of big leaks changes with time as they are fixed and new leaks occur elsewhere.

Overall the distribution of methane emissions is affected by high uncertainty and ground measurements provide a way of verifying their consistency.

4

METHODOLOGY

4.1 Isotopic Analysis as a Way to link Methane Emissions to Specific Sources

As methane sources are isotopically distinct, as explained in Chapter 2, by measuring the isotopic composition of air samples, the actual source of methane emissions in the area surveyed can be identified. If ^{13}C signatures are accurately defined, methane hotspots listed in national inventories can be linked to specific identifiable sources and the actual contribution of each methane source to the atmospheric methane budget constrained.

Several studies attest the value of the isotopic analysis as a tool for categorising methane sources and in verifying inventories (Levin et al., 1999; Lowry et al., 2001; Fisher et al., 2006; Townsend-Small et al., 2012) and, for this purpose, ^{13}C signatures of the methane sources that are listed in the UK inventories need to be defined accurately. However, while there have been many previous studies of ^{13}C in methane, most are based on small scale processes and few have been on UK sources (Stahl, 1977; Deines, 1980; Chung et al., 1988; Hitchman et al., 1990; Bergamaschi et al., 1998; Levin et al., 1999; Whiticar, 1999). Lowry at al. (2001) studied isotopic characterisation of specific methane peaks measured during diurnal air campaigns at the Royal Holloway site, showing that peaks are derived either from natural gas leaks (δ^{13}C -33 ‰ to -35 ‰) or waste treatment emissions (δ^{13}C -51 ‰ to -53 ‰). Nevertheless, the isotopic characteristics of sources may vary over time and season, such as for landfill sites, and isotopic values need to be regularly reassessed.

A large portion of the details given in this chapter and selected highlights of the following chapter have been published in the paper attached at the end of this thesis.

4.2 Analytical Methodology: Measurements at RHUL (Royal Holloway University of London) Atmospheric Laboratory

4.2.1 Methane Concentration Measurements

CH_4 concentrations are measured using a Picarro G1301 CRDS (Cavity Ring-Down Spectroscopy) analyser, which provides CH_4 and CO_2 mole fractions in ppm and water content in %. CRDS is based upon the principles of direct absorption techniques, following the Lambert-Beer law, according to which the intensity of the light transmitted through a sample decays exponentially as a function of the absorption coefficient and path length through the sample. CRDS has a higher sensitivity than conventional direct absorption techniques, since it measures the rate of absorption rather than the absolute magnitude of the absorption of the light transmitted into an optical cavity (Engeln et al., 1998). The cavity inside the instrument, the so called “ring-down cavity” consists of two mirrors, which reflect back and forth a laser pulse. The light intensity decays as it bounces off the mirror, which reflects slightly less than 100 % of the light. The amount of the light intensity leaking through one of the mirrors is measured with respect to time by a photo-detector (http://www.picarro.com). Therefore, the exponential decay of light intensity along the “cavity ring-down” time is proportional to all the losses inside the cavity. If a sample is inserted into the cavity, the light loss will be larger, leading to a shorter ring-down time. The instrument determines continuously the ring down time of the cavity with and without absorption due to the gas species. As the rate of absorption is calculated by measuring the cavity ring-down time rather than the light intensity, the sensitivity is independent from the light source power, which might fluctuate and reduce the accuracy of the measurement. In order to further increase the sensitivity, multi-pass geometries have been developed to increase the absorption path length. In Picarro instruments the path length within the cavity can reach many kilometres, allowing mole fractions the size of ppb or less to be detected. The Picarro instruments used in the atmospheric laboratory at RHUL are calibrated against National Oceanic and Atmospheric Administration

(NOAA) reference gases and the precision achieved for CH_4 is better than 1 ppb at mole fractions ranging from 1850 to 5000 ppb.

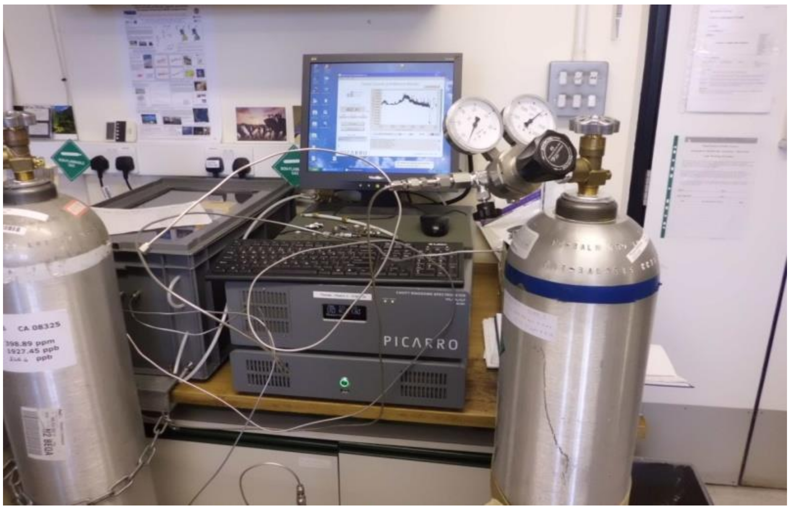

Figure 4.1 Image of the G1301 Picarro CRDS (Cavity Ring-Down Spectroscopy) analyser.

4.2.2 Isotopic Measurements: Trace Gas Instrumentation

The CH_4 isotopic ratio is measured using a Trace Gas preconcentrator coupled with an IsoPrime mass spectrometer. Figure 4.2 shows schematic of the Trace Gas in the CH_4 analysis set-up.

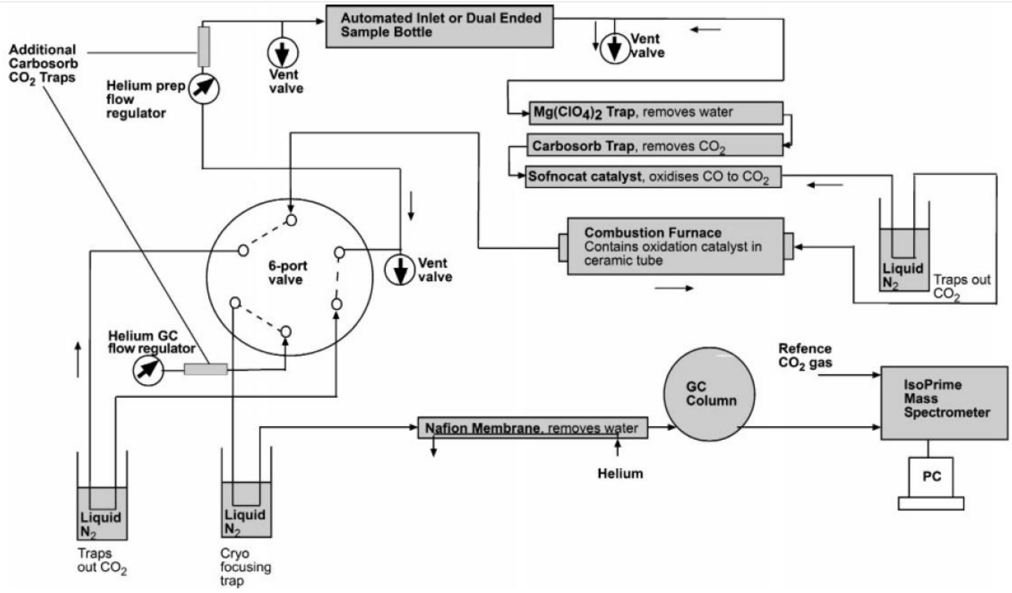

Figure 4.2 Schematic of the Trace Gas in the CH_4 analysis set-up. Black arrows indicate direction of flow of helium and the air sample during CH_4 analysis. Grey arrows show the default helium flow between analyses (Fisher et al., 2006).

The air sample is transported by a 20 mL/min flow of helium. Water and CO_2 are removed through magnesium perchlorate and Carbosorb chemical traps in the Trace Gas. CO is oxidised into CO_2 using a Sofnocat catalyst and the resulting CO_2 is then cryogenically-separated in a liquid nitrogen cryotrap held at -196°C. The Trace Gas consists also of a furnace, where the CH_4 is oxidised into CO_2. The resultant CO_2 is then trapped and cryofocused in the liquid nitrogen and separated from any residual gas components in the sample by a 25m PoraPLOT Q GC column (0.32mm i.d.). The CO_2 is then carried through to the IsoPrime mass spectrometer at a flow rate of 0.3 mL/min, to measure the isotopic molecular species in the gas sample. There the carbon dioxide molecules are ionised and focused into an ion beam, which is deflected by a magnetic field according to the mass of each ion. Ions beams (three for CO_2, mass 44, 45, 46) are then collimated through three different resolving slits, where an electrical current, which is proportional to the total number of ions, is measured. The ratios of the currents are then calculated and compared to the reference gas, giving the $\delta^{13}C$ value for the measured sample. A CO_2 gas cylinder (BOC CP grade) is used as reference for the isotopic measurements.

The average precision achieved for CH_4 isotopes measurements is 0.05 ‰ in triplicate analysis. This level of precision has been obtained by Fisher et al. (2006), who tested several catalysts at specific temperatures and flow rates to enhance the efficiency of the oxidation step in the furnace, which is one of the major variables affecting precision. Palladised quartz wool has been found to be the most efficient catalyst tested and peak heights to reach a maximum and stabilise with optimum precision at 790 °C. An automatic inlet has also been developed in order to reduce the contamination of the sample with laboratory air and to systematise the pump time, the fill time and the time between analyses, and thus to further improve measurement precision.

In this study the continuous flow isotope-ratio mass spectrometry (CF-IRMS) technique, has been employed in the analysis of the ^{13}C signature of air with CH_4 and CO_2 mole fractions higher than background, collected in 3L and 5L Tedlar bags during sampling campaigns. Atmospheric methane samples with mole fractions up to 9 ppm can be measured without a dilution step. For air samples exceeding these mole fraction levels, such as samples from landfill boreholes or from the gas tap of the laboratory at RHUL, dilution was carried out. One-litre Tedlar bags were filled with part of the high concentration sample and nitrogen, diluting the original sample at mole fraction levels between 2 and 5 ppm, the most suitable range for isotopic analyses on the Trace Gras.

A secondary standard tank is measured regularly to check whether there is a drift in the isotopic composition measured over the time of analysis. Each analysis of 75 cc of air takes approximately 20 minutes, making the instrumentation highly advantageous compared to conventional off-line methods (e.g. (Lowe et al., 1994)), which may require tens to hundreds of litres of air and need much longer time for the analyses. Furthermore, the isotopic precision obtained is significantly better than the one achieved with current laser-based isotopic measurement system, such as the CRDS analyser, which is within 1 ‰ for $\delta^{13}C$ of CH_4 (Phillips et al., 2013).

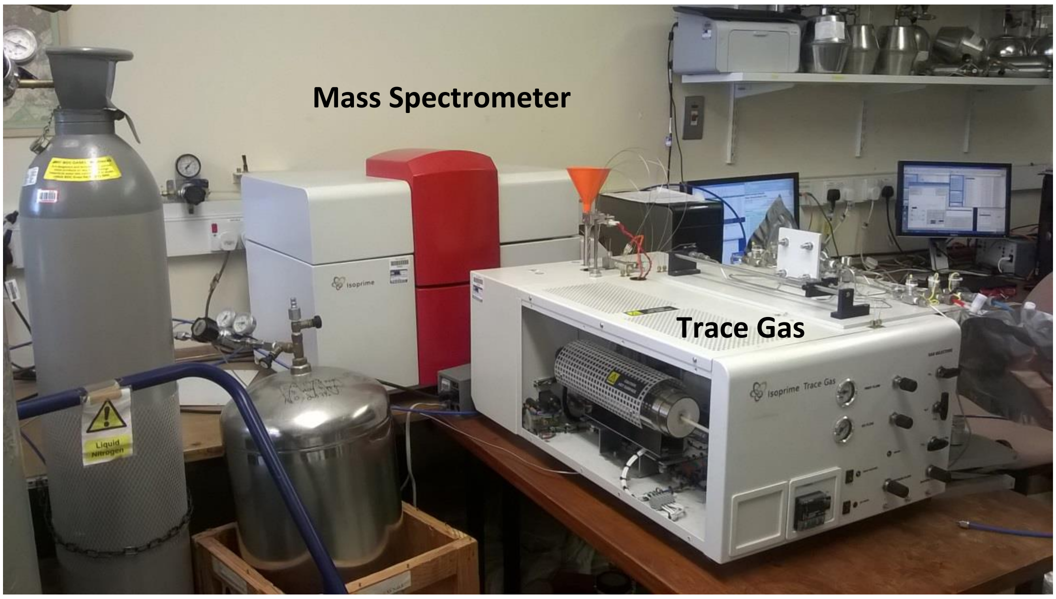

Figure 4.3 Trace Gas preconcentrator coupled and IsoPrime mass spectrometer.

Raw data are calibrated against the secondary standard with an estimated isotopic value of -47.43 ‰. More in detail, for each batch report of analyses, each measured value is corrected by the difference between the value of -47.43 ‰ and the mean isotopic value of the secondary standard measured regularly each day, to take into account the drift in $\delta^{13}C$ of CH_4 of the secondary standard over the time of analysis (≈ 0.05 ‰). Raw data are offset by approximately 0.4 ‰, which Fisher et al. (2006) attributed to the mass spectrometer scaling effect.

4.3 The Keeling Plot Analysis and the Error Estimate

The signature of each methane source (or mixture of sources in a conurbation) is characterised using the Keeling plot method (Keeling, 1958). According to this approach, $\delta^{13}C$ values must be plotted against the inverse of mole fraction data to calculate the isotopic signature of the methane source responsible for the excess over background. Following the Keeling plot procedure, one isotopic signature (with calculated error to allow for some variability of source methane production pathways) is assigned to every methane source explored. Most of the Keeling plots included in this thesis do not display error bars, as they are smaller than displayed symbols.

The Keeling plot method is based on the principle of conservation of mass, so that the atmospheric mixing ratio (mole fraction) of a gas ($\mathbf{c_a}$) in the lower boundary layer results from the combination of the background atmospheric mole fraction ($\mathbf{c_b}$) and the mole fraction of the gas added by the source ($\mathbf{c_s}$) (Pataki et al., 2003):

$$\boldsymbol{c_a = c_b + c_s} \tag{4.1}$$

By assuming the conservation of mass, the following equation is obtained:

$$\delta^{13}C_a\boldsymbol{c_a} = \delta^{13}C_b\boldsymbol{c_b} + \delta^{13}C_s\boldsymbol{c_s}. \tag{4.2}$$

Combining the two previous equations the $\delta^{13}C$ signature of the source input to atmosphere can be calculated as follows:

$$\delta^{13}C_a = \boldsymbol{c_b}\,(\delta^{13}C_b - \delta^{13}C_s)\cdot 1/\boldsymbol{c_a} + \delta^{13}C_s \tag{4.3}$$

$\delta^{13}C_a$ and $1/\mathbf{c_a}$ values are respectively the y and the x values of a best-fit line, whose intercept (at $1/\mathbf{c_a} = 0$) is the isotopic value at which the methane mole fraction tends to infinity. This is interpreted as the isotope signature of the methane source responsible for the excess over background. A linear regression of data must be performed in order to compute the best-fit line slope and intercept.

The lowest mole fraction recorded in a particular setting or time period is usually chosen as background value. In diurnal studies the background value is represented by the daily lowest mole fraction, whereas for source studies the background sample is carefully collected upwind of the studied methane source. The choice of the background plays a key role when there are two or more sources that contribute simultaneously to the methane emissions levels. In this case, if different Keeling plots, each one corresponding to one source, are drawn, then they will include the same background value, whose assessment will constrain the source signatures calculation. In case of one source, the regression technique will allow constraint of the best interpolation line through all the points, and the background value will have the same relevance of each other value.

The estimate of the line parameters might be biased if an ordinary least squared (OLS) method is applied (as in many spreadsheets), which assumes errors are confined to the dependent variable (Leng et al., 2007). For our sources, both variables are measured with errors and another regression model must be implemented. Moreover, our measurements are affected by heteroscedasticity, where the error of a variable changes across the range of values of a second variable that predicts it (Berry and Feldman, 1985). Errors may increase as the value of the independent variable ($1/[CH_4]$) is decreasing, as higher mole fractions are measured with higher standard deviations. Although there are several fitting models that allow for errors in the independent variable (Sokal and Rohlf, 1995), e.g. orthogonal distance regression and geometric mean regression (recommended by Pataki (2003)), few models accommodate for heteroscedastic measurement errors. If a typical OLS approach, intended to minimize $\sum e_i^2$, is applied in case of heteroscedasticity, the calculation of the regression line would give greater emphasis to the extreme values (with greater errors), which are conversely less precise and, hence, contain less information.

Akritas et al. (1996) introduced the BCES estimators procedure (for Bivariate Correlated Errors and intrinsic Scatter). This statistical procedure, designed to overcome the heteroscedasticity case, accounts for correlated errors between the two variables and allows for the magnitude of measurement errors to be dependent on the measurements. These features make the BCES approach well suited for computing the slope and the intercept of the Keeling plot. Therefore the BCES regression program, available to download (http://www.astro.wisc.edu/~mab/archive/stats/stats.html), has been used to find the Keeling plot intercept with the relative uncertainty, and so the δ^{13}C value of the methane source. This technique results in a much more robust calculation of source signature, but will only give very tightly constrained ‰ errors when the precision of both mole fraction and isotopic measurements are very high and the δ^{13}C of the source signature is homogenous across the plume (i.e. single source).

4.4 Sampling Campaigns around Anthropogenic Methane Sources with the Picarro Mobile Analyser

Methane emissions can be measured directly by accessing the source – e.g. landfill gas wells, gas pipe or vehicle exhaust -, but often they are only partially representative of the overall release into the atmosphere from the source area. Therefore, the isotopic composition of methane sources from a 100 m to km-scale spatial area, such as landfills and open-cut coal mines, needs to be evaluated by assessing integrated emissions from the whole site of interest, through measurements of methane mole fractions downwind and upwind of that site. The methane isotopic analysis of air samples collected downwind across the source plume allows assignment of a specific δ^{13}C signature to the source in question.

Each source investigation required a dedicated sampling campaign. By utilising a mobile gas analyser, various potential source sites could be investigated on the same day, measuring methane plumes and spikes while driving on public roads around the target area, and collecting samples whenever mole fractions were relatively high. Subsequent isotopic analysis of the air sampled revealed the origin of methane plumes of local origin. This method was particularly valuable in urban areas with multiple methane sources, where gas leaks can occur in the vicinity of sewage works and landfill sites, since it allowed different sources to be carefully distinguished.

4.4.1 Picarro Mobile System and Sample Collection

The greenhouse gas monitoring system utilised in the survey of the major UK methane sources – i.e. landfill sites, coal mines, sewage works and gas leaks - consists of a mobile Picarro G2301 CRDS (Cavity Ring-Down Spectroscopy) analyser, which provides carbon dioxide and methane mole fractions in ppm, and water vapour in % (see Chapter 4.2.1 for the instrument principles). The mobile module (A0941) consists of a pump, control systems for a Climatronics sonic anemometer and a Hemisphere GPS receiver. Two air inlets, plus the GPS and sonic anemometer are attached to a mast above the roof of a vehicle at 2.2 m above the ground. Three fully charged 12 V, 110 Ah lead-acid batteries allow the instrument to run for up to 9 hours. The airline is ¼” outer diameter and 1.83 m length Nylon tube, with the inlet end blocked and a series of 2mm diameter holes drilled into the first 30 cm to allow ingress of air (air inlet 1 on Figure 4.4a) (Picarro, 2012). This is pumped to the mobile module through a 2 μm Swagelok filter, where the flow splits allowing approximately 300 cc/min to flow through the Picarro and the rest of the air to vent. This greatly reduces the lag time between air entering the inlet and the measurement, allowing successful surveying of small plumes at a vehicle speed of up to 50 km/hr, and large plumes at up to 80 km/hr on first pass. The second air inlet is another ¼” O.D. Nylon tube (air inlet 2 in Figure 4.4a) connected to a battery operated diaphragm pump (KNF Neuberger) used to collect plume and background air samples for later isotopic analysis in the RHUL laboratory. The pump fills a 5L Tedlar air sample bag in 30 seconds.

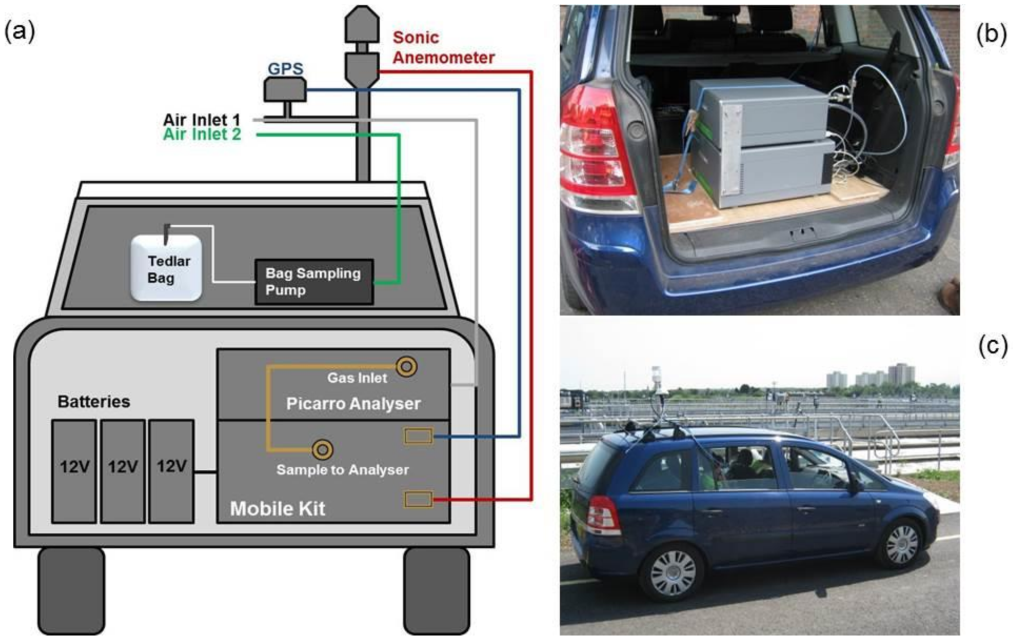

Figure 4.4 a) Schematic set up of the RHUL Picarro mobile measurement system and all the physical connections b) Picarro Mobile c) vehicle used in the sampling campaigns.

The system is controlled by a laptop, so that continuous measurement of CO_2 and CH_4 mole fractions can be observed by the passenger during travel. Communication between the laptop and the Picarro mobile is by WiFi connection to a 3G or 4G system. Both CH_4 and CO_2 mole fractions can be displayed in real time on Google Earth, allowing the gas plumes to be geospatially visualised on site. The time delay between the instantaneous GPS location and the display of Picarro mole fractions has been calculated as approximately 7 seconds by measuring the time lag of the CO_2 peak arrival after blowing into the inlet tube.

The Picarro 2301 instrument was calibrated in the RHUL greenhouse gas laboratory before each survey against two NOAA calibrated air samples, with a resulting precision for CH_4 better than ±0.3 ppb at mole fractions ranging from 1840 to 1975 ppb and accuracies of better than ±1 ppb. A target gas has been analysed using the Picarro instrument while driving in order to test the stability of measurement during motion, with a precision of 0.3 ppb (1 σ) over 2 minutes of analysis.

By driving downwind of the site of interest and by using Google Earth as a platform to visualise mole fractions in real time, the Gaussian shape of plumes was mapped when they were bisected perpendicular to the wind direction. Figure 4.5 demonstrates an example view of data as seen on Google Earth during sampling.

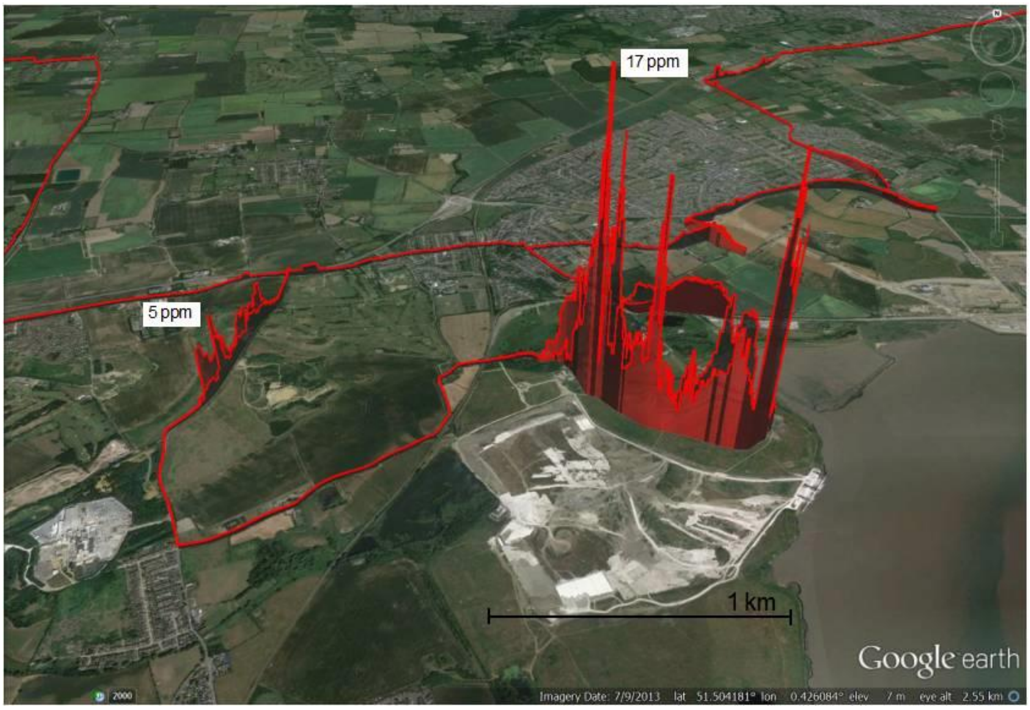

Figure 4.5 Google Earth view of methane plumes detected around Mucking landfill location on 14th October 2013. The maximum mole fractions are labelled for each source plume measured.

Changes in wind direction and speed affect the plume dispersion, and methane peaks might also change position and intensity from one pass to the next downwind of the same methane source. However, the current study was not aimed at calculating fluxes or accurately pinning down the location of small gas leaks, but at proportioning source inputs via the isotopic signatures of the sources. Therefore, a strict accuracy of source position was not required, particularly when surveying large spatial sources such as landfills and open-cut coal mines, where methane plumes can be easily transacted.

Once the methane plume was identified, 5L Tedlar bags were filled as close to the plume centre as possible and at the edges of the plume. When the road traffic conditions allowed, air bags were collected along the plume transect by stopping the vehicle whenever above-background methane mole fractions were observed. When sampling was on a major road and the vehicle could not be stopped, and when the methane mole fraction was not steady during the sampling at a given point (due to a high variability of the wind direction or obstructions between the source and the road), samples were collected while driving, at a speed of approximately 50 km/hr, giving an integrated sample over a distance of up to 400 m.

CH_4 mole fractions of the air samples in Tedlar bags were measured independently in the laboratory at RHUL with the Picarro G1301 CRDS analyser. Each sample was measured for 3 minutes, with an average precision of ±0.5 ppb. The methane isotopic composition of collected samples was measured in triplicate to high precision (±0.05 ‰) using CF GC-IRMS (Trace Gas).

4.4.2 Data Processing

After each measurement campaign a raw file was acquired directly via USB from the instrument, including the following data: CO_2, CH_4 mole fractions in ppm, water content in %, GPS coordinates (latitudinal and longitudinal degrees). Vector wind data (wind direction and speed), even though part of the file, were not processed, as no computational model for plume dispersion, which requires a detailed description of meteorological parameters, was necessary for the isotopic characterisation of the source. The wind direction was estimated independently before each campaign only to verify whether the area downwind of the source site was accessible. The immediate visualisation of mole fractions during the survey itself directed the sample collection. The raw file was converted then into a kml file, and the Google Earth image obtained reproduced the total series of mole fractions measured during the survey. The mole fraction data were re-plotted during post-analysis using ArcMap software, utilising satellite images of the sites as base maps to give a clearer spatial representation of the data and to better display the mole fraction ranges.

4.5 Diurnal Studies

Stable carbon isotopic composition and CH_4 mole fractions of samples collected over a 24 hours period in central London and in Egham were measured to determine the mean $\delta^{13}C\text{-}CH_4$ source signature characterising an urban and a semi-rural environment, and to identify the major methane sources in central London. A detailed description of each diurnal study is in Chapter 6.

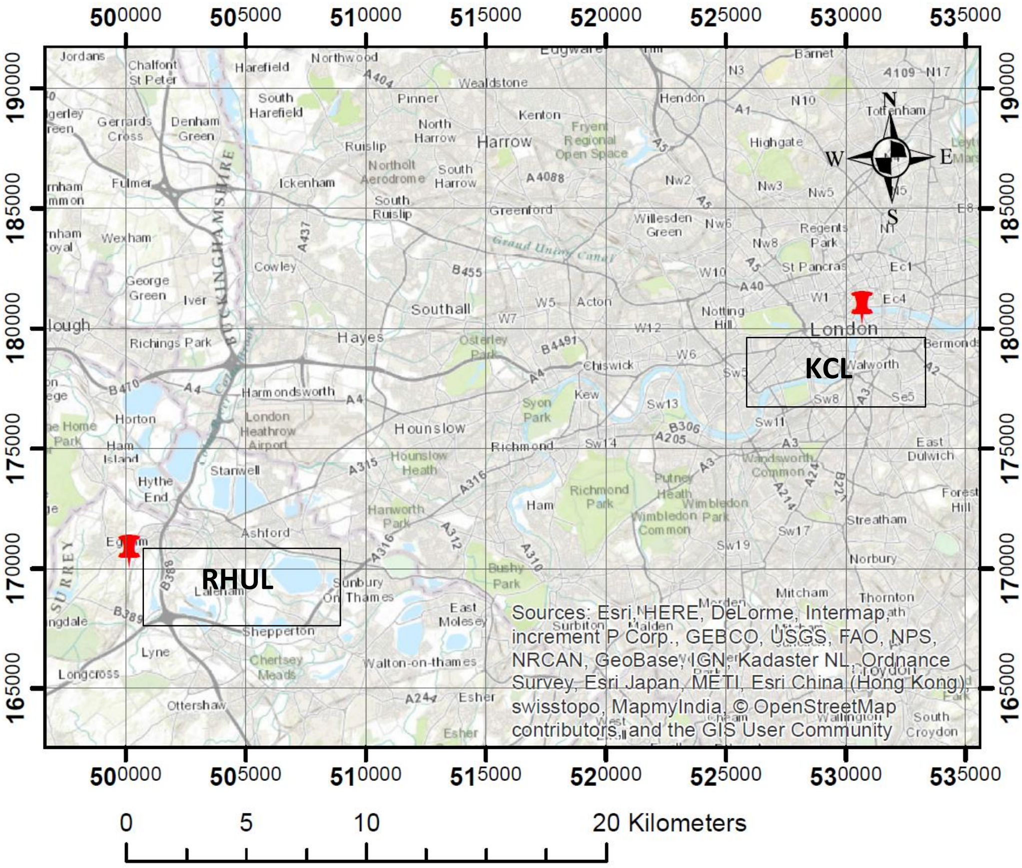

Figure 4.6 Royal Holloway University of London (RHUL) and King's College London (KCL) location.

4.5.1 Diurnal Studies in London: the Development of an Automatic Sampler

The development of an automatic sampler allowed the collection of up to 20 air samples with no requirement for an operator to be present during the sampling. The sampler is controlled by a dedicated program written by Alex Etchells (University of East Anglia), which allows setting of the start time, filling time and interval between samples. Figure 4.7 shows the automatic sampler after one complete sampling session.

Figure 4.7 Automatic sampler after one complete sampling session.

The system has been built on two levels (10 valves on the upper level and 10 on the bottom one) to attach either 20 tanks or bags (Figure 4.8). The inflow of outside air is controlled by a diaphragm pump on the inlet line, connected to the air inlet through a ¼” O.D. nylon tube. Before the valve opening for the collection of each sample, the air is flushed for a fixed time of 20 seconds, and, after the pre-set filling time the valve is immediately closed. Tedlar or Flexfoil bags were found suitable for these studies as they can safely preserve the air collected without leaking during the sampling time, and until collection, and for ease of sample transport. To fill a 3 L bag a filling time of 30 seconds was set. Once the internet connection was established, the whole system could be started remotely and the sampling cycle run with no interruption until the collection of the 20th sample. A time interval between samples of 72 minutes was used in order to cover a 24-hour period. The 20 air samples were picked up the day after and replaced with another 20 empty bags to set up the instrumentation for the next sampling.

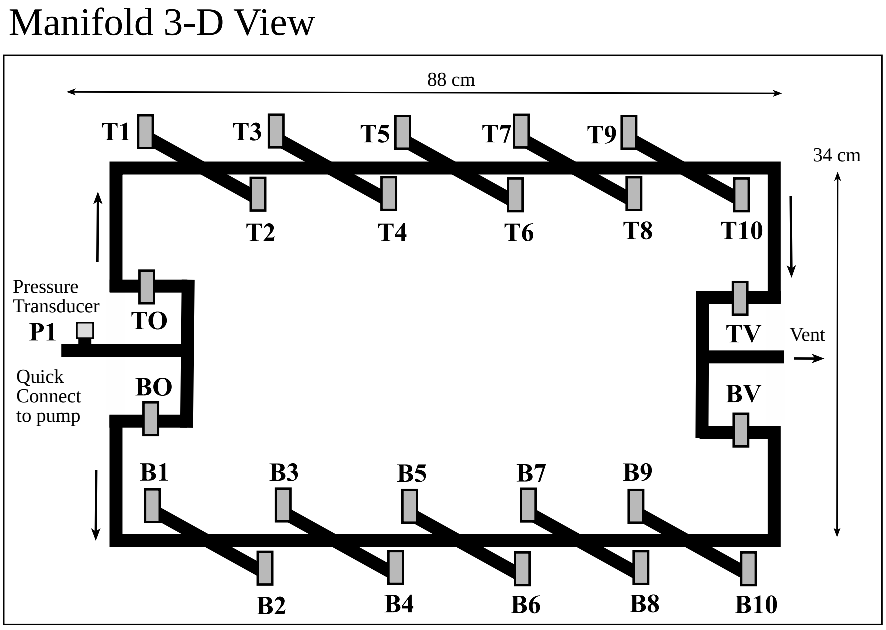

Figure 4.8 Diagram of the automatic sampler. B_i are the bottom valves and T_i the top ones.

In its main use for this project the automatic sampler was connected to an air inlet placed at 7 meters above roof height and 48.6 m above ground level on a triangular tower (Aluma T45-H) installed on the rooftop at the Strand Campus of King's College London (KCL, 51°30′ N, 0°7′ W), approximately 32 km ENE of Egham. The Strand Campus is located in the borough of Westminster, characterised by a dense cover of buildings, except to the south where the River Thames is located, and heavy traffic in all directions.

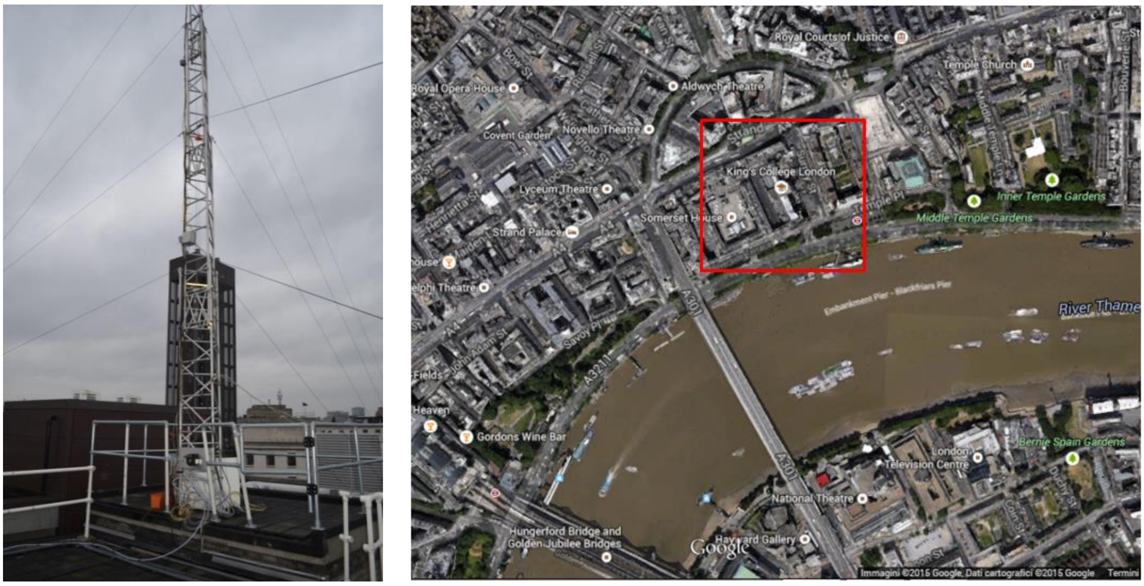

Figure 4.9 Tower on the the rooftop at the Strand Campus of King's College London and Google Earth image of the Strand Campus location (in the middle of the red square) and the city centre.

The Picarro G2301, used for mobile measurements, was detached from the mobile module and connected to the inlet on the tower to measure continuous CH_4 and CO_2 mole fractions from 10th December 2013 to 31st January 2014 and from 24th July to 11th August 2014. Sample mole fractions were measured in the RHUL laboratory by the Picarro G1301 GRDS, thus allowing verification of the consistency between the continuous measurements performed by the Picarro G2301 at King's College and the laboratory measurements of the sampled bags. Isotopic composition of samples was measured using the Trace Gas analyser at RHUL in triplicate to high precision (±0.05 ‰). Meteorological data (wind speed and direction, atmospheric stability) were measured with a weather station (WXT510 model) fitted to the air-sampling tower and provided by the Earth and Environmental Dynamics Group, Department of Geography, King's College London.

The Keeling plot analysis based on mole fractions and isotopic measurements allows determination of the $\delta^{13}C\text{-}CH_4$ source signature of the mixed air in central London. Some Keeling plots used only those values characterising a significant build-up in mole fractions, to identify the emitting methane source. The wind direction recorded in central London, averaged every 30 minutes, gives an indication on the provenance of methane plumes, whereas the wind speed and the stability parameter suggest the dynamic of the boundary layer during the diurnal cycle. The Hybrid Single-Particle Lagrangian Integrated Trajectory model

(HYSPLIT) has been used to compute air trajectories originating at 50 meters above ground in order to assess the provenance of air masses at regional scale (Draxler R.R. and Rolph G.D., 2015; Rolph G.D., 2015).

4.5.2 Diurnal Studies in Egham

The RHUL Earth Science Department (52°25.6’N, 0°33.7’W) is located 32 km WSW of the city of London, at the edge of the Greater London conurbation (Figure 4.6), and it is affected by the London air pollution when easterly winds occur. Air is continuously pumped into the atmospheric laboratory from a sampling intake above the roof, at 15 m above ground height and 45 m above the London basin. CH_4 mole fractions have been measured every 30 minutes since 1995 by GC and CO_2 mole fractions every 5 minutes since 1999 using a LiCor NDIR analyser. Since 2009 measurements of CO_2 and CH_4 have been made using the Picarro G1301 analyser at higher resolution (5 to 10 seconds). Meteorological data (wind direction and speed, pressure, relative humidity and temperature) are recorded by a meteorological station situated on the department roof.

When diurnal studies were planned, the air coming from the roof of the building through ½” O.D. Synflex (Dekoron) tubing was pumped into the Trace Gas for continuous isotopic measurements. Outside air was measured at 20-minute intervals and a standard tank (RHS 662) between every 5 sample measurements. The liquid nitrogen for the cryotrap was refilled approximately every 4 hours. Two diurnal studies of 24 and 48 hours duration respectively were performed in October and December 2012. The intercept of Keeling plots based on values characterising peaks in mole fractions represents the $\delta^{13}C$ source signature of the methane plume, thus revealing its origin.

5

SOURCE STUDIES

This chapter introduces all the surveys carried out in order to identify and isotopically characterise methane plumes from the main UK source categories: landfill sites, coal mines, natural gas, vehicles and ruminants. Each section includes details on samples location, mole fractions levels measured and comparison between the $\delta^{13}C$ source isotopic signatures attributed to the sources investigated and those found in previous studies.

5.1 Landfill $\delta^{13}C$-CH_4 Signatures

Methane emissions from landfills occur and change over a long time frame from the initial waste disposal, and the $\delta^{13}C$ isotopic characterisation of landfill sites vary accordingly. Several studies have investigated isotopic signatures of methane emissions using flux chambers to capture methane fluxes from soil and collect air samples (Liptay et al., 1998; Chanton et al., 2000). In order to ensure that a representative area is covered, many chambers need to be arranged across site, often highlighting the large spatial variability of the $\delta^{13}C$ signature measured and making it difficult to define an overall isotopic value characterising the whole landfill.

The measured isotopic signature of methane might vary depending on whether the top-soil is in place. Bergamaschi et al. (1998) obtained values highly ^{13}C enriched (-45.9 ±8.0 ‰) in covered areas relative to those observed in uncovered areas (-55.1 ±5.2 ‰), showing that methane passing through the topsoil is subjected to oxidation by methanotrophic bacteria (^{12}C is preferentially oxidised increasing the proportion of ^{13}C in the remaining methane). Further variability is associated with the change in the well isotopic composition across the site, which might be related to the waste age. In order to overcome spatial variability and get the isotopic signature of integrated emissions downwind of the landfill, measurement campaigns were carried out using the Picarro mobile system (see Chapter 4), which allowed methane plumes to be directly identified and sampled on transects.

Weather conditions were checked before every survey, specifically wind direction, to verify that the downwind area of the landfill site was accessible, and wind speed, which shapes the plume dispersion. Although surveys were not aimed at calculating fluxes, and therefore no study of plume dispersion, which requires the measurement of the wind speed, was carried out, moderate and constant wind speeds (5-10 km/hr) were sought, as they support sustained methane plumes that can be easily transected using the Picarro mobile system. The barometric pressure also strongly affects methane emissions from landfill sites, which are augmented when the barometric pressure is falling and the landfill gas is transported away from the surface by the air turbulence (Xu et al., 2014). Most of measurement campaigns were carried out in April, July and October, when temperatures were not particularly low and the barometric pressure was not that high to suppress the gas release.

The eight landfill sites that have been surveyed in this study, both still active and recently closed, are all located within 70 km of London, and they are all considered methane hotspots by national inventories, except for Greatness Quarry (see Figure 5.1). The sampling and the isotopic characterization of each landfill site is described in the following chapters.

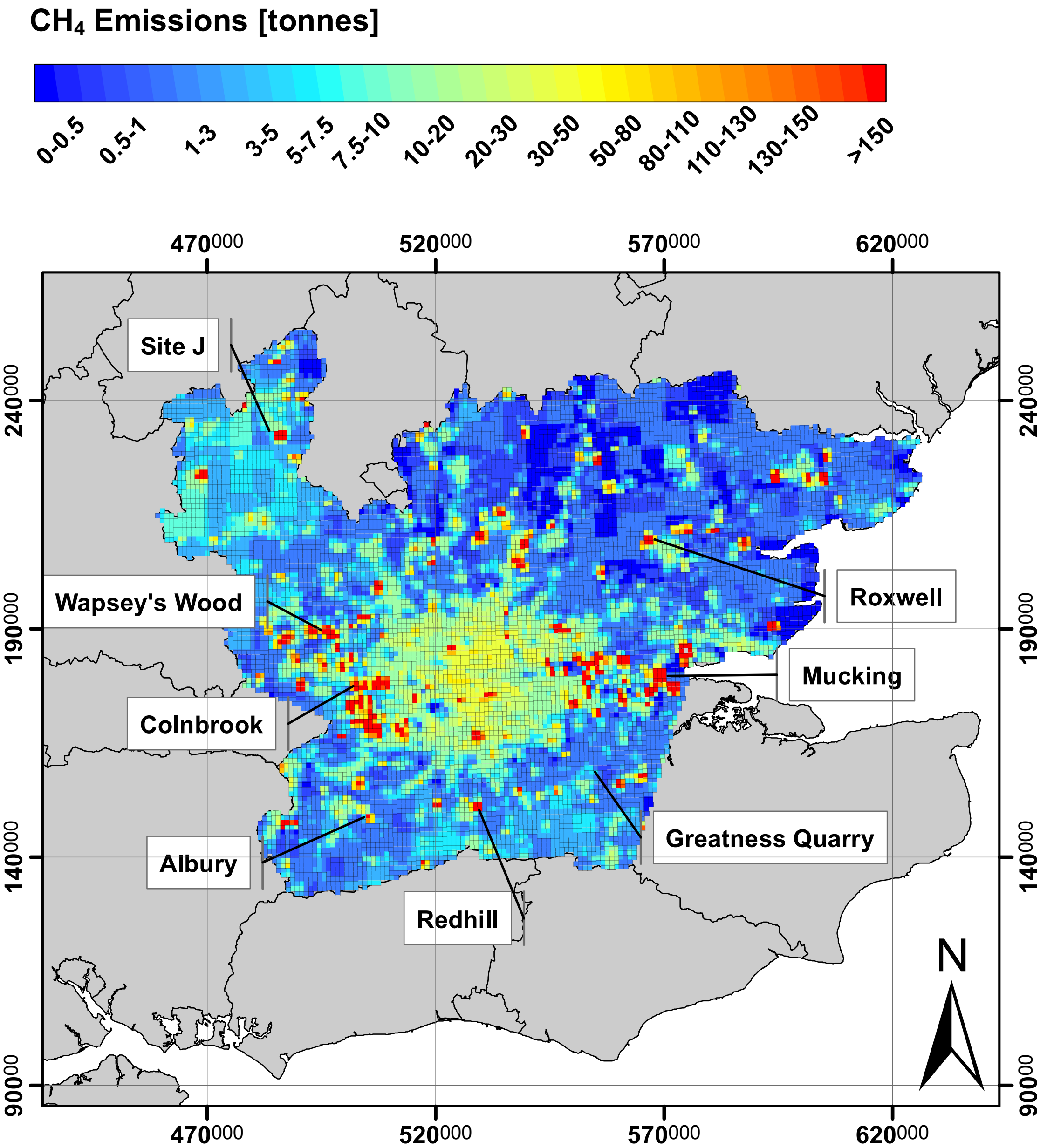

Figure 5.1 2012 emission map of the areas where the surveyed landfill sites are located. The grid coordinates are displays in the British National Coordinate System.

5.1.1 Colnbrook Landfill Site

Colnbrook landfill site is situated in Berkshire, north-east of Heathrow airport, in between the M4 to the north, A4 Colnbrook Bypass to the south and Sutton Lane to the west. The site was closed at the end of 2012, following landscaping works in order to restore the agricultural use of the site. It was active for 26 years, although subjected to complaints arising from the residents living in close proximity of the landfill area. According to the Environmental Agency, the landfill was a major contributor of carbon dioxide, dioxins and nitrogen oxides emissions, whereas methane emissions were not mentioned. In 2010 a landfill gas utilisation plant has become operational, greatly reducing the biogas realise. Nevertheless, during the survey with the Picarro mobile system on 11th July 2013, a methane plume was detected, with a recorded maximum mole fraction of 2.1 ppm.

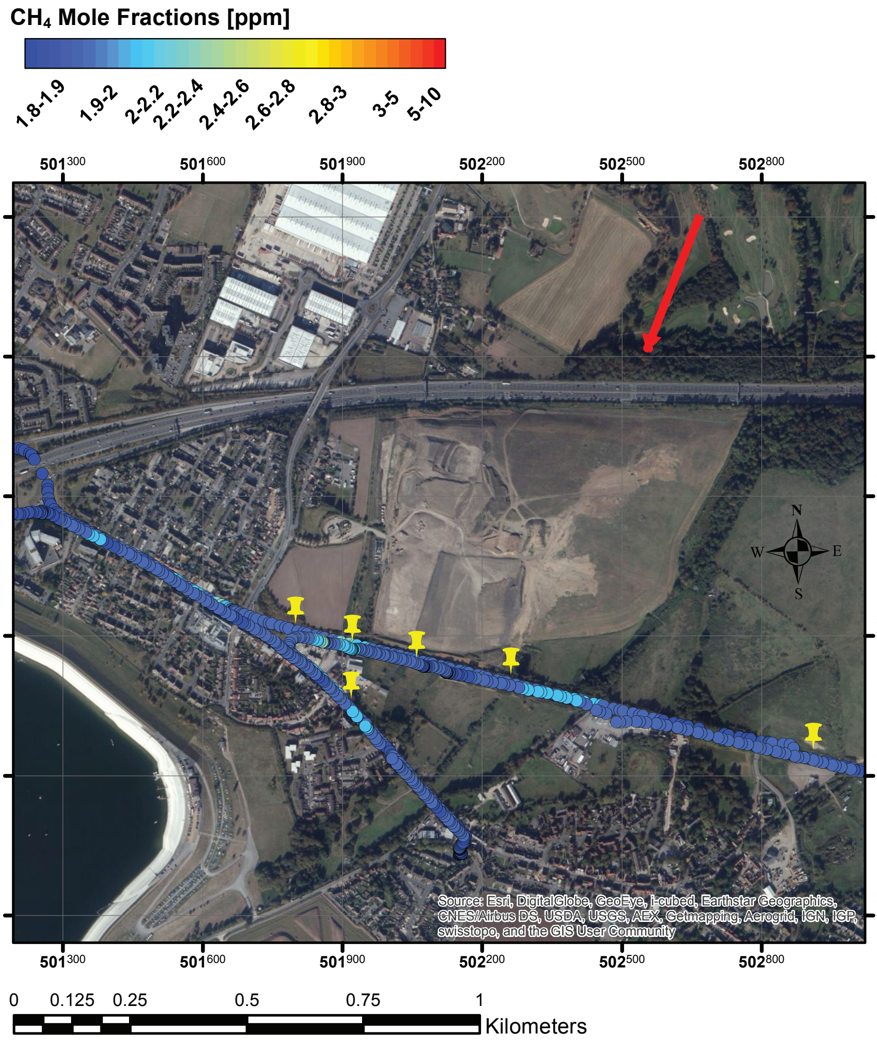

Figure 5.2 ArcGIS plot of methane mole fractions in ppm recorded on 11th July 2013 around Colnbrook landfill site. The grid coordinates are displayed in the British National Coordinate System. The red arrow represents the wind direction and yellow markers the location of the air samples collected.

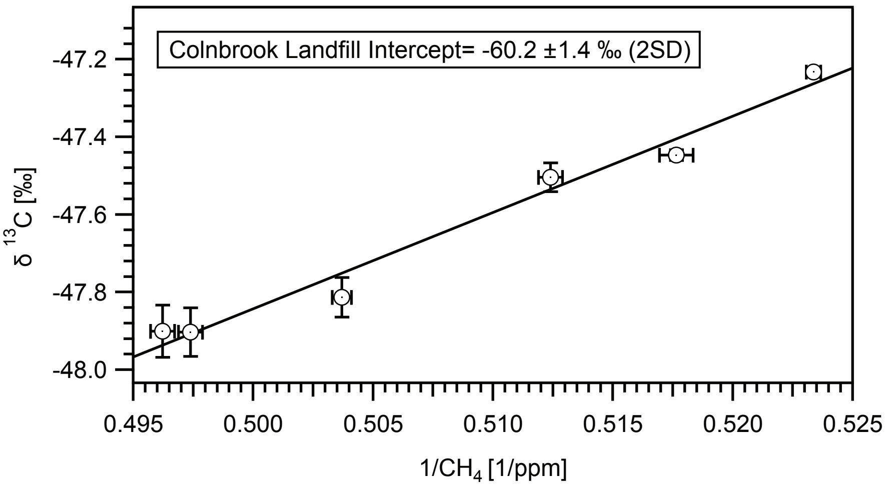

Figure 5.3 Keeling plot based on the samples collected around Colnbrook landfill site.

Even though methane mole fractions were not significantly above the background (see Figure 5.2), precise isotopic measurements in the RHUL laboratory allow isotopic source calculation with a small range of mole fraction values. A source signature of -60.2 ±1.4 ‰ was found by Keeling plot analysis (Figure 5.3), the lowest among all the source signatures of the landfill sites surveyed. The ^{13}C depletion in the methane plume intercepted might indicate that the biogas is emitted through leaking boreholes rather than from the topsoil cover, overtaking the oxidation process in the soil cap.

5.1.2 Wapsey's Wood Landfill Site

Wapsey's Wood landfill site has been surveyed twice, in July 2013 and April 2014. Located near Gerrards Cross, this landfill area is still open, collecting household and industrial waste, but the closure is planned for the end of 2017, when the site will become full in capacity. Topsoiling and seeding works have already started as part of the restoration process of this site. The gas extraction from cells is implemented as soon as their landfilling is complete.

Being still active, the area is affected by methane emissions, and maximum mole fractions of 3 ppm were measured during the first survey. Five samples were collected downwind of the methane plume that was directed towards SW (Figure 5.4). The Keeling plot based on these five samples gives an intercept of -57.6 ±0.5 ‰ (Figure 5.5).

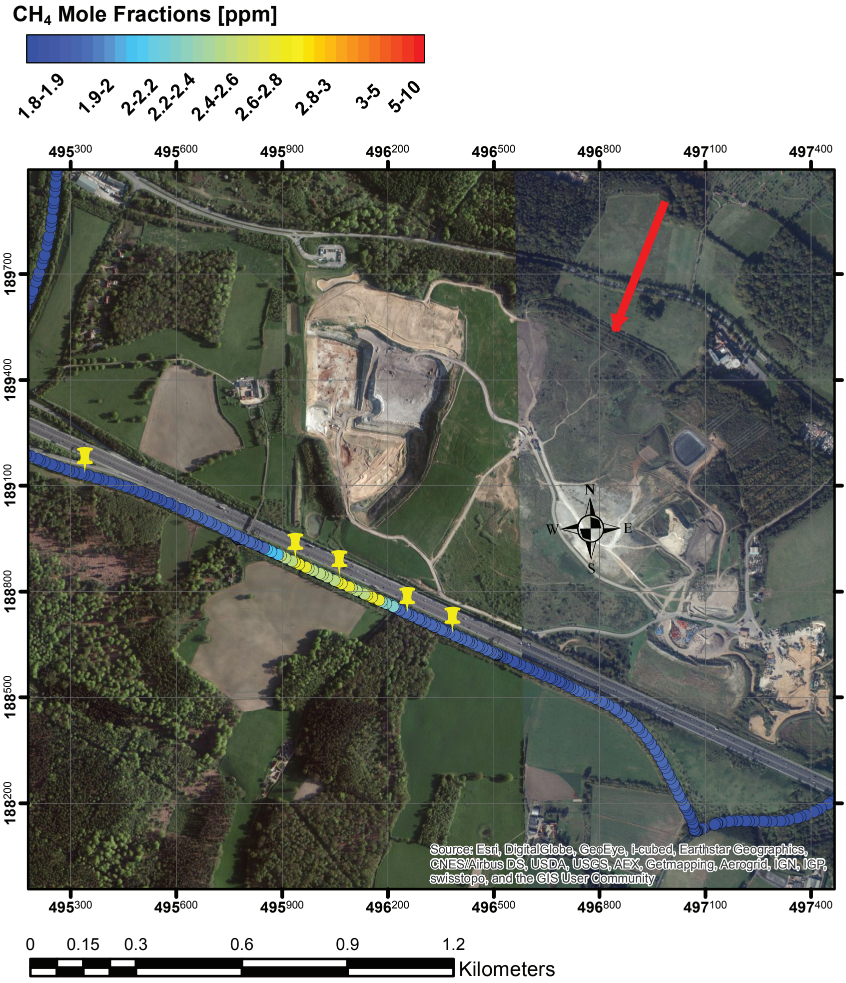

Figure 5.4 ArcGIS plot of methane mole fractions in ppm recorded on 11th July 2013 around Wapsey's Wood landfill site. The grid coordinates are displayed in the British National Coordinates System. The red arrow represents the wind direction and the yellow markers the location of the air samples collected.

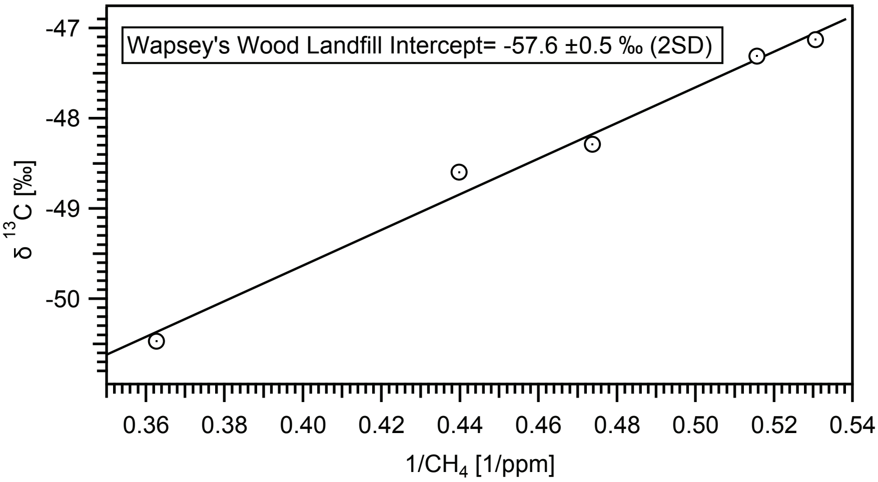

Figure 5.5 Keeling plot based on the samples collected around Wapsey's Wood andfill site in July 2013.

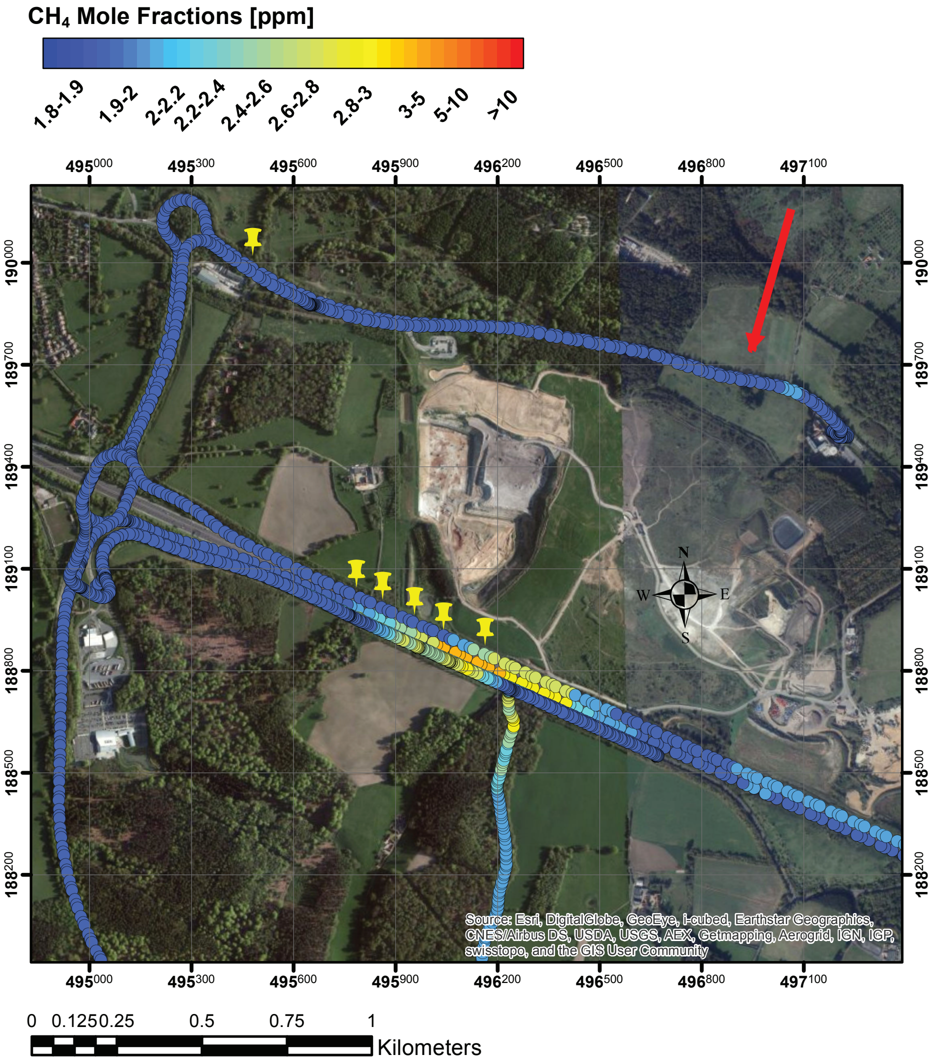

Source: Esri, DigitalGlobe, GeoEye, i-cubed, Earthstar Geographics, CNES/Airbus DS, USDA, USGS, AEX, Getmapping, Aerogrid, IGN, IGP, swisstopo, and the GIS User Community

Figure 5.6 ArcGis plot of methane mole fractions in ppm recorded in April 2014 around Wapsey's Wood landfill site. The grid coordinates are displayed in the British National Coordinates System. The red arrow represents the wind direction and the yellow markers the location of the air samples collected.

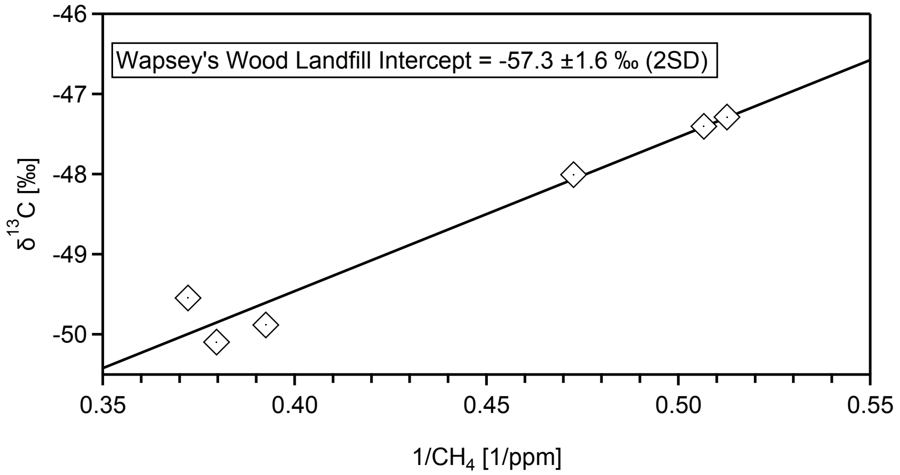

Figure 5.7 Keeling plot based on the samples collected around Wapse's Wood landfill site in April 2014.

During the survey carried out in April 2014 (see Figure 5.6), methane mole fractions the same order of the previous measurement campaign (below 3 ppm) were found and the isotopic source signature of -57.3 ±1.6 ‰ calculated on 6 samples collected was very consistent with the value previously determined (see Figure 5.7). Within 2014, while some cells were subjected to the process of restoration (topsoiling and gas extraction), another containment cell was constructed, in order to provide continuity of landfill during the final operational years of the site (see planned activities on this website:
http://217.114.88.49/Southbucks/Wapseys-Wood-Site-Activities). Therefore the amount of waste collected and emissions were not significantly curtailed after one year and the isotopic signature was not changed.

5.1.3 Albury Landfill Site

Albury landfill is located next to the town of Dorking in the county of Surrey. It collects only household waste and includes a biogas plant for electric power generation. When the site was surveyed on 24th October 2013, wind was coming from the SSE direction and the methane plume was encountered on a major road, where it was not possible to stop the vehicle for sampling (Figure 5.8). Therefore air samples were collected in sequence while driving, in order to get at least three samples representative of integrated methane emissions downwind of the landfill. A Keeling plot analysis based on a narrow range of four values gave an intercept value of – 59.7 ±1.1 ‰ (2SD) (see Figure 5.9).

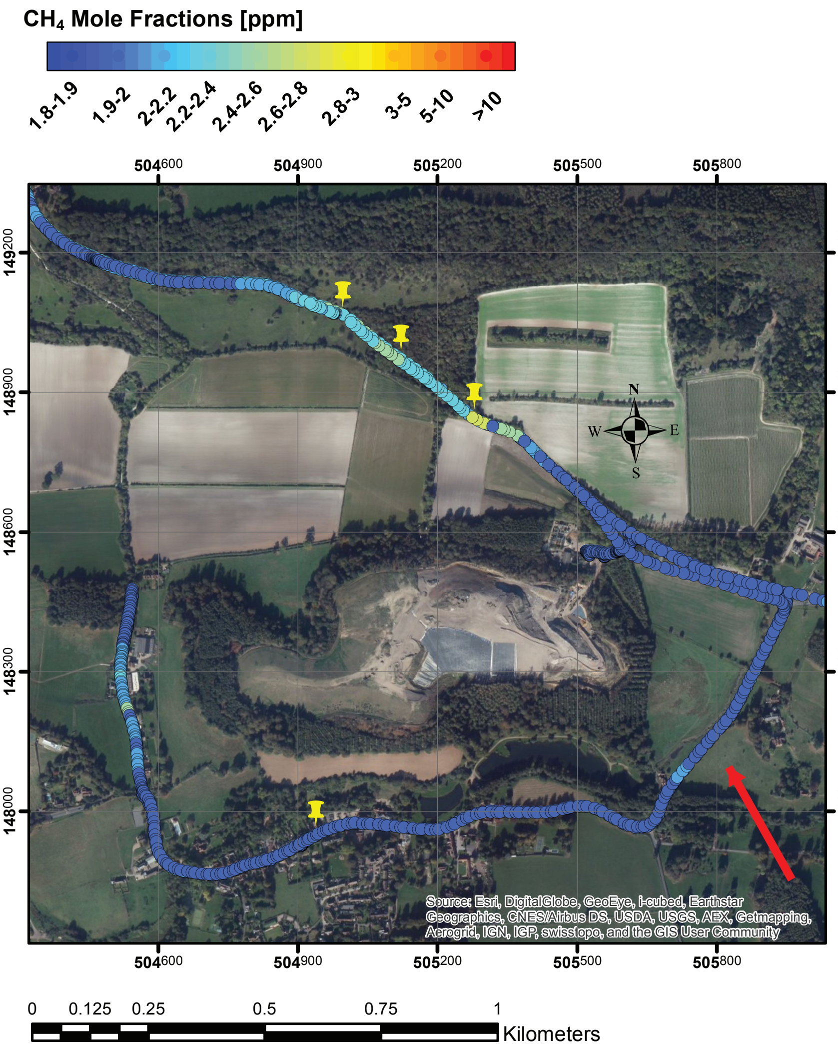

Figure 5.8 ArcGIS plot of methane mole fractions in ppm recorded on 24th October 2013 around Albury landfill site. The grid coordinates are displayed in the British National Coordinates System. The red arrow represents the wind direction and the yellow markers the location of the air samples collected.

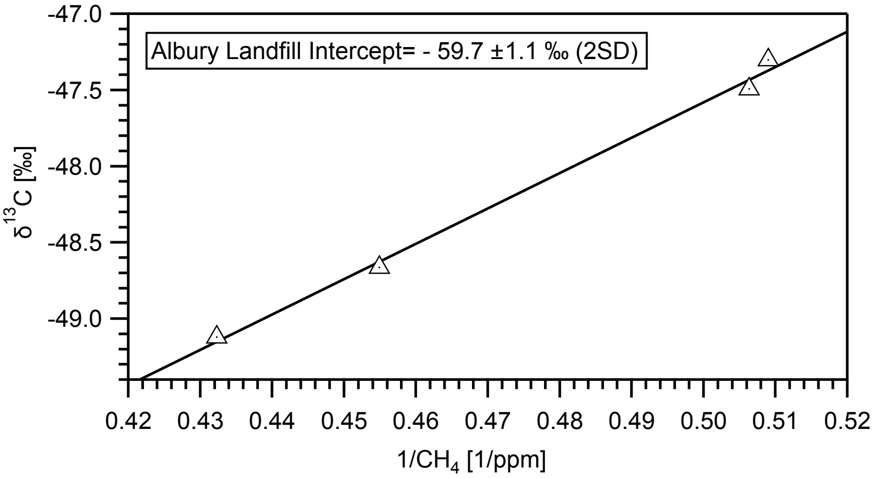

Figure 5.9 Keeling plot based on the samples collected around Albury landfill site.

5.1.4 Redhill Landfill Site

Redhill is an active landfill site in Surrey and it is expected to operate until 2030. Gas wells and gas carrier lines have been installed through different cells and the captured gas is used to produce electricity (http://www.biffa.co.uk/waste-processing/landfill/redhill-landfill.html). Most of the cells have been restored and currently waste is disposed of in one cell (the cell in the yellow square in Figure 5.10). The site was surveyed on 24th October 2013; as wind was coming from SSE, the methane plume could be sampled by driving on the residential area on the NNE side of the landfill, where five samples were collected. The area next to the landfill was carefully explored and several peaks in methane mole fractions were detected also upwind of the site of interest, as Figure 5.10 shows. The highest methane peak was passed through twice with the Picarro mobile, in order to confirm its location and to collect an air sample of it. The isotopic value of that sample turned out being ^{13}C enriched (-44.2 ‰) relatively to the background, suggesting that the methane peak was associated with a leak in the natural gas network. The Keeling plot analysis based on the samples collected in the area affected by landfill emissions gave a source signature of – 59.6 ±0.7 ‰ (2SD) (Figure 5.11).

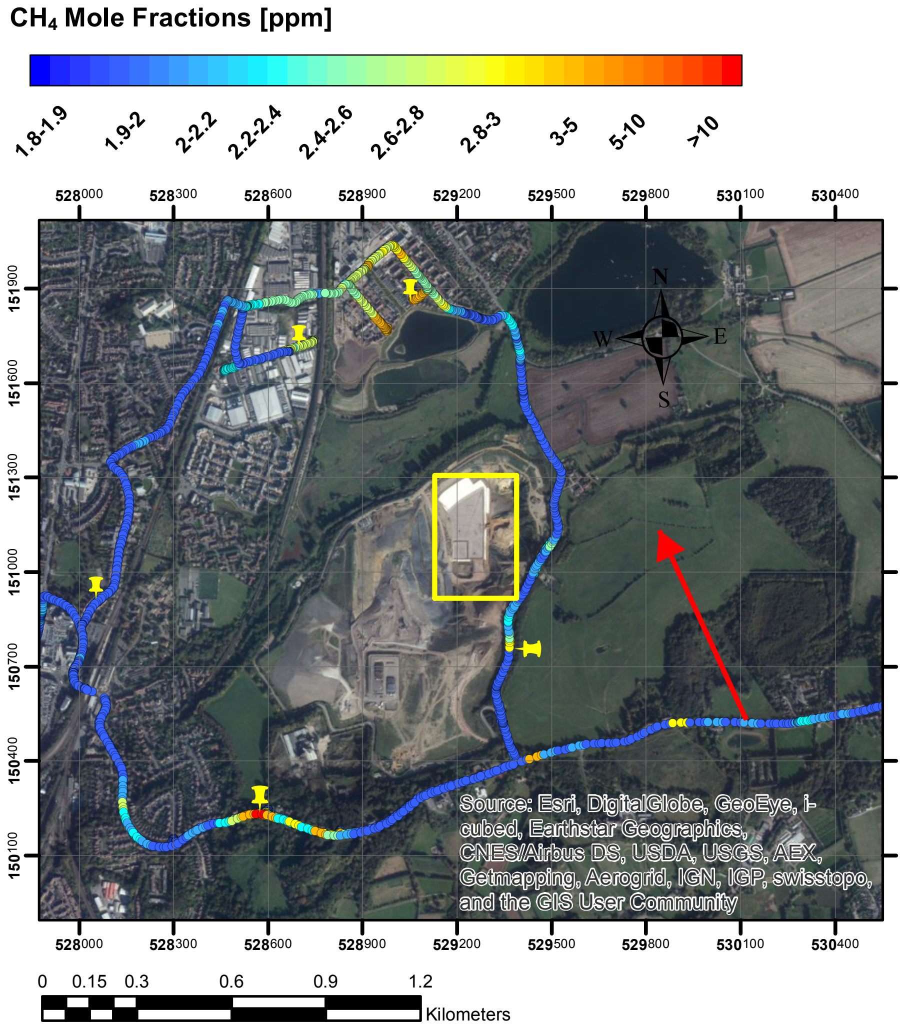

Source: Esri, DigitalGlobe, GeoEye, i-cubed, Earthstar Geographics, CNES/Airbus DS, USDA, USGS, AEX, Getmapping, Aerogrid, IGN, IGP, swisstopo, and the GIS User Community

Figure 5.10 ArcGIS plot of methane mole fractions in ppm recorded on 24th October 2013 around Redhill landfill site. The grid coordinates are displayed in the British National Coordinates System. The red arrow represents the wind direction and the yellow markers the location of the air samples collected.

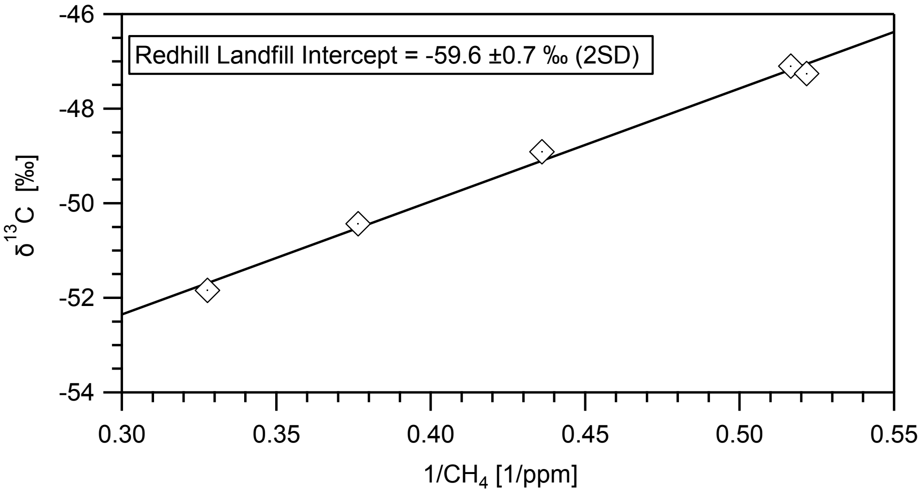

Figure 5.11 Keeling plot based on the samples collected around Redhill landfill site.

5.1.5 Greatness Quarry Landfill Site

Greatness Quarry landfill site, in Kent, is permitted to accept non-hazardous waste until 2015. While surveying the site on 24th October 2013, methane emissions were detected by driving on the west side of the landfill area, finding peaks in methane mole fractions of approximately 5 ppm. Eight air samples with methane mole fractions ranging from 1.9 to 3.9 ppm were collected, giving a Keeling plot intercept of -57.4 ±0.2 ‰ (2SD). The ArcGIS basemap in Figure 5.12 shows a body of water on the east side of the landfill, which might be a drainage basin and might trigger the production of biogenic methane.

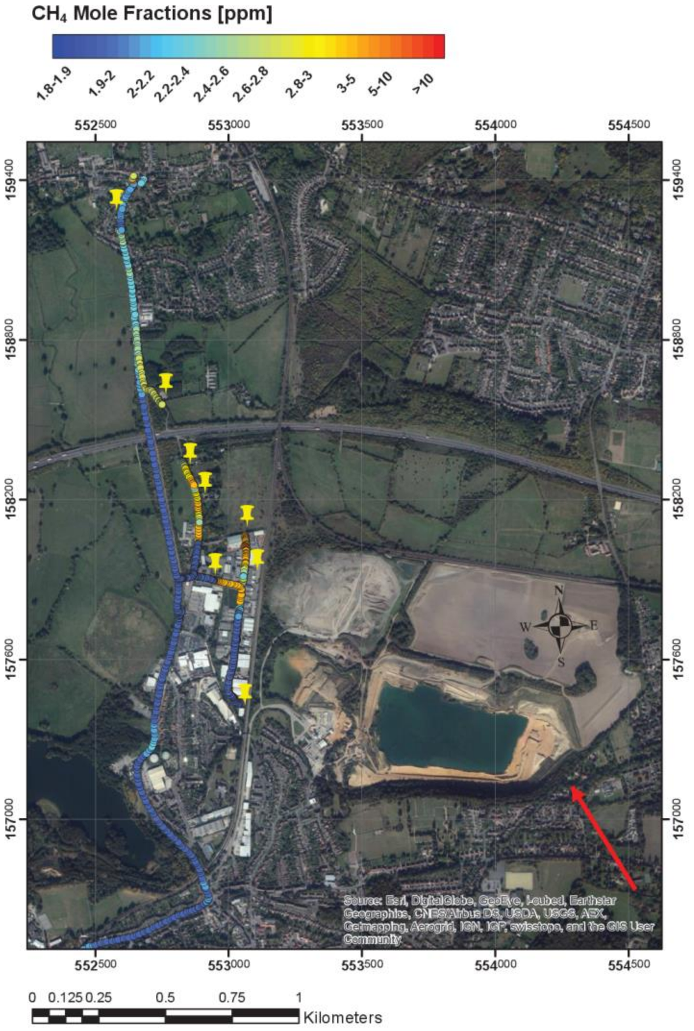

Figure 5.12 ArcGIS plot of methane mole fractions in ppm recorded on 24th October 2013 around Greatness Quarry landfill site. The grid coordinates are displayed in the British National Coordinates System. The red arrow represents the wind direction and the yellow markers the location of the air samples collected.

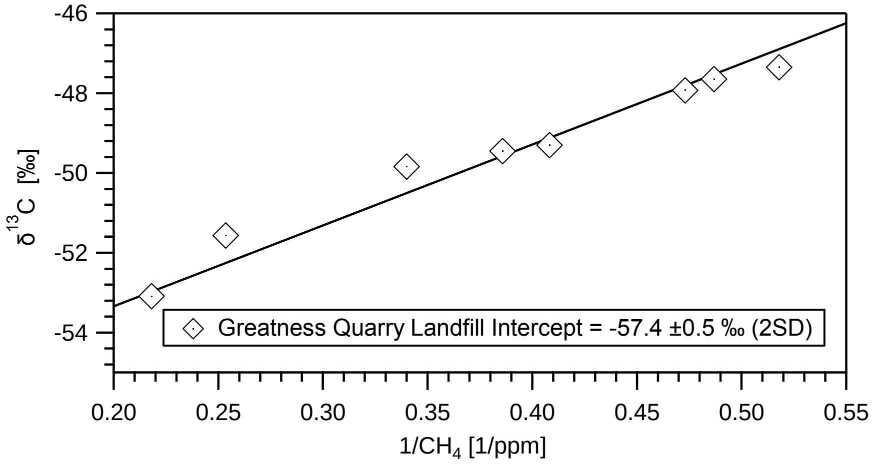

Figure 5.13 Keeling plot based on the samples collected around Greatness Quarry landfill site.

5.1.6 Mucking Landfill Site

Mucking landfill site, in Thurrock, Essex, ceased taking waste at the end of 2010 and was closed in 2012. As it was reclaimed for community and environmental use, it is now accessible to anyone, and the area can be easily explored. Despite its closure, the landfill is still emitting a large amount of methane: the maximum mole fraction recorded in the measured part of the plume was approximately 17 ppm. With wind from the SSW, on 14th October 2013 it was possible to intersect the plume on 4 transects at different distances from the NNE side of the landfill and 11 samples were collected (Figure 5.14), covering a wide range of mole fractions, ideal for precise Keeling plot analysis.

The calculated source signature of -56.1 ±0.5 ‰ (2SD) is one of the heaviest values found for UK landfill sites (Figure 5.15). Indeed, closed landfills, where biogas is oxidised in the topsoil cover, are usually characterised by more ^{13}C-CH_4 enriched emissions relatively to more recent and still active landfill sites.

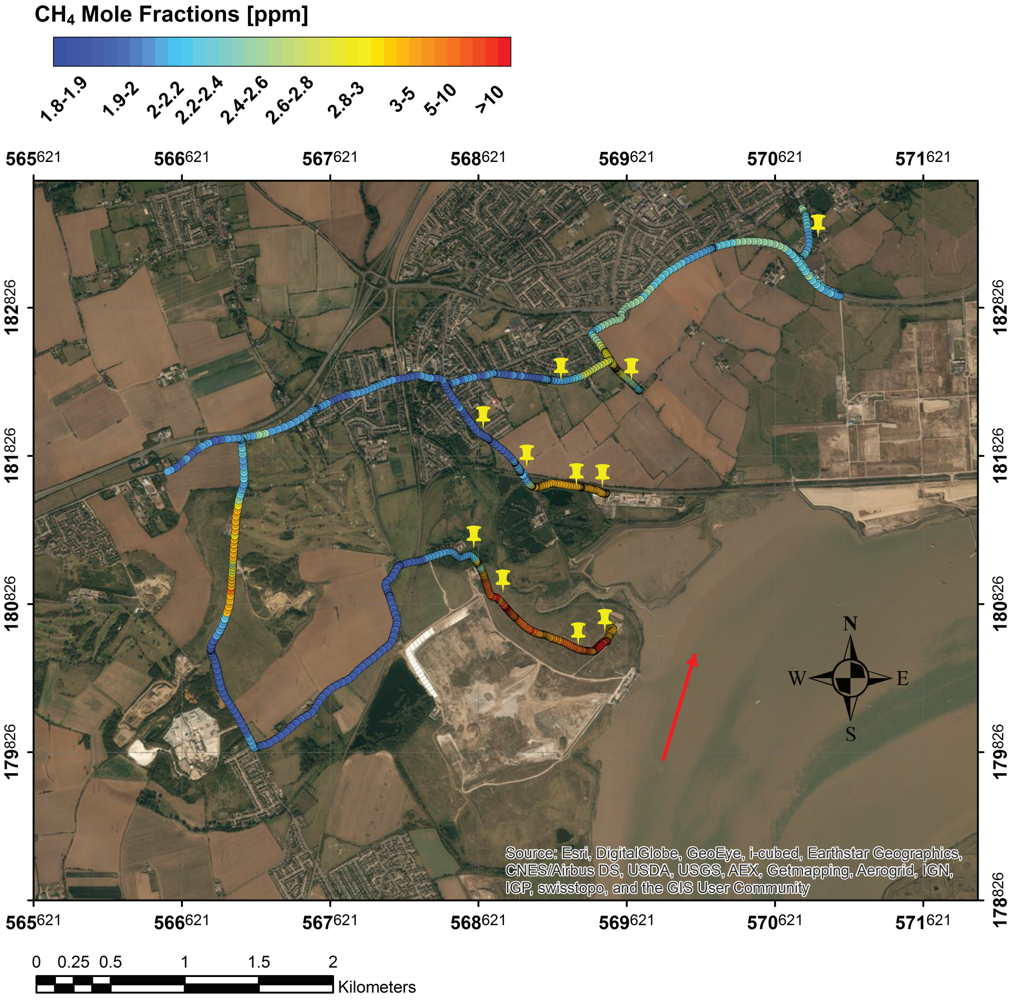

Figure 5.14 ArcGIS plot of methane mole fractions in ppm recorded on 14th October 2013 around Mucking landfill site. The grid coordinates are displayed in the British National Coordinates System. The red arrow represents the wind direction and the yellow markers the location of the air samples collected.

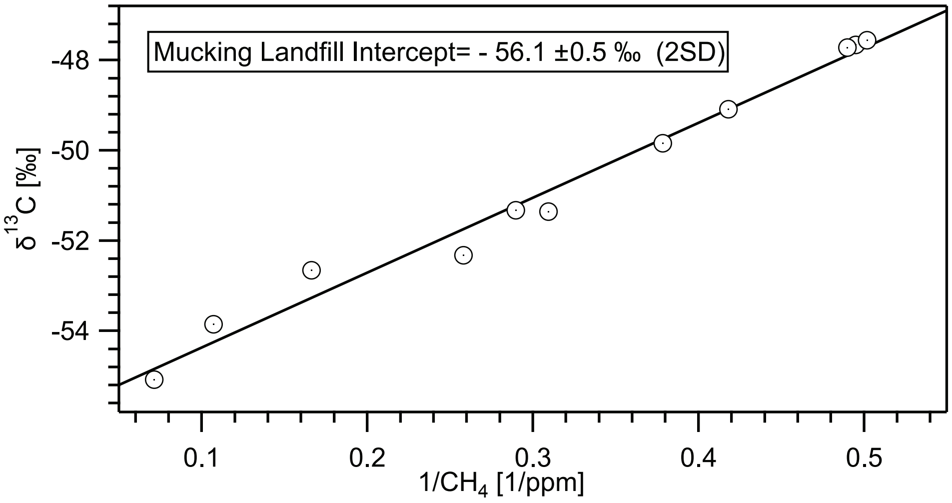

Figure 5.15 Keeling plot based on the samples collected around Mucking landfill site.

5.1.7 Roxwell Landfill Site

Next to the village of Chignal St. James, in Essex, Roxwell landfill site is still active and its complete restoration has been planned to be concluded by the end of 2015. Gas extraction for electricity production is in operation. The area was explored on 24th October 2013 and five samples were collected while transecting the main plume on the NE side of the landfill (see Figure 5.16), where methane mole fractions ranging from 2 to 4 ppm were measured. The Keeling plot based on those 5 samples gives a source signature value of -55.2 ±0.6 ‰ (2SD), which is the most ^{13}C enriched signature found so far (Figure 5.17).

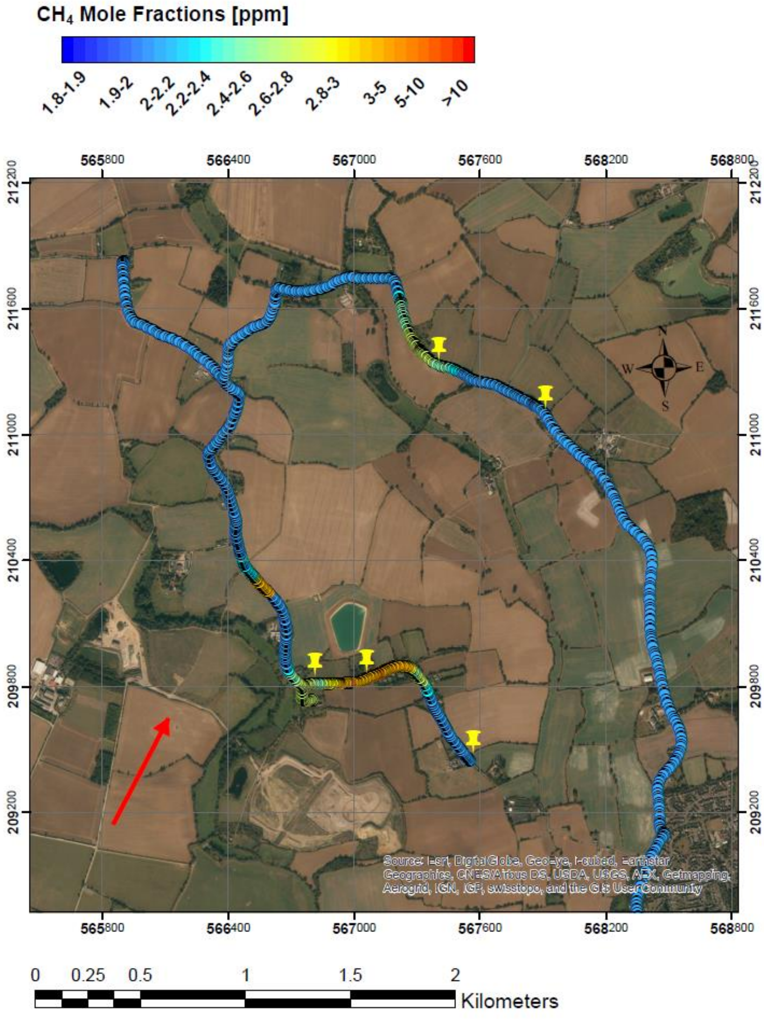

Figure 5.16 ArcGIS plot of methane mole fractions in ppm recorded on 24th October 2013 around Roxwell landfill site. The grid coordinates are displayed in the British National Coordinates System. The red arrow represents the wind direction and the yellow markers the location of the air samples collected.

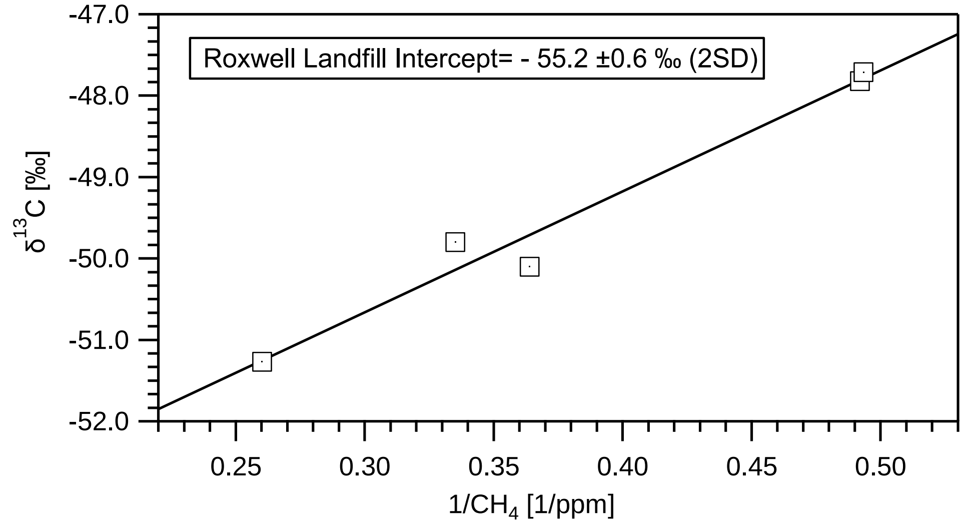

Figure 5.17 Keeling plot based on the samples collected around Roxwell landfill site.

5.1.8 Landfill Site J

By utilising the Picarro mobile system, different sites can be measured on the same day, but also thorough measurement campaigns on large areas can be carried out. One landfill site was carefully explored and sampled for three days on March 2013, as part of a project with NPL and DEFRA. The landfill site is a modern landfill, comprising an area of active filling. The area highlighted in yellow in Figure 5.18 is the zone including active filling cells and slopes with temporary cover. Each day a different sampling scheme was planned: downwind and transect locations were dependent on the site perimeter and the wind direction, assessed before sampling started. As this project included an exhaustive onsite survey and not only driving offsite on public roads to sample the downwind methane plume, weather parameters such as wind speed and atmospheric pressure were measured. Figure 5.18 represents methane mole fractions recorded on the third day of the measurement campaign (5th March 2013) in the afternoon. The wind direction moved from SSE to SE, measured wind speeds were 0 to 12 km/h and the atmospheric pressure was progressively falling (1004 to 1002 hPa). Where no cover was involved in weakening biogas emissions, resulting methane mole fractions were higher. The biggest plume, with peaks 35 ppm above background, was associated with the active filling cells (yellow square in Figure 5.18). Elevated concentrations were recorded also downwind of the gas and leachate plant.

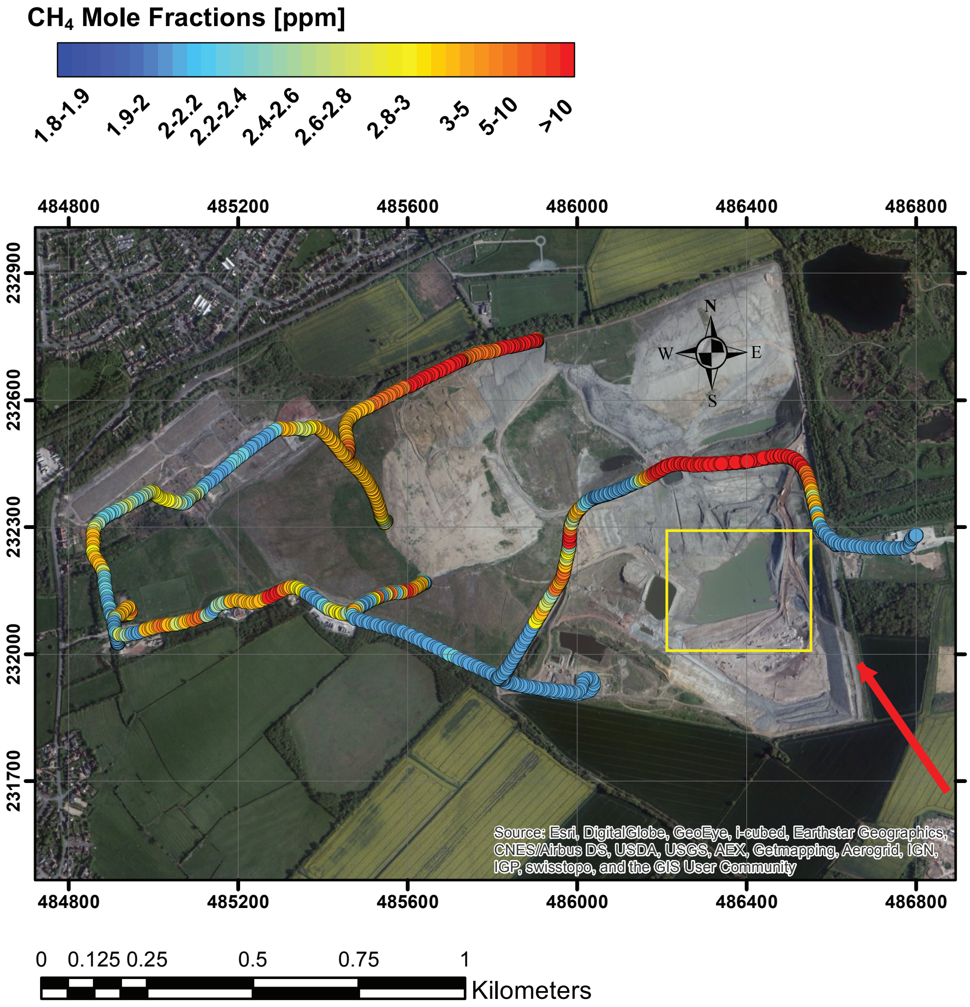

Source: Esri, DigitalGlobe, GeoEye, i-cubed, Earthstar Geographics, CNES/Airbus DS, USDA, USGS, AEX, Getmapping, Aerogrid, IGN, IGP, swisstopo, and the GIS User Community

Figure 5.18 ArcGIS plot of methane mole fractions in ppm recorded on 5th March 2013 around landfill site J. The grid coordinates are displayed in the British National Coordinates System. The red arrow represents the wind direction. The yellow square represents the active cell.

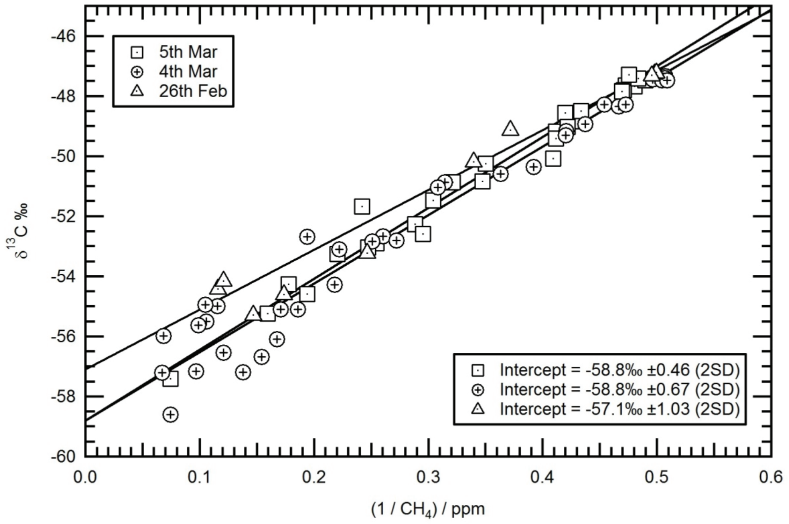

Figure 5.19 Keeling plot of all air samples collected at Site J. Intercepts for 3 different days are shown.

As methane leaks from the gas extraction network represent one of the main pathways of methane release, the isotopic composition of methane from gas wells distributed all over the site was measured (see Chapter 4 for the analysis of methane high concentrations gas samples). Isotopic values span a range from -63 to -53 ‰. The more ^{13}C enriched values are thought to be correlated to the oldest parts of the landfill, where methane has been oxidised for longer time.

Figure 5.19 shows the Keeling plots based on all the ambient air data for each day of measurements at Site J. The intercept of the Keeling plots represent the bulk isotopic composition of the methane emitted from the area: -57.1 ±1.0 ‰ on day 1, -58.8 ±0.7 ‰ on day 2 and -58.8 ±0.5 ‰ on day 3. Overall, the averaged isotope values recorded for the Site J are in agreement with the value of -58 ‰, taken as a reference value for methane emissions from SE England landfills.

5.1.9 Summary

Landfill sites surveyed are listed in Table 5.1, together with the δ^{13}C source signatures calculated and the relative errors.

Landfill	Current Status	Sampling Date	Max measured Mole Fractions [ppm]	δ^{13}C Signature [‰]
Albury	Active	Oct-13	2.3	-59.7 ±1.1
Colnbrook	Closed (2012)	Jul-13	2.1	-60.2 ±1.4
Greatness Quarry	Active	Oct-13	4.6	-57.4 ±0.5
Mucking	Closed (2011)	Oct-13	14.0	-56.1 ±0.5
Redhill	Active	Oct-13	3.1	-59.6 ±0.7
Roxwell	Active	Oct-13	3.9	-55.2 ±0.6
Wapsey's Wood	Active	Jul-13	2.8	-57.6 ±0.7
		Apr-14	2.7	-57.3 ±1.6
Site J	Active	Feb-13	8.6	-57.1 ±1.0
		Mar-13	17.5	-58.8 ±0.7
		Mar-13	36.7	-58.8 ±0.5
Site L	Active	Mar-13	50.1	-58.5 ±0.6
Masons	Active	Aug-14	16.7	-57.5 ±0.4

Table 5.1 Landfill sites surveyed with the calculated δ^{13}C signature. Errors are calculated as 2 standard deviations. Surveys on Site L and Masons were conducted as part of different projects involving the Atmospheric Research Group at RHUL.

Isotopic signatures observed span a range from -60.2 ±1.4 to -55.2 ±0.6 ‰ (2SD), with an averaged value of -58.0 ±3 ‰ (2SD), which could be safely taken as representative of SE England landfills.

The three days survey of the Site J showed that total methane emissions principally originate from the uncapped active tipping area and from leaks in the gas extraction system in the topsoil-covered parts of the landfill. In case of a soil capping, both cover type and age affect the extent of methane oxidised, and therefore the isotopic composition of the methane released.

Although all the surveyed landfill sites are associated with high methane emissions in the national inventories, according to my measurements, Albury and Colnbrook landfill sites do not release high level of biogas. On the other hand, high methane mole fractions levels have been detected next to Greatness Quarry landfill site, which does not correspond to a methane hotspot in the 2012 inventories. The 4.6 ppm CH_4 measured at Greatness was the highest offsite mole fraction measured. All higher mole fractions are from sites where access was granted for methane oxidation studies, or on the public access road that crosses the Mucking site.

5.2 English and Welsh Coal Mines

In order to assign a representative $\delta^{13}C-CH_4$ signature to emissions from coal mines, English deep mines and Welsh deep and opencast mines have been surveyed and their emissions isotopically characterised. The isotopic composition of methane from coal mines in South Yorkshire, Warwickshire and South Wales has been found to vary significantly. The following section discusses the process of coalification and the parameters that might affect the isotopic signature of methane releases associated with coal.

5.2.1 Process of Coalification

The process of coalification involves both biochemical and geochemical reactions. The vegetal matter firstly decays under water, in the absence of oxygen; then, with increasing burial, it is subjected to a thermal maturation, which implicates more geochemical changes. As coalification proceeds, the carbon content increases, accompanied by a relative depletion in volatile compounds, such as hydrogen and oxygen, emitted in the form of water, methane, carbon dioxide and higher hydrocarbons through decarboxylation and dehydration reactions (Stach and Murchison, 1982). At higher degree of coalification and temperature, the liquid hydrocarbons formed in previous stages are thermally cracked to methane, increasing the amount of methane produced. Peat represents the first stage of the coalification process. The vertical pressure exerted by accumulating sediments converts peat into lignite. The intensification of the pressure and heat from movements of the Earth's crust facilitates the transition from lignite to anthracite (the highest rank).

The isotopic signature of the methane produced is certainly affected by the methane origin pathway (Whiticar, 1996). Thermogenic methane (produced at great depth by thermal modification of sedimentary organic matter) is isotopically enriched in ^{13}C (> -50 ‰) compared to biogenic methane (< -50 ‰ for acetate fermentation and <-60 ‰ for the CO_2 reduction pathway) that is generated at shallow depths and lower rank stages, as a consequence of the ^{12}C-^{12}C bonds being broken more easily than ^{13}C-^{13}C by thermal processes (Rice, 1993). Biogenic methane is generated during early coalification stages and it is then dissolved in water and released during burial; during more mature stages, its production is triggered by the meteoric water inflow into the coal, following basin uplift (Rice, 1993; Scott et al., 1994).

Intermediate isotopic compositions of methane might reflect a mixing between microbial and thermogenic gases or secondary processes. Indeed, many controlling factors co-drive the fractionation process, and several contentions about their leverage still persist in literature. Deines et al. (1980) assert that no significant trend is observed in the isotopic signature of methane in relation to the degree of coalification. Conversely, Chung et al. (1979) observed that the composition of the parent material does affect the isotopic composition of the methane accumulated, together with the temperature and the time of formation. They experimented that the methane accumulated from pyrolysis of coal at 500° becomes more enriched in ^{13}C with increasing degree of coalification, and they ascribed this result to the methane precursor functional groups, which were also enriched in ^{13}C. These assumptions were made on the basis of long-term laboratory pyrolysis of coal and by extrapolating the results to the extensive thermal degradation occurring during the natural maturation of organic matter. However, the application of these experiments to the actual coalification process might be misleading, due to the enormous difference in the rate of heating between laboratory experiments and geological conditions.

Whereas the link between isotopic composition and coal rank is not that straightforward, studies carried out in different worldwide coal seams confirm a stronger relation between coal bed gas composition and depth. Rice et al. (1993) using data from Australian, Chinese and German coal beds, show that shallow coal beds tend to contain relatively isotopically lighter methane when compared to those at greater depths. In the presence of intrusion of meteoric water, biogenic methane, isotopically lighter, can be generated and mixed with the thermogenic gas previously produced. Colombo et al. (1970) documented a distinct depth correlation in the Ruhr Basin coal in Germany, with methane becoming more ^{13}C-depleted towards the surface zone, independently from coalification patterns. This tendency can be explained either by bacterial methanogenesis, or by secondary processes such as absorption-desorption of methane. Also Scott et al. (2002), in a study about coal seams in the Bowen Basin, Australia, ascribe the progressive methane ^{13}C-enrichment with depth to the meteoritic recharge in the shallowest seams, associated with a higher bacteria activity and a preferential stripping of ^{13}C-CH_4 by water flow.

The migration of methane from the primary zone as a consequence of local pressure release can affect the isotope composition, since $^{12}CH_4$ diffuses and desorbs more readily than $^{13}CH_4$ (Deines, 1980). However, the migration effect on the isotopic composition of methane is limited. Fuex et al. (1980) affirm that this fractionation would not exceed 1 ‰ ^{13}C-depletion and generally the quantitative experimental data on isotopic fractionation effects have been carried out mostly under laboratory conditions and few through natural sedimentary rocks (Zhang and Krooss, 2001). Although secondary processes such as diffusion and desorption may affect the δ^{13}C of coal methane, a much larger variation in the isotopic composition is associated with different pathways (30 ‰) and thermal maturation stage (25 ‰) (Clayton, 1998).

The great scatter in the δ^{13}C values, according to several authors (Whiticar, 1999; Schlegel et al., 2011; Hamilton et al., 2014), might be also caused by the process of substrate depletion in a partially closed microbial system, although it involves very gradual changes in the isotopic composition of the carbon reservoir. The progressive depletion of the carbon reservoir, associated with a progressive removal of the lightest molecules from the carbon pool, may result in a ^{13}C-enrichment of the residual carbon, with a related ^{13}C-enrichment in the methane subsequently formed.

Overall, the δ^{13}C values of methane from coal show an extremely wide range (-80 ‰ to -17 ‰) (Rice, 1993). Therefore the understanding of those processes driving the methane isotopic composition must be restricted to a particular set of geological conditions.

5.2.2 Geology of English and Welsh Coalfields

The major coalfields of England and Wales belong to the same stage in the regional stratigraphy of northwest Europe, the Westphalian Stage, between roughly 313 and 304 Ma (Upper Carboniferous). Nottinghamshire, Yorkshire, South Lancashire, Warwickshire, North and South Staffordshire contain some of the largest coalfields, but mining has long since ceased in many of these areas. Most of the coal mines observed in this study are located in South Yorkshire (Hatfield and Maltby collieries), where 50% of the coalfield's output came from the Barnsley seam, the most valuable one, which embraces soft coal on the top and harder coal in the bottom portion. Seams >2m in thickness are common in the southern half of the Yorkshire coalfield. Upper Carboniferous coal measures typical of Yorkshire extend into the East Midlands coalfields (IMC Group Consulting Limited, 2002). The exposed coalfields are found into the west of this belt, where the coal measures outcrop (roughly from Nottingham to Bradford and Leeds via Chesterfield, Sheffield and Barnsley) and then dip eastwards beneath younger rocks. Indeed, coal is deeply buried towards the east, where the coal is said to be 'concealed'.

Daw Mill Colliery is another UK mine whose methane emissions have been analysed in this study. The coal exploited is part of the Warwickshire Coalfield comprising Carboniferous rocks of 354-290 million years old and the seam varies in thickness from 6.6 to 7.5 m (IMC Group Consulting Group, 2002). In the south of this coalfield the main seam of interest is the Warwickshire Thick Coal, mined exclusively in Daw Mill Colliery (Jones N S, 2004).

The coal of the South Wales basin exhibits a well-defined regional progression in rank, which varies from highly volatile bituminous coal in the south and east margin to anthracite in the north-west part (Alderton et al., 2004).

5.2.3 English Coal Mines

The English coal mines that have been surveyed are shown in the emission map created with 2012 emission inventories for the related counties (Figure 5.20), and they are all corresponding to methane hotspots in the NAEI (red squares).

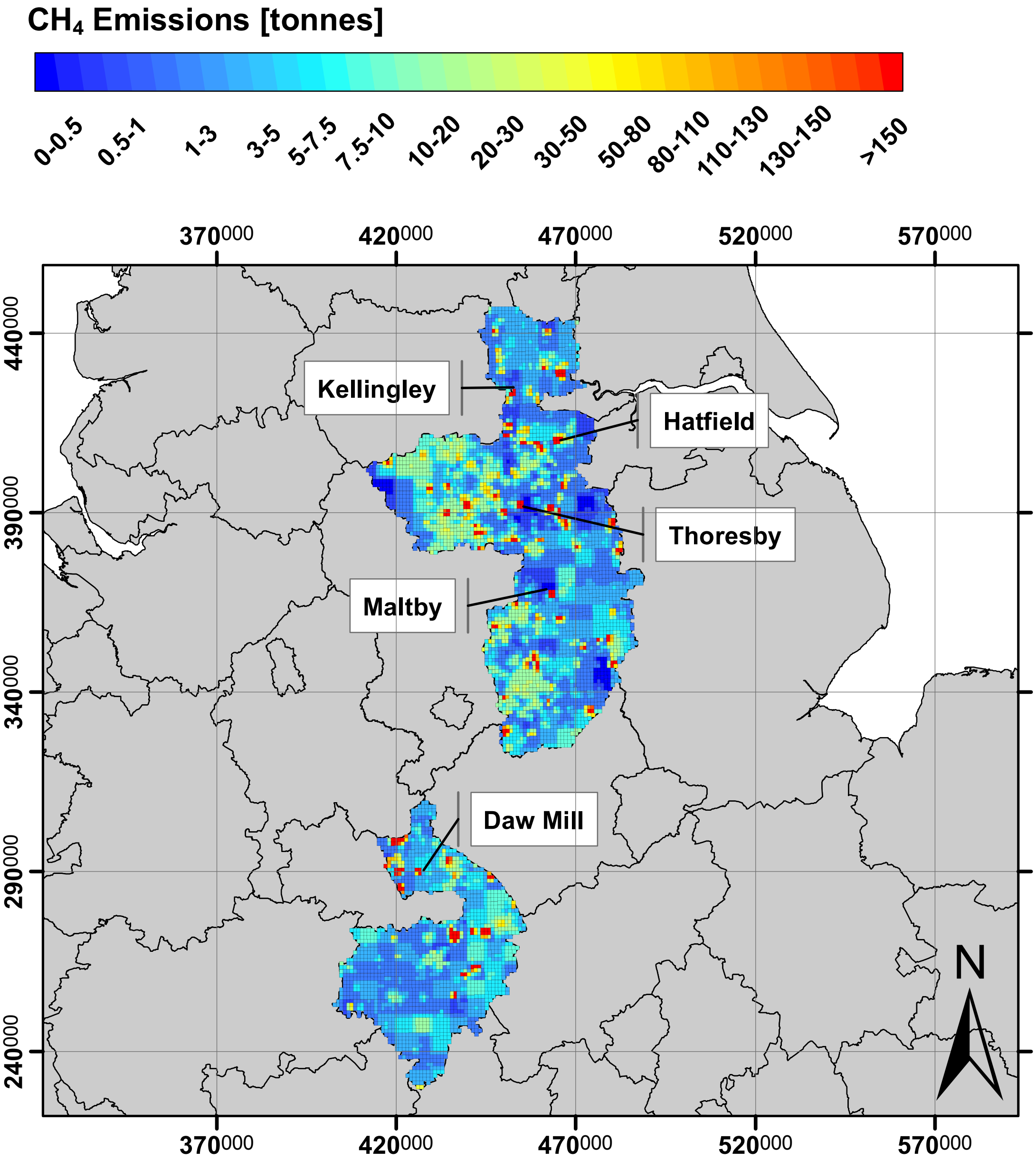

Figure 5.20 2012 emission map of the areas where the explored English coal mines are located. The grid coordinates are displays in the British National Coordinate System.

5.2.3.1 Hatfield Colliery

Hatfield is one of the few UK deep mines still open. New investments in deep mine production have been made and abandoned developments have been reopened (Mineral Planning Factsheet British Geological Survey, 2010). The main seams that have been worked since the 1920s are the Barnsley, the Dunsil and the High Hazel seams, at approximate depth of 401-365 m, 414-376 and 313-284 m respectively (Hill, 2001).

According to Jones et al. (2004) the gas content of these seams is relatively low and their permeability is uncertain, and methane emissions to the atmosphere are expected to be negligible. However, mole fractions over 7 ppm were recorded during both surveys carried out in the Hatfield colliery area in July and October 2013, giving evidence of methane releases from the coal mine. The methane desorbed from coal piles within the colliery area and methane vented from wells may explain the relatively high mole fractions measured.

On 10th July 2013 a mole fraction of over 7.2 ppm was recorded on the SW side of the colliery and four samples were collected when transecting the methane plume (see Figure 5.21a).

On 26th September 2013 the plume spread out towards the WNW side of the coal mine, driven by south-easterly winds. By driving with the Picarro mobile downwind of the colliery, the methane plume was transected three times (see Figure 5.21b) and 5 samples were collected.

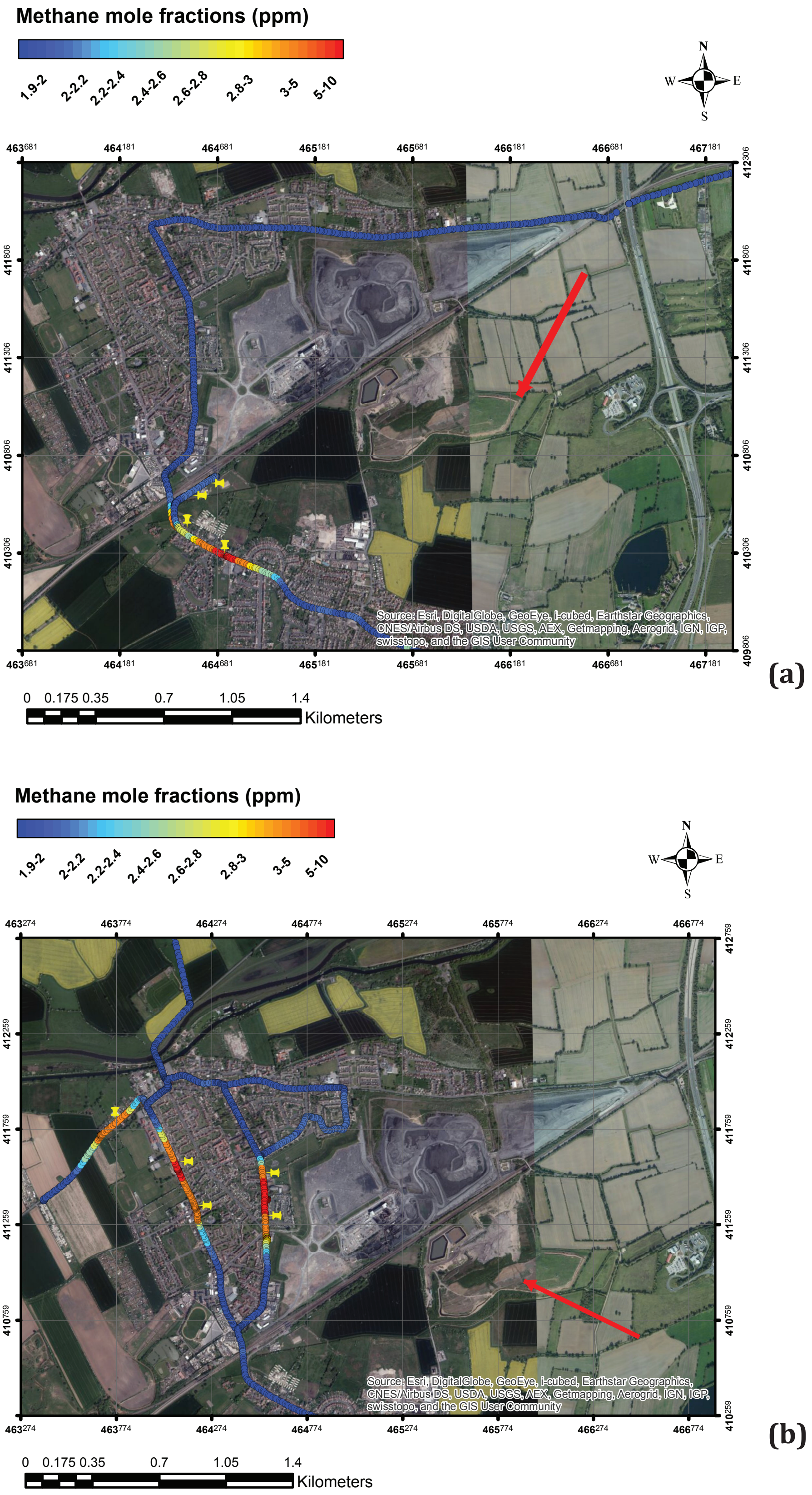

Source: Esri, DigitalGlobe, GeoEye, i-cubed, Earthstar Geographics, CNES/Airbus DS, USDA, USGS, AEX, Getmapping, Aerogrid, IGN, IGP, swisstopo, and the GIS User Community

Source: Esri, DigitalGlobe, GeoEye, i-cubed, Earthstar Geographics, CNES/Airbus DS, USDA, USGS, AEX, Getmapping, Aerogrid, IGN, IGP, swisstopo, and the GIS User Community

Figure 5.21 ArcGIS plot of methane mole fractions in ppm recorded downwind of Hatfield coal mine in July 2013 (a) and September (b). The grid coordinates are displayed in the British National Coordinate System. The red arrow represents the wind direction and yellow push-pins samples collected.

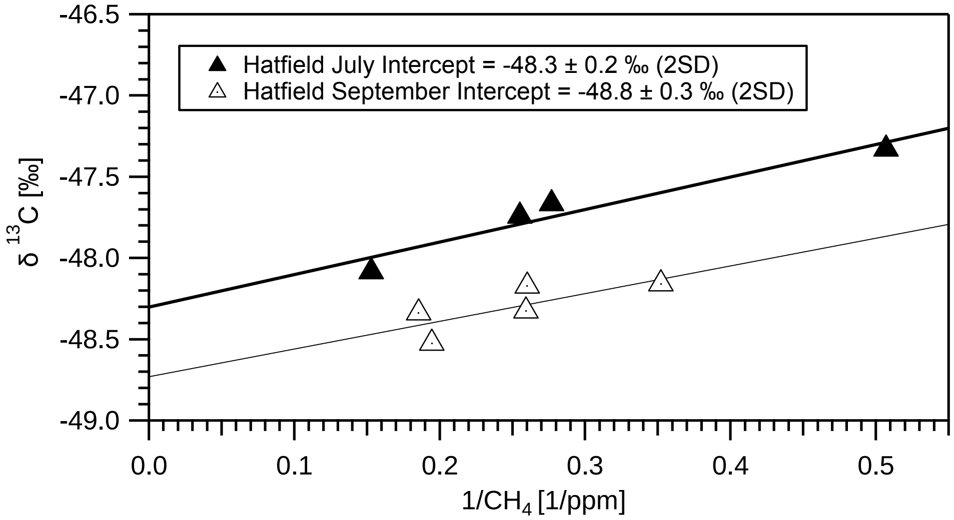

Figure 5.22 Keeling plots based on samples collected around Hatfield Colliery on two different sampling days (26th September and 10th July 2013).

The Keeling plots based on samples collected around Hatfield in July and September (see Figure 5.22) give an intercept value of -48.3 ±0.2 and -48.8 ±0.3 ‰ (2SD) respectively. It has to be pointed out that the atmospheric background composition differed greatly between the two sampling days, from 1.89 ppm and -47.4 ‰ in July to 1.92 ppm and -47.8 ‰ in September, due to the methane isotopes seasonal cycle (see Figure 2.6 in Chapter 2) driven by the balance between methane destruction by OH radicals, enhanced in July, and source production.

Most of the coal mined in South Yorkshire is bituminous coal and the measurements are consistent with the range of -49 and -31 ‰ suggested by Colombo et al. (1970) for in situ coal bed methane in the Ruhr basin in Germany, which contains the most important German bituminous coal of Upper Carboniferous age.

5.2.3.2 *Maltby Colliery*

Maltby colliery is one of the largest underground mines in England and it has been recently closed (March 2013). In 2007 it was estimated to be the deepest UK mine, reaching 991 m in depth. The coal exploited is part of the Yorkshire coalfield, a high volatile bituminous coal with a seam gas content of between 4.1 and 6.1 m^3 CH_4 per tonne (McEvoy et al., 2006). The two seams worked are the Barnsley and the recently exploited Parkgate one, whose coal is a good quality industrial one used for gas manufacture (Hill, 2001). The coal mine methane is drained and used for electricity, as well as at Thoresby and Welbeck mines. Over 3 ppm methane mole fractions were detected while driving with the Picarro mobile system downwind of the colliery on two different days, in July and September 2013.

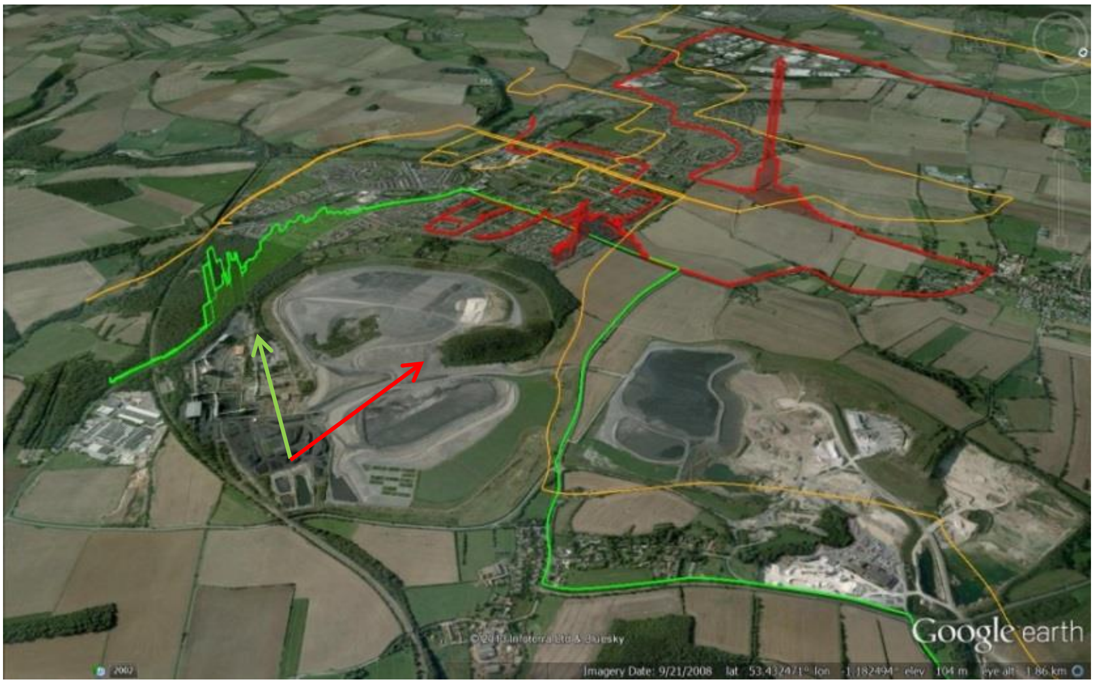

Figure 5.23 Google Earth view of the methane mole fractions recorded both in July (green line) and September (red line) in Maltby. The yellow line represents the 5 ppm threshold. The arrows represent the respective wind directions.

By displaying methane mole fractions for both sampling days on a Google Earth interface, and drawing the respective wind directions, the source of methane plumes could be deduced. Figure 5.23 suggests that methane emissions derive from the area where the coal is stored, from the degassing of coal heaps, whereas the north area of the coal pit (the area on the right in Figure 5.23) seems not to emit, as no plume has been intercepted driving downwind of that site. Ventilation shafts and leaks in the recovery methane network for electrical power generation might also be the origin of the plume, but, as collieries were not accessible and the survey was limited to public roads surrounding the coal mine area, the exact provenance of the plume remains unknown.

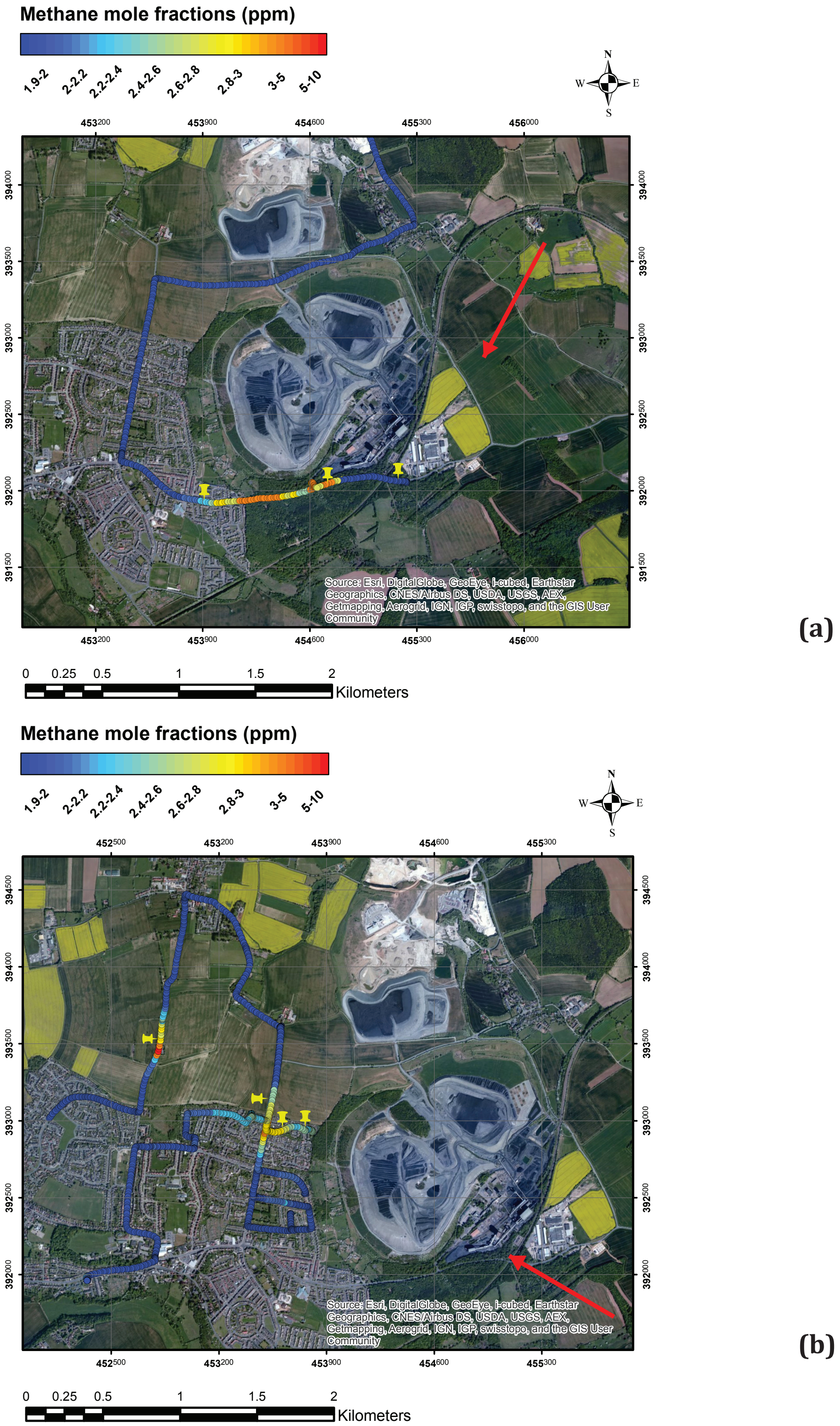

Source: Esri, DigitalGlobe, GeoEye, i-cubed, Earthstar Geographics, CNES/Airbus DS, USDA, USGS, AEX, Getmapping, Aerogrid, IGN, IGP, swisstopo, and the GIS User Community

Source: Esri, DigitalGlobe, GeoEye, i-cubed, Earthstar Geographics, CNES/Airbus DS, USDA, USGS, AEX, Getmapping, Aerogrid, IGN, IGP, swisstopo, and the GIS User Community

Figure 5.24 ArcGIS plot of methane mole fractions in ppm recorded downwind of Maltby coal mine in July 2013 (a) and September (b). The grid coordinates are displayed in the British National Coordinate System. The red arrow represents the wind direction and yellow pushpins samples collected.

The Keeling plot intercept based on the samples collected in July and in September are -45.9 ±0.3 ‰ (2SD) and -45.4 ±0.2 ‰ (2SD) respectively (Figure 5.25), more than 2 ‰ higher than the one obtained with samples collected in Hatfield on the same day. Both source signatures are in good agreement with the value of -44.1 ‰ observed for desorbed methane of the Barnsley coal seam, in a study conducted by Hitchman et al. (1990).

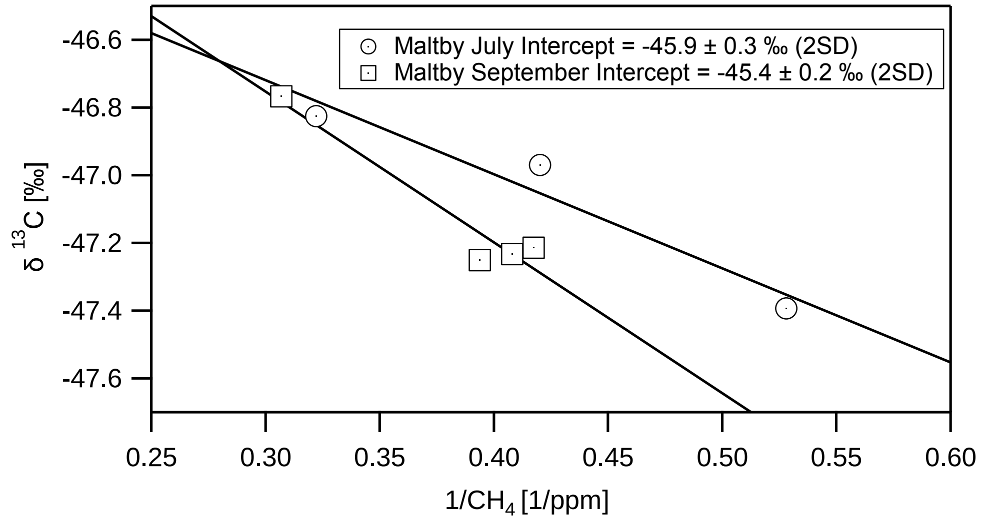

Figure 5.25 Keeling Plots based on samples collected around Maltby Colliery in July and September 2013.

5.2.3.3 Kellingley Colliery

Although mining has considerably declined, the Kellingley colliery is still open. It is a deep mine situated in North Yorkshire and its production potential is estimated to be exploited beyond 2020, working the Warren House seam. So far the Beeston and the Silkstone coal seams were mined, all of Upper Carboniferous age, characterised by a high quality, low sulphur coal used for coke manufacture. As Kellingley is one of the newest deep mines in England, a system of methane drainage and power generation is implemented (Holloway et al., 2005). Despite the coal methane recovery, over 9 ppm methane mole fractions were observed while driving on the north side of the coal mine on 10th July 2013. (see Figure 5.26).

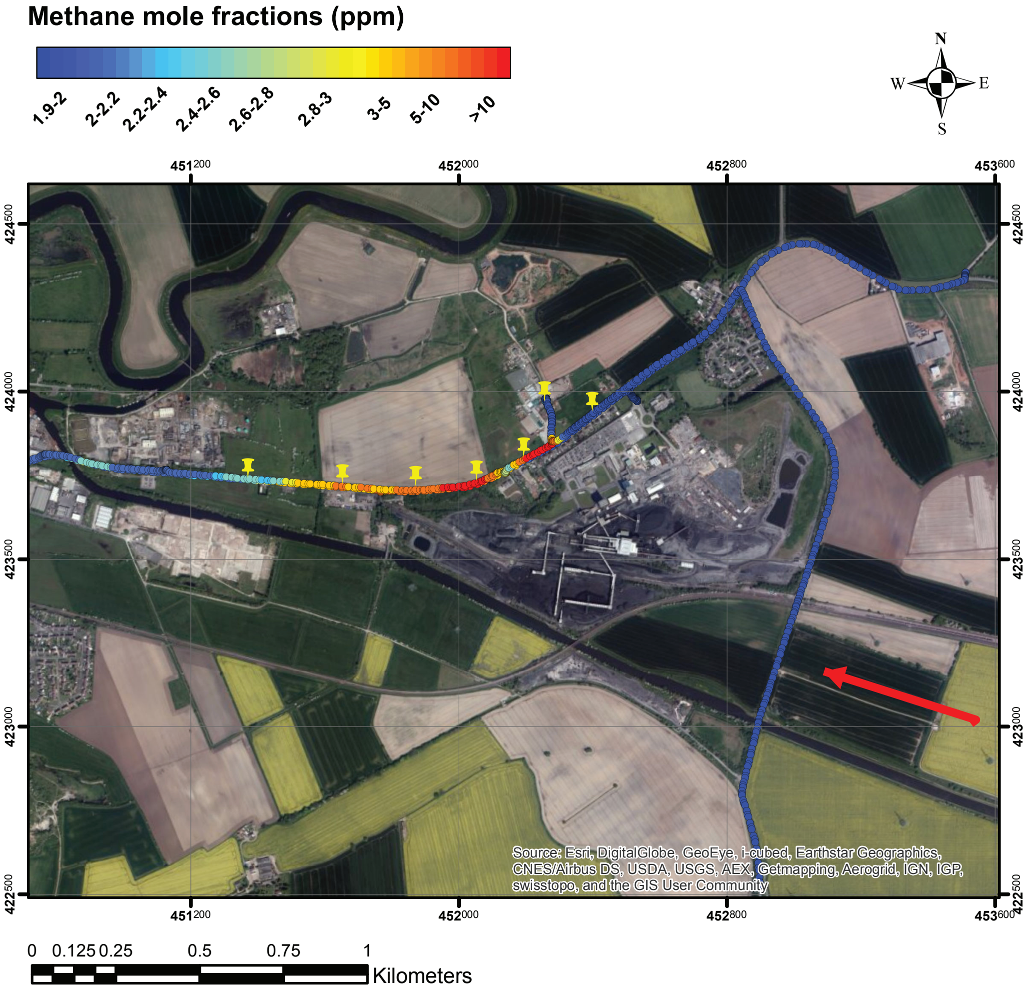

Source: Esri, DigitalGlobe, GeoEye, i-cubed, Earthstar Geographics, CNES/Airbus DS, USDA, USGS, AEX, Getmapping, Aerogrid, IGN, IGP, swisstopo, and the GIS User Community

Figure 5.26 ArcGIS plot of methane mole fractions in ppm recorded downwind of Kellingley coal mine in July 2013. The grid coordinates are displayed in the British National Coordinates System. The red arrow represents the wind direction and yellow pushpins the samples collected.

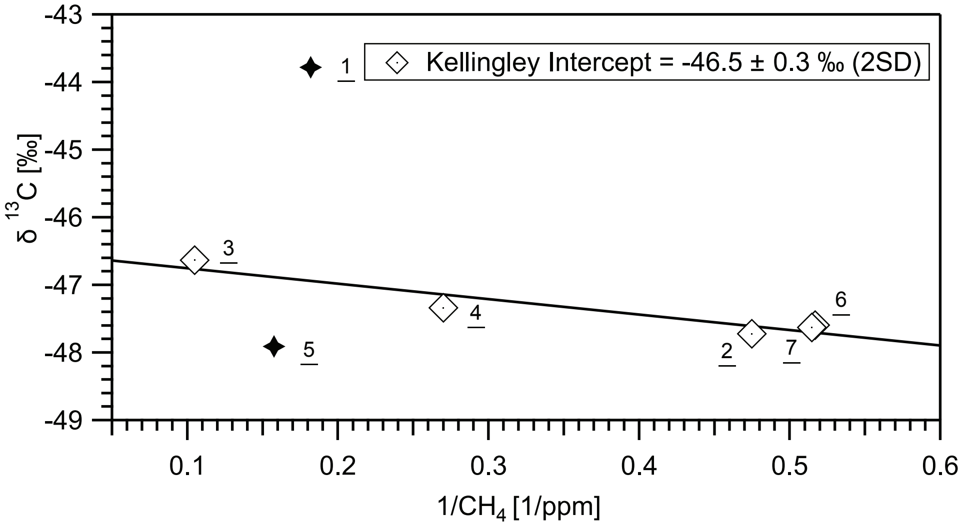

Figure 5.27 Keeling plot based on samples collected around Kellingley Colliery on 10th July 2013

Five out of seven samples collected were used for the Keeling Plot analysis and an intercept value of -46.5 ±0.3 ‰ (2SD) was obtained (Figure 5.27). Samples number 1 and 5 are thought to be representative of other small methane sources than the main methane plume originating from the colliery (e.g. gas leak for sample number 1).

5.2.3.4 Thoresby

Thoresby is one of the UK's largest coal mines in Nottinghamshire, exploiting the Parkgate seam. The mining is currently taking place at about 650 m underground. Although methane is drained, used for 2.8 MWe electrical power generation (Holloway et al., 2005), mole fraction levels of 4.6 ppm were observed in the downwind plume.

The methane plume was transected three times and 9 samples were collected (see Figure 5.28).

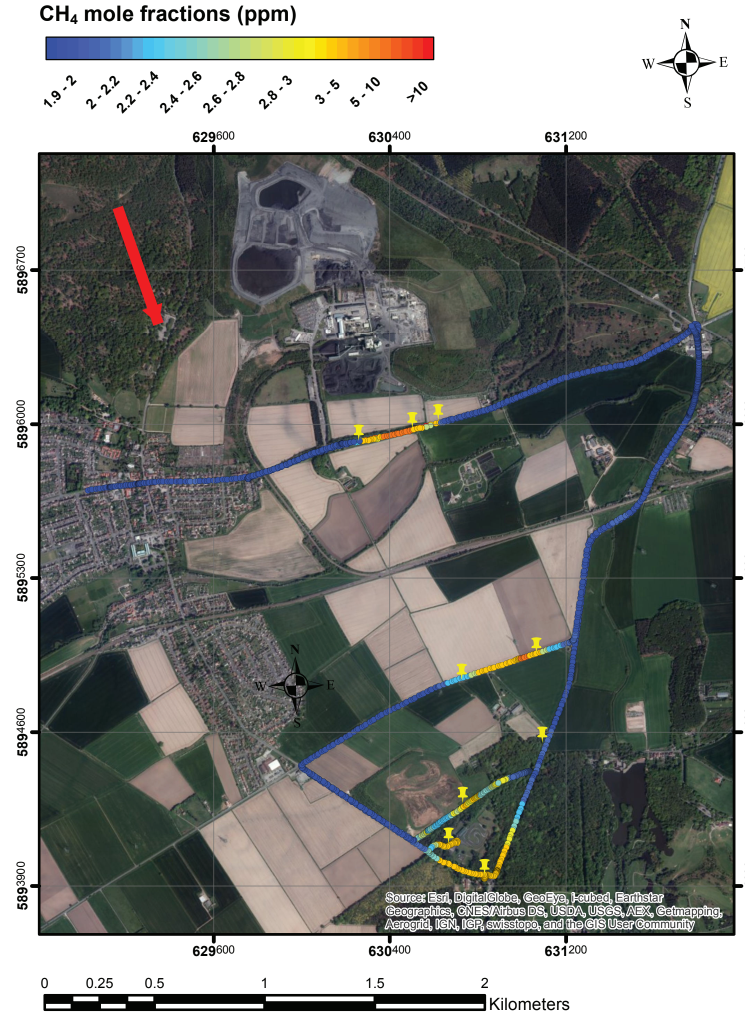

Figure 5.28 ArcGIS plot of methane mole fractions in ppm recorded downwind of Thoresby coal mine in November 2013. The grid coordinates are displayed in the British National Coordinates System. The red arrow represents the wind direction and the yellow pushpins the samples collected.

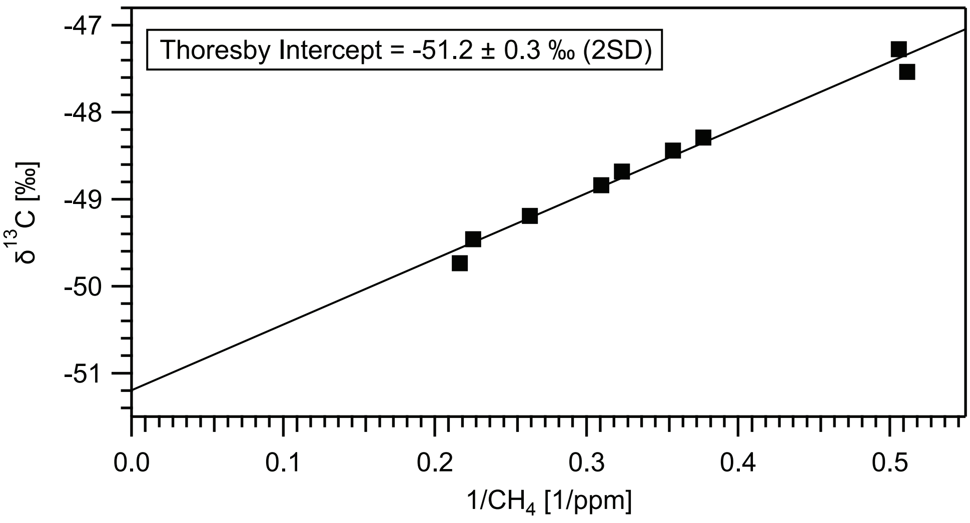

Figure 5.29 Keeling plot based on samples collected around Thoresby Colliery on 22nd November 2013.

The Keeling plot intercept of -51.2 ±0.3 ‰ (2SD) (Figure 5.29) indicates more ^{13}C depleted methane emissions than those sampled from the South Yorkshire mines. The Parkgate seam is the one exploited also in Maltby colliery, meaning that the difference in the isotopic signature between emissions from Maltby and Thoresby cannot be entirely ascribed to the coal type. For instance, a lighter source signature can be caused by the mixing with recently formed biogenic methane in association with incursion of meteoric water (see Chapter 5.2.1).

5.2.3.5 Daw Mill

The Daw Mill colliery, before its closure in March 2013, was Britain's biggest coal producer, exploiting the Warwickshire Thick seam, which lies between 500 and 1000 m in depth. The estimated methane content of this seam is low (typically about 1.7 m^3/tonne) and, furthermore, a ventilation system is implemented, so that the coal mine methane potential is curtailed (Drake, 1983). During the sampling, the highest methane mole fractions (≈5 ppm) were recorded only at the edge of the colliery (Figure 5.30), whereas, driving downwind of the site at further distances, only background values were measured. A source isotopic signature of -51.4 ±0.2 ‰ (2SD) is found by Keeling plot analysis (Figure 5.31), consistent with the one characterising Thoresby colliery.

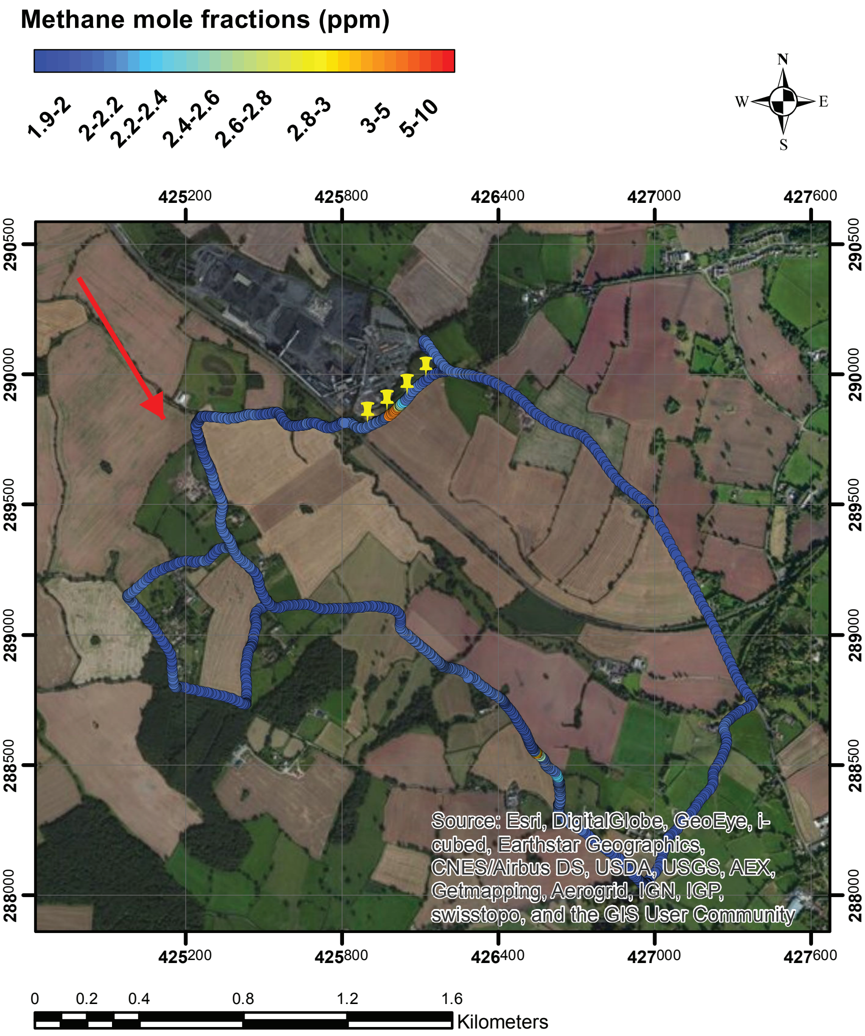

Source: Esri, DigitalGlobe, GeoEye, i-cubed, Earthstar Geographics, CNES/Airbus DS, USDA, USGS, AEX, Getmapping, Aerogrid, IGN, IGP, swisstopo, and the GIS User Community

Figure 5.30 ArcGIS plot of methane mole fractions in ppm recorded downwind of Daw Mill coal mine in November 2013. The grid coordinates are displayed in the British National Coordinates System. The red arrow represents the wind direction and the yellow markers the air samples collected.

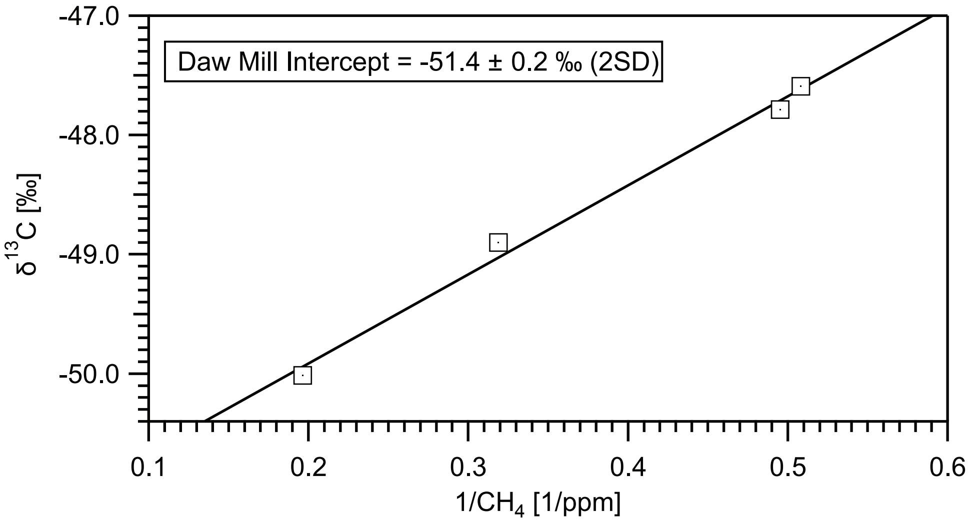

Figure 5.31 Keeling plot based on samples collected ardownwind of Daw Mill on 22nd November 2013.

5.2.4 Welsh Coal Mines

Methane emissions from coal mines in Wales were sampled in order to characterise methane releases from a different rank of coal. The area investigated extended from Cwmllynfell to Merthyr Tydfil, embracing the anthracite belt (see Figure 5.32).

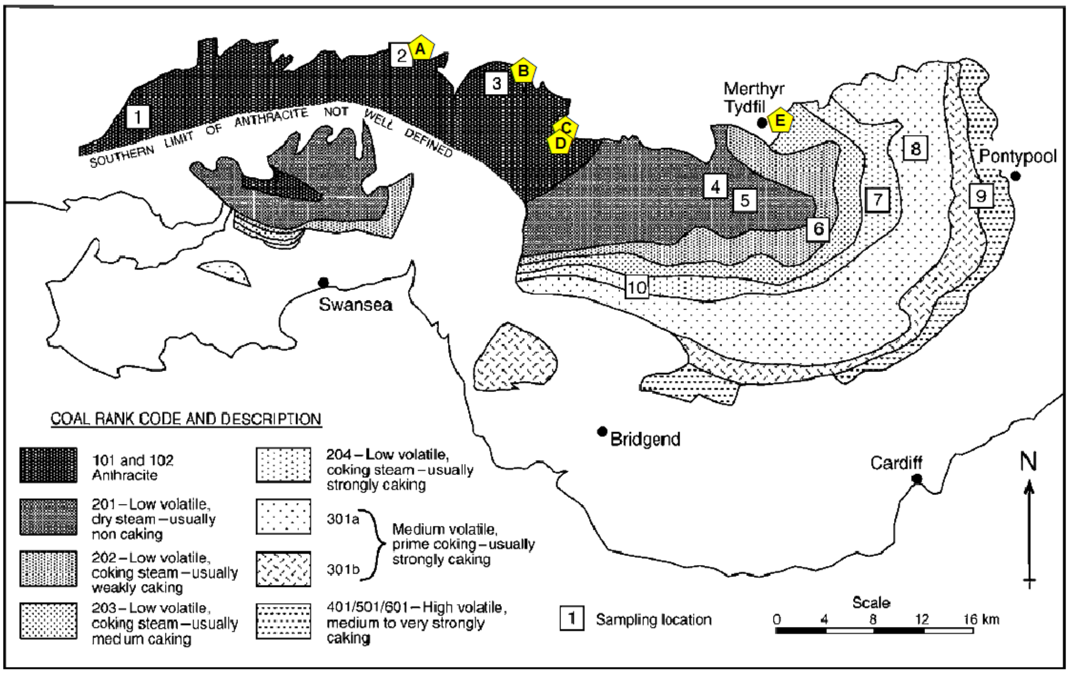

Figure 5.32 Coal rank variation in the South Wales basin (Alderton et al., 2004). The coal rank has been classified according to the British Coal Board rank classification scheme, which is based on coal volatile content and coking properties (Adams, 1967; Williamson, 1967). Symbols in yellow represent the sites sampled for this study: Cwmllynfell (A), Abercrave (B), Unity coal mine (C), Aberpergwm coal mine (D), Merthyr Tydfil (E).

A comparison between the isotopic composition of methane emissions from anthracite mines and English collieries, all mining bituminous coal, gives an insight into the link between coal rank and the methane isotopic signature. Both deep and opencast coal mines in Wales were explored on 17th October 2013. High methane mole fractions were observed just downwind of deep mines, whereas only slightly above background methane mole fractions were recorded next to opencast mines. No significant methane emissions were measured in Merthyr Tydfil and Hirwaun, where two big opencast mines are located.

The South Wales coalfield is estimated to have the highest measured seam gas content in the UK (Creedy, 1991). The Tower colliery (the opencast mine in

Hirwaun) had to cope with several issues related to methane emissions and in 1999 the colliery began to utilise the methane drained to generate electricity. Conversely, the deep mine Aberpergwm, which closed in December 2012, did not operate coal mine methane schemes and methane is vented up to the surface as part of standard operation systems (Holloway et al., 2005). That might explain the high methane mole fractions recorded when approaching Aberpergwm deep coal mine. Air samples were also collected near Unity deep mine, Wales' largest drift mine, which reopened in 2007 and is located in the town of Cwmgwrach, only one mile away from Aberpergwm. Methane mole fraction peaks of 6 ppm were observed downwind of both deep mines. All the surveyed anthracite mines are listed in the 2012 methane inventories as methane hotspots, as shown in Figure 5.33.

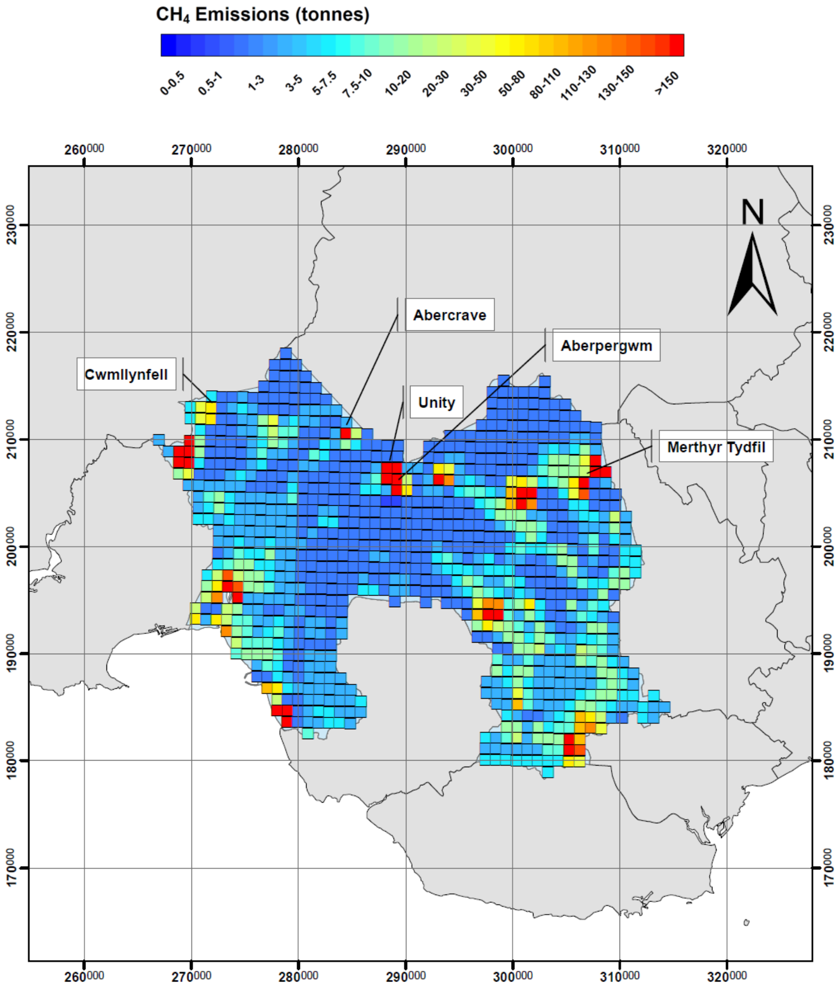

Figure 5.33 2012 emission map for the surveyed Welsh coal mines. The grid coordinates are displays in the British National Coordinate System.

5.2.4.1 Welsh Deep Mines: Aberpergwm and Unity Coal Mines.

An isotopic source signature of -33.3‰ and -30.9‰ result from the Keeling plots based on samples collected respectively near Aberpergwm and Unity colliery, both highly ^{13}C enriched relative to Thoresby colliery, one of the English mines surveyed for this study (Figure 5.34). Despite what is asserted by several authors (see 5.2.1 Chapter), according to our measurements the link between the ^{13}C/^{12}C isotopic ratio and the coal rank seems appreciable: higher-grade coal is associated with a heavier isotopic signature of methane emissions. However, other parameters might explain the variety of δ^{13}C isotopic values, such as the depth at which the coal is mined, the occurrence of water incursion and the actual methane provenance (e.g. coal piles degassing, mining wells).

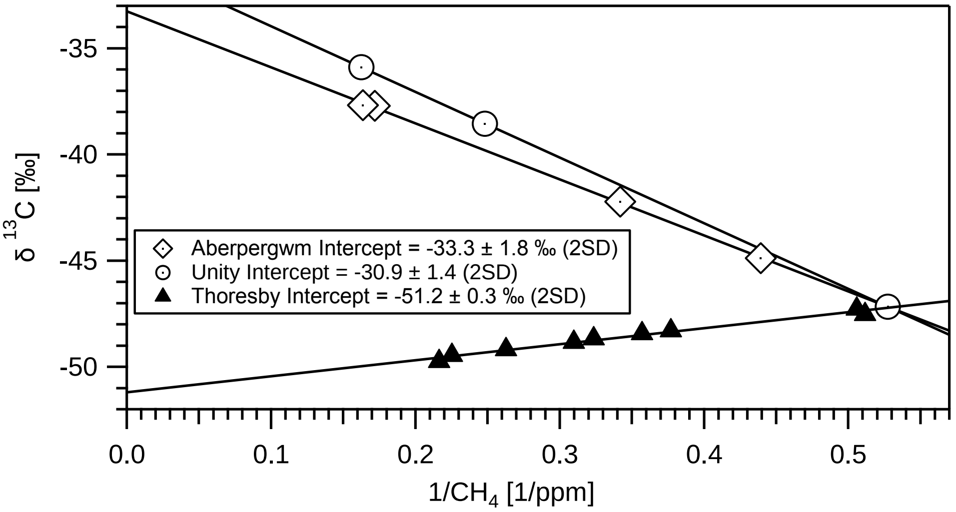

Figure 5.34 Keeling Plots based on samples collected in Aberpergwm and Unity colliery on 17th October 2013, compared with the Keeling plot based on samples collected downwind of Thoresby mine.

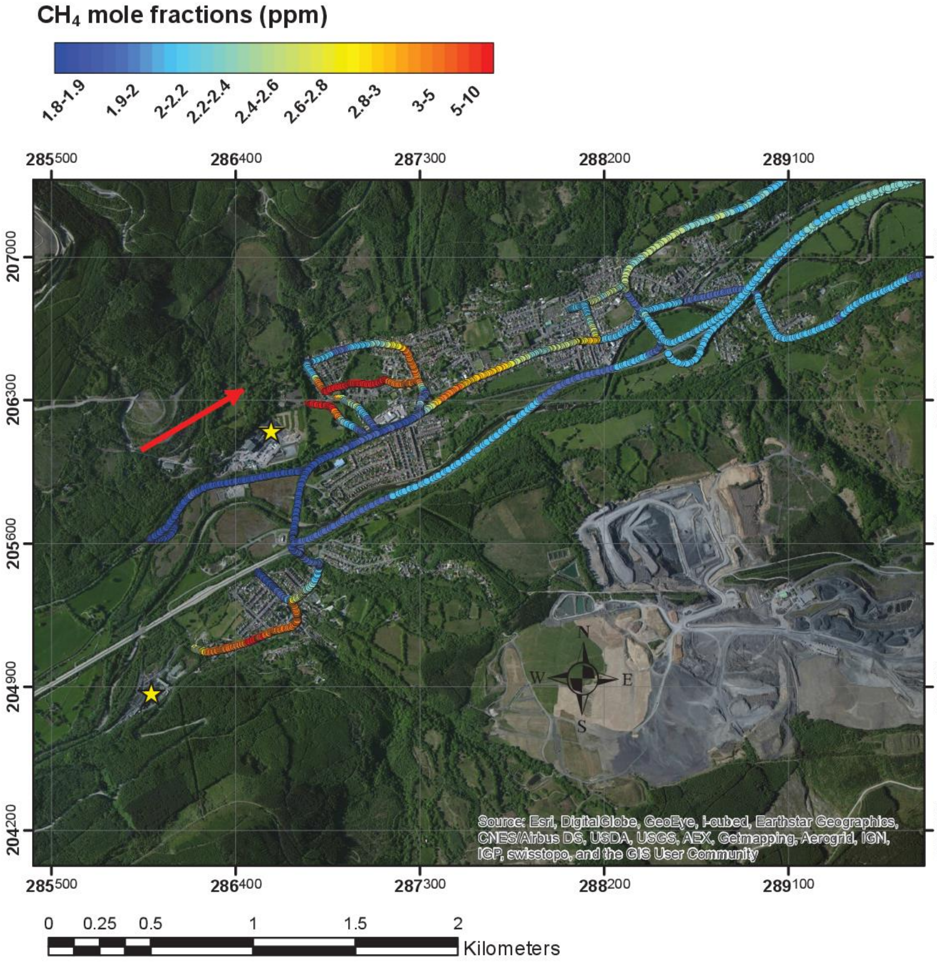

Source: Esri, DigitalGlobe, GeoEye, i-cubed, Earthstar Geographics, CNES/Airbus DS, USDA, USGS, AEX, Getmapping, Aerogrid, IGN, IGP, swisstopo, and the GIS User Community

Figure 5.35 ArcGIS plot of methane mole fractions in ppm recorded on 17th October 2013 downwind of Aberpergwm and Unity deep mines in Wales –yellow stars. The grid coordinates are displays in the British National Coordinate System. The red arrow represents the wind direction and yellow pushpins the samples location.

5.2.4.2 Welsh Opencast Mines

The Picarro mobile system was driven around opencast mines in Cwmllynfell, Abercrave, in the Swansea Valley, and Hirwaun and Merthyr Tydfil. Above 2 ppm methane mole fractions were recorded near the first two mines (Figure 5.36), whereas only background mole fractions were observed approaching the other two sites. Cwmllynfell and Abercrave collieries were closed in the 1960's as drift mines and are currently exploited as opencast mines. Nevertheless, our measurements confirm that they are still emitting methane, albeit at levels which are not significantly above background. Tower colliery in Hirwaun, still working, and the open cast mine in Merthyr Tydfill, authorized in 2006, follow the criteria of methane recovery and no relevant methane emissions stood out while sampling.

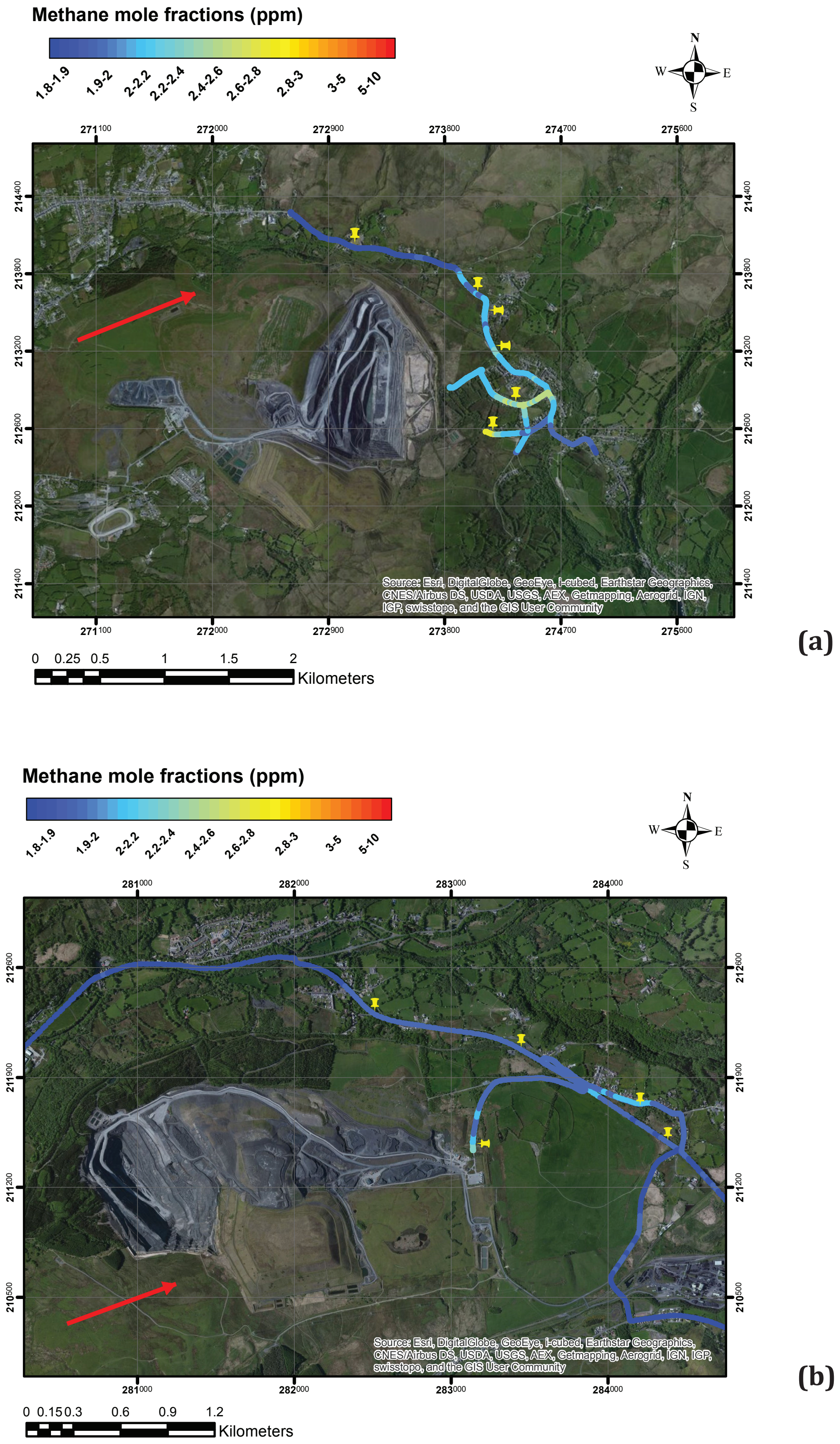

Source: Esri, DigitalGlobe, GeoEye, i-cubed, Earthstar Geographics, CNES/Airbus DS, USDA, USGS, AEX, Getmapping, Aerogrid, IGN, IGP, swisstopo, and the GIS User Community

Source: Esri, DigitalGlobe, GeoEye, i-cubed, Earthstar Geographics, CNES/Airbus DS, USDA, USGS, AEX, Getmapping, Aerogrid, IGN, IGP, swisstopo, and the GIS User Community

Figure 5.36 ArcGIS plot of methane mole fractions in ppm recorded on 17th October 2013 downwind of Cwmllynfel (a) and Abercrave (b) Colliery. The grid coordinates are displayed in the British National Coordinate System. The red arrow represents the wind direction and yellow pushpins the samples collected.

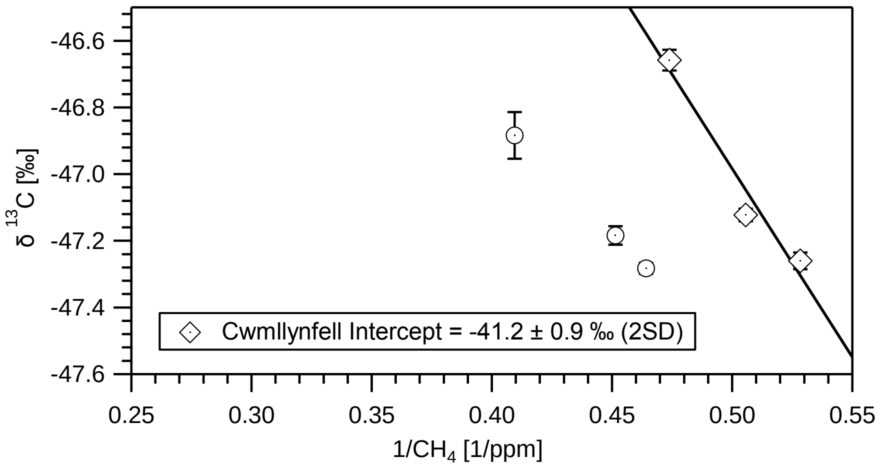

Figure 5.37 Keeling Plots based on samples collected in Cwmlynnfell coal mine on 17th October.

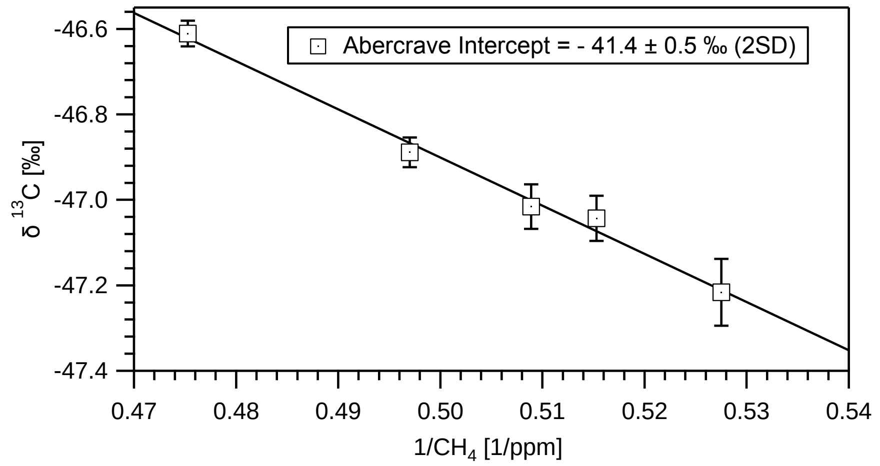

Figure 5.38 Keeling Plots based on samples collected in Abercrave coal mine on 17th of October.

A ^{13}C signature ranging from -41.4 ±0.5 to -41.2 ±0.9 ‰ (2SD) results from isotopic analysis of samples collected downwind of the opencast mines (Figure 5.37 and 5.38), approximately 10 ‰ lower than the isotopic signature characterising Welsh deep mines. Three samples collected in Cwmlynfell mine (rounded markers in Figure 5.37) do not fit in the same Keeling line of the other samples, and they might be related to a different methane source within the area, which has not been localised during the survey. Although both opencast and deep mines with relevant emissions exploited the same type of coal (pure anthracite), the shallower coal deposits in the open cast mines have been more exposed to the weathering and meteoric water, most likely associated with the production of some microbial methane, isotopically lighter.

5.2.5 Summary of ^{13}C Signatures of Coal

As Table 5.2 shows, there is a large variety of δ^{13}C-CH_4 values observed for different ages and coal rank. The global isotopic range for coal is therefore very large (Rice, 1993), but can be narrowed down when the study is focused on a specific basin. In this study, methane emissions from deep coal mines in South Yorkshire, Warwickshire and some anthracite mines in South Wales display a range of δ^{13}C values between -51 and -30 ‰ (Table 5.3), with emissions from coal mines in Wales being ^{13}C enriched relative to the other UK coal mines.

Site	Age and Rank	δ^{13}C (‰)	Author
Australia	From Miocene to Permian; maturity from brown coal to low volatile bituminous coal.	-73.0 to -43.5	J.W. Smith et al. (1981)
Queensland Basin, Australia	From Sub-bituminous to high volatile bituminous	-57.3 to -54.2	Papendick et al. (2011)
Ruhr basin, Germany	Bituminous Coal, Anthracite	-37 (-60 to -14)	Deines (1980)
Hunter Valley, Australia	Bituminous Coal	-65.1 ±1.1	RHUL unpublished data
Maules Creek, Australia	Bituminous Coal	-55.5 ±1.3	RHUL unpublished data
Western Germany	Late Carboniferous; High-volatile bituminous to anthracite.	-70.4 to -16.8	Colombo et al. (1970)
Eastern China	Carboniferous, Permian, and Triassic to Tertiary; Sub-bituminous to anthracite	-66.9 to -24.9	Dai et al. (1987)
UK, Barnsley seam	Upper Carboniferous; Bituminous Coal	-44.1	S. P. Hitchman (1990)

Table 5.2 Literature isotope values obtained by coal mines, boreholes and seam coals samples. Errors are not included in the sources, except for the calculated isotopic signatures based on samples collected during the surveys carried out by the Atmospheric Research Group at RHUL (RHUL unpublished data).

Sampling Site	Sampling Date	Max measured Mole Fractions [ppm]	δ^{13}C Signatures [‰]
Kellingley Colliery (North Yorkshire)	Nov-2013	9.54	-46.5 ±0.3
Maltby Colliery	Jul-2013	3.10	-45.9 ±0.3
(South Yorkshire)	Nov-2013	3.26	-45.4 ±0.2
Hatfield Colliery	Jul-2013	6.54	-48.3 ±0.2
(South Yorkshire)	Sept-2013	5.39	-48.8 ±0.3
Thoresby Colliery (Nottinghamshire)	Nov-2013	4.62	-51.2 ±0.3
Daw Mill Colliery (Warwickshire)	Nov-2013	5.09	-51.4 ±0.2
Cwmllynfell Colliery (Welsh)	Oct-2013	2.93	-41.2 ±0.9
Abercrave Colliery (Welsh)	Oct-2013	2.47	-41.4 ±0.5
Unity Colliery (Welsh)	Oct-2013	6.16	-30.9 ±1.4
Aberpergwm Colliery (Welsh)	Oct-2013	6.11	-33.3 ±1.8

Table 5.3 δ^{13}C-CH_4 signatures measured in this study. Errors are calculated as 2 standard deviations.

The difference in the isotopic composition has been ascribed mainly to a progression in coal rank, as it varies from bituminous coal in the English mines to pure anthracite in the north-west coalfield area of Wales (see paragraph 5.2.2). However, other parameters seem to have smaller secondary effects on the methane isotopic composition, such as the methanogenic path and the incursion of water in a coal basin. According to our measurements, two stages process can be suggested: the progression in coal rank that explains a value of -50 ‰ for bitumen and -30 ‰ for anthracite, followed by a 10 ‰ meteoric water biological depletion resulting in -40 ‰ for Welsh anthracite opencast and -60 ‰ for Australian bituminous opencast.

The highest methane mole fractions were detected next to deep mines both in England and Wales, where methane is either vented towards the surface or captured and used to generate electricity, and coal is piled on the surface (Hatfield and Maltby collieries). Since atmospheric methane mole fractions were continuously measured by driving the Picarro mobile system outside the colliery margins, and samples from wells could not be collected, the provenance of methane plumes was only inferred, after processing mole fractions and wind direction data.

Welsh and English deep mines have been proved to contribute significantly to the atmospheric methane budget, but opencast mines were identified only as a minor methane source, whereas UK national methane inventories estimate high emission levels from both deep and opencast mines (see Figure 5.20 and Figure 5.33).

5.3 Other Sources Studied: Natural Gas Distribution System, Vehicles and Ruminants.

5.3.1 Gas Distribution System

The UK has been a net importer of gas since 2004, with net import in 2013 accounting for 50 % of supply from Norway, Belgium (sourced from Norway), Netherlands and LNG by ship, mainly from Qatar (MacLeay et al., 2014). The completion of the interconnector from Netherlands at the end of 2006 and of two new LNG terminals in 2009 changed the UK's import scheme –i.e. natural gas imports from Belgium and Norway substantially increased in 2013. Accordingly, the isotopic value of the natural gas supply to SW London has changed a little in recent years, being close to -34 ‰ over 1998-99 period (Lowry et al., 2001) and close to -36 ‰ since at least 2002. Surveys around Staines, Bacton, and downwind of the Fawley refinery, in Southampton, are described in the following sections.

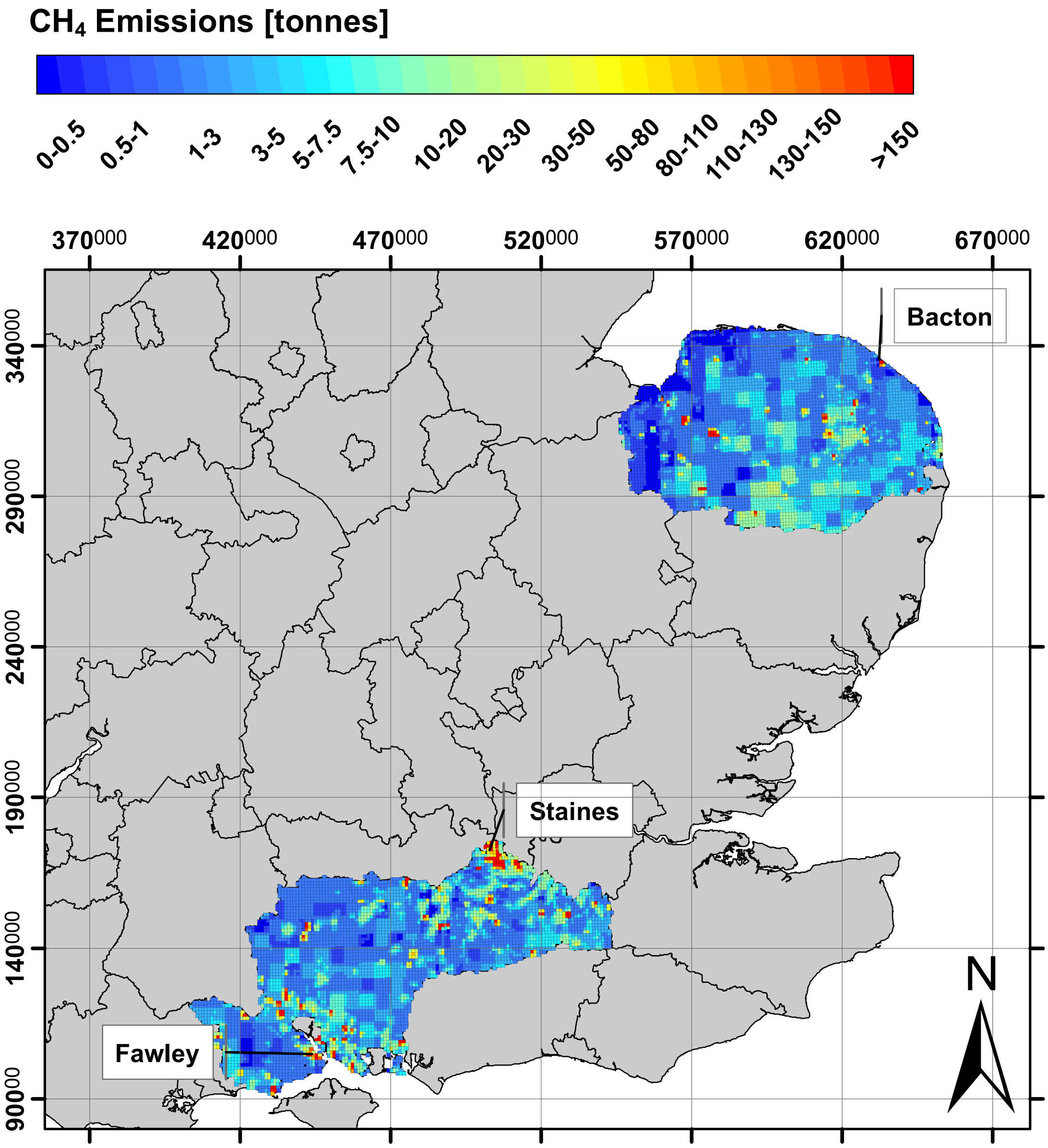

Figure 5.39 2012 emission map of the areas where the surveyed natural gas emissions are located. The grid coordinates are displays in the British National Coordinate System.

5.3.1.1 *Bacton 22nd February 2012*

The first measurement campaign to assign a new δ^{13}C-CH_4 isotopic signature to natural gas was carried out in Bacton, on the Norfolk coast, before the development of the RHUL Picarro mobile system. The map in Figure 5.40 shows the national gas transmission system and highlights the importance of this gas installation, where pipelines bring all southern and much northern North Sea Norwegian gas onshore, as well as gas from the interconnector pipeline to Belgium.

Source: International Energy Agency and DECC

Figure 5.40 National gas transmission system in 2013. Source: (MacLeay et al., 2014).

Seven samples were collected downwind of the gas works ("Bac" samples in Figure 5.41) and 4 along the coast (Figure 5.41 and Figure 5.42). The first five samples downwind of the gas plant were interpolated in a different Keeling plot from the two samples collected further south. The air sample on the coast in Figure 5.41 was used as background of "Bac5" and "Bac6" samples, as the wind was coming from east, and a δ^{13}C-CH_4 source signature of -36.1 ±0.3 ‰ (2SD) was found by Keeling plot analysis (see Figure 5.43). The δ^{13}C-CH_4 source signature resulting from the Keeling plot based on the first five samples was slightly enriched, -34.9 ±2.4 ‰ (2SD), which might indicate a small proportion of methane emissions derived from incomplete gas combustion during flaring operations. The intercept value of -56.7 ±1.5 ‰ (2SD), calculated with the samples along the coast, represented the isotopic signature of continental air, according with back-trajectories computed with the NOAA HYSPLIT (Hybrid Single Particle Lagrangian Integrated Trajectory) model for the previous 72 hrs, which show the continental provenance of air masses.

Figure 5.41 Location of samples collected downwind of the refinery in Bacton.

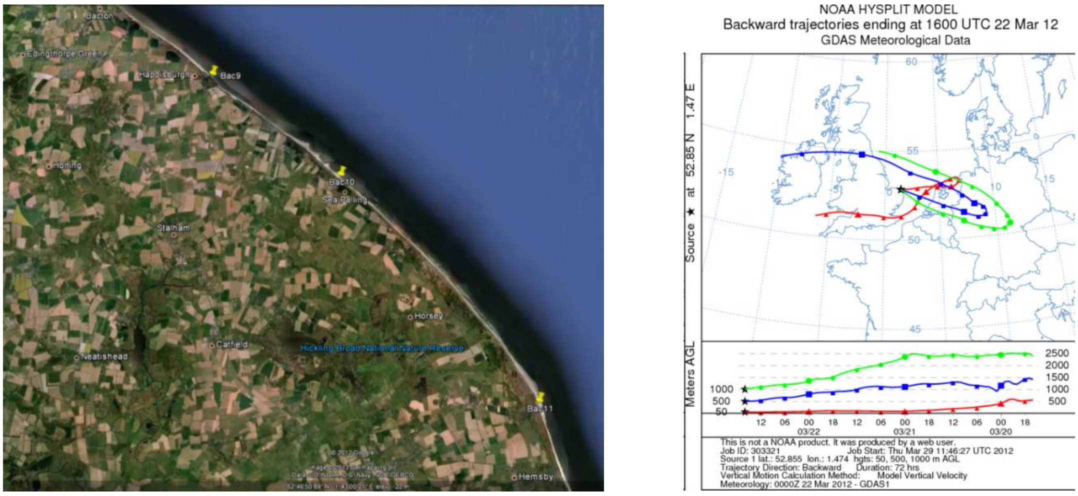

Figure 5.42 Location of samples collected along the coast at the southern side of the refinery in Bacton (on the left); NOAA HYSPLIT back-trajectories (on the right).

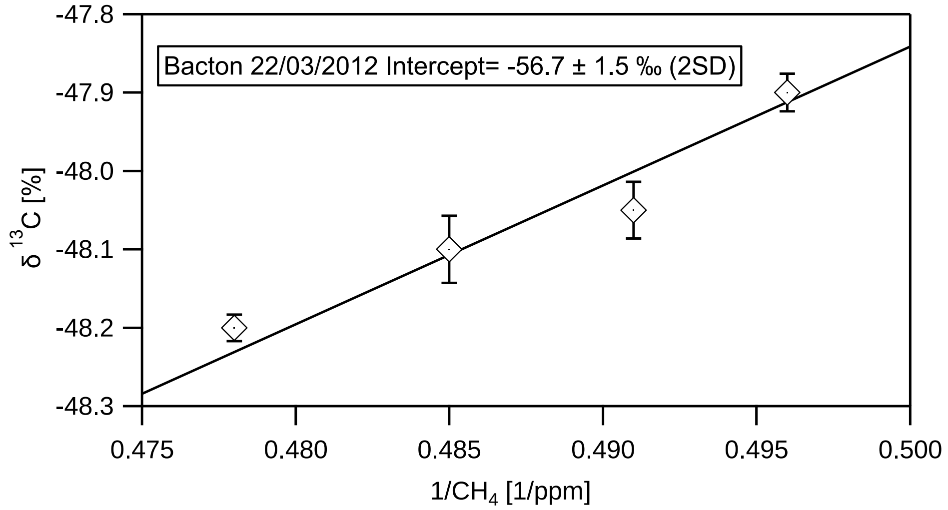

Figure 5.43 Keeling plot of samples collected in Bacton on 22nd February 2012.

5.3.1.2 Bacton 30 April 2014

Another measurement campaign in Bacton was carried out on 30th April 2014, by driving the mobile Picarro system on public roads in the area. The downwind plume was transected three times and 17 samples were collected. The background sample was collected further north along the coast. Red pushpins in Figure 5.44 represent samples with the highest methane mole fractions, all located on the closest transect to the gas works. The maximum concentration found approached 7.6 ppm. The source signature of the Keeling plot based on the three highest mole fraction samples was -32.3 ±0.3 ‰ (2SD), more ^{13}C enriched than the one calculated with all the other samples collected (-35.7 ±1.2 ‰ (2SD)), confirming the occurrence of another methane source than leaks and releases from venting operations. Since the distributed natural gas is supposed to be characterised by the same isotopic signature, the most ^{13}C enriched methane emissions might originate from the incomplete combustion of natural gas within the refinery, as inferred after the previous survey.

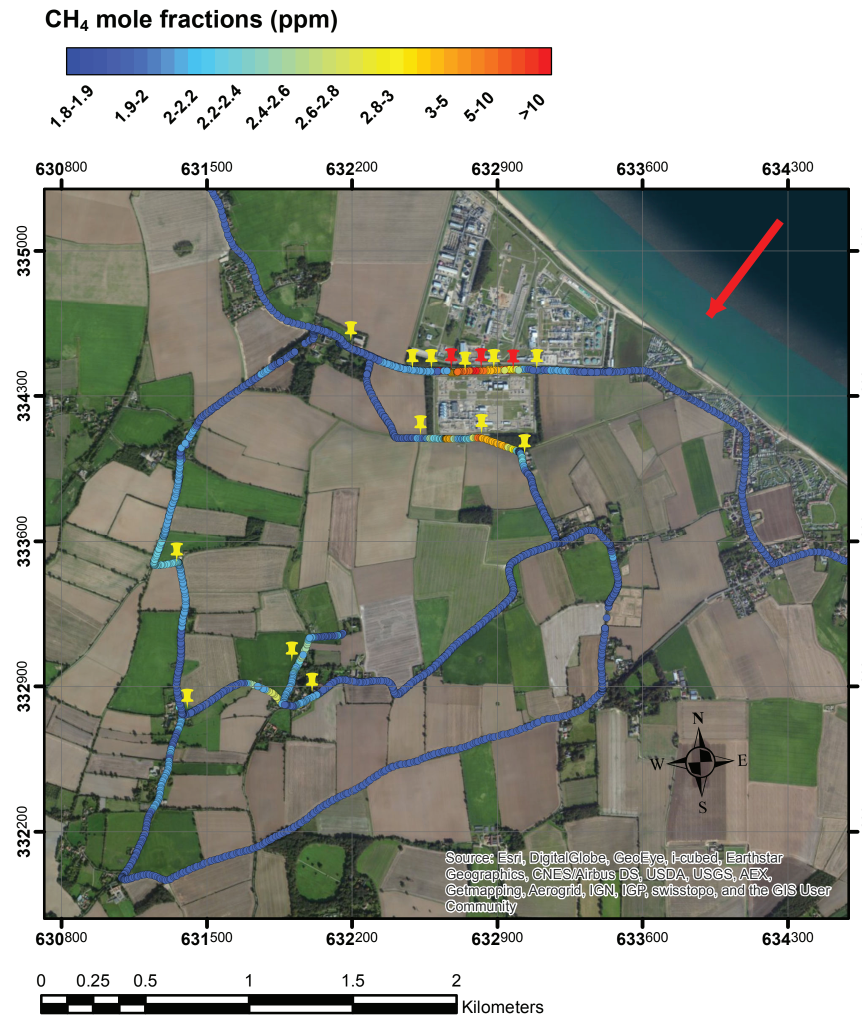

Source: Esri, DigitalGlobe, GeoEye, i-cubed, Earthstar Geographics, CNES/Airbus DS, USDA, USGS, AEX, Getmapping, Aerogrid, IGN, IGP, swisstopo, and the GIS User Community

Figure 5.44 ArcGIS plot of methane mole fractions recorded downwind of Bacton refinery on 30th April 2014. The grid coordinates are displayed in the British National Coordinates System. The red arrow represents the wind direction and the yellow markers the location of the air samples collected.

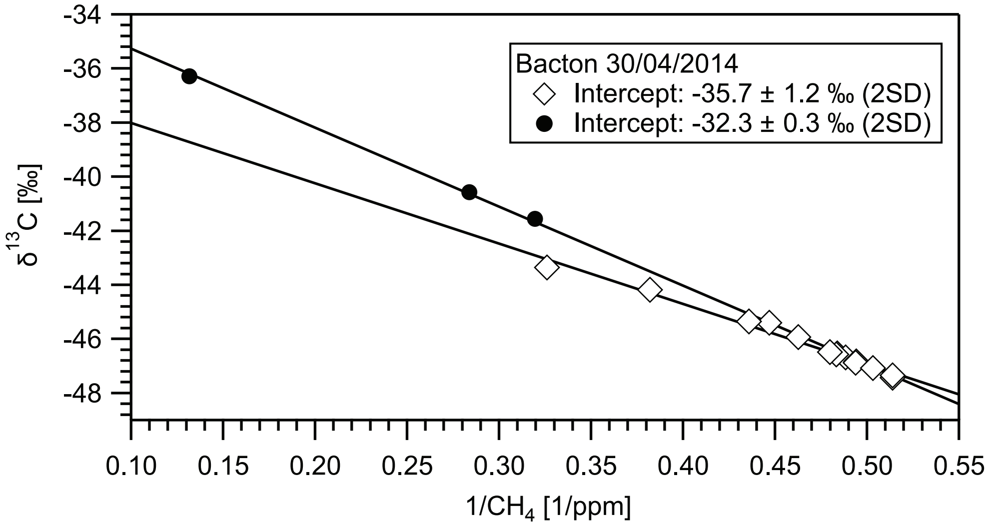

Figure 5.45 Keeling plot based on samples collected in Bacton on 30th April 2014. Black markers represent the three highest mole fraction samples.

5.3.1.3 Staines 11th April 2014

A 1.2 km path was surveyed on the south (downwind side) of the Staines storage facility, and 16 samples were collected for isotopic analysis with mole fractions ranging from 1.98 to 3.85 ppm. Figure 5.46 shows that peaks were observed approximately at the same location by driving back and forth for a few times along the same downwind transect through the emission plume. The three methane peaks highlighted suggest that there are several leaks in the gas distribution system along with the storage tank ("gasometer") that is located in the middle of the transect. The Keeling plot for the whole transect (Figure 5.47) shows a constant origin for the methane of -36.3 ±0.3 ‰ (2SD) that is consistent with a dominant thermogenic North Sea gas source.

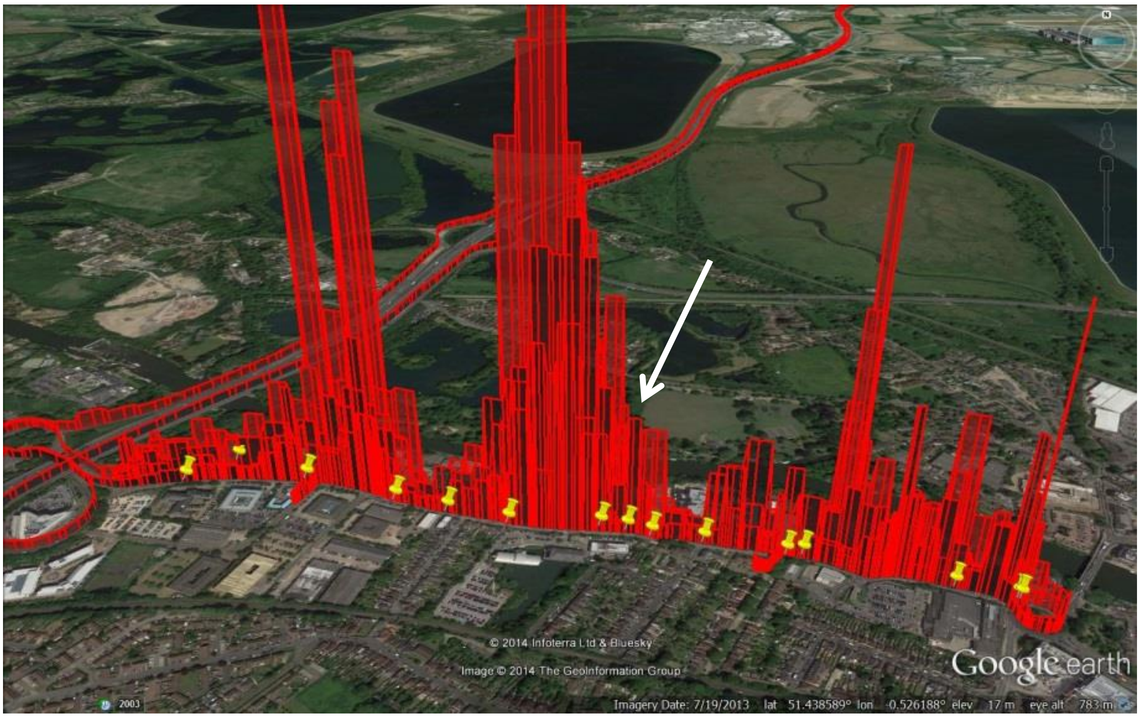

Figure 5.46 Google Earth view of methane mole fraction columns measured along the transect downwind of the gasometer that is located on the A308 in Staines, on 11th April 2014. Yellow markers represent samples location. The white arrow indicates the gasometer location.

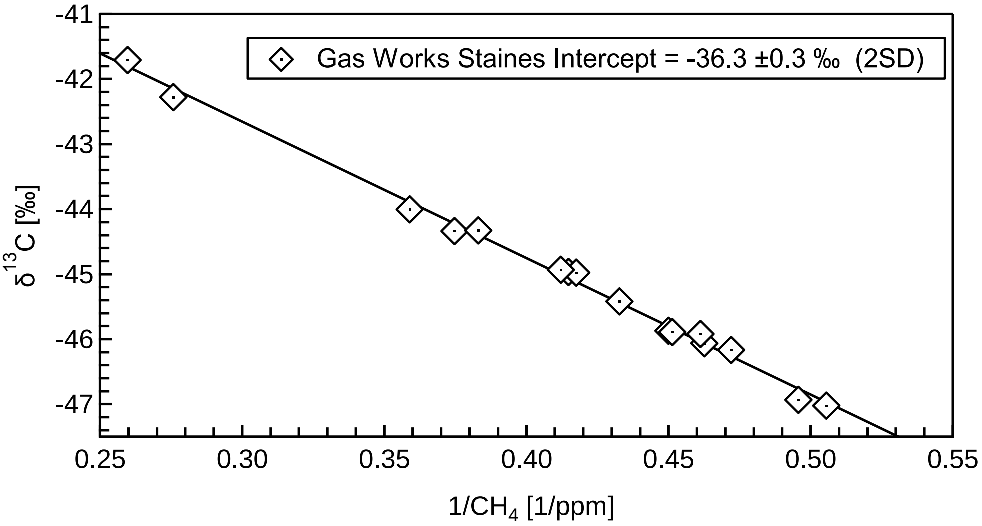

Figure 5.47 Keeling plot based on samples collected downwind of gas works in Staines on 11th April 2014.

5.3.1.4 *Fawley Refinery 18th March 2015*

Fawley refinery, in Southampton, is the largest refinery in the UK. Within the refinery the crude oil is split into separate fractions in distillation towers, called "pipe stills", which are treated further in the chemical facility that is integrated with the refinery, producing a wide range of higher olefins[7].

As natural gas is usually found dissolved in the oil, during oil production methane emissions result primarily from venting and flaring gas from oil wells and oil storage tanks. During the survey carried out on 18th March 2015, the Picarro Mobile system was driven downwind of the refinery and three main methane peaks were observed (see Figure 5.48). The biggest methane plume was intercepted downwind of the north side of the refinery, where some of the oil storage tanks are located, measuring over 5 ppm methane mole fractions. Another methane peak was measured a further 200 m south, and another one on the southern side of the refinery, downwind of pipe stills and the Cogen (Combine heat and power generation) generator that burns refinery gas.

A source signature of -38.5 ±0.6 ‰ (2SD) was calculated with all the 8 samples collected (see yellow pushpins in Figure 5.48), which is fairly consistent with the

---

[7] http://www.exxonmobil.co.uk/UK-English/about_what_refining_fawley.aspx

isotopic range ascribed to the natural gas distributed to SE England, although the crude oil processed in Fawley, and thus the joint natural gas, comes from the North Sea, Russia, West Africa and South America.

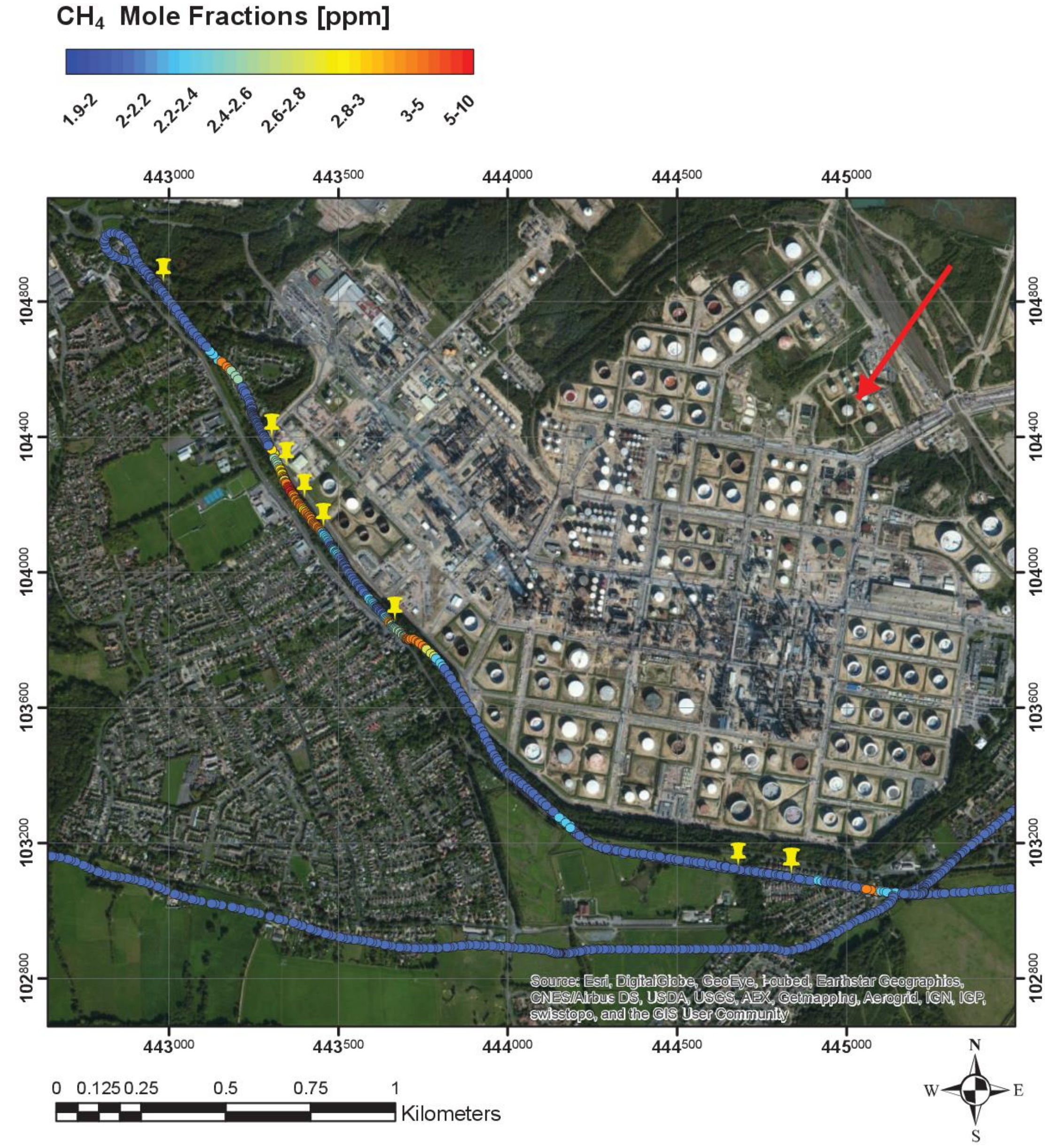

Figure 5.48 ArcGIS plot of CH_4 mole fractions recorded downwind of Fawley refinery on 18th March 2015. Red arrow represents the wind direction, yellow pushpins sample locations.

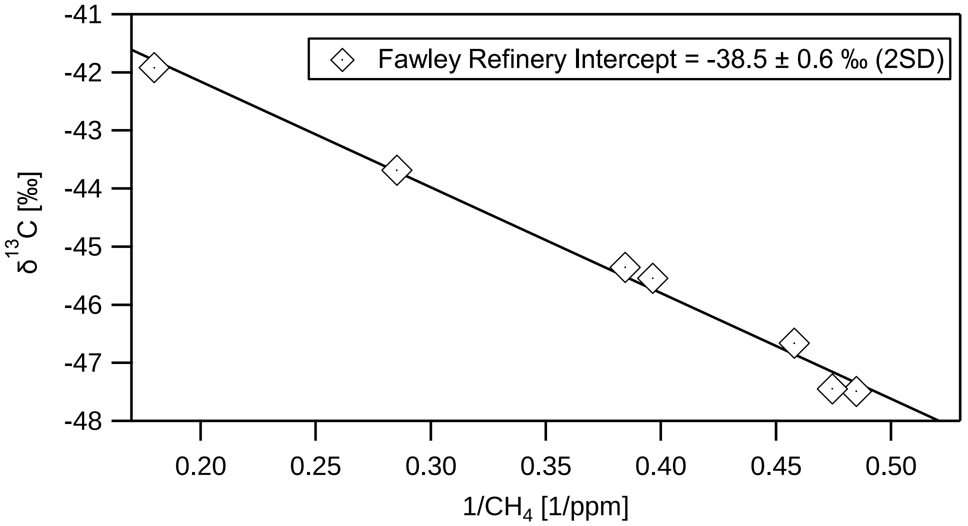

Figure 5.49 Keeling plot based on samples collected downwind of Fawley refinery on 18th March 2015.

5.3.1.5 Natural Gas Measurements in RHUL Laboratory

The isotopic signature of natural gas was measured also in the geochemistry laboratory of the Earth Science Department at RHUL, collecting samples from the gas tap monthly and measuring their isotopic signature. Results are shown in Table 5.4.

Date of sampling	**δ^{13}C-CH$_4$**
24/11/2011	-37.60 ±0.02
21/12/2011	-37.09 ±0.02
26/01/2012	-38.16 ±0.03
06/03/2012	-35.92 ±0.04
29/03/2012	-37.44 ±0.04
01/05/2012	-37.77 ±0.04
03/09/2012	-37.99 ±0.04
13/11/2012	-35.79 ±0.02

Table 5.4 Isotopic signatures of natural gas samples collected from the gas tap of the geochemistry laboratory at RHUL.

The average value of -37.3 ±0.9 ‰ (2SD) is in good agreement with the source attributions calculated after the measurement campaigns described in previous sections.

5.3.1.6 Summary

The $\delta^{13}C-CH_4$ range for the natural gas has been constrained to a value of -36 ‰. Table 5.5 summarises the $\delta^{13}C$ source signatures of methane plumes sampled downwind of the gas installations and the refinery surveyed, and the isotopic values of the samples collected in the RHUL laboratory.

Gas Installation	**$\delta^{13}C$ source signature calculated [‰]**
Bacton	-36.1 ±0.3
	-35.7 ±1.2
Staines	-36.3 ±0.3
Fawley Refinery	-38.5 ±0.6
RHUL geochemistry laboratory	-37.3 ±0.9

Table 5.5 $\delta^{13}C$ source signatures of methane plumes sampled and of the natural gas measured in the RHUL laboratory. Errors in the $\delta^{13}C$ signatures are calculated as 2 standard deviations.

Natural gas samples from Holland and Italy were also analysed at RHUL, giving values of -29.5 ±0.9 ‰ (2SD) and -47.6±0.9 ‰ (2SD) respectively. In the NW European Atlas report (Lokhorst, 1997), carbon isotope ratios between -33 and -36 ‰ for the Carboniferous reservoir gas in the North Sea and between -30 and -24 ‰ for the Rotliegend strata in the Southern North Sea are indicated. The natural gas supply from western Siberia has been measured near source, and in St. Petersburg by the RHUL group and in Heidelberg by Levin et al. (1999), and it is characterised by an isotopic signature of -50 ‰. Because of different gas source provider countries, the isotopic characterisation of the natural gas changed over time and the new value assessed in this study can be safely taken as representative of the current natural gas supplied to the whole of SE England.

5.3.2 Vehicles

The vehicle exhaust was isotopically characterised by collecting samples directly from the exhaust of 10 cars available in the RHUL campus of different age and fuel type. Samples were collected on the same day at approximately 0.5 m from the exhaust after running the engine for ≈3 minutes. Source $\delta^{13}C-CH_4$ signatures were calculated based on one background air sample collected at the same time away from the car exhausts ($\delta^{13}C-CH_4$ value of -47.46 ±0.02 ‰ and 1.97 ±0.001 ppm mole fractions). Results are listed in Table 5.6. Two cars (Astra 2009 and Volvo 2014) were not included in the calculation of the source isotopic signature, since methane mole fractions of their exhausts were too close to background, 1.97 and 1.99 ppm respectively.

Car Make	**Year**	**Fuel Type**	**CH_4 mole fractions (ppm)**	**$\delta^{13}C-CH_4$ (‰)**	**Source $\delta^{13}C-CH_4$ (‰)**
Golf MK2	1987	Leaded	4.892 ±0.050	-26.69 ±0.09	-12.7
Mazda MX3	1998	Leaded	17.585 ±0.500	-13.11 ±0.10	-8.8
Opel Corsa	2003	Unleaded	5.149 ±0.001	-26.88 ±0.04	-14.1
Ford Focus 1.6	2007	Diesel	3.867 ±0.050	-30.46 ±0.05	-12.8
Mini Cooper	2009	Unleaded	3.202 ±0.050	-34.99 ±0.04	-15.1
Zafira	2012	Diesel	3.720 ±0.003	-32.88 ±0.01	-16.5
Twingo	2012	Unleaded	7.007 ±0.050	-21.06 ±0.06	-10.7
Audi	2013	Unleaded	2.227 ±0.001	-42.33 ±0.03	-2.9
		Mean			**-11.7 ±4.3**

Table 5.6 Methane emissions from a selection of cars from the RHUL campus. The source signature is derived from a 2-point Keeling plot.

The most recent car is the one characterised by the most ^{13}C enriched emissions, due to a high combustion efficiency of the engine, in agreement with what is stated by Chanton et al. (2000). Methane emissions from the Mazda MX3, which is one of the oldest cars, were also highly ^{13}C enriched. In a study of methane emissions from cars carried out by R. Fisher (2006) results show that, among the unleaded petrol cars, the Nissan Micra was the only car without a catalytic converter producing relatively ^{13}C enriched methane, leading to the preliminary conclusion that Japanese engines might generate methane emissions distinctively enriched in ^{13}C.

The averaged value of -11.7 ±4.3 ‰ is consistent with the value of -9 ±0.3 ‰ calculated by Nakagawa et al. (2005). Figure 5.50 shows the 2-points Keeling plots including the background and each exhaust sample.

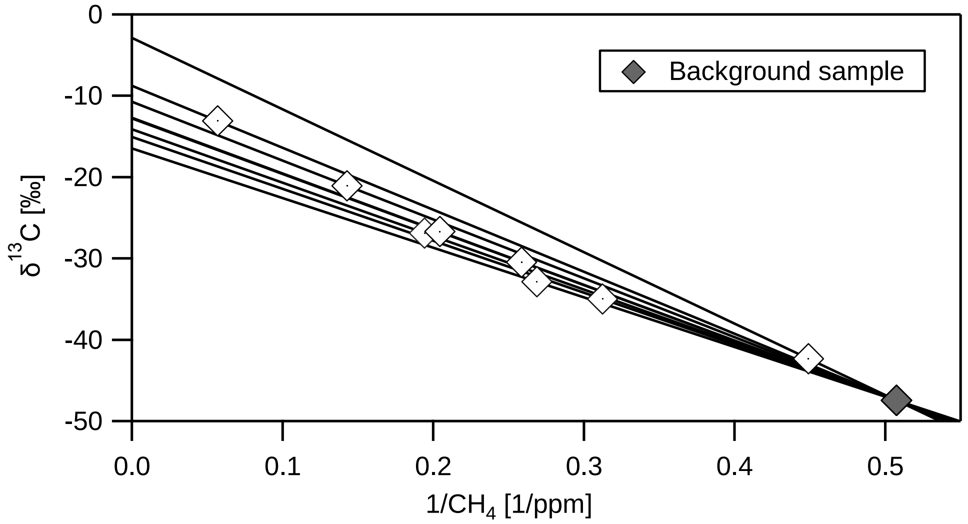

Figure 5.50 Keeling plots based on the cars exhaust samples. Each line includes the background and the exhaust sample.

5.3.3 Ruminants

The δ^{13}C source signature of methane emissions from enteric fermentation was determined firstly by sampling methane emissions inside a shed located in North Yorkshire on December 2012, and then collecting samples near a group of cows found in a farm in Dorset, during the survey with the Picarro mobile system on March 2015.

The shed in North Yorkshire hosted 80 Holstein Fresian cows, and spanned an area of 15x25 m, containing 4 rows of cubicles. Two air samples were collected each day around 9 a.m., for 5 days, one inside the shed and the second one of background air upwind of the shed at a distance of approximately 50 m. The cows' waste products were regularly removed by an automatic manure scraping system; therefore methane emissions from manure should not have interfered with emissions derived exclusively from enteric fermentation.

The Keeling plot in Figure 5.51 shows two clusters of samples, the high CH_4 mole fractions ones representing emissions inside the shed, and the background air ones, as no sample with intermediate methane mole fractions was collected in between the shed and the background location. A δ^{13} source signature of -66.3 ±0.3 ‰ (2SD) resulted from the study.

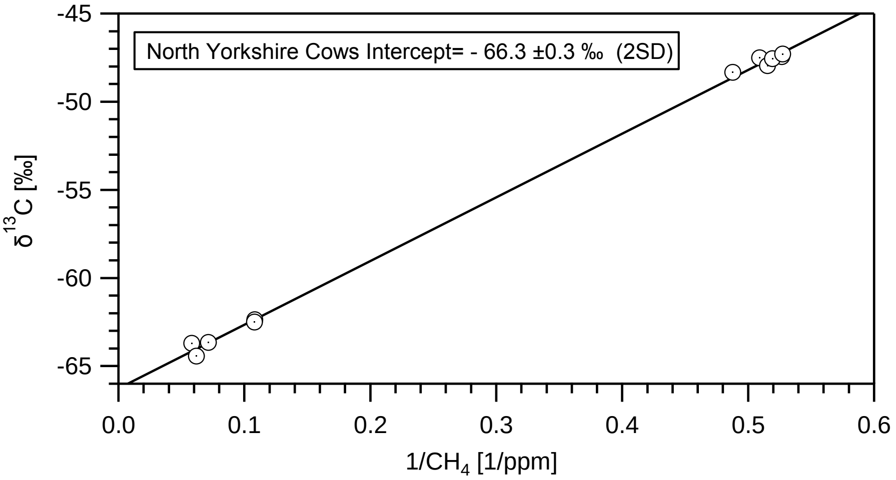

Figure 5.51 Keeling plot based on samples collected during an experiment with dairy cows conducted in December 2012.

In the search for methane plumes from cattle farming during the survey with the Picarro mobile system carried out on 19th March 2015 in Dorset, a group of 20 rare breed cows in open field were spotted next to Wytch Farm. Three samples were collected in close proximity to group, sampling the cows' breath, and the resulting Keeling plot showed an intercept of -69.4 ±3.7 ‰ (2SD), in agreement with the value previously calculated.

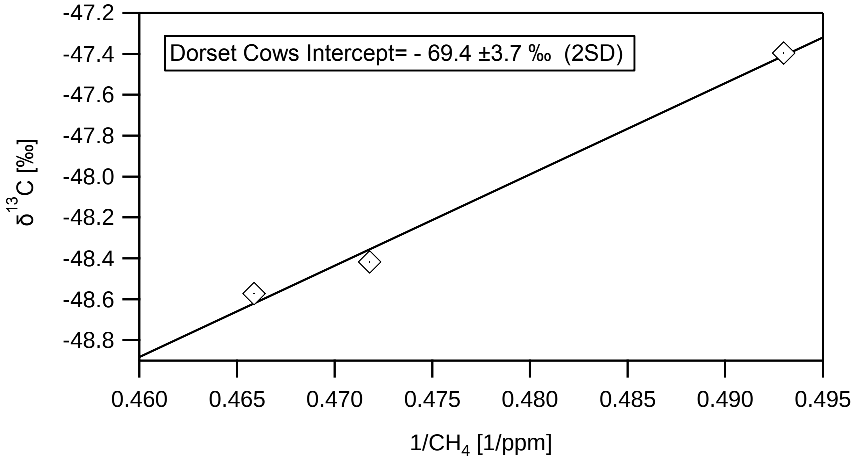

Figure 5.52 Keeling plot based on samples collected in proximity of a group of cows in Dorset.

A wide range of isotopic signatures (from -45 to -75 ‰) has been observed by Levin et al. (1993), taking as a case study a sample of cattle in the Heidelberg region. Different diets might explain this large variability, as the difference in the δ^{13} signature between C3 and C4 plants (≈14 ‰) is reflected in the emitted CH_4 isotopic value, as several studies prove (see Chapter 2.4.1). Klevenhusen et al. (2010) investigated the diet effect on the isotopic signature of milk, excreta and methane produced by a group of dairy cows in Switzerland, feeding them either with maize (C4 plant) or C3 plants. The $\delta^{13}C$-CH_4 signature of methane emitted by cows fed with maize were more enriched, averaging -57.5 against -67.6 ‰ with a C3 diet. The North Yorkshire cows' diet was C3 based and indeed the value of -67.6 ‰ is highly consistent with the first result of this study (-66.3 ‰). Bilek at al. (2001) also conducted a series of experiments to determine the effects of different diets on the isotopic signature of methane emissions from dairy cattle. An average $\delta^{13}C$-CH_4 value of -70.6 ±4.9 ‰ was found, and they demonstrated that variations in the C3/C4 content in diet does play a key role in determining the $\delta^{13}C$ of emitted CH_4, confirming the Levin et al. finding that lighter CH_4 is associated with a C3-dominated diet

5.4 Sewage Works: a Complicated Case

Sewage works embrace several methane sources, such as the biological treatment of wastewater and the anaerobic digesters, and the $\delta^{13}C$ signature of the downwind plume changes according to the variation of methane emissions from each single source, making it difficult to pin down a distinct sewage $\delta^{13}C$ signature. Mogden sewage works site, located in west London (51° 27.69' N; 0° 20.43'W), at the east side of Hounslow, was chosen as a case study for sewage treatment, as it is surrounded by public roads on which the Picarro mobile could be driven and thus methane plumes detected from any direction.

The structure of wastewater treatment is shown in Figure 5.53. The process involves firstly the passage of the sewage through the primary treatment (A) where the wastewater is held in a quiescent basin to let heavier solids settle to the bottom. Then, after the discharge of the solids, called primary sludge, the remaining liquid undergoes a biological or secondary treatment (B), performed by microorganisms in an aerobic environment. These bacteria and protozoa degrade the organic matter and bind the less soluble fractions into coagulated ones that are heavier and then can subside to the bottom of the tank. The effluent passes through a secondary clarifier (C), where the microbial biomass is separated from the treated water by gravity. The residual sludge is treated by pasteurisation and anaerobic digestion (D) and the biogas produced during this step, on average approximately 60,000 Nm^3/day, is burned in the power station (E), to power the combined heat and power engines (2.4MW each)[8].

---

[8] http://www.water-technology.net/projects/mogden-sewage-treatment-works-isleworth-london/

Figure 5.53 Mogden sewage works structure. A represents the primary treatment, B secondary treatment, C secondary clarifiers, D anaerobic digestions and E the power station.

As methane is produced by the anaerobic decomposition of organic matter, within the wastewater treatment methane is generated mainly in the primary treatment area and sludge holding tanks (see Chapter 3.1.7). During our surveys methane emissions were detected also downwind of the secondary treatment, suggesting that methane produced in the primary settling tanks may be transported in dissolved form into the secondary treatment area following the turbulent liquid flow, and the mechanical aeration may cause the gas to be stripped. However, the most important methane releases come from the ultimate disposal of sludge, from leakages in the digesters (IPCC, 2006). Those in Mogden are floating roof digesters with a sludge seal, which, due to their design, occasionally have some localised biogas releases.

The isotopic signature of the biogas generated is determined by the microbial consortia involved in the anaerobic digestion and the temperature. During anaerobic digestion, heterogeneous microorganisms degrade complex organic matter into substrates that are converted in a second stage by methanogens into methane and carbon dioxide (Toerien and Hattingh, 1969). Methanogenic bacteria occurring into the sludge are thought to be the same species living in other environments, but they are dependent on the operational temperature in digesters (Golueke, 1958). Sewage sludge in Mogden is treated in mesophilic reactors at temperatures around 35°C, which support most of bacteria of the mesophilic group. The chemical composition of the biogas produced is 60-65 % CH_4, 30-33 % CO_2 and small quantities of H_2, N_2, H_2S and H_2O[9]. During biogas combustion, residual methane derived from incomplete combustion might be released, which is isotopically heavier than the original biogas.

The variety of methane sources involved in the sewage treatment results in methane plumes that have $\delta^{13}C$ signatures correlating with the technology employed and therefore highly site specific. Methane plumes from the Mogden site were isotopically characterised driving outside the perimeter of the sewage plant. Only during the first measurement campaign the site was entirely explored, when we had full access to the site under agreement with Thames Water. The surveys carried out are described in the following sections.

5.4.1 9th July 2013

The first survey of Mogden Sewage works was carried out on 9th July 2013. Mole fractions measured are displayed in Figure 5.54. As the whole area was explored, five samples could be collected near the secondary treatment and four next to the power station, where over 20 ppm mole fractions were recorded. Methane emitted from the secondary treatment was characterised by a $\delta^{13}C$ source signature of -59.2 ±1.2 ‰ (2SD), which falls within the range of -65 and -50 ‰ suggested for fermentative processes (Whiticar et al., 1986).

The high CH_4 peak detected downwind of the power engines suggests evident leakages in that area. The Keeling plot based on the four samples collected (see black markers in Figure 5.55) shows a $\delta^{13}C$ signature relatively heavier (-48.6 ±0.7 ‰ (2SD)) than the one characterising purely biogenic methane, indicating a component of methane derived from incomplete combustion of the biogas generated.

---

[9] http://homepage.ntlworld.com/philiptomlinson/ben/mogden%20wwtp.pdf

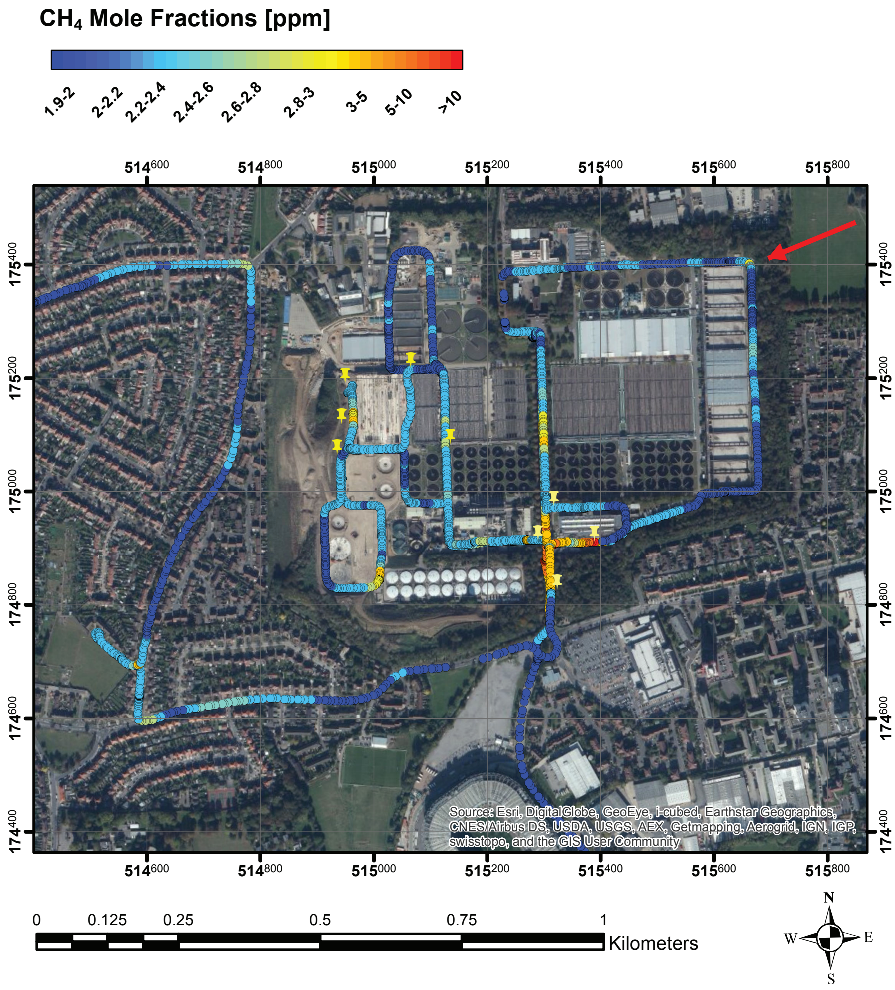

Source: Esri, DigitalGlobe, GeoEye, i-cubed, Earthstar Geographics, CNES/Airbus DS, USDA, USGS, AEX, Getmapping, Aerogrid, IGN, IGP, swisstopo, and the GIS User Community

Figure 5.54 ArcGIS plot of methane mole fractions in ppm recorded on 9th July 2013 around Mogden sewage works. The grid coordinates are displayed in the British National Coordinates System. The red arrow represents the wind direction and the yellow markers the location of the air samples collected.

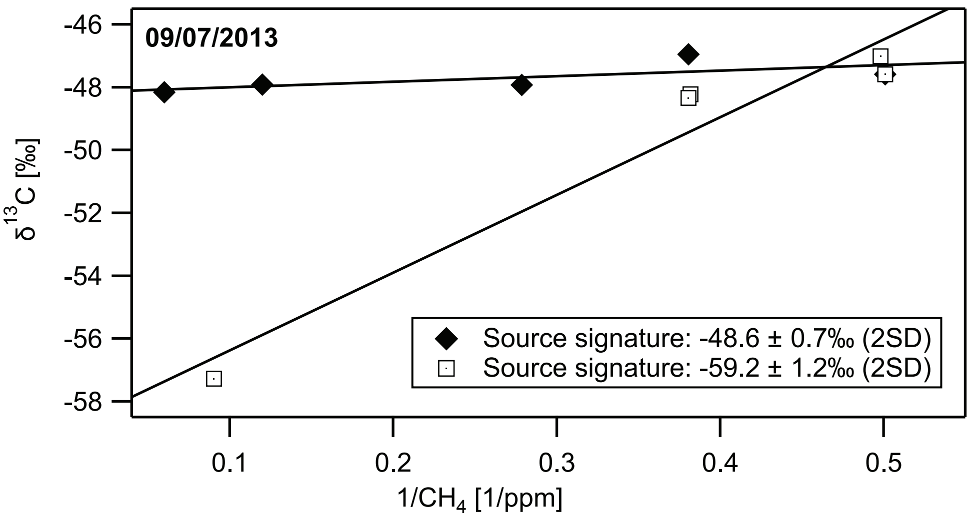

Figure 5.55 Keeling plot based on the samples collected on 9th July 2013 around Mogden sewage works. Black markers represent the samples collected downwind of the power engines.

5.4.2 4th June 2014

The survey on 4th June 2014 was carried out driving in a circuit on public roads around the outside of the sewage treatment works, trying to intersect the downwind plume from the sewage plant area. While driving, other methane sources than those involved in the sewage works were distinguished, identifiable as gas leaks. In fact, the intercept value of -38.1 ±1.2 ‰ (2SD), resulting from the Keeling plot of samples collected upwind of the sewage treatment plant and on the third transect parallel to the east side of the circuit (red pushpins in Figure 5.56), is characteristic of methane releases from the natural gas network.

Four samples were collected downwind of the sewage works, and they were interpolated in two different Keeling trends. Yellow diamonds in Figure 5.56 are associated to a source signature of -50.1 ±0.3 ‰ (2SD) (Figure 5.57), whereas yellow pushpins, which are more downwind of the power station, are linked to a slightly ^{13}C enriched isotopic signature (-47.3 ±0.3 ‰ (2SD)), revealing a partial contribution of methane released from the biogas combustion.

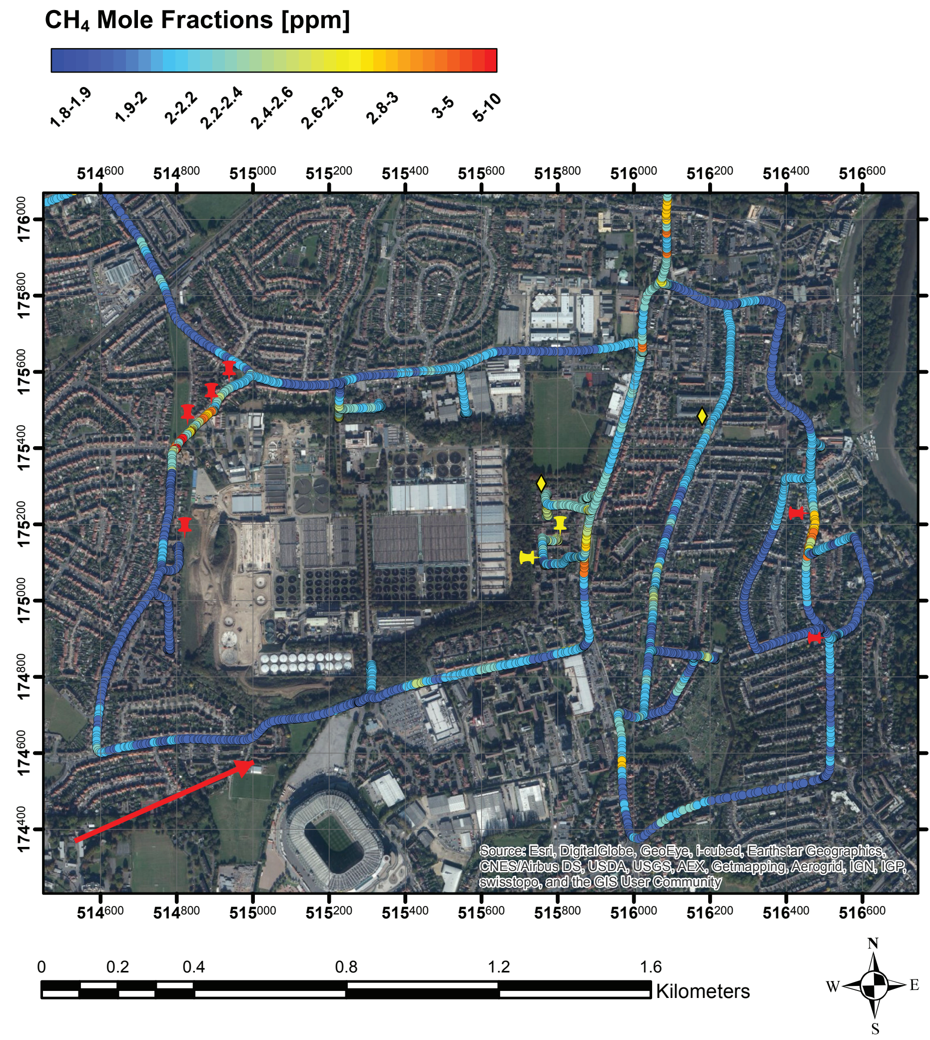

Source: Esri, DigitalGlobe, GeoEye, i-cubed, Earthstar Geographics, CNES/Airbus DS, USDA, USGS, AEX, Getmapping, Aerogrid, IGN, IGP, swisstopo, and the GIS User Community

Figure 5.56 ArcGIS plot of methane mole fractions in ppm recorded on 4th June 2014 around Mogden sewage works. The red arrow represents wind direction, yellow pushpins and diamonds represent the samples collected downwind of sewage works, red pushpins samples related to gas leaks.

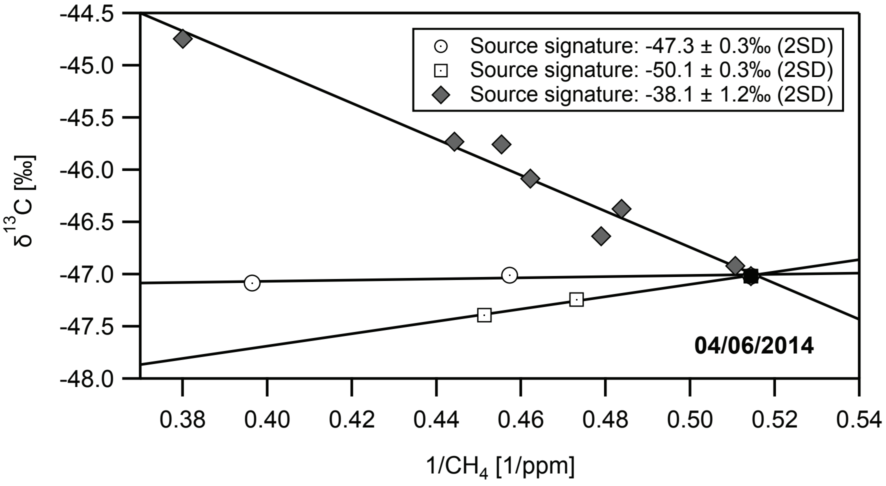

Figure 5.57 Keeling plot based on the samples collected on 4th June 2013 around Mogden sewage works. Grey markers represent samples related to gas leaks. Squared markers correspond to diamonds and circles to pushpins in Figure 5.56.

5.4.3 11th July 2014

On 11th July 2014 methane emissions from the sewage works were intercepted while driving on the southern side of the sewage plant, due to north-westerly wind. High methane mole fractions were measured also at further distance from the sewage treatment (see red markers in Figure 5.58), but a source signature of -40.3 ±0.8 ‰ (2SD), calculated using the two samples collected on the east side and the one on the north-west corner, revealed a correlation with local gas leaks rather than sewage works as thought during the survey (grey markers on the Keeling plot in Figure 5.59).

Yellow pushpins in Figure 5.58 represent samples of methane emissions from anaerobic digesters and biological treatment, which were interpolated in the same Keeling line, giving a $\delta^{13}C$ signature of approximately -51.1 ±1.0 ‰ (2SD). In fact, according to our measurements, the biogas produced in the anaerobic digesters has a fairly distinctive source signature, which is more ^{13}C enriched than the value of -59.2 ‰ characterising emissions from the secondary treatment, although falling within the range of -65 to -50 for methane derived from acetate fermentation suggested by Whiticar et al (1986). The other samples collected on the south side (yellow diamonds in Figure 5.58 and white diamonds in Figure 5.59) are thought to represent a mixture of methane emissions coming from anaerobic digesters, biogas combustion and biological treatment.

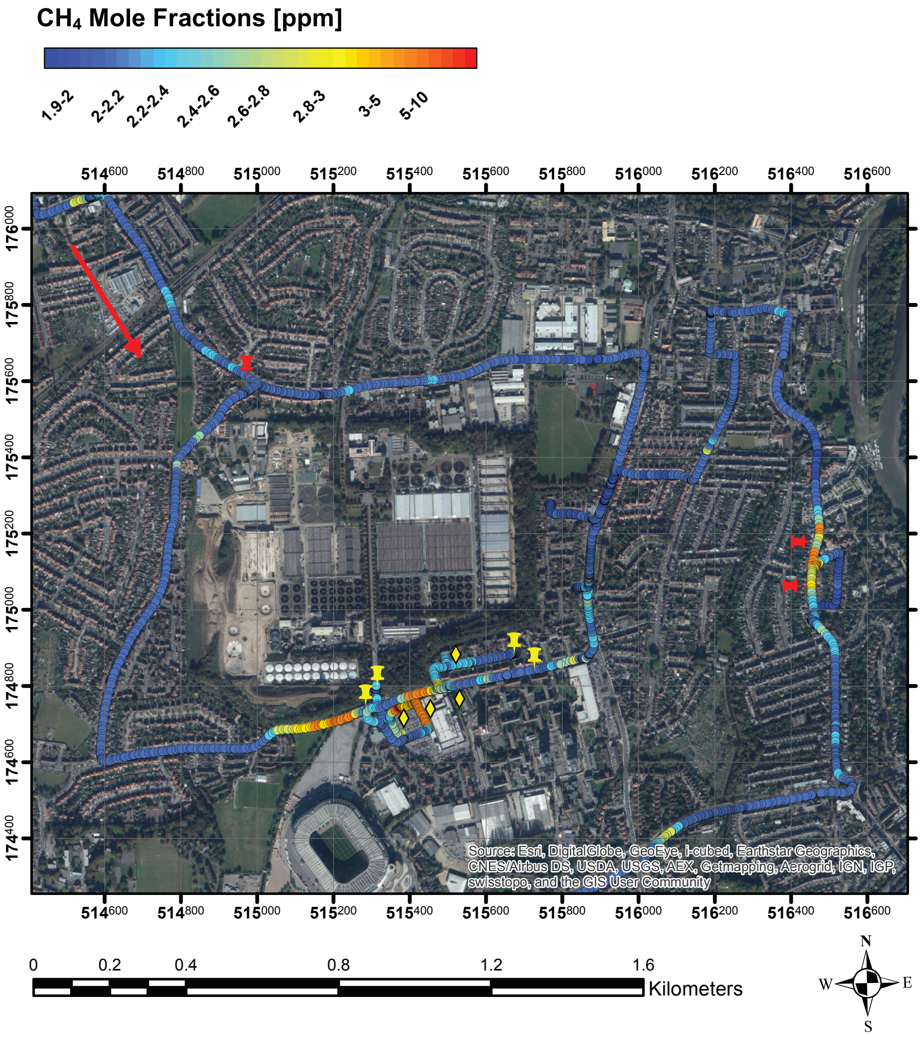

Figure 5.58 ArcGIS plot of methane mole fractions in ppm recorded on 11th July 2014 around Mogden sewage works. The red arrow represents wind direction, yellow pushpins and diamonds the samples collected downwind of sewage works, red pushpins samples related to gas leaks.

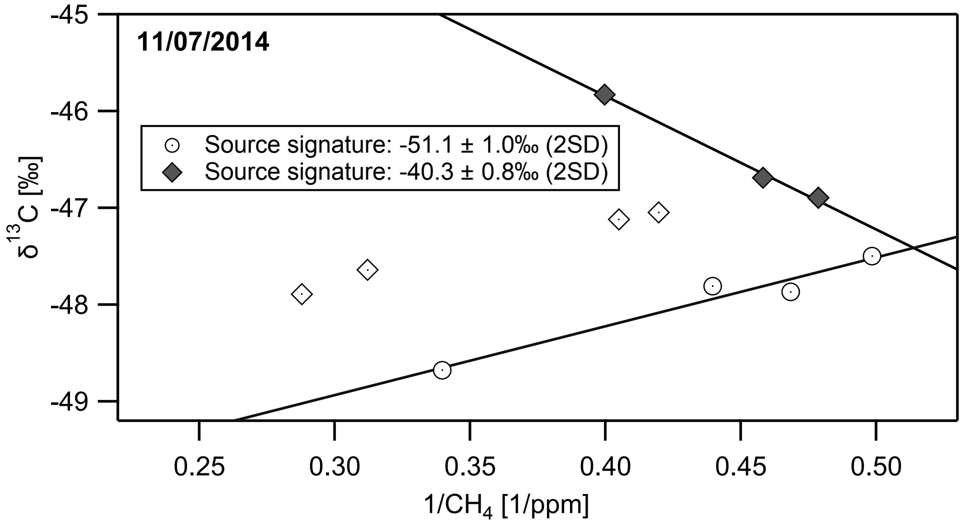

Figure 5.59 Keeling plot based on the samples collected on 11th July 2014 around Mogden sewage works. Grey markers represent samples related to gas leaks, squared markers correspond to diamonds and circles to pushpins in Figure 5.58.

5.4.3.1 20th March 2015

On 20th March 2015 the measurement campaign was carried out during night time, when the stable stratification of air in the nocturnal boundary layer suppresses convective motions and vertical mixing, and methane mole fractions are higher. Methane plumes intercepted during previous surveys were sampled again, in order to confirm their location and source. Six samples were collected along the main road at the south side of Mogden, two of them downwind of anaerobic digesters (first two pushpins on the left in Figure 5.60) and other four while driving towards east. The Keeling plot based on the first two samples gave an intercept of -50.8 ±0.2 ‰ (2SD) (Figure 5.61), consistent with the $\delta^{13}C$ signature found on 11th July 2014 for biogas produced in the anaerobic digesters (-51.1 ±1.0 ‰ (2SD)). The next three samples were interpolated in another Keeling line with an intercept of -48.5 ±1.3 ‰ (2SD), which was ^{13}C enriched relative to the biogas signature and might be associated with the interposing of methane releases from the power station. The sixth sample was undoubtedly related to a gas leak, as the Keeling plot built on that sample and the background that was collected upwind of sewage works had an intercept of –39 ‰, falling within the natural gas signature range.

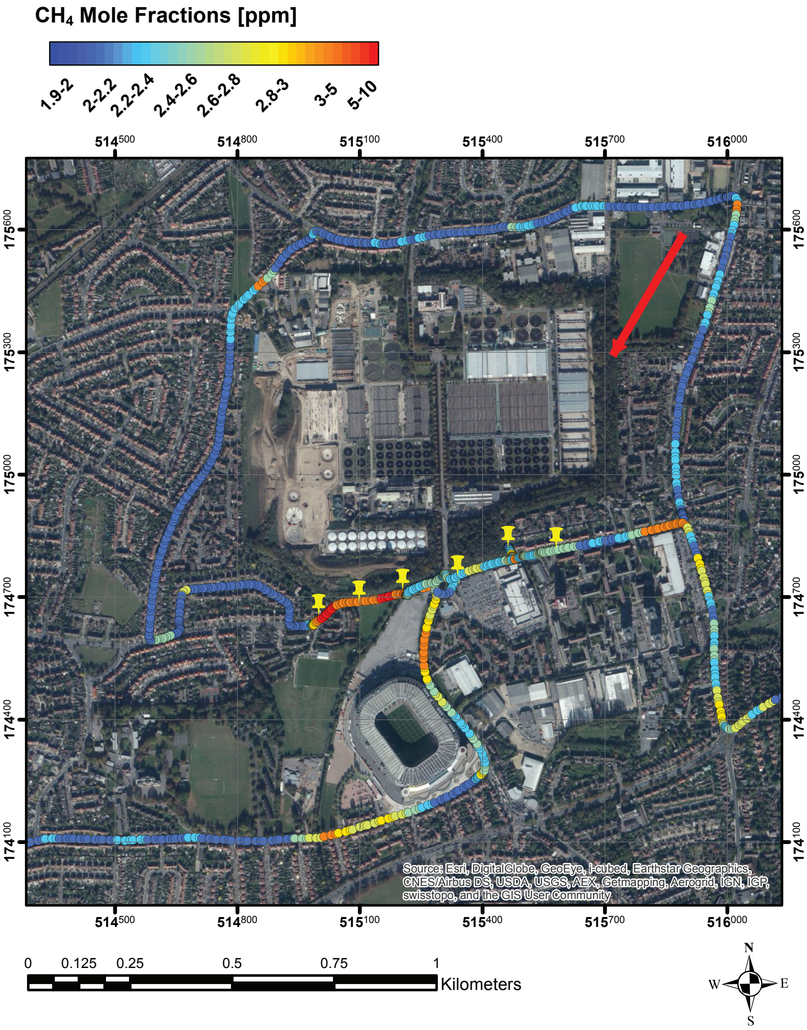

Figure 5.60 ArcGIS plot of methane mole fractions in ppm recorded on 20th March 2015 around Mogden sewage works. The red arrow represents wind direction and the yellow markers the air samples collected.

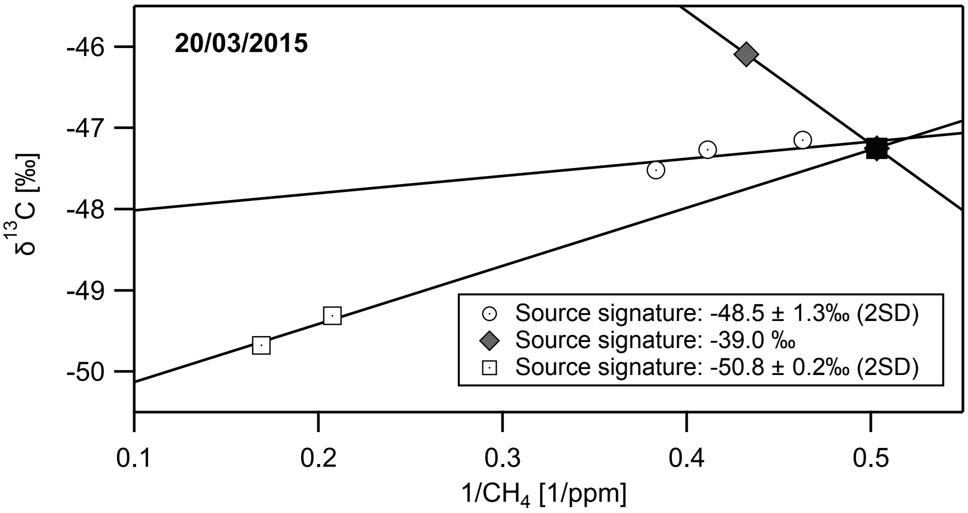

Figure 5.61 Keeling plot based on samples collected on 20th March 2015 around Mogden sewage works. The grey marker represents the sample related to a gas leak (first on the left on Figure 5.60), squared markers correspond to the first two samples in Figure 5.60 and circles to the other three samples; the black square represents the background value.

5.4.4 Summary

Methane source	$\delta^{13}C$ isotopic signature
Anaerobic digesters	-50.7 ±1.1 ‰ (2SD)
Secondary treatment	-59.2 ±1.2 ‰ (2SD)
Power station	-48.1 ±1.5 ‰ (2SD)

Table 5.7 Averaged values of $\delta^{13}C-CH_4$ isotopic signature assigned to methane sources involved in sewage works.

By sampling around Mogden sewage works, three main methane sources were identified:

i. biogas releases from the anaerobic digesters;
ii. biological treatment;
iii. releases of uncombusted biogas from the power station.

The $\delta^{13}C$ signature of methane emissions from the biological or secondary treatment is found more ^{13}C depleted relative to the isotopic value of the biogas generated in the anaerobic digesters. Indeed, mesophilic temperatures inside the anaerobic digesters might favour different methanogen groups, leading to more ^{13}C enriched methane. Methane emissions detected downwind of the power station are characterised by an even heavier isotopic signature, suggesting a component of methane derived from the incomplete combustion of biogas.

6

DIURNAL STUDIES

6.1 Long-Term Methane Record for Royal Holloway

An assessment of 18 years of methane mole fraction measurements at RHUL allows comparison between the methane record for a background site (e.g. Mace Head) and an area embracing the most important urban methane sources, such as gas leaks, landfill sites and sewage works. Monthly averages over the period between October 1995 and December 2014 are shown in Figure 6.1. From 1995 methane mole fractions were measured at 30-minute intervals using HP 5890 GC-FID (Egham Record). Since 2009 measurements have been made at 5-second intervals using a Cavity Ring Down Spectrometer (Picarro measurements).

Over the first decade of measurements methane mole fractions declined by approximately 9 ppb/year, as a result of a reduced leakage from the natural gas distribution system, and decreased emissions from landfill sites and vehicles; then an increasing trend has been observed from 2008 until December 2014. Methane mole fractions from 2000 until 2012 recorded in Mace Head, on the west coast of Ireland (53.33°N, -9.90°W), show the same pattern, suggesting that the latest growth in methane mixing ratio is not confined to the SE of England, but has to be interpreted in terms of global events.

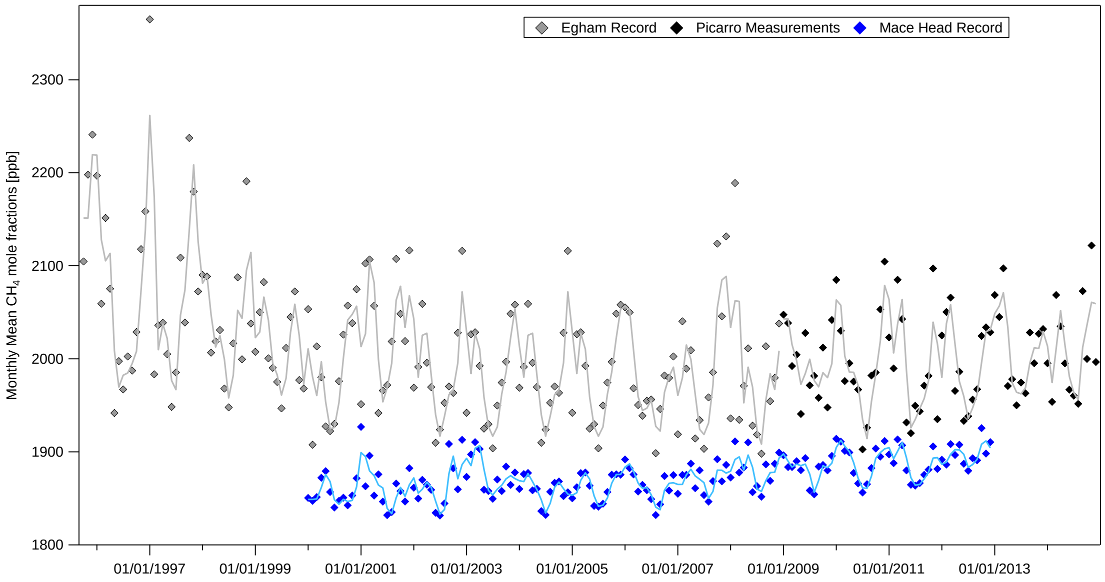

Figure 6.1 Methane mole fractions recorded at Egham from 1996 until 2014 (grey and black markers) and at Mace Head (blue markers) from 2000 until 2012. The continuous lines represent mole fractions computed with a moving average calculation. Mace Head continuous record is available from the website http://ingos-atm.lsce.ipsl.fr.

Both measurements from Egham and Mace Head exhibit the annual cycle in methane mole fractions, due to the prevalence of methane uptake via OH oxidation and a major atmospheric mixing during summer, and the build-up of methane emissions under a lower boundary layer and perhaps enhanced fossil fuel consumption during winter.

Pollution roses and diurnal cycles based on the Egham record have been used as a preamble for studying those methane sources that are supposed to have driven the methane increase in the SE England area. Pollution roses calculated using the 2014 methane record (Figure 6.2) indicate that mole fractions at background levels come from the SW sector, and that the E sector, corresponding with the London region, is associated with the highest mole fractions (>5 ppm), especially in September, November, March and April. The contribution of urban sources in the London region to the local methane budget has been verified by the source studies described in Chapter 5.

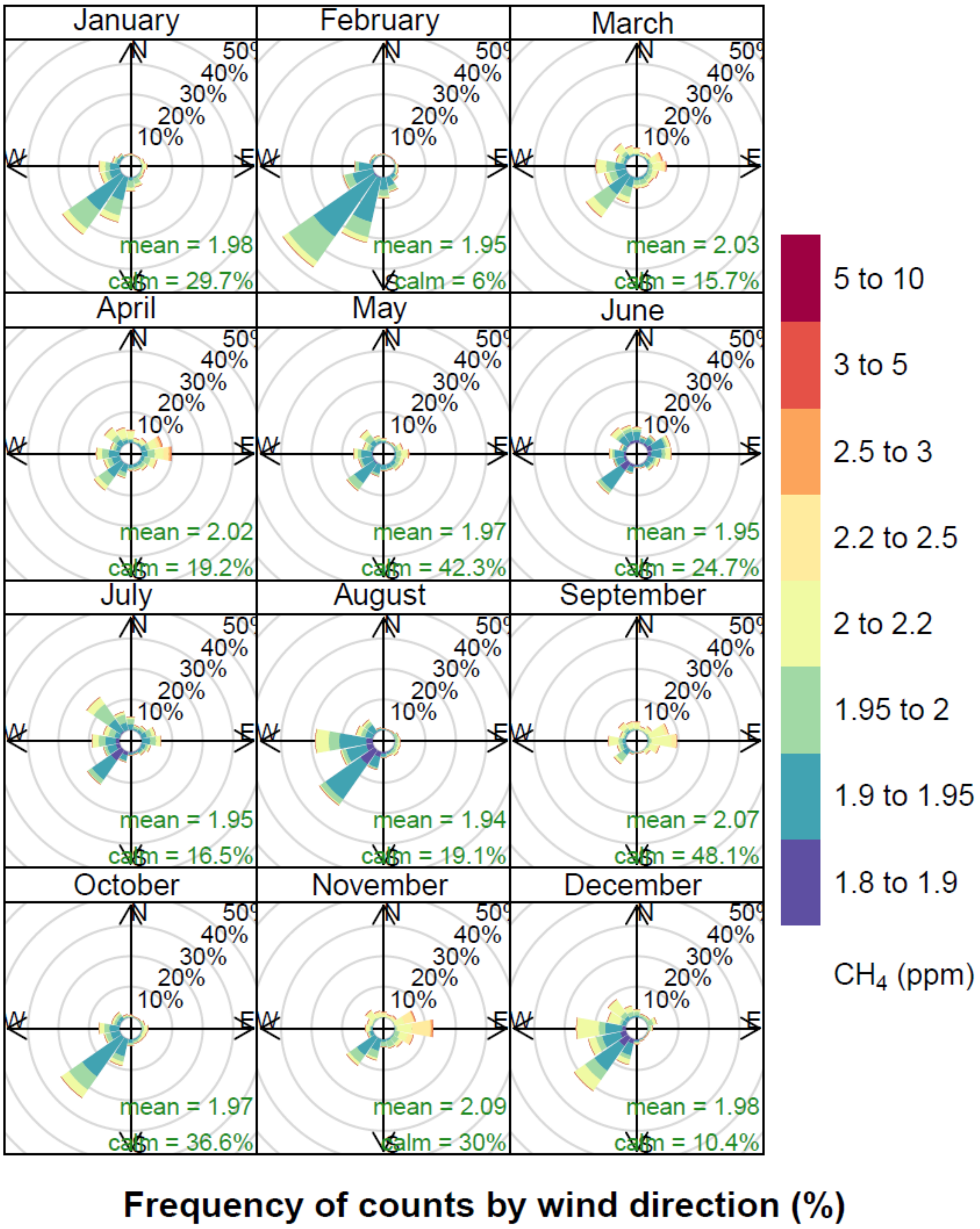

Figure 6.2 Pollution roses built using Open Air package and methane mole fraction data measured in 2014 in Egham.

Diurnal cycles have been computed by aggregating methane mole fraction data recorded at RHUL. Figure 6.3 displays the 2014 diurnal cycle for summer and winter months, highlighting how methane mole fractions in winter are constantly higher throughout the day, except for the period from 1 a.m. to 6 a.m. Methane sources that prevail in winter (i.e. heating systems), combined with a lower boundary layer during winter anticyclonic conditions, which allows methane mole fractions to build-up, can explain the higher mole fractions observed in winter. The stronger atmospheric turbulence characterising summer months leads to a major dispersion of gases and a more pronounced diurnal cycle.

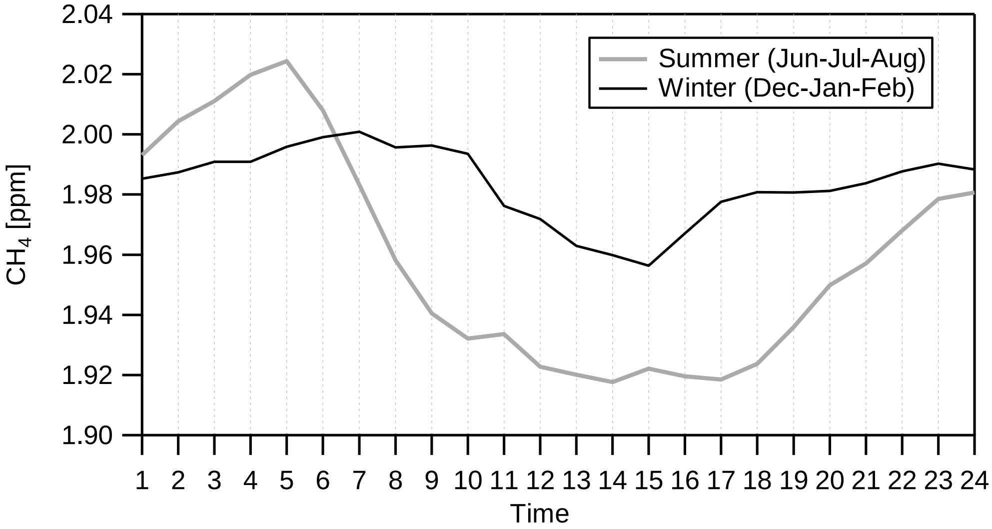

Figure 6.3 Diurnal cycle calculated aggregating methane mole fractions recorded in summer (grey line) and winter (black line) 2014.

The seasonality of diurnal cycles can be associated with both weather conditions and sources whose emissions are enhanced during a specific time of the year. The isotopic analysis of the source mix during diurnal cycles, both in Egham and in London, has been used to achieve a better understanding of the main processes affecting the methane mixing ratio.

6.2 Introduction to Diurnal Studies

Stable carbon isotopic composition combined with CH_4 mole fraction measurements allow determination of the mean $\delta^{13}C$-CH_4 source signature characterising a region and estimation of the proportion of CH_4 sources in a source mix. Diurnal studies have been carried out at RHUL (Lowry et al., 2001; Fisher, 2006). Following the development of an automatic inlet on the Trace Gas, numerous diurnal studies have been performed and a mean $\delta^{13}C$-CH_4 source signature of -50.1 ±0.7 ‰ has been calculated for 2004 (Fisher et al., 2006), indicating a large contribution of landfill emissions (-52 ‰ in 1998) in the CH_4 budget for the region of London, relative to natural gas emissions (-36 ‰).

A better understanding of urban CH_4 sources can be achieved by the analysis of the source mix directly in the centre of the city, where impervious surfaces and the absence of large green areas create a micro-environment that strongly affects the air dynamics and therefore the emissions from local sources. Several diurnal studies have been carried out in the centre of London, benefitting from an air inlet located at 7 meters height on a tower mounted on the rooftop at the Strand Campus of King's College London (see Chapter 4.5).

The nocturnal temperature inversion leads to CH_4 accumulation overnight that dissipates in the late morning, following vertical air mixing. These diurnal fluctuations in mole fractions were observed in the majority of the diurnal studies carried out, and the $\delta^{13}C$-CH_4 signature characterising the source mix in central London was calculated by the isotopic anlysis of the overnight build-up. However, irregular local emissions can disturb the usual mole fraction cycle, making the interpretation of diurnal studies difficult. In fact, due to the arrangement of buildings surrounding King's College, some very local emissions may interfere with the measurement of surface sources (Kotthaus and Grimmond, 2012) and occasional CH_4 mole fraction peaks may occur. Although the isotopic analysis of these peaks indicated different isotopic source signatures, a predominant component of fossil CH_4 in the source mix, related to leakages in the natural gas system and exhaust gas from vehicles, could be confirmed, an outcome shared by several studies carried out in other big conurbations (Moriizumi et al., 1998; Vinogradova et al., 2007; Townsend-Small et al., 2012).

6.3 Identification of Regional and Continental Isotopic Signals

The isotopic characterisation of the methane build-up measured in central London and in Egham during diurnal studies entails the identification of the atmospheric background, as the increment in methane mole fractions can be interpreted on the basis of a ^{13}C-enrichment or depletion relative to the isotopic background. The high precision achieved with the Trace Gas for isotopic measurements (see Chapter 4) allows analysis of isotopes in background air and identification of remote regional isotopic source signatures using Keeling plot analysis.

Three background sites for the London region were chosen: Dover in Kent for the SE background, Bacton on the Norfolk coast for the NE background and Portland in Dorset for the SW background.

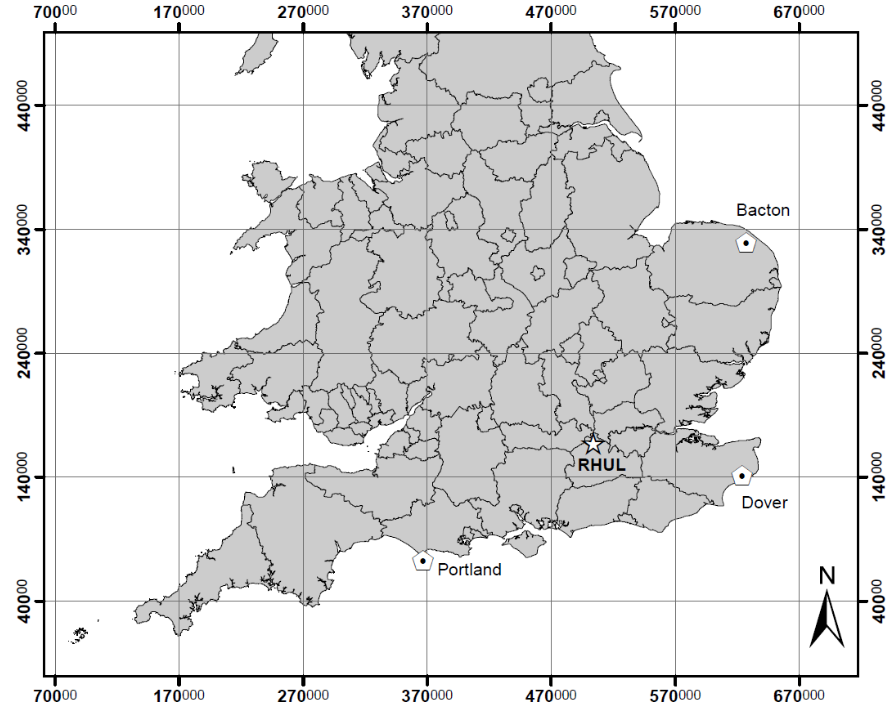

Figure 6.4 Background sites. The star indicates the Royal Holloway University of London in Egham.

6.3.1 Dover

Six samples were collected at half hour intervals in Dover, on top of the cliffs, from 10 a.m. until 12:30, on 10th February 2012. The wind direction was ENE at 10 a.m., turning into SE after 11 a.m. According to the backward trajectories model for the previous 72 hrs (see Chapter 6.3.4), continental air reached Dover passing through the Baltic Sea, North of Germany and Netherlands. The Keeling plot in Figure 6.5 shows an intercept of -56.5 ±2.5 ‰ (2SD), which is highly depleted relative to the isotopic signature characterising central London (see Chapter 6.5), due to the a different source proportion in the source mix characterising Europe (see European Inventories in Chapter 3.2) and a different isotopic composition of the leading methane sources.

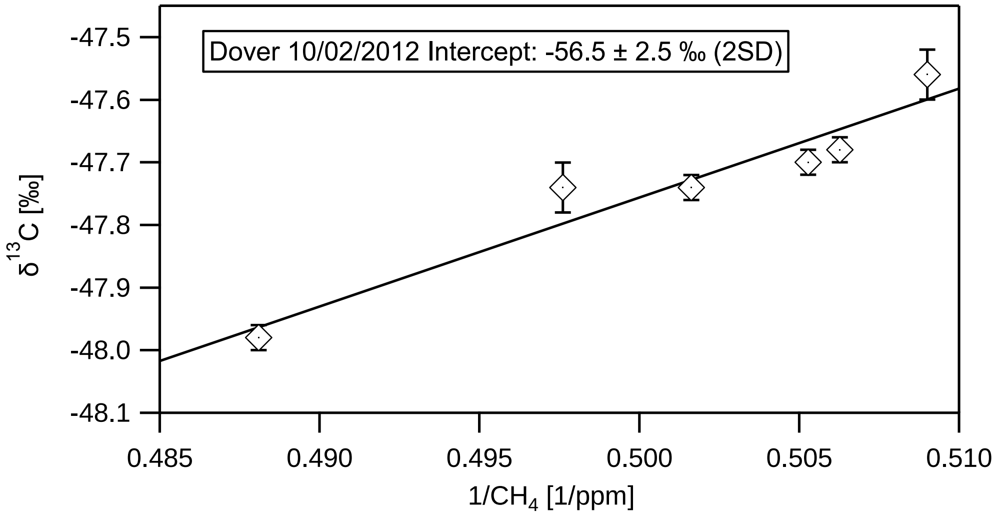

Figure 6.5 Keeling plot based on samples collected in Dover on 10th February 2012.

6.3.2 Portland

On 25th June 2012 6 samples were collected in Portland at hourly intervals, from 10 a.m. According to back-trajectories based on the previous 72 hrs (see Chapter 6.3.4), air masses were coming from the North Atlantic, crossing South of Ireland and part of Cornwall. The air route may explain the ^{13}C depleted source signature of -61.0 ±2.1 ‰ (2SD) calculated for the air reaching Portland, as biogenic methane emissions derived from cows and sheep might have added to the air masses coming from the ocean.

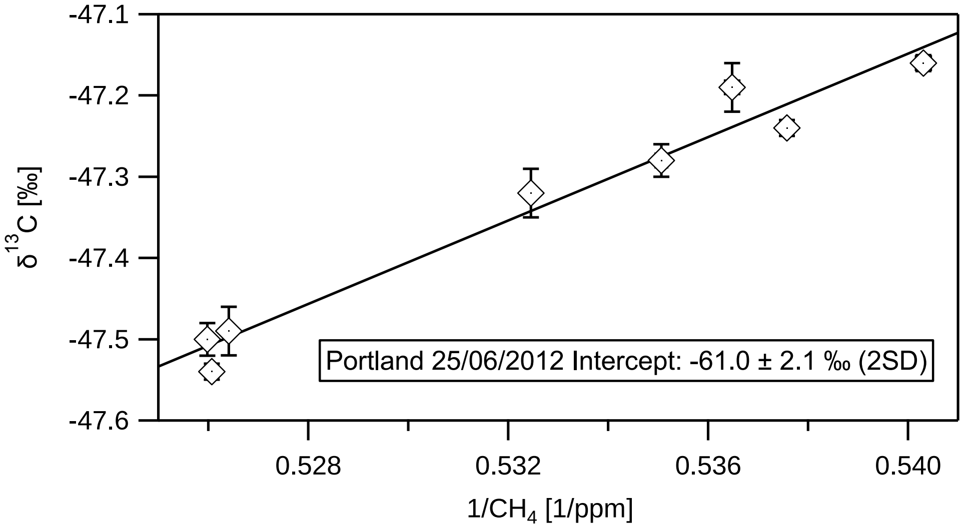

Figure 6.6 Keeling plot based on samples collected in Portland on 25th June 2012.

6.3.3 Bacton

Bacton was the site chosen to isotopically characterise air coming from NE, and 4 samples were collected along the coast on 22nd March 2012. Air masses were coming from Europe, mainly from north of Germany and Netherlands (see Chapter 6.3.4), and the source signature of -56.7 ±1.5 ‰ (2SD) (Figure 6.7) is indeed consistent with the isotopic value characterising the background air in Dover, where continental air coming from the same regions was sampled.

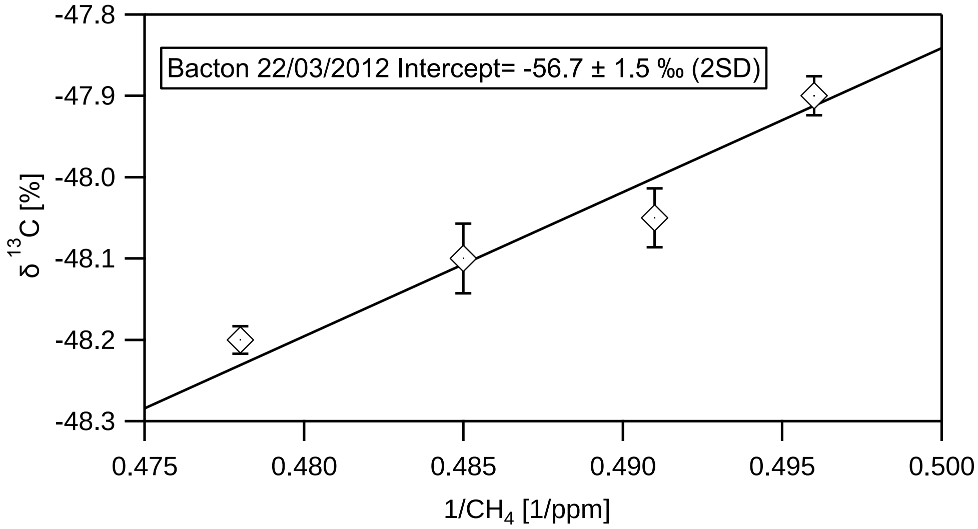

Figure 6.7 Keeling plot based on samples collected in Bacton on 22nd March 2012.

6.3.4 Backward Trajectories

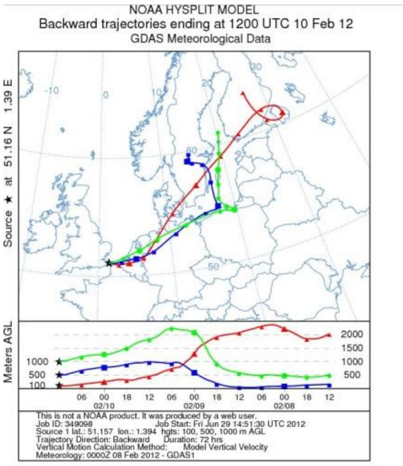

This is not a NOAA product. It was produced by a web user.
Job ID: 349098 Job Start: Fri Jun 29 14:51:30 UTC 2012
Source 1 lat.: 51.157 lon.: 1.394 hgts: 100, 500, 1000 m AGL
Trajectory Direction: Backward Duration: 72 hrs
Vertical Motion Calculation Method: Model Vertical Velocity
Meteorology: 0000Z 08 Feb 2012 - GDAS1

Figure 6.8 Backward trajectory model for Dover, calculated for a duration of 72 hrs air movement.

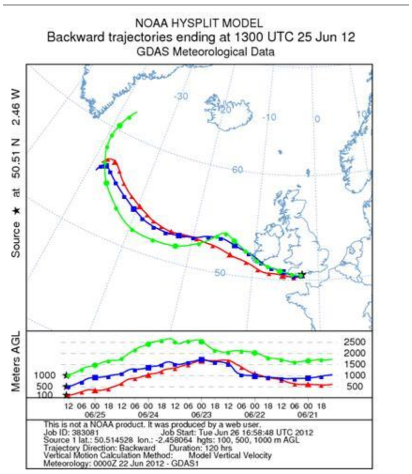

This is not a NOAA product. It was produced by a web user.
Job ID: 383081 Job Start: Tue Jun 26 16:58:48 UTC 2012
Source 1 lat.: 50.514528 lon.: -2.458064 hgts: 100, 500, 1000 m AGL
Trajectory Direction: Backward Duration: 120 hrs
Vertical Motion Calculation Method: Model Vertical Velocity
Meteorology: 0000Z 22 Jun 2012 - GDAS1

Figure 6.9 Backward trajectory model for Portland, calculated for a duration of 72 hrs air movement.

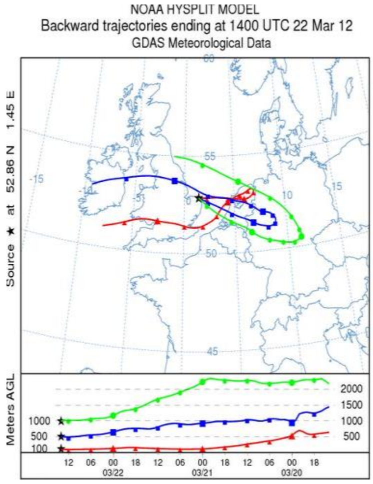

Figure 6.10 Backward trajectory model for Bacton, calculated for a duration of 72 hrs air movement.

6.4 Diurnal Measurements in Egham

At RHUL Earth Science department CH_4 mole fractions at background levels can be measured when the air is coming from SW and CH_4 emissions from London can be detected with easterly winds, making this location strategic for continuous sampling. Still, anticyclonic conditions or steady winds can lead to significant CH_4 build-up associated with identifiable sources. However, when wind speed approaches 0 ms^{-1}, local sources will affect the measured methane, and this may be the cause of the large variation in the isotopic composition that has been found throughout the sampling period. In fact, during one diurnal cycle different peaks in CH_4 mole fractions occurred and, due to fluctuations in wind direction and the variety of methane sources, only some measured values could be interpolated in a Keeling plot. Two examples of diurnal studies carried out in Egham are presented in this section.

6.4.1 18th-19th October 2012

During the diurnal study on 18th and 19th October, shown in Figure 6.11, mainly westerly winds were recorded on the first day; then wind directions started varying, concurrently with the overnight drop in wind speed. From 1 a.m. to 11 a.m. a build-up in CH_4 was recorded, accompanied by a ^{13}C-enrichment. The most enriched value corresponded to the peak of 2.5 ppm at 6 a.m., when wind direction was from ESE but associated with a zero wind speed, and therefore unreliable.

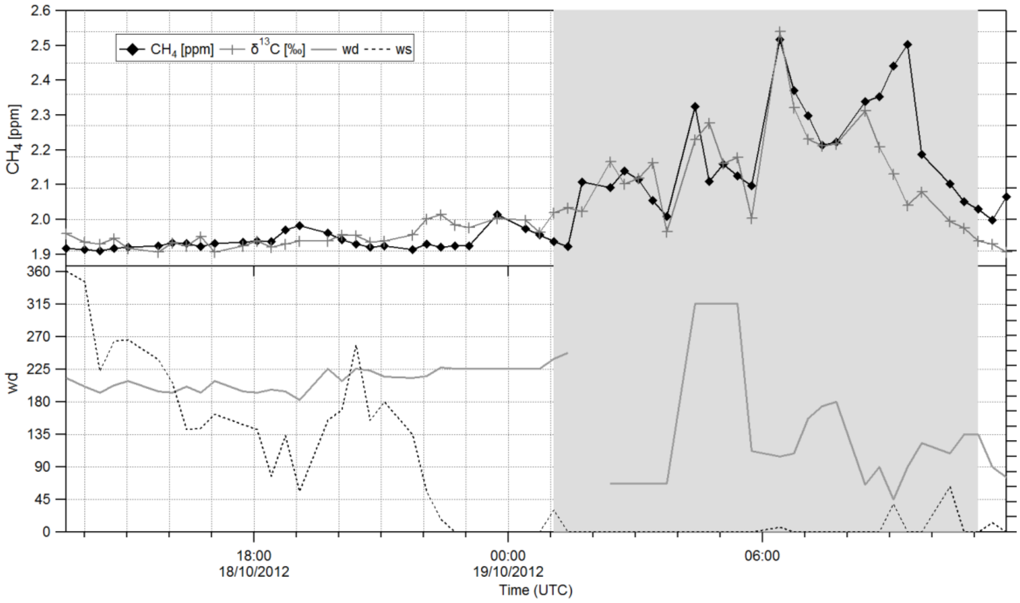

Figure 6.11 CH$_4$ mole fractions and δ^{13}C values, wind speed and direction recorded on 18th and 19th October 2012. The grey area highlights the build-up in CH$_4$ mole fractions.

The Keeling plot (Figure 6.12) based on values measured throughout the build-up period (grey area in Figure 6.11), shows a δ^{13}C source signature of -40.7 ±1.8 ‰ (2SD), which can be attributed to a prevalent fossil component in methane emissions, such as local gas leaks.

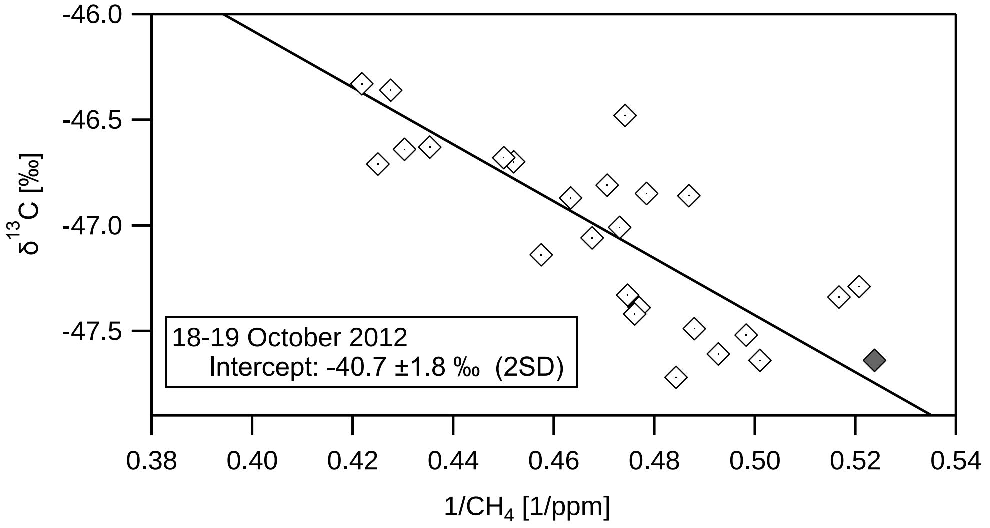

Figure 6.12 Keeling plot based on values measured from 1 a.m. to 11 a.m. on 19th October 2012. The grey marker represents the background value.

6.4.2 11th-12th-13th December 2012

A diurnal study of three consecutive days was carried out from 11th to 13th December 2012. The build-up in CH_4 mole fractions was associated with a drop in wind speed, a decrease in temperature from 6 to 3 °C and a consistent barometric pressure of 1010 hPa. CH_4 mole fractions peaked at 10 p.m. on 12th December (2.98 ppm), as well as the $\delta^{13}C$ value (-45.3 ‰).

The Keeling plot based on the values recorded on the period between 1 and 7 a.m. on 13th December (Figure 6.13), when the wind speed was appreciable and the wind direction was consistently from ESE-E (see grey area in Figure 6.14), shows an intercept value of -38.6 ±0.6 ‰, which is very indicative of a fossil fuel source.

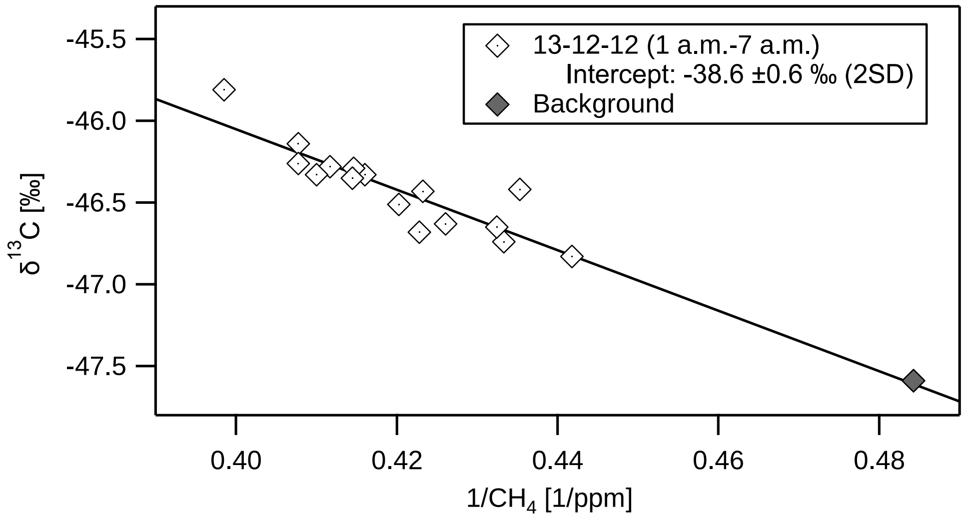

Figure 6.13 Keeling plot based on values measured from 1 a.m. to 7 a.m. on 13th December 2012.

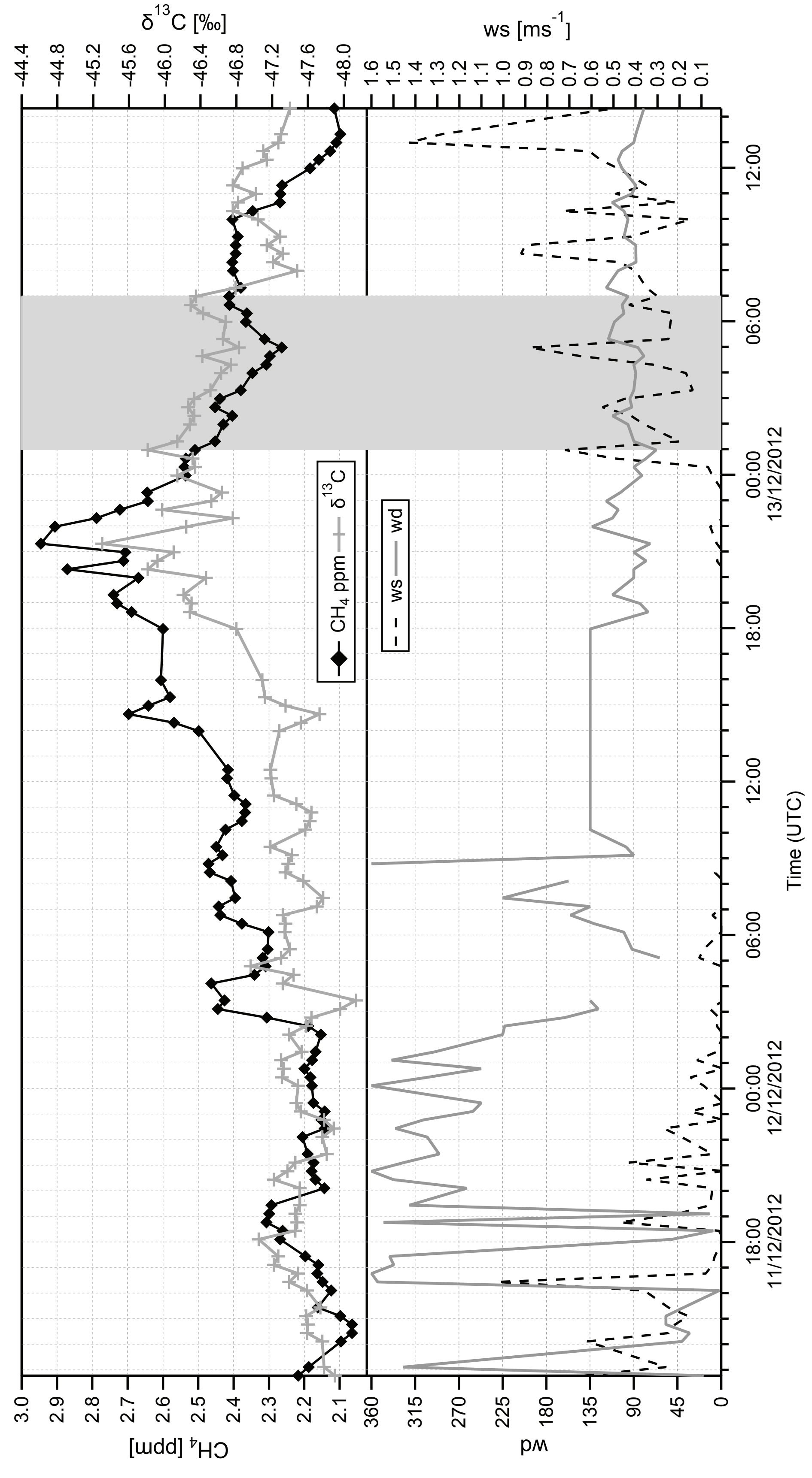

Figure 6.14 CH$_4$ mole fractions and δ^{13}C values, wind speed and direction recorded on 11th, 12th and 13th December 2012. The grey area highlights the isotopic values included in the Keeling Plot.

6.4.3 Methane Source Signature Variation with Wind Direction

The plot in Figure 6.15 was made by considering all the episodes of methane mole fractions 100 ppb higher than the background used for the diurnal studies in Egham and associated with wind speed > 0 ms^{-1}, and by plotting all the related δ^{13}C-CH$_4$ source signatures by wind direction (the source signature is the intercept of a 2-points Keeling plot calculated with the over-background and the background values). During the two diurnal studies most of the air masses were coming from the E sector, which produced isotopic source signatures ranging from -50 to -34 ‰. The ENE sector was dominated by only relatively ^{13}C enriched signatures, which might have been related to a fossil fuel source located in this direction. The mean calculated source δ^{13}C for the London sector (45° to 110°) was -40.7 ±3.8 ‰ (n=19), more ^{13}C enriched than the value of -50.1 ±0.7 ‰ (n=46) found by Fisher (2006), although it is based on only two diurnal studies carried out over three nights. The ^{13}C-enrichment of air coming from the London sector might be explained with a significant input of fossil fuel sources to the regional source mix, such as gas leaks in the natural gas network.

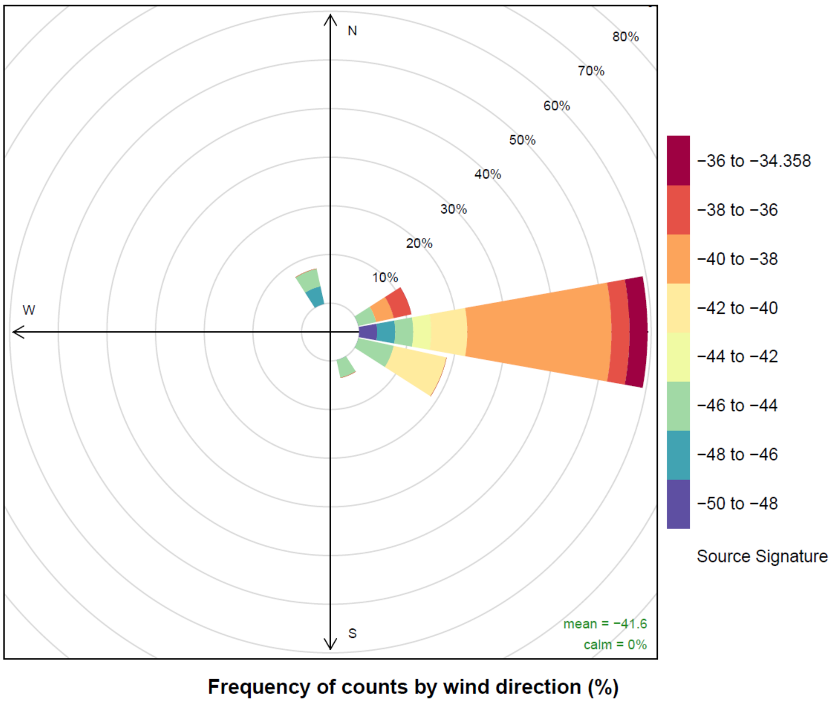

Figure 6.15 Frequency of calculated δ^{13}C source signatures split by wind direction.

6.5 Diurnal Measurements of CH_4 in Central London

Continuous CH_4 and CO_2 mole fractions were measured by a Picarro G2301 greenhouse gas analyser situated on the roof of King's College from 10th December 2013 to 31st January 2014 and from 24th July to 11th August 2014. Collection of air samples in bags for detailed diurnal studies was carried out when a large build-up in mole fractions was expected, during high pressure and low wind speed conditions.

Each diurnal study includes the calculation of an isotopic signature of the source mix in central London, an analysis of continuous CO_2 and CH_4 mole fractions at King's College station, a comparison between London and Egham CH_4 trends and an investigation on the wind pattern.

The diurnal measurements carried out in this study are described in the following sections. During each diurnal cycle an automatic sampler was activated remotely, allowing twenty air bags to be collected for methane isotopic analysis (Chapter 4 for details on the automatic sampler and measurements).

6.5.1 Diurnal Measurements before the Development of the Automatic Sampler

Before development of the automatic sampler, only one diurnal study was carried out, on 9th July 2012, which involved sample collection at hourly intervals on the roof of King's College and approximately at the same time in Egham (excluding the night), using the sampling intake above the roof of the RHUL Earth Science Department.

CH_4 mole fractions in London were higher than in Egham (Figure 6.16), except for the 2.1 ppm peak between 2 and 3 a.m., which was not isotopically characterised, as no sample was collected overnight.

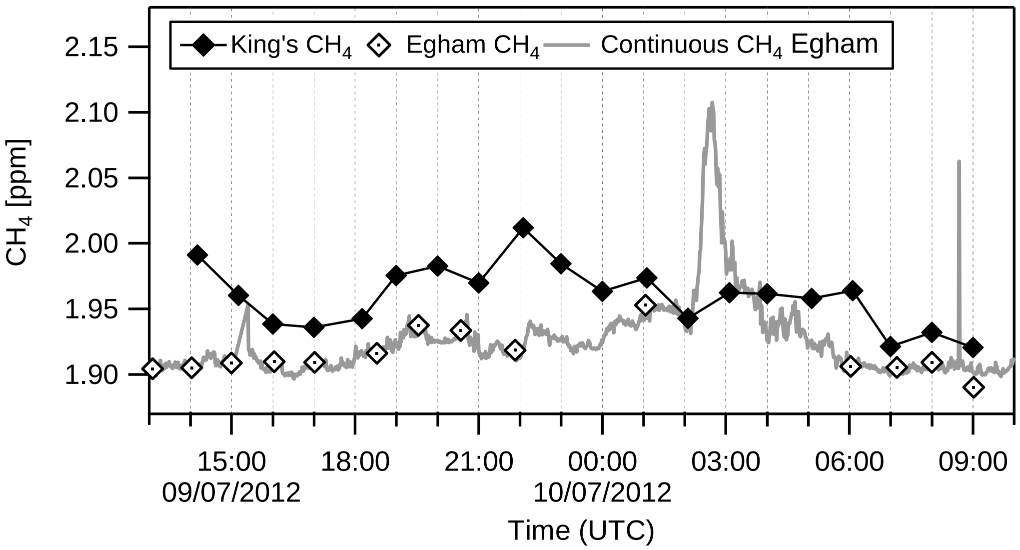

Figure 6.16 CH_4 mole fractions measured at King's College (black line), continuous measurements in Egham (grey line) and samples collected at RHUL (white markers) on 9th and 10th July 2012.

The source signature of -38.1 ±4.7 ‰ (2SD) resulting from the Keeling plot based on all the samples analysed (Figure 6.17), indicates the predominance of fossil CH_4 emissions. Samples collected in Egham are characterised by overall lower isotopic values than the ones collected in London, suggesting a stronger proportion of CH_4 from biogenic emissions.

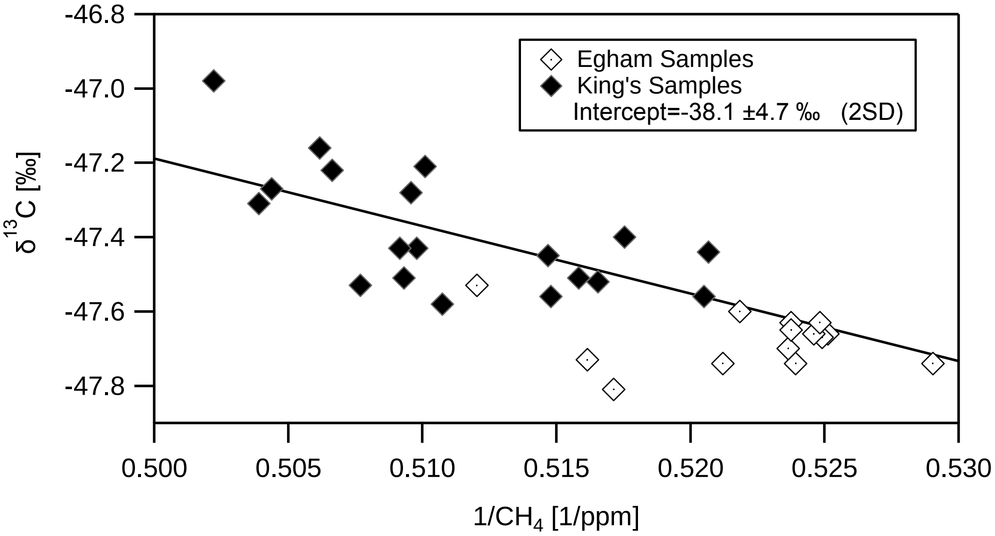

Figure 6.17 Keeling plots based on all the samples collected at King's College (black markers) and in Egham (white markers).

6.5.2 2nd-3rd December 2013

On 2nd and 3rd December 2013, the CH_4 mole fraction trend at King's College was inferred by the CH_4 mole fractions of samples collected, as continuous concentrations could not be retrieved for those days. According to the sample measurements, CH_4 and CO_2 mole fractions in Egham showed a nocturnal build-up that was not recorded in central London (Figure 6.18). As NOAA back trajectories display (Figure 6.19), air masses were passing through the London region before reaching Egham, and they might have been loaded by CH_4 emissions from CH_4 sources in rural areas and from landfill sites.

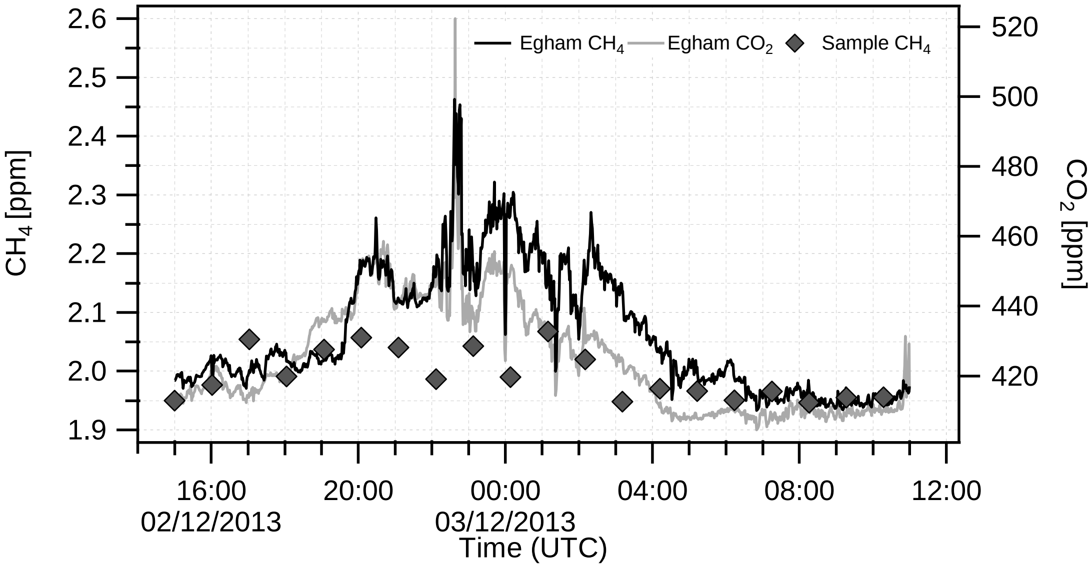

Figure 6.18 CH_4 (black) and CO_2 (grey line) mole fractions recorded in Egham on 2nd and 3rd December 2013 and CH_4 mole fractions of samples collected on the King's College roof (grey markers).

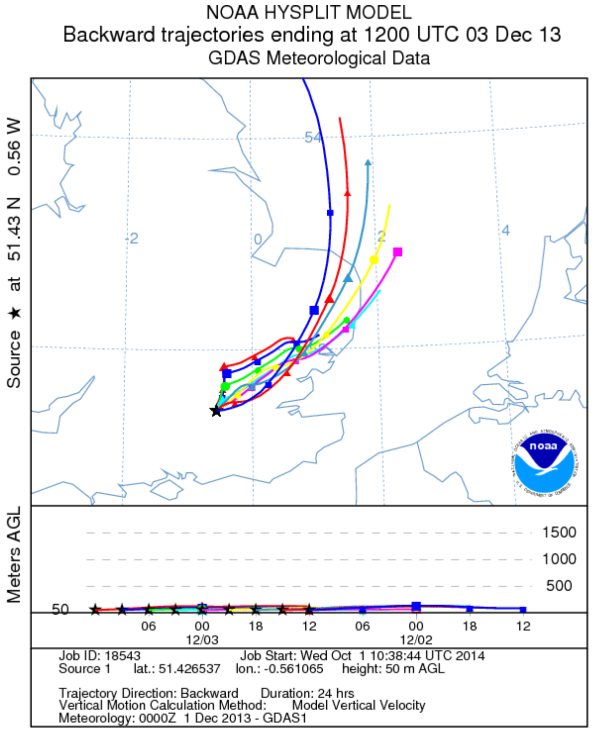

Figure 6.19 Back trajectories calculated using Hysplit trajectory model provided by NOAA. 9 back trajectories, one every 3 hrs, are shown for the 3rd December 2013 for air arriving at the Earth Sciences Department of RHUL (Egham).

The source signature determined from Keeling plot intercept for the bags collected at King's College (Figure 6.20), calculated for the period from 2nd December 3 p.m. to 3rd December 10 a.m., is -38.8 ±1.7 ‰ (2SD). This relatively ^{13}C enriched isotopic signature can be explained by fossil CH$_4$ sources such as natural gas losses, heating and vehicle exhausts. A single well constrained Keeling plot based on all the samples collected during the same diurnal study is an exceptional result, as several sources play a role into the CH$_4$ balance in central London and the CH$_4$ peaks occurring in a diurnal CH$_4$ cycle, often associated with a wind direction change, are usually characterised by multiple isotopic source signatures.

During this study the wind was predominantly from the eastern sector and the wind speed constantly below 3.5 ms^{-1} (Figure 6.21). Mole fraction peaks are associated with the NE and ESE sector.

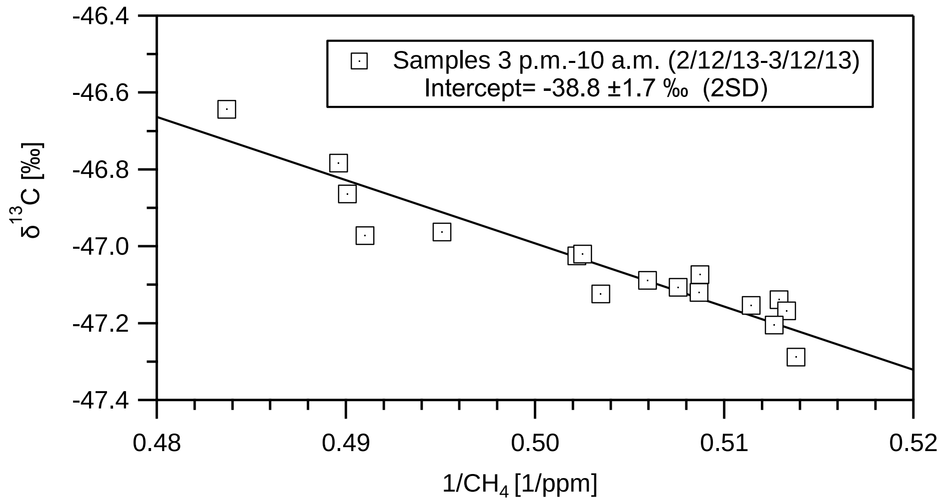

Figure 6.20 Keeling plot based on all the samples collected on 2nd December 2013 at King's College.

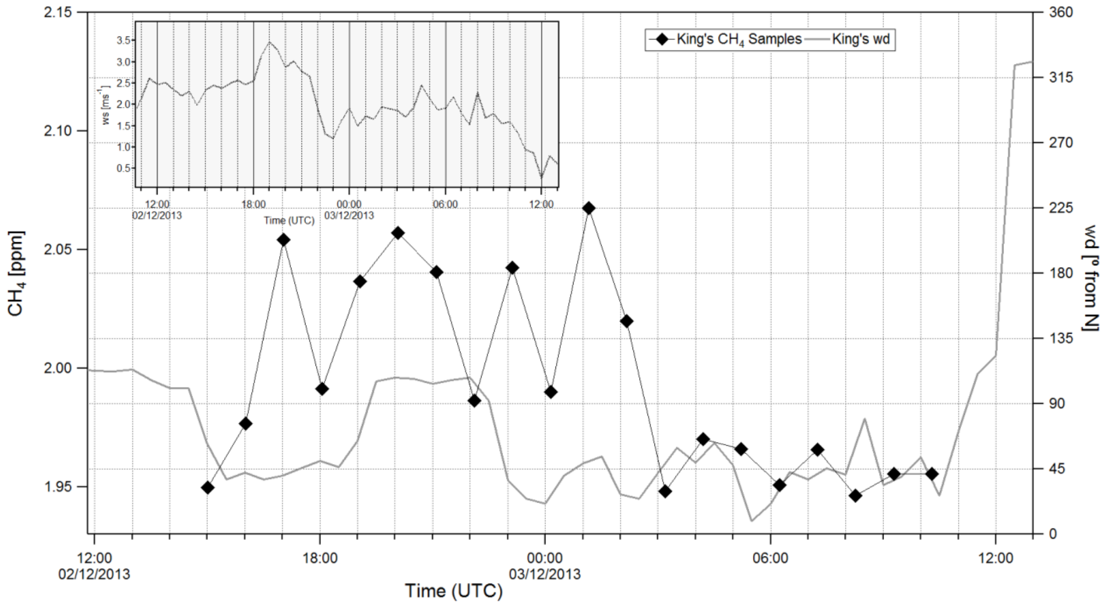

Figure 6.21 Wind direction (grey line) and wind speed (in the embedded graph) recorded on King's College roof, compared with the samples CH_4 mole fractions.

6.5.3 10th-11th December 2013

CH_4 and CO_2 mole fractions recorded at King's College on 10th and 11th December 2013 showed a peak around 1 a.m., before falling and then progressively increasing from 5 a.m., following a drop in wind speed below 1 ms^{-1} (see Figure 6.26). By 1 p.m., CH_4 and CO_2 mole fractions had reached 3.2 ppm and more than 600 ppm respectively (Figure 6.22). The extremely foggy conditions and the atmospheric stratification occurring during that night led to a constant build-up from 4 a.m.. CH_4 mole fractions in Egham started decreasing after 9 a.m., whereas in central London high levels of CH_4 mole fractions persisted until the early afternoon (Figure 6.23). During the 10th/11th December CH_4 mole fractions in Egham overall were increasing until 1 a.m., showing occasionally higher peaks than in London, perhaps due to the prevalence of biogenic sources as the air masses came from SSE sector, as shown by the NOAA back trajectories (Figure 6.24).

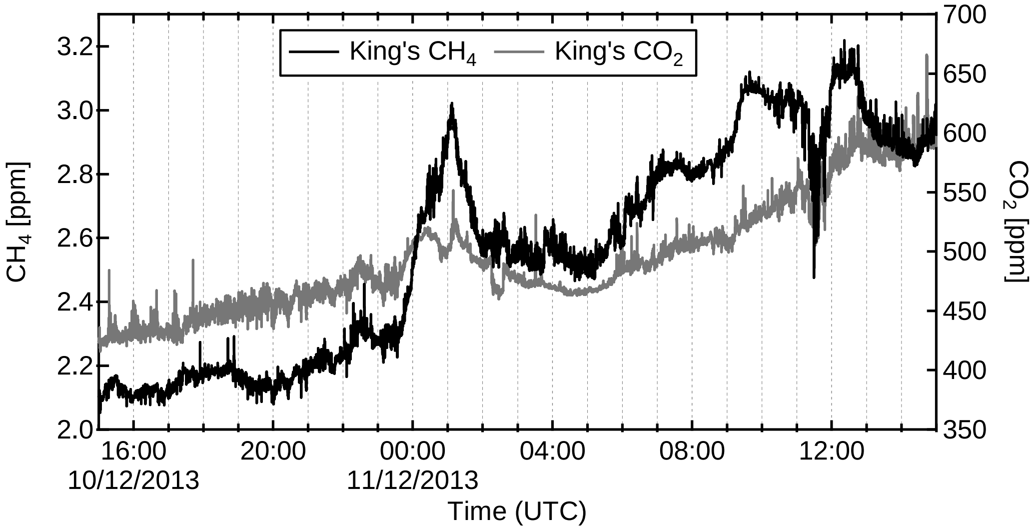

Figure 6.22 CH_4 (black line) and CO_2 (grey line) mole fractions recorded on King's College roof on 10th and 11th December 2013.

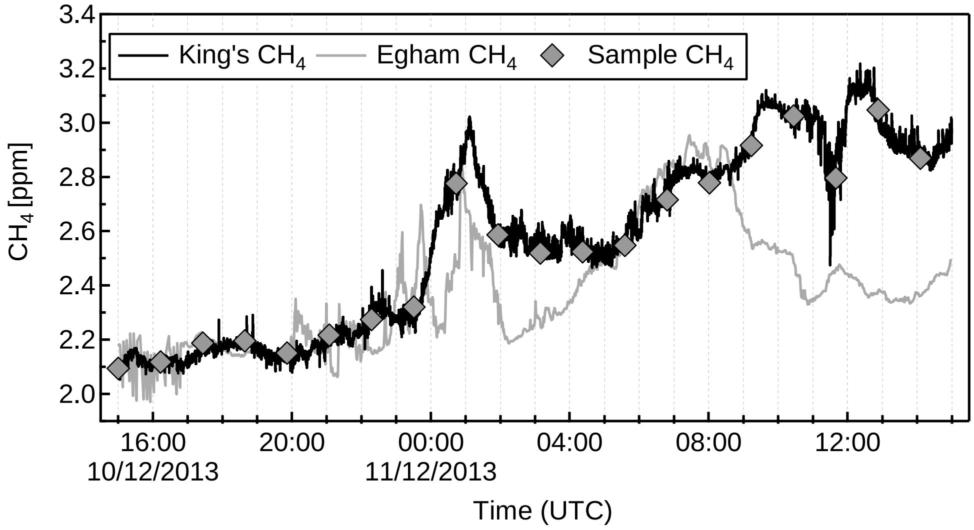

Figure 6.23 CH_4 mole fractions recorded at King's College (black) and in Egham (grey line) on 10th and 11th December 2013. Grey markers are CH_4 mole fractions of samples collected on the King's College roof.

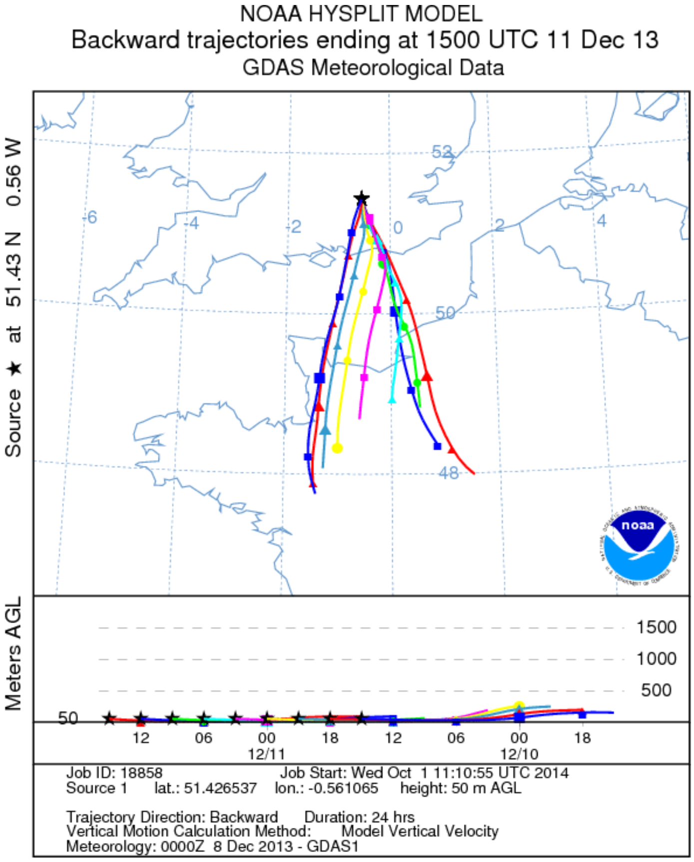

Figure 6.24 Back trajectories calculated using Hysplit trajectory model provided by NOAA. 9 back trajectories, one every 3 hrs, are shown for the 13th December 2013 for air arriving at the Earth Sciences Department of RHUL (Egham).

Two interpolation lines follow the Keeling plot analysis (see Figure 6.25), one based on the period from 3 p.m. to 10 p.m. on the 10th December and the other one constructed with samples collected during the night and morning of the 11th December from 2 a.m. to 11 a.m., resulting in two distinct source signatures, -36.8 ±2.2 ‰ (2SD) and -55.2 ±2.6 ‰ (2SD) respectively. The grey marker represents the peak at 00:40, which does not fit in any of the two interpolation lines, and it is associated with a mix of sources.

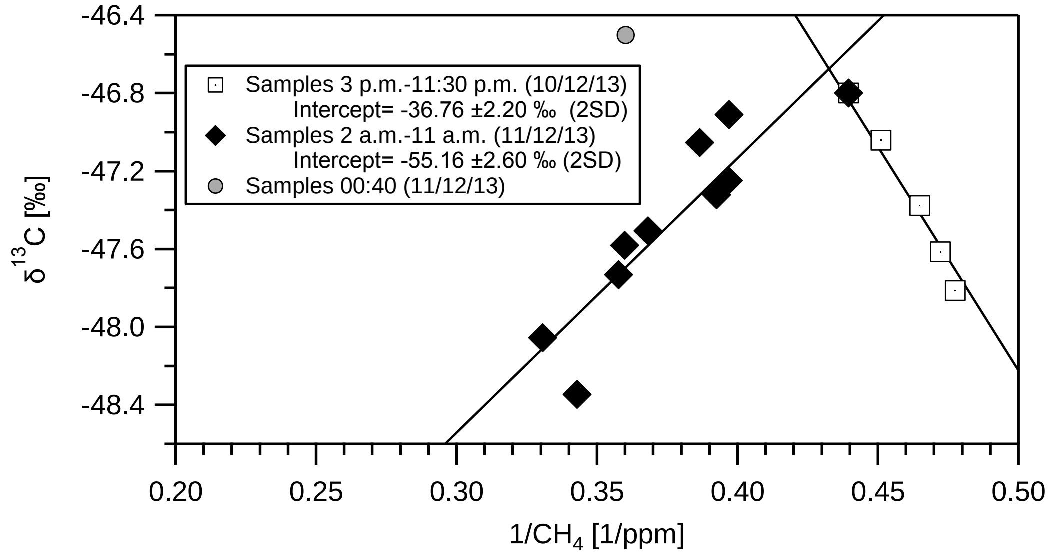

Figure 6.25 Keeling plots based on the samples collected during the afternoon and the evening of the 10th December 2013 (white markers) and during the night and the morning of the 11th December 2013 (black markers). The grey marker represents the peak at 00:40, which does not fit in any of the two interpolation lines

Two different backgrounds are used in this analysis, considering that the system might have alternated between the two sources, and one source plume acted as background when the other source became dominant. In fact, the complete absence of vertical mixing conditions, associated with wind speeds consistently below 1 ms^{-1}, might have led to an accumulation of CH_4 near the ground and the superimposition of one source plume on the other one.

The early morning build-up, whose source signature was relatively ^{13}C depleted, was associated with a SSE-SE wind direction, which did not vary until after 12 p.m., when CH_4 mole fractions started decreasing (Figure 6.26). The morning CH_4 plume might have originated from a biogenic source sited in the SE sector. A measurement campaign has been carried out in central London to evaluate to what extent the River Thames is involved as a methane emitter (see Chapter 6.6).

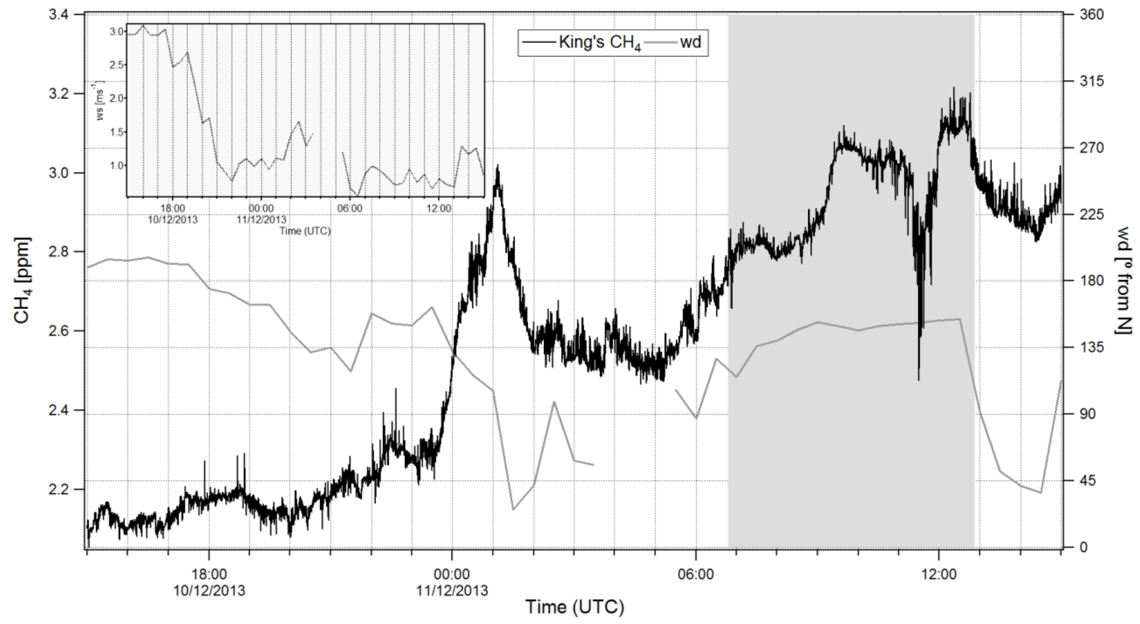

Figure 6.26 Wind direction trend (grey line) recorded at King's College and CH$_4$ mole fractions (black line) continuously measured on King's College roof on 10th and 11th December 2013. The grey section highlights the time interval of those samples which are thought to be associated with a biogenic CH$_4$ source. Wind speed is on the graph embedded.

6.5.4 20th-21st January 2014

A strong nocturnal build-up was recorded on 20th January, when CH_4 was trapped in the lower boundary layer under typical winter high pressure conditions. Mole fractions peaked at 3.5 ppm during the night and reached almost 3 ppm at 10 a.m. on the 21st (Figure 6.27).

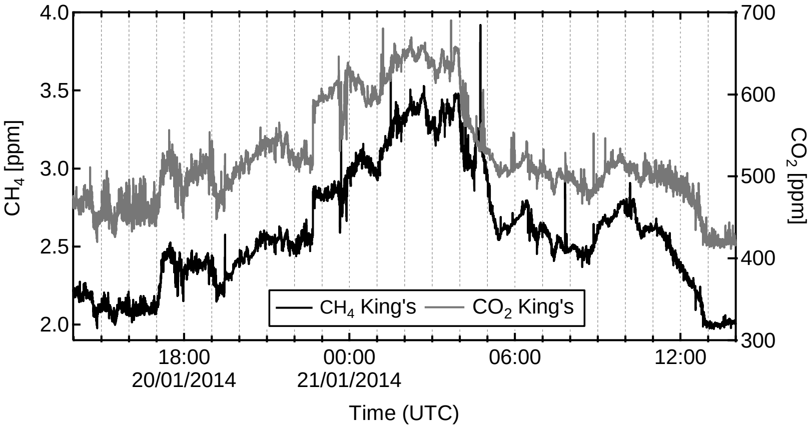

Figure 6.27 CH_4 (black line) and CO_2 (grey line) mole fractions recorded on the King's College roof on 20th and 21st January 2014.

CH_4 mole fractions in Egham did not exhibit the same nocturnal build-up, but followed a similar trend after 5 a.m., even though the increase in CH_4 mole fractions after 9 a.m. was much smaller than the London one (Figure 6.28). During the night, air masses in Egham were coming from the western sector, as suggested by the NOAA back trajectories (Figure 6.29), so that emissions in the London area should have not affected the mole fractions recorded at Egham.

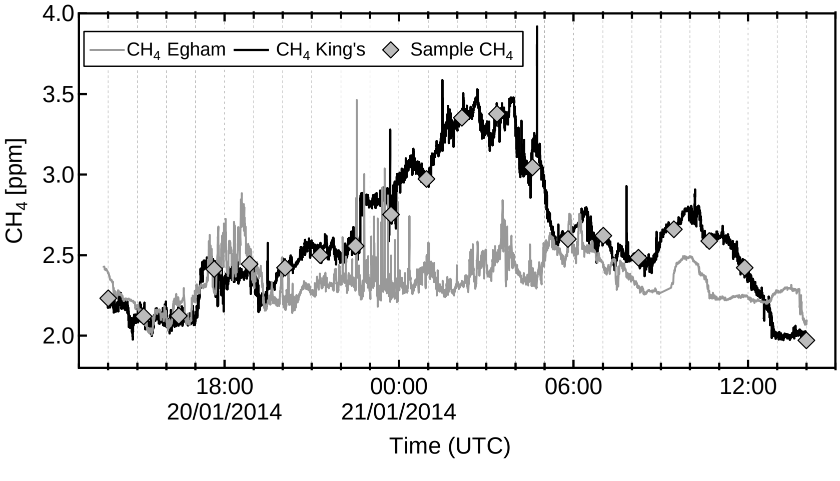

Figure 6.28 CH_4 mole fractions recorded at King's College (black line) and in Egham (grey line) on 20th and 21st January 2014. Grey markers are CH_4 mole fractions of samples collected on the King's College roof.

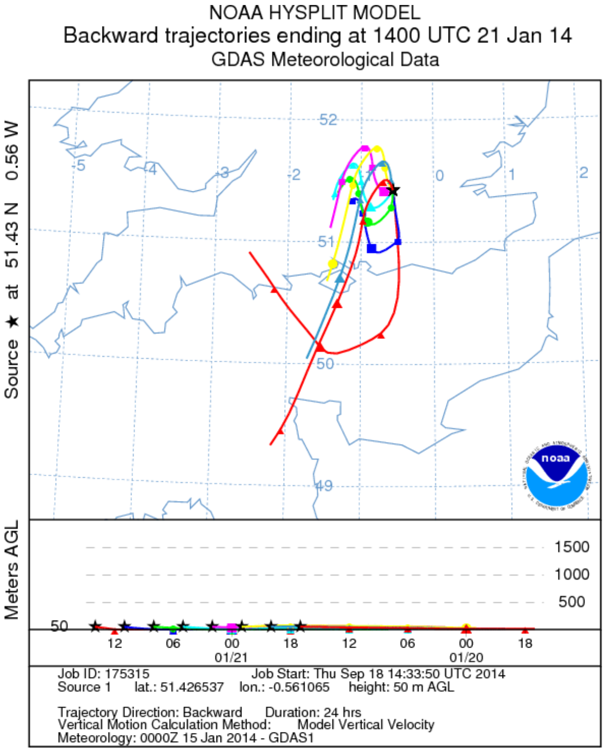

Figure 6.29 Back trajectories calculated using Hysplit trajectory model provided by NOAA. 9 back trajectories, one every 3 hrs, are shown for the 21st January 2014 for air arriving at the Earth Sciences Department of RHUL (Egham).

A ^{13}C enriched signature of -40 ‰ for air sampled between 2 p.m. and 7 a.m. revealed a mainly fossil CH_4 contribute to the CH_4 emissions in central London (Figure 6.30). Conversely, samples collected during the morning of the 21st showed a more ^{13}C depleted signature and, by including those samples and the background value (grey marker in Figure 6.30) in a Keeling plot, a source signature of -51.5 ±2.6 ‰ was obtained. The wind direction from 9 a.m. and 11 a.m., during the CH_4 peak, was from SSE (Figure 6.31), which is the wind sector where biogenic CH_4 emissions seem to come from during the morning.

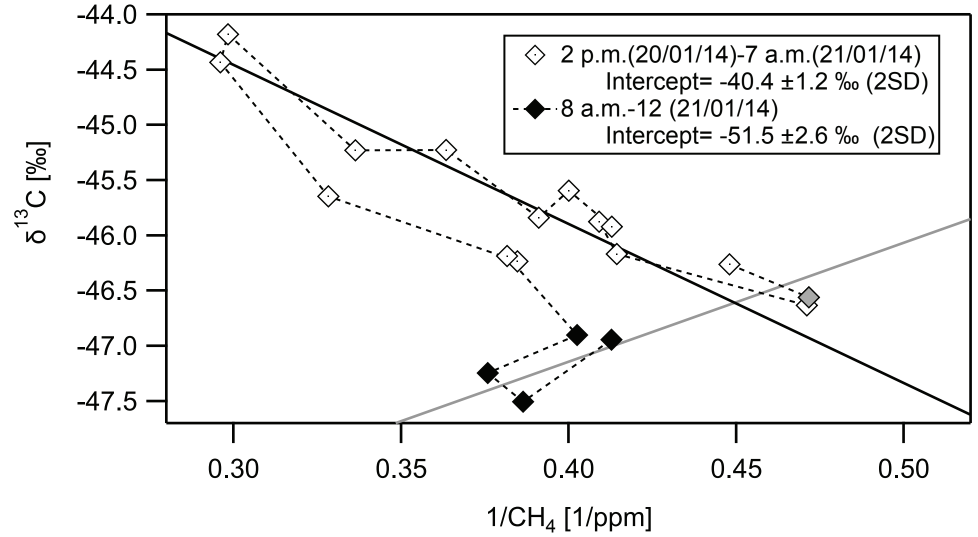

Figure 6.30 Keeling plots based on the samples collected during the 20th and the early morning of the 21st January 2014 (white markers) and during the morning of the 21st January 2014 (black markers). The dotted line follows the order of sampling.

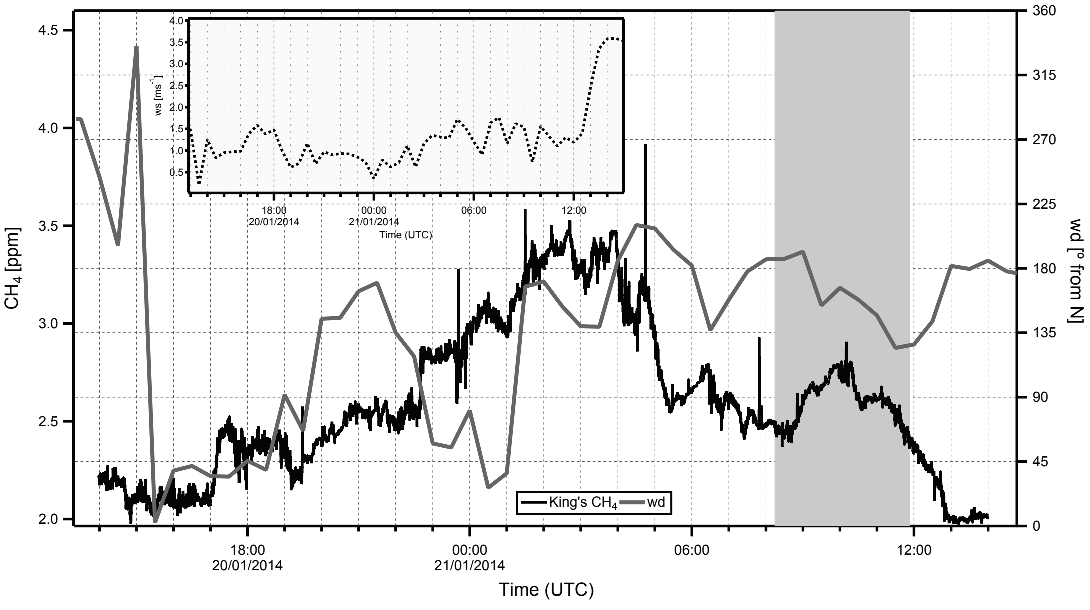

Figure 6.31 Wind direction (grey line) and speed (line in the embedded graph) trend recorded at King's College on the 20th and 21st and CH$_4$ mole fractions (black line) continuously measured on King's College roof. The grey section highlights the time interval of those samples which are thought to be associated with a biogenic CH$_4$ source.

6.5.5 30th-31st January 2014

CO_2 and CH_4 mole fractions on 30th and 31st January were highly fluctuating and no persistent nocturnal build-up was recorded, and mole fractions of both gases abruptly decreased after 8 a. m. on 31st (Figure 6.32). CH_4 mole fractions in London were higher than in Egham throughout the whole sampling period (Figure 6.33), suggesting that different weather conditions occurred at the two stations (i.e. wind direction and speed, atmospheric stability) and different sources contributed to the CH_4 peaks.

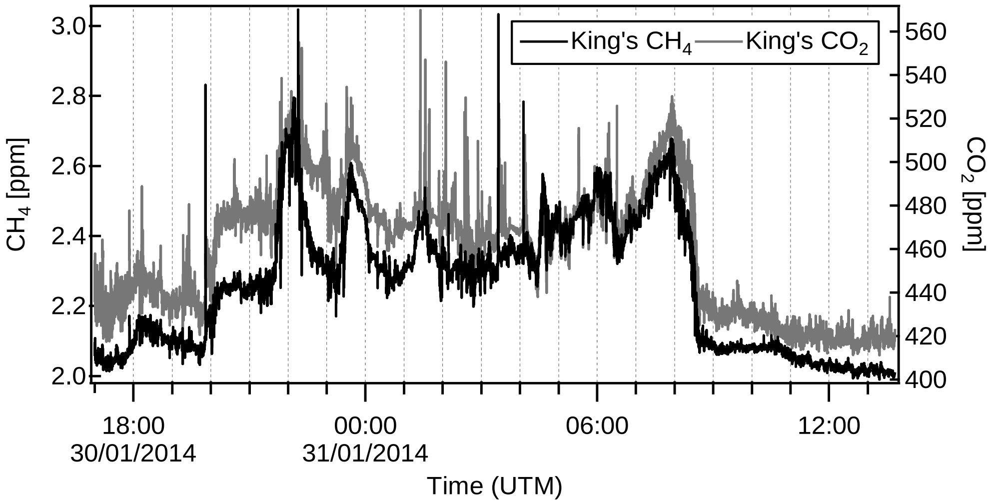

Figure 6.32 CH_4 (black line) and CO_2 (grey line) mole fractions recorded on King's College roof on 30th and 31st January 2014.

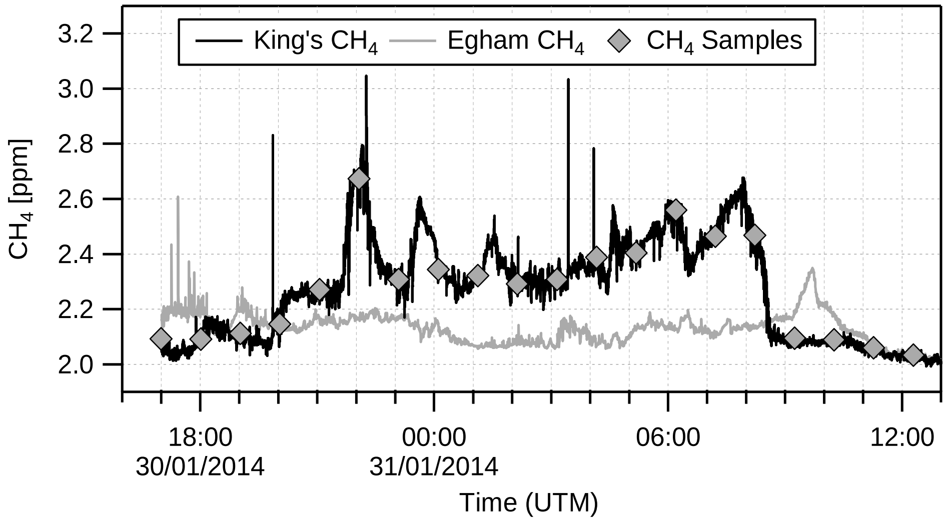

Figure 6.33 CH_4 mole fractions recorded at King's College (black line) and in Egham (grey line) on 30th and 31st January 2014. Grey markers are CH_4 mole fractions of samples collected on the King's College roof.

Natural gas losses are likely to have determined CH_4 peaks between 5 and 9 p.m. on the 30th in central London, as suggested by a source signature of -35.9 ±0.5 ‰ (2SD) (Figure 6.34). A more ^{13}C depleted signature calculated on some samples collected overnight indicated a more mixed CH_4 source. Isotopic values greatly differed overnight, following the discontinuous mole fraction trend. By linking with a Keeling plot the sample collected at 10 a.m. on the 31st (black circle in Figure 6.34) with the one taken as the background, a source signature of -51.1 ‰ resulted, which might have been related to the biogenic source previously identified in the sampling campaign of the 10th December 2013.

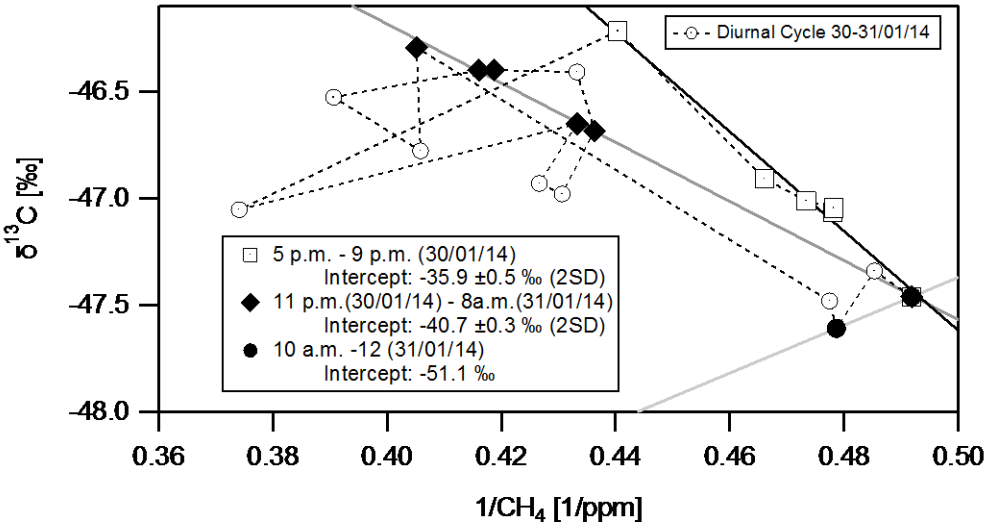

Figure 6.34 Keeling plots for the period 30th January 5 p.m. to 9 p.m. (white squared markers) and 30th January 11 p.m. to 31st January 8 a.m. (black squared markers). The circle black marker is the sample collected the 31st January at 10 a.m.. The dotted line follows the order of sampling.

Wind direction in central London was extremely variable, mainly southerly; the 10 a.m. sample was specifically associated with the SSE wind direction, strengthening the hypothesis of a biogenic CH_4 source on the SSE side of King's College (see Figure 6.35). The nocturnal build-up is associated to low wind speeds (<2ms^{-1}), whereas the mole fraction collapse occurred when the turbulence intensity and wind speeds started increasing (after 8 a.m.).

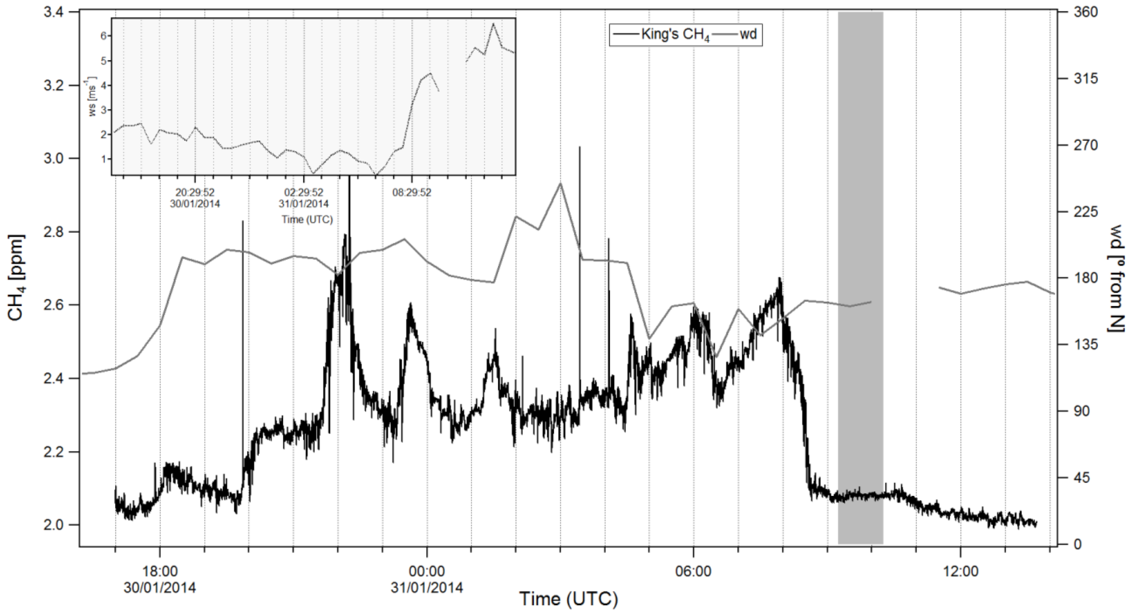

Figure 6.35 Wind direction (grey line) and speed (line in the embedded graph) trend recorded at King's College on 30th and 31st January, and CH_4 mole fractions (black line) continuously measured at King's College. The grey section highlights the time interval of the sample which is thought to be associated with a CH_4 biogenic source.

6.5.6 12th-13th-14th March 2014

Sampling was carried out over two consecutive nights from 12th to 14th March. Figure 6.36 shows CH_4 mole fractions recorded in Egham and samples collected at King's College, since the Picarro instrument was not available for continuous CH_4 measurements in March. NOAA back trajectories show that air masses in Egham were coming from the London region and a similar trend between the two stations was expected (Figure 6.37). In fact, both samples collected and CH_4 continuous mole fractions exhibited two daily cycles that are fairly comparable, except for CH_4 mole fractions recorded in Egham from 4 a.m. to 1 p.m. on the 13th, which were 0.4 ppm higher than in London, and a mole fraction peak at 11:30 p.m in London. The build-up occurring during both nights is concomitant with the nocturnal drop of the wind speed (see Figure 6.40).

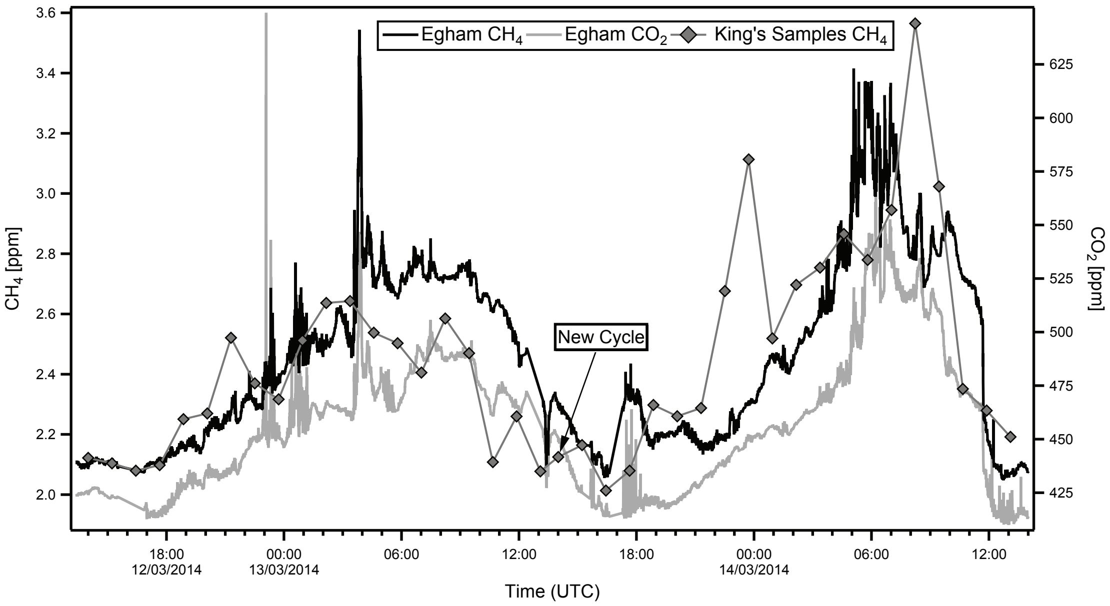

Figure 6.36 CH_4 (black line) and CO_2 (grey line) mole fractions recorded in Egham on the 12th, 13th and 14th March 2014 and CH_4 mole fractions of samples collected on King's College roof (grey markers).

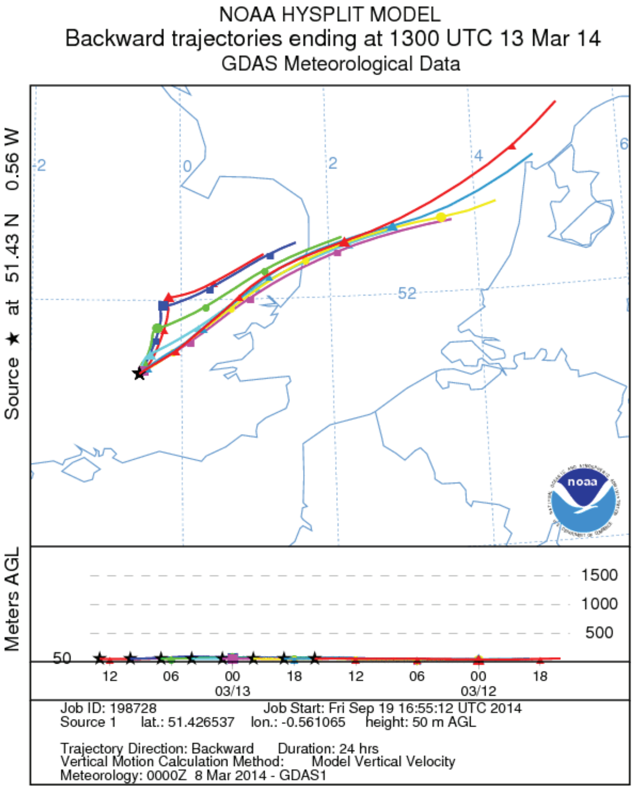

Figure 6.37 Back trajectories calculated using Hysplit trajectory model provided by NOAA. 9 back trajectories, one every 3 hrs, are shown for the 13th March 2014 for air arriving at the Earth Sciences Department of RHUL (Egham).

Not all the samples collected were included in a Keeling plot, due to the mixed nature of CH_4 emissions in London and the consequent variety of isotopic values. However, two similar patterns can be identified with the Keeling plot analysis, which gives a source signature of approximately -43 ‰ in both diurnals (Figure 6.38 and 6.39). Furthermore, a ^{13}C depleted source signature (<-50 ‰) indicative of a biogenic source, is calculated from the Keeling plot based on samples collected around midnight for both samplings. The biogenic CH_4 emissions that in previous samplings were spotted during the morning, seem to be detected around midnight. The wind direction associated with those emissions was SSE for the first sampling and ESE for the second one, consistently with the sector ascribed to the biogenic source detected during previous winter samplings.

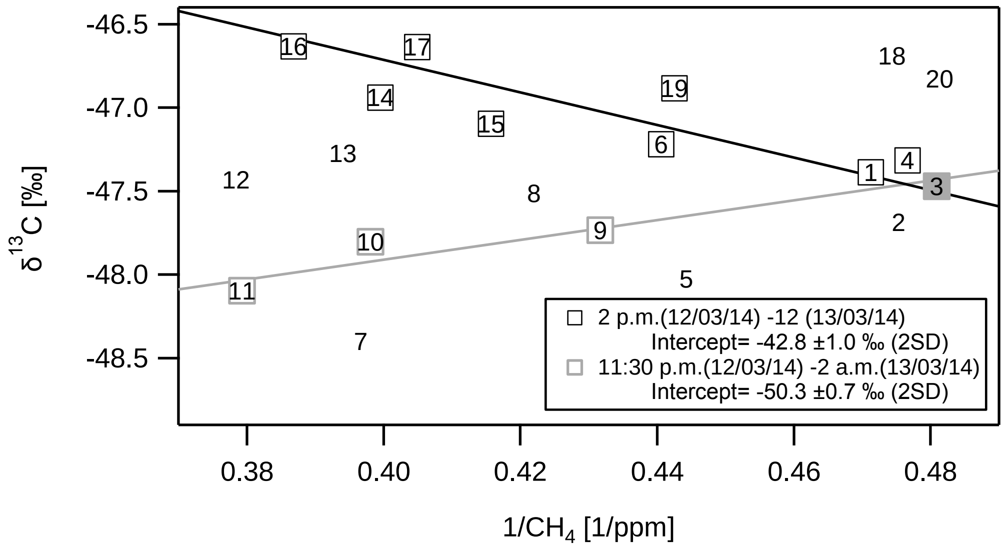

Figure 6.38 Keeling plots for the period 12th March 2014 2 p.m. to 13th March 12 (black line). In grey is the Keeling plot based on samples collected from 11:30 p.m. on 12th March to 2 a.m. on 13th March. The grey marker represents the background value.

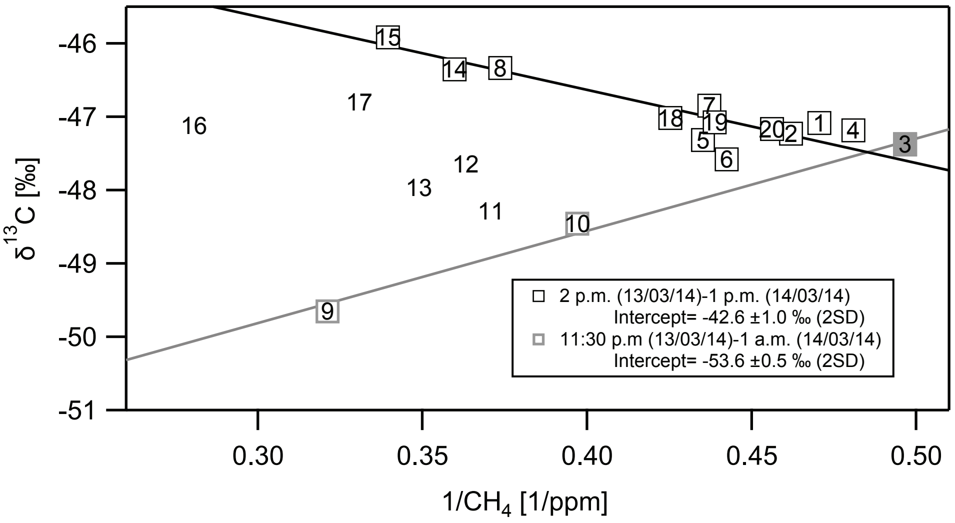

Figure 6.39 Keeling plots for the period 13th March 2014 2 p.m. to 14th March 1 p.m. (black line). In grey is the Keeling plot based on samples collected from 11:30 p.m. on 13th March to 1 a.m. on 14th March. The grey marker represents the background value.

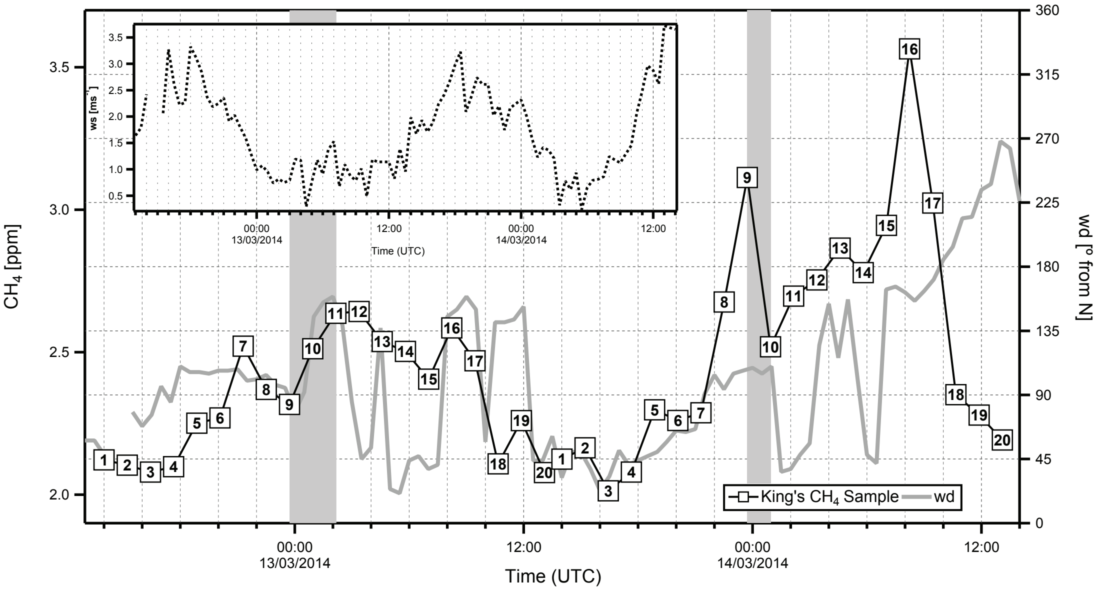

Figure 6.40 Wind direction (grey line) and speed (line in the embedded graph) trend recorded at King's College on 12th, 13th and 14th March 2014 and CH_4 mole fractions (white markers) of samples collected at King's College. The grey sections highlight the time intervals of those samples that are thought to be associated with a biogenic CH_4 source.

6.5.7 24th-25th July 2014

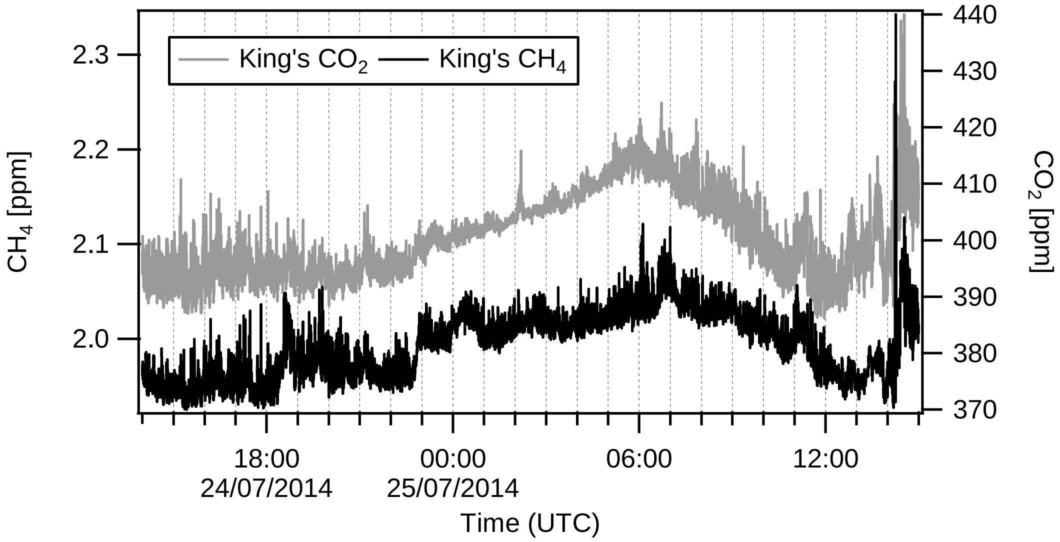

Figure 6.41 CH$_4$ (black line) and CO$_2$ (grey line) mole fractions recorded on King's College roof on 24th and 25th July 2014.

Both CH$_4$ and CO$_2$ mole fractions recorded at King's College between the 24th and 25th July showed a nocturnal build-up and a sharp peak in the early afternoon approximately at 3 p.m. (Figure 6.41).

Mole fractions recorded at Egham followed the same trend but were lower throughout the whole cycle, except for a peak measured from 7 to 9 p.m. caused by a putative local methane source (Figure 6.42).

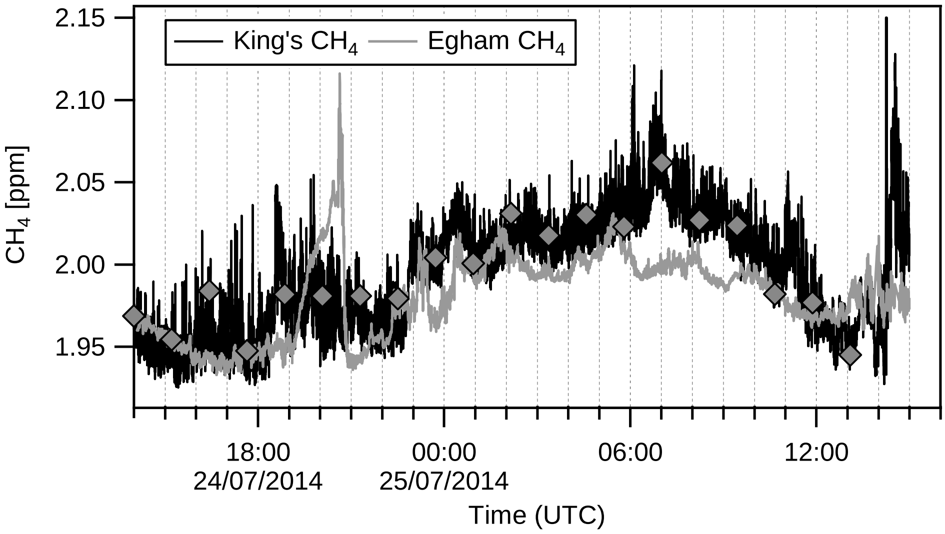

Figure 6.42 CH$_4$ mole fractions recorded at the King's College (black line) and in Egham (grey line) on 24th and 25th July 2014. Grey markers are CH$_4$ mole fractions of samples collected on the King's College roof.

NOAA back trajectories for the 25th of July suggest that air was coming from the NE sector at the Egham station (Figure 6.43), and so from the London region, explaining the consistency of methane mole fractions trends between King's College and Egham.

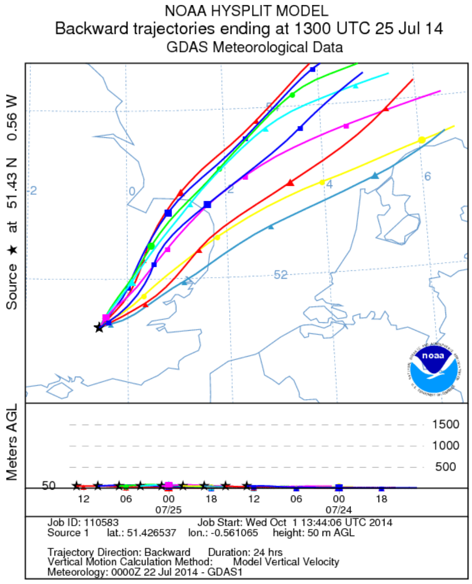

Figure 6.43 Back trajectories calculated using Hysplit trajectory model provided by NOAA. 9 back trajectories, one every 3 hrs, are shown for the 25th July 2014 for air arriving at the Earth Sciences Department of RHUL.

The Keeling Plot based on samples collected from 2 p.m. to 8 a.m. gives an intercept of -44.2 ±2.0 ‰ (2SD), which reflects a combination of different sources (Figure 6.44).

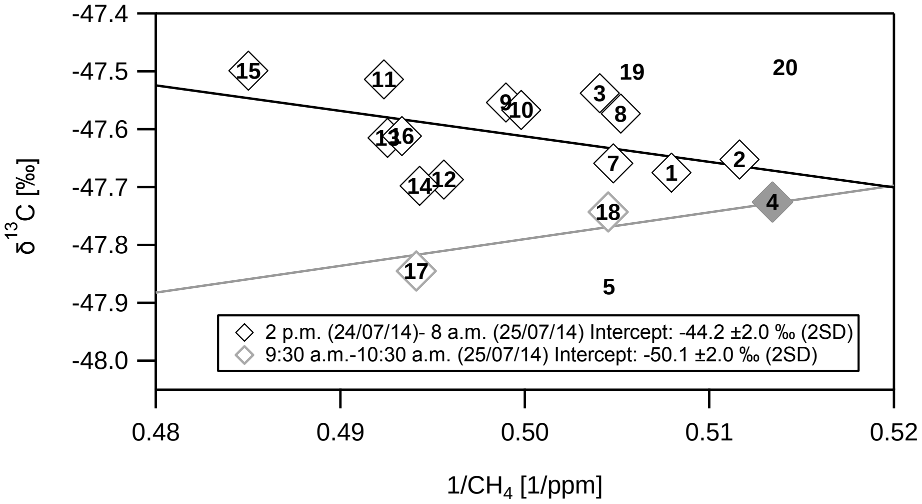

Figure 6.44 Keeling plots for the period 24th July 2 p.m. to 25th July 8 a.m. (black line) and for the period 25th July 9:30 a.m. to 10:30 a.m. (grey line). The grey marker represents the background sample.

The 9:30 a.m. and 10:30 a.m. samples are ^{13}C depleted relative to all the other samples, in particular the 9:30 a.m. sample (number 17 in Figure 6.44), which might be related to the hypothesized biogenic CH_4 source characterising morning emissions.

Wind was steadily coming from the NNE sector during the overnight build-up, becoming more variable during the morning and the early afternoon after 12 p.m., when wind speed increased (Figure 6.45) and the level of atmospheric stability was recorded as extremely unstable (Figure 6.46).

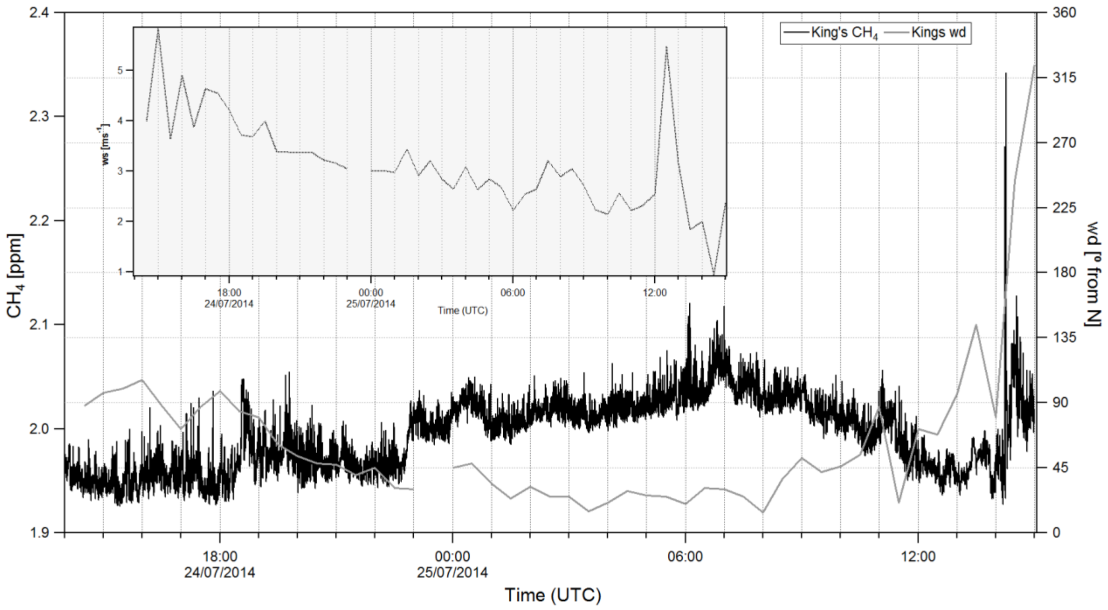

Figure 6.45 Wind direction (grey line) and direction (line in the embedded graph) trend recorded at King's College on 24th and 25th July 2014 and CH_4 mole fractions (black line) continuously measured on King's College roof.

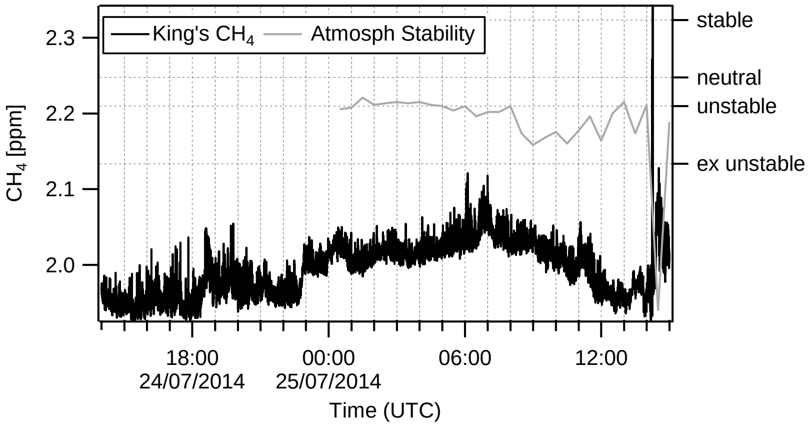

Figure 6.46 Atmospheric stability trend (grey line) recorded at King's College on 24th and 25th July 2014 and CH_4 mole fractions (black line) continuously measured on King's College roof.

6.5.8 7th-8th August 2014

During the sampling on 7th and 8th August no clear nocturnal build-up was recorded, but both CO_2 and CH_4 mole fractions started increasing in the morning after 6 a.m., reaching a peak between 8 and 9 a.m (Figure 6.47).

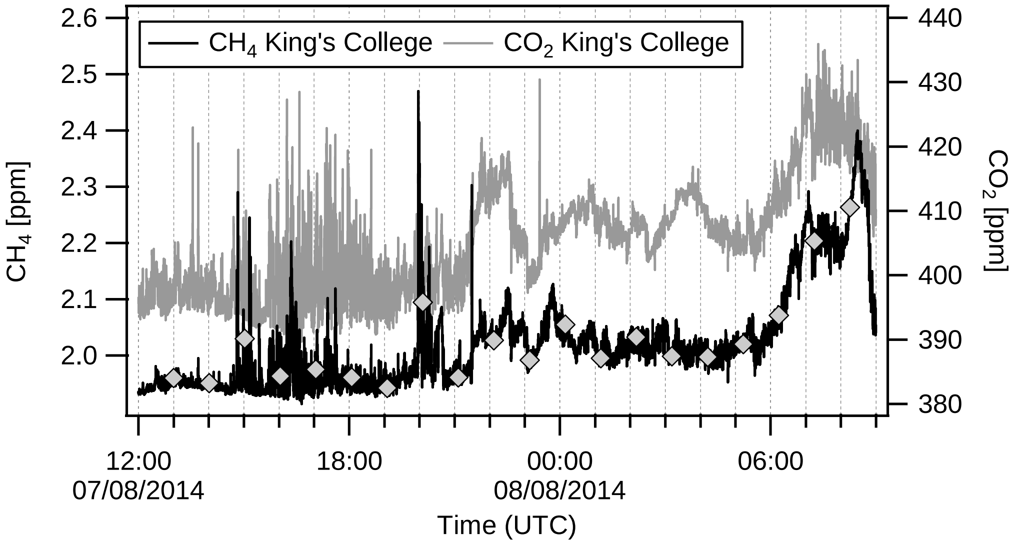

Figure 6.47 CH_4 (black line) and CO_2 (grey line) mole fractions recorded on King's College roof on 7th and 8th August 2014. Grey markers are CH_4 mole fractions of samples collected on the King's College roof.

Conversely CH_4 mole fractions in Egham were much higher overnight than in central London, and decreased in the morning after 7 a.m. (Figure 6.48). This discrepancy in mole fractions between the two stations can be better understood by observing the air back trajectories for Egham (Figure 6.49), which show the southern provenance of air masses. CH_4 releases originating either from the agricultural areas or from the Trumps Farm landfill located to the south of Egham might have contributed to the nocturnal build-up.

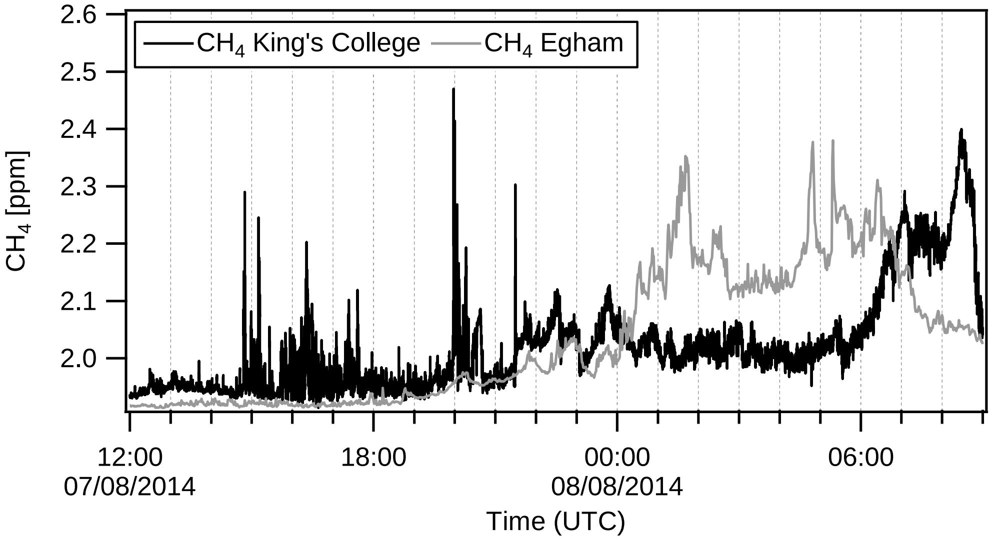

Figure 6.48 CH$_4$ mole fractions recorded at the King's College (black line) and in Egham (grey line) on 7th and 8th August 2014.

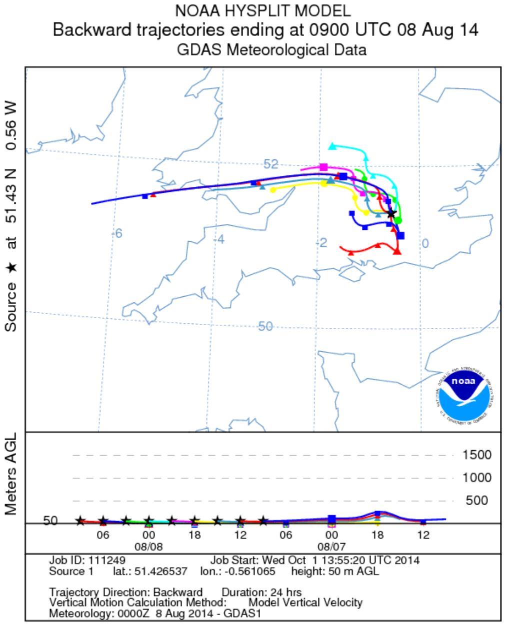

Figure 6.49 Back trajectories calculated using Hysplit trajectory model provided by NOAA. 9 back trajectories, one every 3 hrs, are shown for the 8th August 2014 for air arriving at the Earth Sciences Department of RHUL.

An intercept of approximately -40 ‰ resulted from the Keeling plot obtained with the samples collected on 7th August (Figure 6.50). The Keeling plot based on the three samples collected during the morning build-up defines an intercept of -54.7 ±2.5 ‰ (2SD), suggesting a $\delta^{13}C$ signature distinctive of a biogenic source. Air was steadily coming from ESE from midnight onwards and the morning build-up might be explained by the drop in wind speed occurring after 5 a.m. (see Figure 6.51).

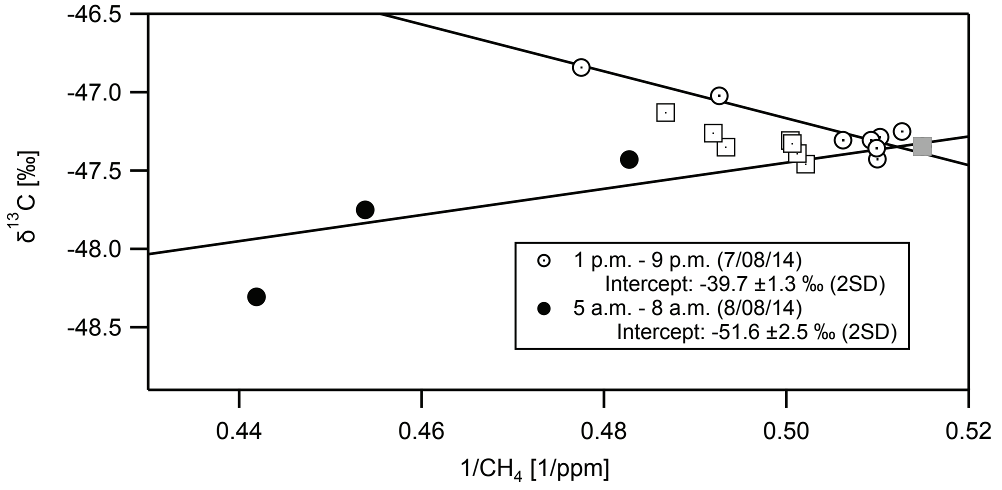

Figure 6.50 Keeling plots for the period 7th August 1 p.m. to 9 p.m. (white circular markers), for the period 7th August 10 p.m. to 8th August 4 a.m. (white square markers) and for the period 8th August 5 a.m. to 8 a.m. (black markers). The grey square represents the value taken as background.

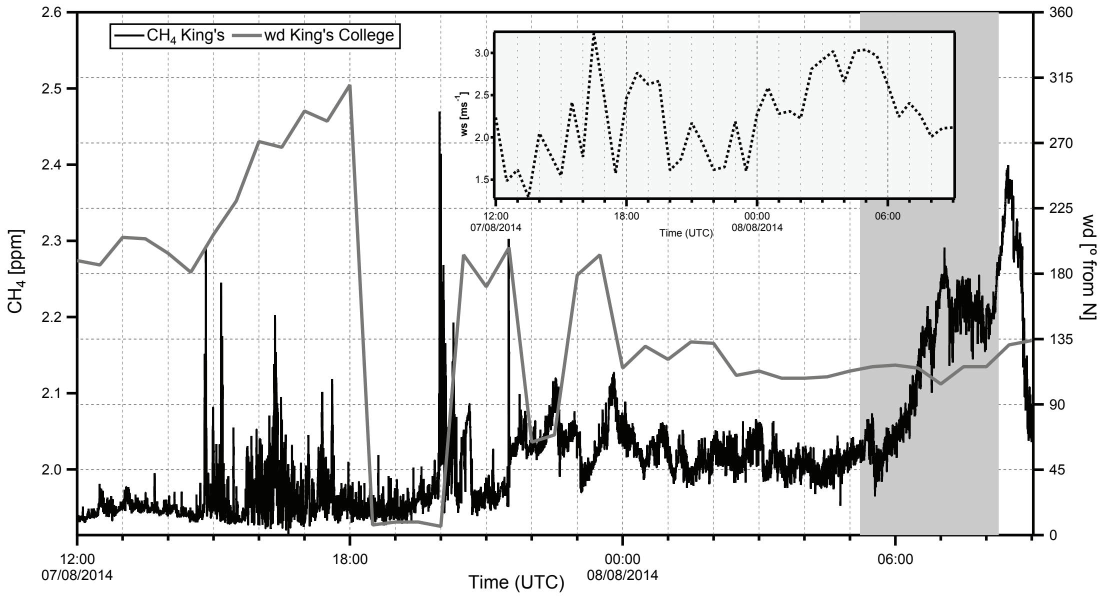

Figure 6.51 Wind direction (grey line) and speed (line in the embedded graph) trend recorded at King's College on 7th and 8th August 2014 and CH_4 mole fractions (black line) continuously measured on King's College roof.

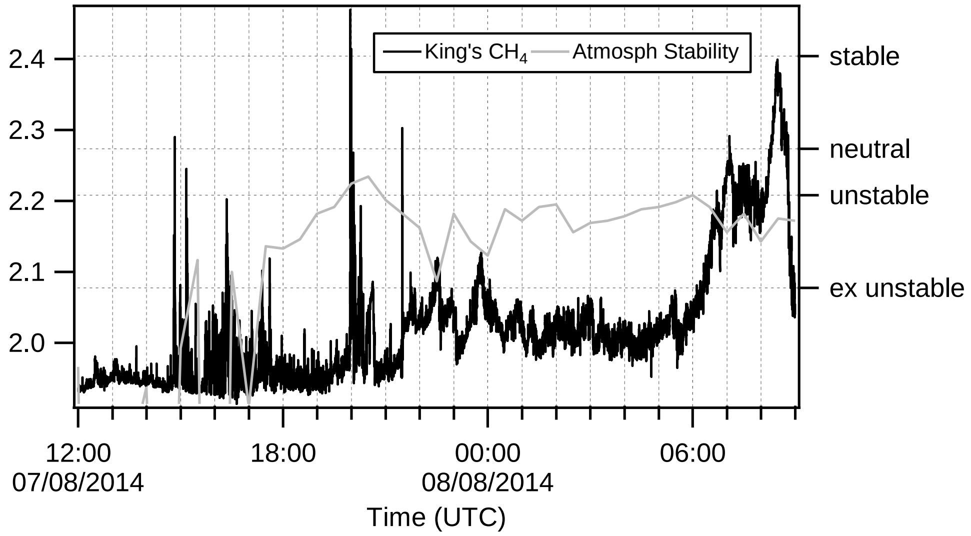

Figure 6.52 Atmospheric stability trend (grey line) recorded at King's College on 7th and 8th August 2014 and CH_4 mole fractions (black line) continuously measured on King's College roof.

6.5.9 Comparison between Winter and Summer Diurnal Studies

CH_4 mole fractions recorded in central London peaked at 3.4 ppm during winter time (December and January) and 2.4 ppm in the summer period (July and August). A stronger CH_4 build-up during winter reflects the occurrence of shallower inversions overnight and a less intense atmospheric turbulence.

The winter pollution rose in Figure 6.53a indicates SSW as the preferential wind provenance for CH_4 background (1.9-1.95 ppm) and attributes the highest CH_4 mole fractions to the eastern sector. Similarly, during summer, most of the lowest CH_4 mole fractions come from SSW, but wind directions tend to be more variable due to the stronger thermal turbulence taking place in summer.

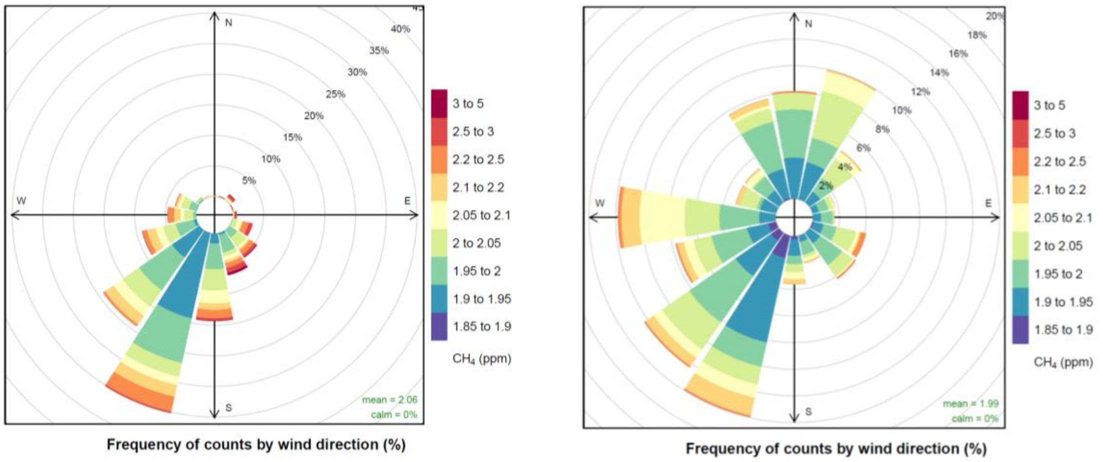

(a) **(b)**

Figure 6.53 Pollution roses based on CH_4 mole fraction and wind data measured in central London in winter 2013-2014 (a) and summer 2014 (b).

Polar plots, which show the mean mole fractions by wind speed and wind direction, were created for CO_2 and CH_4 mole fractions recorded at King's College during the winter and summer period.

The plots based on winter data (Figure 6.54) display a similar pattern, with high mole fractions uniformly distributed around the measuring station and associated with low speed winds.

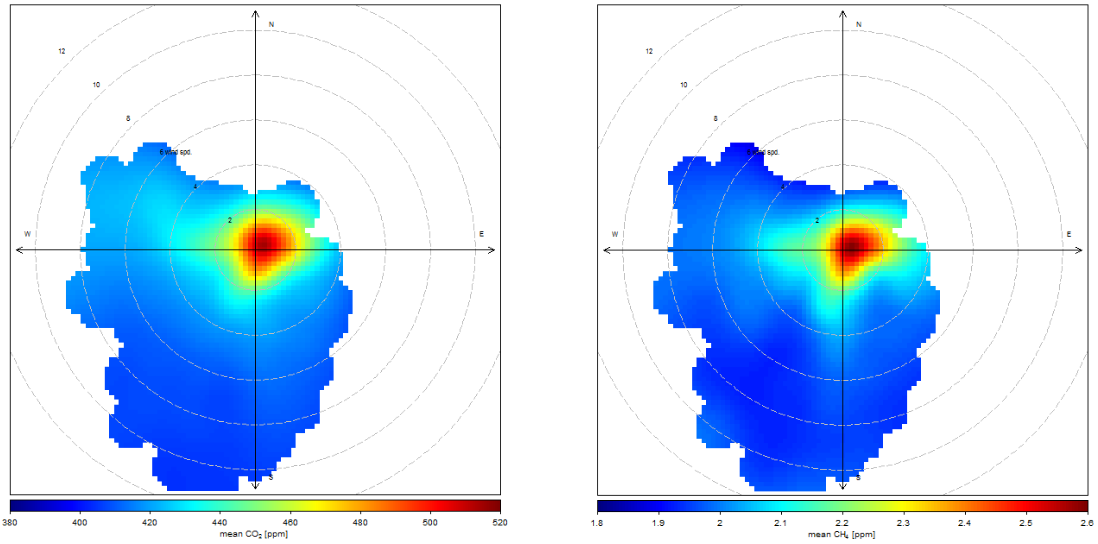

(a) **(b)**

Figure 6.54 Polar plots of CO_2 (a) and CH_4 (b) mole fraction data (in ppm) recorded in December 2013 and January 2014 in central London.

The summer period CH_4 polar plot does not show the "concentric" mole fraction pattern observed during the winter (Figure 6.55), due to higher wind speeds and a wider range of wind directions. Higher CH_4 mole fractions are polarised on the eastern and western sectors (Figure 6.55b) and are particularly associated with south-westerly and surprisingly with high speed winds. This different behaviour during summer might indicate that CH_4 emissions originate from other sources than in winter, for instance from a biogenic source, whose releases are augmented by higher temperatures, or from occasional gas leaks. CO_2 mole fractions are consistent in all directions (Figure 6.55a), with slightly higher mole fractions associated with low wind speed. During summer, the photosynthetic uptake of CO_2 by the vegetation and a reduced usage of the gas central heating lead to lower CO_2 mole fractions and a different CO_2 pattern. However, considering central London as the only area of influence, the plants overnight respiration and the photosynthesis do not play a central role in the CO_2 balance.

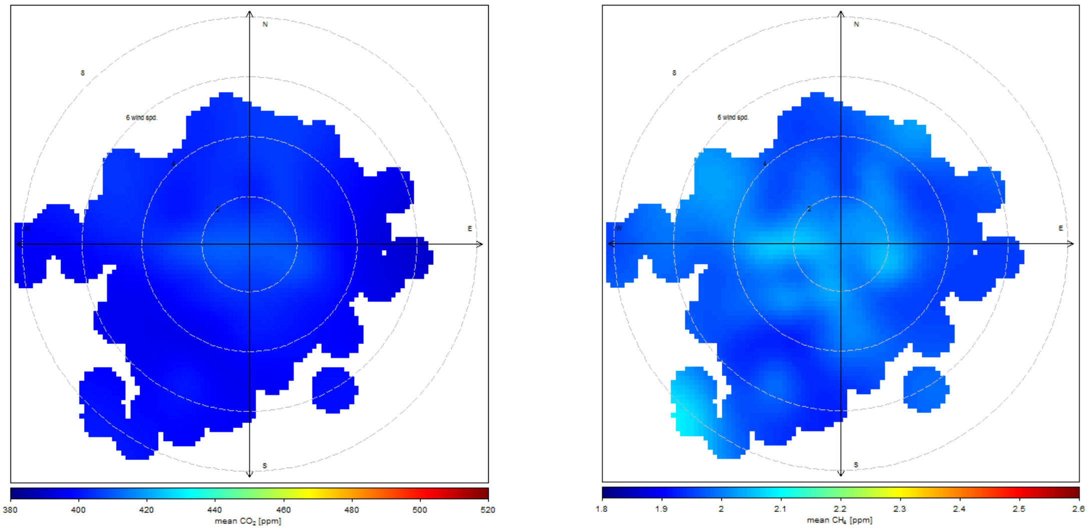

(a) **(b)**

Figure 6.55 Polar plots of CO_2 (a) and CH_4 (b) mole fractions (ppm) measured in central London in July and August 2014.

For the Egham station, during winter, CO_2 and CH_4 polar plots (Figure 6.56) show the same pattern: high mole fractions are associated mostly with the ENE sector, corresponding with the Staines gas works and the M25.

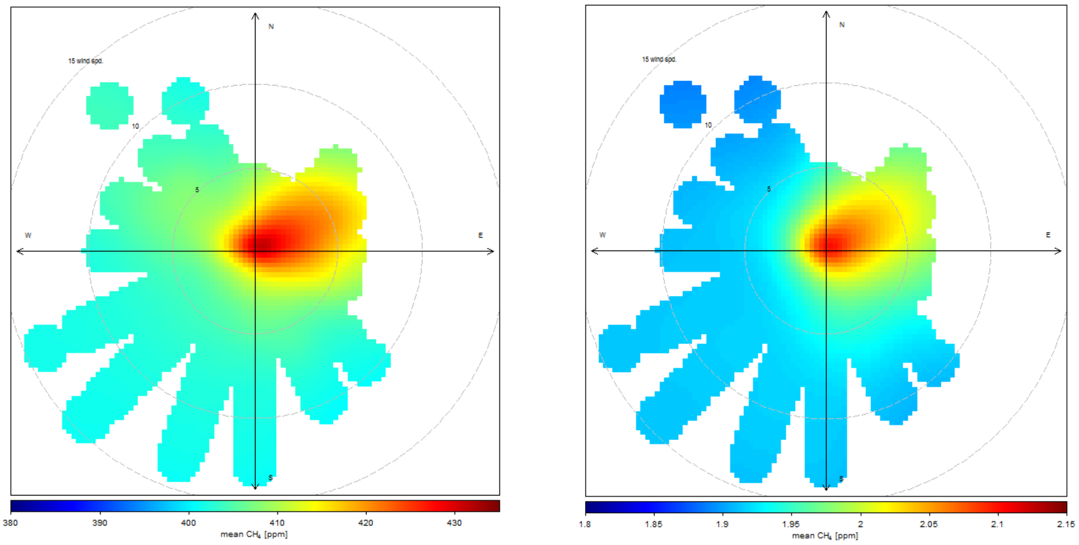

(a) **(b)**

Figure 6.56 Polar plots of CO_2 (a) and CH_4 (b) mole fractions (ppm) measured in Egham in December 2013 and January 2014, based on the continuous measurements recorded at RHUL for the same period that the Picarro was at King's College. Wind directions are available only for the main sectors and no intermediate values are recorded.

During summer CH_4 mole fractions seem to be more uniformly distributed around the measuring station than in London (Figure 6.57). The RHUL Earth Sciences department is located in a semi-rural area and therefore not subjected to the alteration of the local wind pattern created by the city buildings and the so called "urban island effect". Higher CH_4 mole fractions come also from the NW of the sampling site, where very local sources such as a boiler house and buildings in the campus have been attested to contribute to the measured mole fractions (Fisher, 2006). Higher CO_2 mole fractions seem to be associated with more northerly winds.

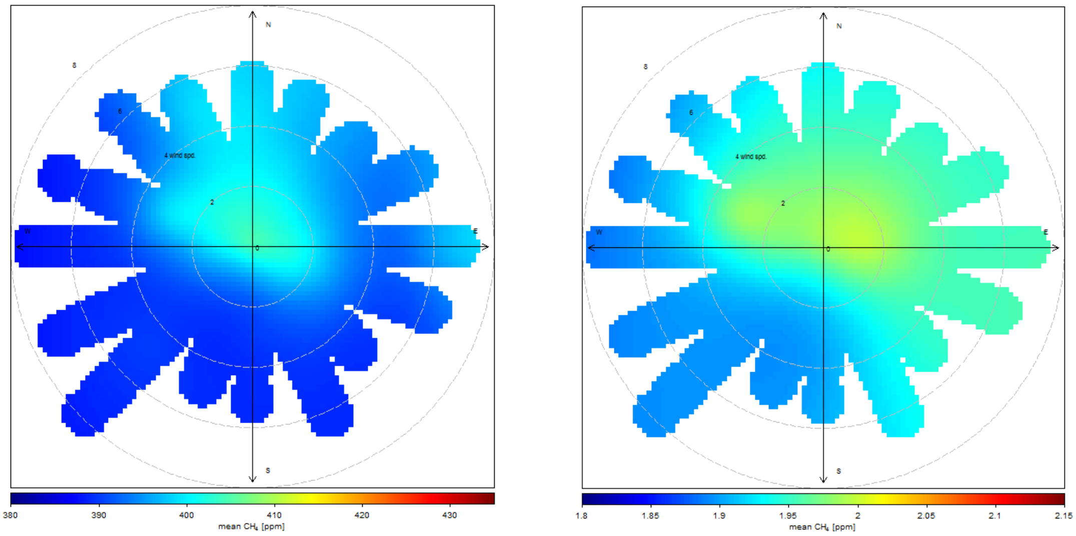

(a) **(b)**

Figure 6.57 Polar plots of CO_2 (a) and CH_4 (b) mole fractions (in ppm) measured in Egham in July and August 2014.

A CH_4 diurnal profile built with median values of mole fractions for each hour of the day (Figure 6.58) to minimise the influence of residual local CH_4 plumes, as Rigby et al. (2008) did with CO_2 records, calculated with continuous measurements from King's College and RHUL, indicates that on average mole fractions recorded at King's College are higher, and shows a stronger over-night build-up. The median mole fraction at 8 a.m. in London represents the peak mole fraction of the morning build-up that was detected in central London during most of the sampling campaigns carried out and was not observed in Egham. During winter the morning collapse of mole fractions is occurring later than in summer, as the persistence of the inversion cap in the morning delays the growth of the boundary layer with the related incursion of clean air. Summer diurnal cycles, which refer only to the two weeks that the Picarro instrument was installed in central London, are more pronounced, reflecting a stronger intensity of the atmospheric turbulence due to a higher surface warming. The difference in CH_4 mole fractions between the two measuring stations is narrowed, and the diurnal cycles exhibit similar behaviour. Furthermore, the CH_4 mole fractions characterising the nocturnal build-up in Egham (0-4 a.m.) approach the values recorded in London and are higher than in winter, suggesting an increase in CH_4 emissions from biogenic sources (i.e. landfill sites) around Egham.

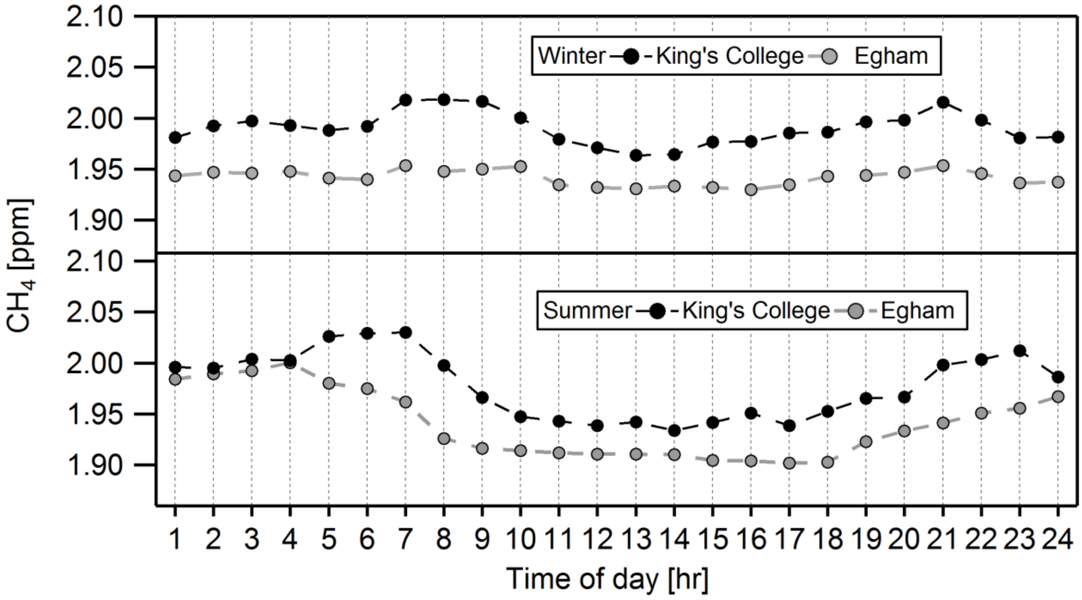

Figure 6.58 Diurnal cycle in winter and summer made with median mole fractions at each hour of the day. Median values are calculated according to the UTC time standard.

6.6 The Search for the Biogenic Methane Source in Central London

On 20th March 2015 a survey with the Picarro mobile system in central London was carried out, in order to identify methane sources directly while driving. The time slot between 8 and 9 o'clock was chosen, based on the time the biogenic source was detected when the Picarro analyser was set up on the King's College roof. Figure 6.59 shows the methane mole fractions measured in the borough of Westminster along the river banks.

Two samples were collected on the Westminster Bridge, on the east corner, where high methane mole fractions were found. During the survey the methane peak sampled was thought to be related to a methane source located on the north east side of the river, as the wind direction was NNE (red arrow in Figure 6.59). The Keeling plot intercept (Figure 6.60) calculated with the two samples collected in that corner and the background sample (-36.5 ±2.3‰ (2SD)) reveals the occurrence of a natural gas leak.

Since the excess of sewage discharged into the river without treatment is assumed to be the sought after biogenic methane source, it will be detected only after heavy rains, when the over flow is realised into the river to prevent the system backing up into people's home and streets. If the sewage is released significantly upriver from central London, it might take many days to reach the King's College London area according to its flow rate, by which point it would have mixed to give a delocalised source. Therefore, the biogenic source intercepted during diurnal studies must be very local, for instance from a storm relief located next to the King's College London. The complete absence of a detected biogenic signature during the survey in March 2015 might be explained by the dry conditions characterising that day and the whole previous week, as the Thames was not loaded with any untreated sewage.

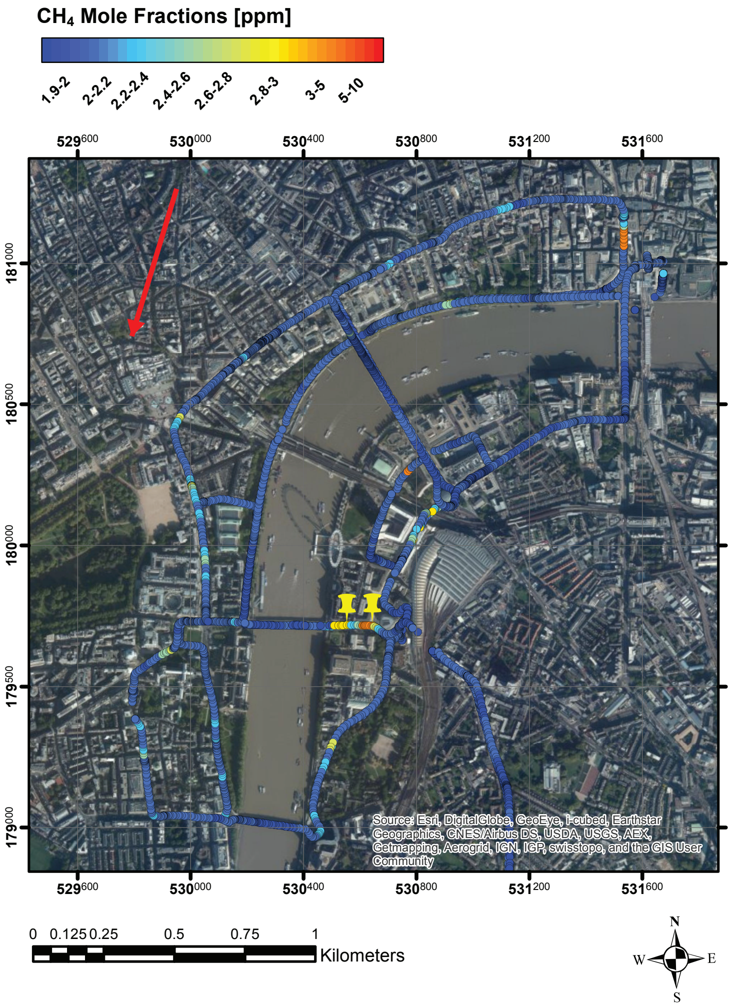

Figure 6.59 ArcGIS plot of methane mole fractions in ppm measured in central London, in the Borough of Westminster, on 20th March 2015. Yellow pushpins represent samples location and the red arrow the wind direction. The grid coordinates are displayed in the British National Coordinates System.

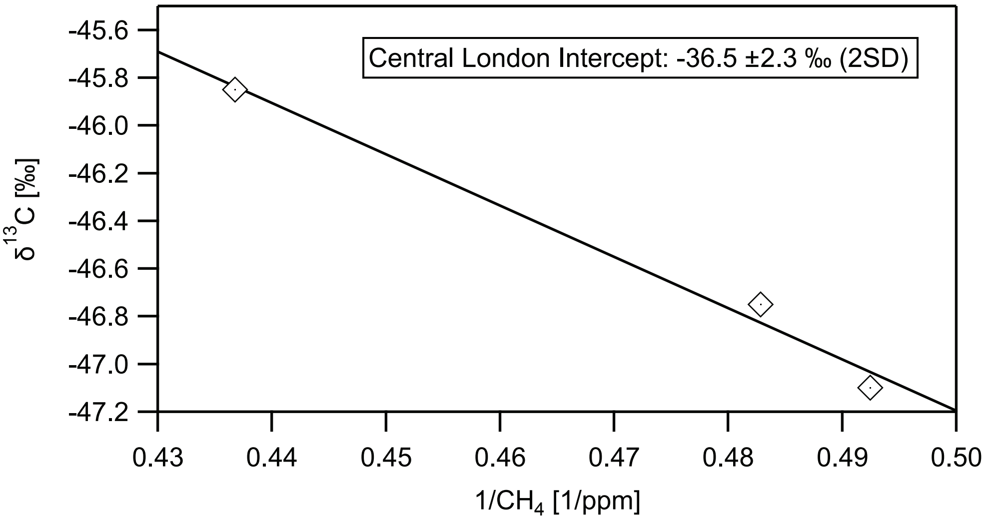

Figure 6.60 Keeling plot based on samples collected in central London on 20th March 2015.

6.7 Summary

Date	$\delta^{13}C$ isotopic signature (‰)	Time of samples included in the Keeling Plot
9th-10th Jul 2012	-38.1 ±4.7	2 p.m. (09/07/2012) -9 a.m. (10/07/2012)
2nd-3rd Dec 2013	-38.8 ±1.7	3 p.m. (2/12/2013) – 10 a.m. (3/12/2013)
10th-11th Dec 2013	-36.8 ±2.2	3 p.m.-10 p.m. (10/12/2013)
	-55.2 ±2.6	2 a.m.- 11 a.m. (11/12/2013)
20th-21st Jan 2014	-40.1 ±1.2	2 p.m. (20/01/2014) – 7 a.m. (21/01/2014)
	-51.5 ±2.6	8 a.m. -12 (21/01/2014)
30th-31st Jan 2014	-35.9 ±0.5	5 p.m. – 9 p.m. (30/01/2014)
	-40.7 ±0.3	11 p.m. (30/01/2014) – 8 a.m. (31/01/2014)
	-51.1 ±0.9	10 a.m. – 12 (21/01/2014)
12th-13th-14th March 2014	-42.8 ±1.0	2 p.m. (12/03/2014) – 12 (13/03/2014)
	-42.6 ±0.4	2 p.m. (13/03/2014) – 1 p.m. (14/03/2014)
	-50.3 ±0.7	11:30 p.m. (12/03/2014) – 2 a.m. (13/03/2014)
	-53.6 ±0.5	11:30 p.m. (13/03/2014) – 1 a.m. (14/03/2014)
24th-25th Jul 2014	-44.2 ±2.0	2 p.m. (24/07/2014) – 8 a.m. (25/07/2014)
	-50.1 ±2.0	9:30 a.m. -10:30 a.m. (25/07/2014)
7th-8th Aug 2014	-39.7 ±1.3	1 p.m. – 9 p.m. (07/09/2014)
	-40.6 ±3.7	10 p.m. (07/08/2014) – 8 a.m. (08/08/2014)
	-54.7 ±2.5	5 a.m. – 8 a.m. (08/08/2014)

Table 6.1 $\delta^{13}C$ source signatures calculated with the Keeling plot analysis for each diurnal study. Time is in UTC.

In a very densely populated and urbanised area like central London daily variations in CH_4 mole fractions are thought to be associated with the atmospheric turbulence and thus with the growth and the shrinkage of the boundary layer, rather than with the balance between sources and sinks (Vinogradova et al., 2007). The influence of natural sources is expected to be negligible and the photo-reaction with the radical OH, which represents the main sink, takes place in the middle troposphere. In every diurnal study carried out, CO_2 and CH_4 mole fractions were strongly correlated, with the exception of occasional local emissions, further evidence that the boundary layer dynamics and the variation in the wind regime are driving the daily trend in mole fractions. Therefore, the CH_4 isotopic source signature observed for the source mix in London should be fairly constant, especially during winter months, when the biogenic production of CH_4, which is highly variable and temperature dependant, is minor. Nevertheless, the winter source signature recorded during the afternoon and the nocturnal build-up ranged from -36.8 ±2.2 ‰ (2SD) to -40.7 ±0.3 ‰ (2SD), meaning that the relative contribution to the CH_4 budget of CH_4 sources was changing. Indeed, in central London the heating and the fossil fuel use varies with time of day and season.

The isotopic source signature during summer spans values between -39.7 ±1.4 ‰ (2SD) and -44.2 ±2.0 ‰ (2SD), lower than values observed during winter months. This seasonal variation might be ascribed to higher temperatures in summer that trigger the CH_4 production from urban biogenic sources (e.g. sewage works, landfills, River Thames).

Overall, the mean $\delta^{13}C$ source signature recorded in central London was -40.2 ±2.6 ‰ (2SD), not taking into account the most ^{13}C depleted signatures (<-50 ‰) characterising some mole fraction peaks. This value, being isotopically heavier than the background, confirms the primacy of fossil CH_4 emissions in the CH_4 budget in central London. However, in almost all diurnal studies, also a biogenic component was identified, mostly in the early morning. The consistency of this result does not question the main conclusion of this study -i.e. fossil fuel CH_4 sources represent the major contribution to the source mix- but highlights the occurrence of a biogenic source that might correspond to the River Thames, as the wind direction analysis demonstrates how the biogenic signature regularly coincides with the SSE wind sector (Figure 6.61).

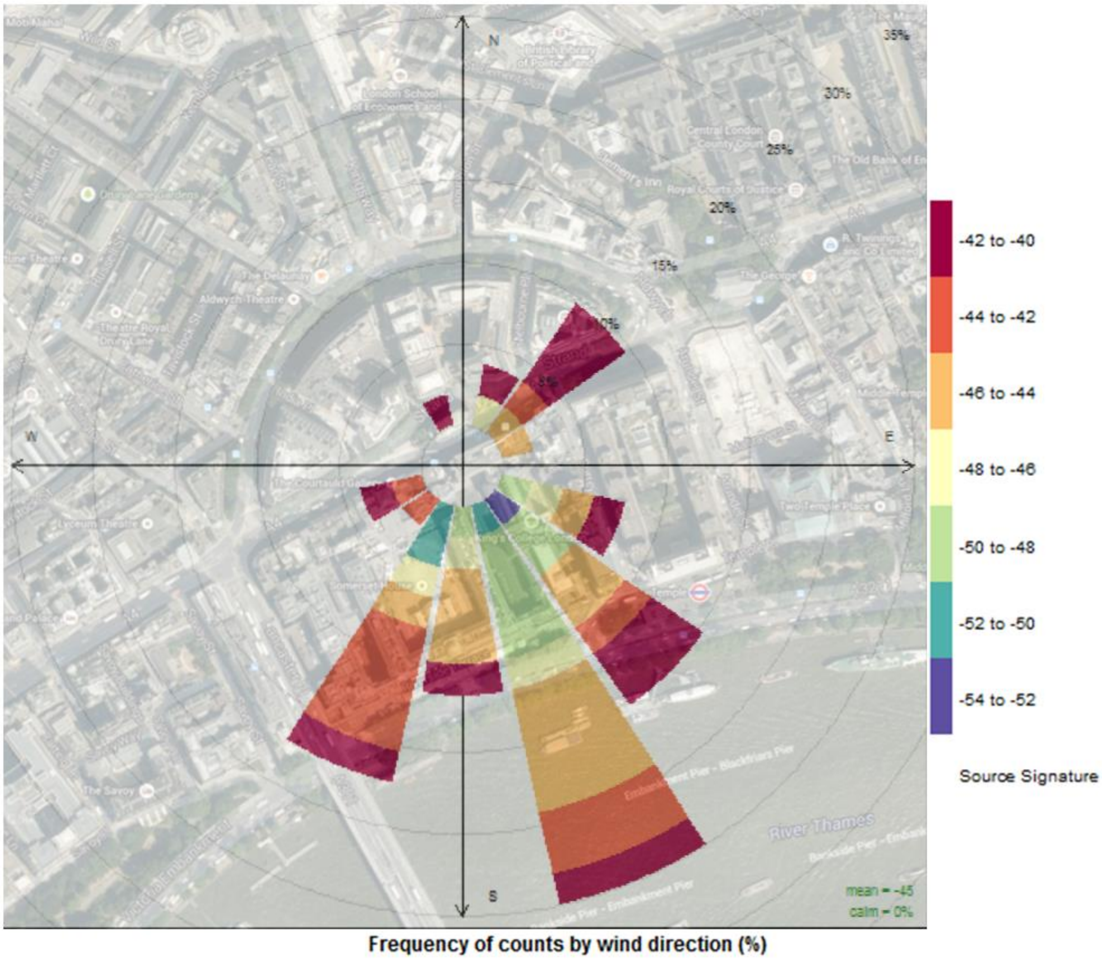

Figure 6.61 δ^{13}C Source Signature Rose made using the same method used for Figure 6.15.

The diurnal studies in winter were carried out on particularly foggy days, following heavy rain periods. Sewage plants in London still partly rely on the old collecting system and allow excess flows during heavy rain episodes to discharge directly the overflow into water courses, and this creates the suitable conditions for the anaerobic production of CH_4.

A comparison between CH_4 mole fractions in central London and Egham was also made, but each diurnal trend exhibits different features, according to the provenance of air masses, and this does not allow generalisations. Therefore diurnal cycles, made with median values calculated for each hour of the day during the whole period that the Picarro instrument was installed at King's College, were plotted, leading to important conclusions. Winter CH_4 mole fractions in central London were always higher than in Egham, demonstrating that fugitive emissions from the natural gas network and combustion are the main responsible sources for CH_4 accumulation in the city. This was verified also by comparing the isotopic values of air samples collected in London and in Egham at the same time during the diurnal study of the 9th July 2012, when the isotopic values observed for the London samples were all more enriched in ^{13}C than the Egham ones.

The sampling on the rooftop of King's College has proven to be extremely useful both for comparing the isotopic source signature between an urban and a semi-rural area and for a better comprehension of the CH_4 source scenario in a big conurbation.

6.7.1 An Insight into the London Inventories

The National Atmospheric Emission Inventory (NAEI) website makes available total emission in tonnes per km^2 for 2012 by source categories (see National Inventories in Chapter 3.3). With CH_4 emissions divided by sources categories, whose isotopic signatures have been assessed in this thesis work, a weighted isotopic value for central London was estimated. The main contribution to the CH_4 emissions detected at the King's College station comes from sources in a radius of about 300-1000 m around the King's College tower (Kotthaus and Grimmond, 2013), and it is then limited to centre of London. An isotopic signature of -38 ‰ results from the calculation if an area of about 1 km^2 around the Strand Campus of King's College London is considered, which is fairly consistent with the mean $\delta^{13}C$ source signature measured in central London (-40.2 ±2.6 ‰ 2SD). Since methane emission inventories show high uncertainty (see Chapter 3.3), the calculated isotopic signature represents only approximately the actual CH_4 source mix, but provides further confirmation that fossil CH_4 emissions, such as gas leaks, vehicle exhausts and other combustion sources are the major contributors to the CH_4 urban budget.

7

DISCUSSION

7.1 Regional Isotopic Characterisation and the Validation of Inventories

7.1.1 Revised $\delta^{13}C-CH_4$ Signatures

By the identification and sampling of methane emissions plumes during source studies (see Chapter 5) and the calculation of a source isotopic signature by Keeling plot analysis, typical $\delta^{13}C-CH_4$ values have been allocated to the major methane sources in the UK. All the $\delta^{13}C-CH_4$ values that have been revised in this study (values with the asterisk) are listed in Table 7.1.

UK Methane Sources	Emission Kt (2012)	Typical $\delta^{13}CH_4$ (‰)
Waste disposal and Landfills	884	-58*
Enteric Fermentation (cows)	745	-66*
Agriculture (Manure Management)	316	-58
Gas transmission and distribution	189	-36*
Wastewater handling	78	-53*
Coal Mining	76	-45*
Combustion (Industrial and Domestic)	43	-25
Biomass Burning	3	-28
Road transport	3	-12*
UK Total	**2337**	**-57.2**

Table 7.1 $\delta^{13}C$ signatures of UK methane sources, based on measured values (Lowry et al., 2001; Fisher, 2006) and literature review. * indicates values which have been revised by this study. 2012 NAEI emission inventories are provided without errors. Errors of measured isotopic values are within ±3 ‰. The isotopic values for coal mining range between -51 and -30 ‰. A value of -45 ‰ has been used, considering the prevalence of ^{13}C depleted emissions from mines in Yorkshire over the ^{13}C enriched ones in Wales.

Each revised isotopic value represents the mean of all the $\delta^{13}C-CH_4$ source signatures calculated for that source. These values are an improvement on the previous measured ones. Using the Picarro mobile system for identification of methane emission plumes and their sampling for isotopic analysis, the isotopic signature of integrated emissions from each source area could be measured. The new values are therefore more representative than the former ones of emissions from large areas such as landfill sites. In fact, the landfill gas is commonly measured with the flux chamber technique, which requires a large number of measurements to overcome the spatial variability, whereas the sampling of the downwind plume allows the characterisation of the gas released from the whole site.

Each new signature is the result of extensive measuring campaigns on many sites. The value for waste disposal and landfills has been calculated from 10 detailed surveys around closed and still active landfill sites, and the value for coal has been calculated surveying 9 coal mines exploiting different types of coal. Furthermore, isotopic signatures may vary over time and season, such as for landfill sites, where the reliance on methane oxidation by topsoil and gas flaring have been largely replaced by gas extraction systems, for natural gas, as the providing countries changed throughout the last years, and for combustion sources, following efficiency improvements to engines and boilers.

7.1.2 Production of Isotopic Maps

As mentioned in Chapter 3.3, emission data in inventories are classified by UNECE sector (see table Table 3.1) on a 1 km^2 grid. By assigning an isotopic value to each category, using the revised values in Table 7.1, and computing a weighted average of $\delta^{13}C\text{-}CH_4$ for each km^2, emissions data have been converted to isotopic signatures and then plotted using the ArcMap software for comparison with emission maps. The calculated isotopic signature for each square represents the expected isotopic signature of the emissions from that grid cell, based on the mix of sources assessed in the emission inventories.

UNECE sector code	Description	$\delta^{13}C\text{-}CH_4$ (‰)
1	Combustion in energy production and transfer	-25
2	Combustion in commercial, institutions, residential and agricultural sector	-25
3	Combustion in industry	-25
5	Offshore	-36
7	Road Transport	-20
8	Other transport and machinery	-20
9	Waste treatment and disposal	-58
10	Agriculture	-66

Table 7.2 $\delta^{13}C\text{-}CH_4$ values assigned to 2012 UNECE sectors used for national methane inventories. Agriculture sector includes both enteric fermentation and manure; offshore category refers to emissions from fossil fuels (natural gas and coal); waste treatment sector includes both landfill sites and sewage works. The natural gas isotopic value of -36 ‰ has been attributed to the "offshore" sector, as no coal mines are located within the London area. For the agriculture and waste treatment sector the enteric fermentation and landfill isotopic signatures have been used respectively. The isotopic value of -20 ‰ from Fisher (2006) has been attributed to the transport sector, prior to a recent revision experiment, but this is only a very minor source component (Table 7.1).

The 2012 emission and isotopic maps for the London region are shown in Figure 7.1. The centre of London is homogenously characterised by methane emissions in the range 50-100 tonnes/year/km^2 and is ^{13}C enriched relative to the surrounding boroughs, meaning that ^{13}C enriched sources, such as vehicles and leaks from the natural gas distribution network and other combustion sources are suggested to prevail in central London. This validates the primary result of the diurnal studies carried out at King's College (see Chapter 6.5), which reveal the dominance of thermogenic methane emissions in central London. Methane hotspots are mainly located on the west side of the London region and along the River Thames on the east side. In accord with national inventories, those spots are associated mostly with ^{13}C depleted areas, being affected by emissions from the waste treatment sector. Methane hotspots within the London region are also highlighted as green squares in the isotopic map (^{13}C depleted), related to either landfill sites or wastewater treatment plants.

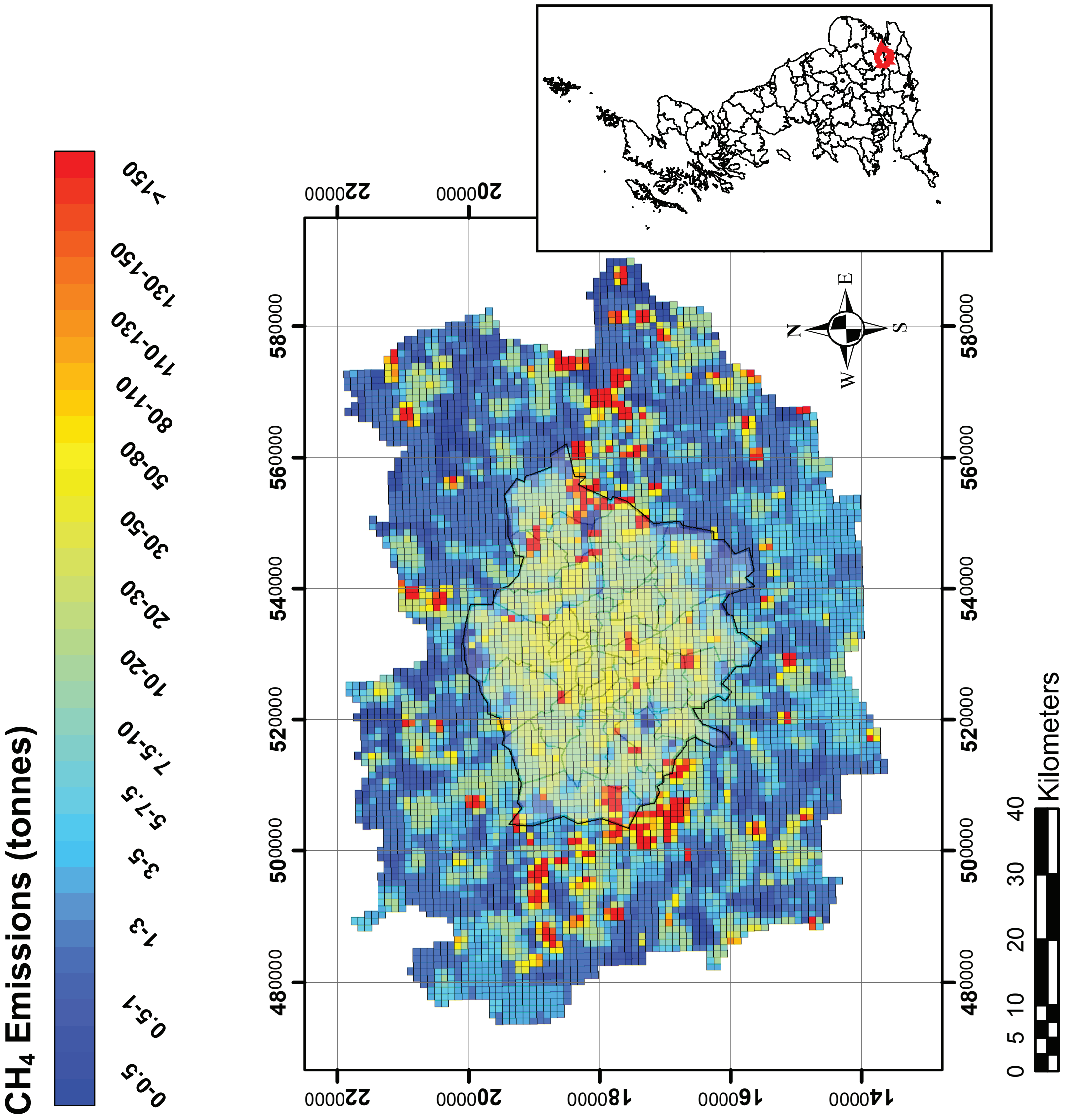
CH$_4$ Emissions (tonnes)
0-0.5
0.5-1
1-3
3-5
5-7.5
7.5-10
10-20
20-30
30-50
50-80
80-110
110-130
130-150
>150
220000
200000
180000
160000
140000
480000
500000
520000
540000
560000
580000
N
E
S
W
0
5
10
20
30
40
Kilometers

(a)

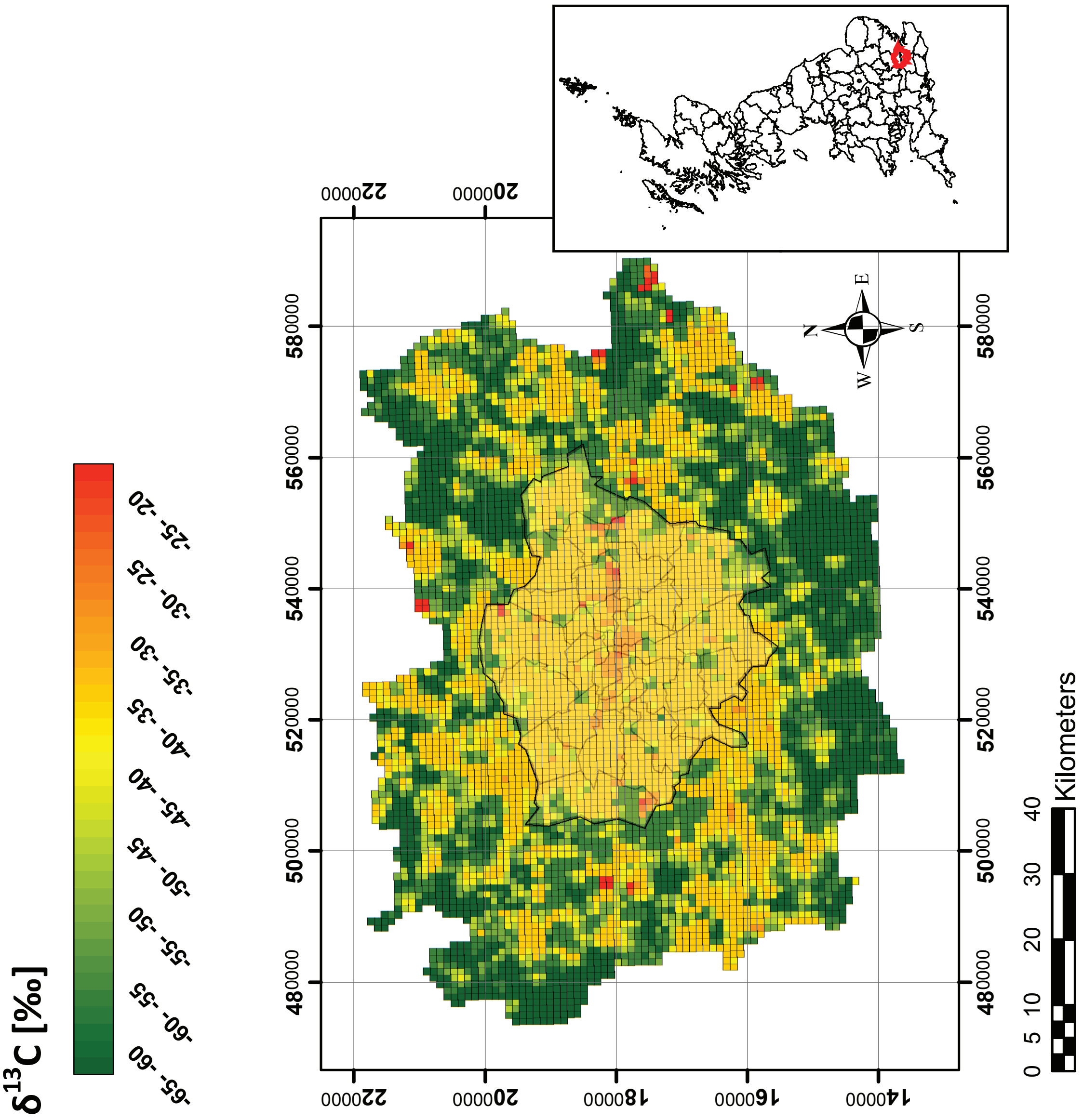

(b)

Figure 7.1 2012 methane emission map (a) and isotopic map (b) created with ArcMap software.

7.1.3 Verification of Local Methane Sources

A focus on a single borough puts emphasis on local emissions and their relative isotopic characterisation. Emission and isotopic maps for Runnymede Borough (Figure 7.2) show that expected methane hotspots correspond to ^{13}C depleted emissions areas, all coinciding with landfill sites. Mobile methane mole fraction measurements in Runnymede borough have been carried out as part of an ongoing project to identify local methane sources and verify their consistency with the inventories. During these surveys no methane plumes have been intercepted in the area between the 166080 and 167080 northings and 498320 and 500320 eastings (see Figure 7.2), where the now closed Trumps Farm Landfill is located.

Isotopic analysis of air samples collected in April 2014 on the A308 in Staines, in the area corresponding to the emission hotspot between 171080 and 172080 northings and 501320 and 502320 eastings, revealed the occurrence of thermogenic methane emissions (source $\delta^{13}C$ signature of -36 ‰), most likely originating from leaks from the Staines storage facilities (see Figure 5.46 in Chapter 5). This facility has now closed, but emissions were still significant in June 2015, probably from the main distribution pipeline. Conversely, national inventories suggest that the area is affected by emissions from the waste sector (see green square in the isotopic map in Figure 7.2), as they incorporate modelled data of methane releases expected from the long-since closed Hythe End Landfill, located at the north of this hotspot, without verification by atmospheric measurements.

Although occasional gas leaks might be the prevailing methane source in certain areas, they cannot be directly included in the methane inventories, as they are highly variable and often spatially unpredictable, but are an emission based on the activity and population density of the grid square. Furthermore, the calculated emissions from methane sources provided by the inventories might differ greatly from the reconstruction using recent atmospheric measurements, due to a progressive reduction in methane emissions from closed landfill sites and better methane recovery from the active ones.

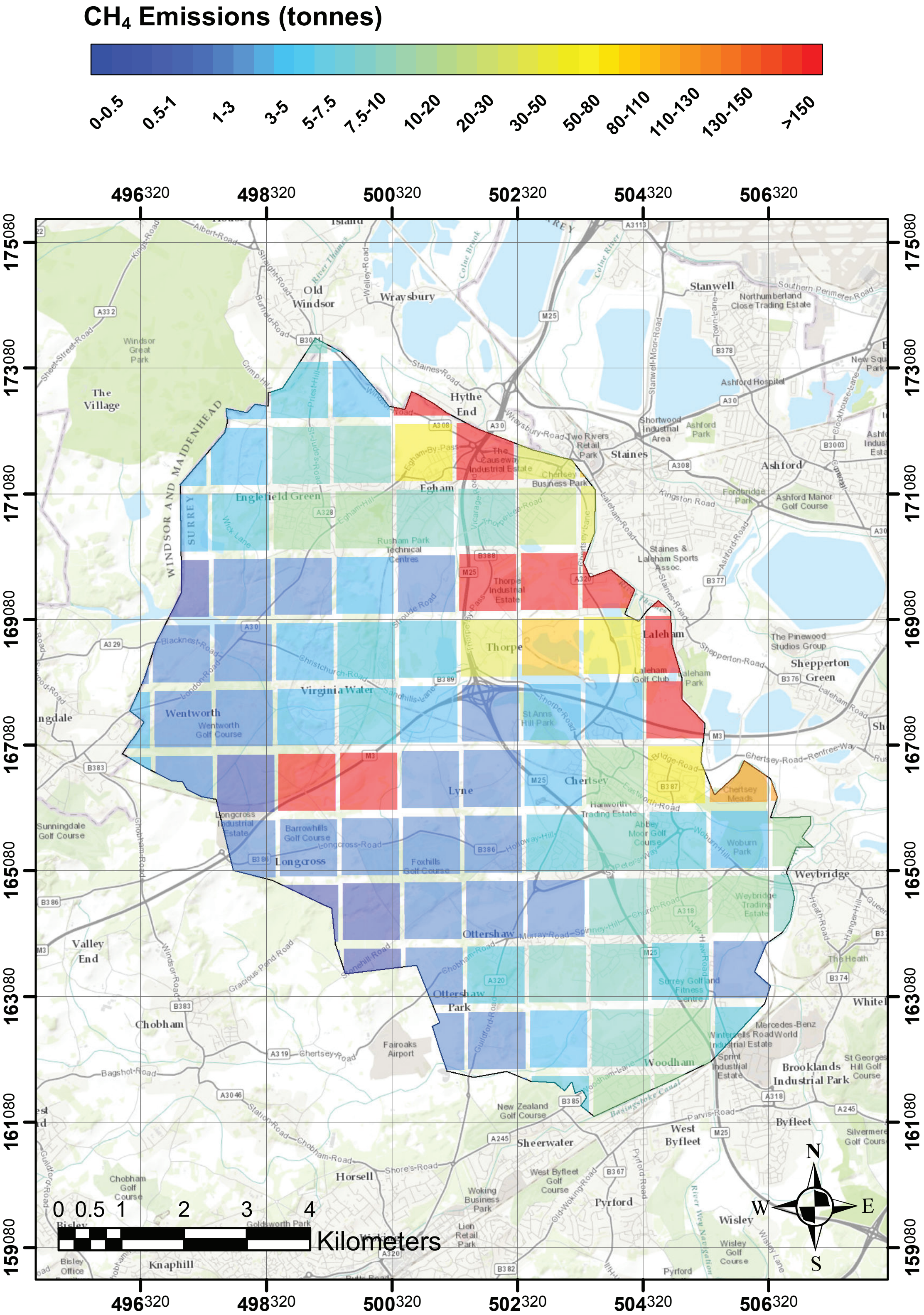
CH$_4$ Emissions (tonnes)
0-0.5
0.5-1
1-3
3-5
5-7.5
7.5-10
10-20
20-30
30-50
50-80
80-110
110-130
130-150
>150
496320
498320
500320
502320
504320
506320
175080
173080
171080
169080
167080
165080
163080
161080
159080
0 0.5 1 2 3 4
Kilometers
N
E
S
W
Egham
Thorpe
Chertsey
Virginia Water
Longcross
Lyne
Ottershaw
Woodham
Staines
Laleham
Englefield Green
Wentworth
Addlestone
Weybridge
Chobham
Old Windsor
Wraysbury
Hythe End
Stanwell
Ashford
Shepperton Green
Byfleet
West Byfleet
Sheerwater
Pyrford
Horsell
Valley End
Knaphill

(a)

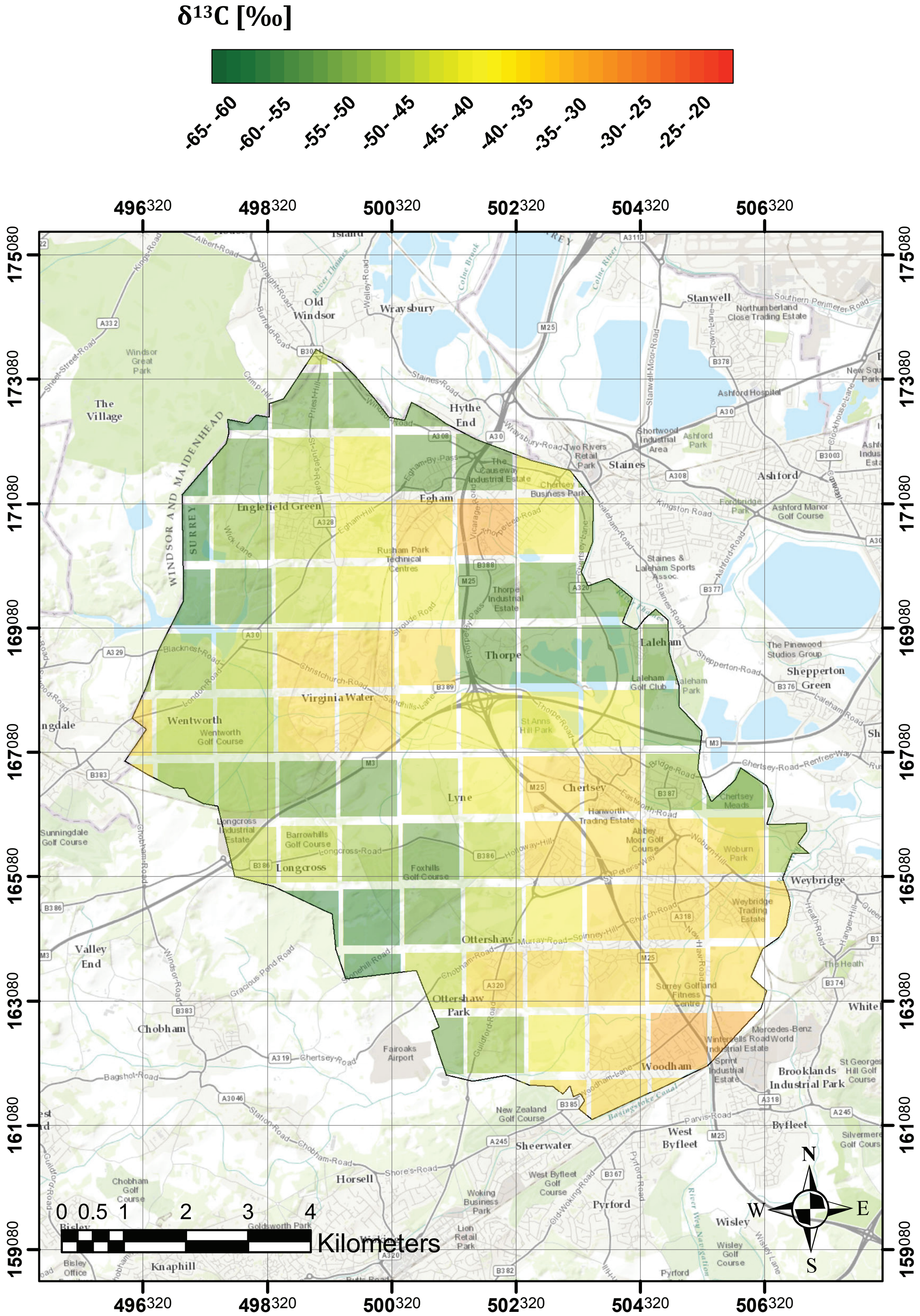

(b)

Figure 7.2 2012 emission (a) and isotopic (b) map for Runnymede Borough.

Following revisions to the inventories, the emissions map based on 2012 data offer a very different picture of methane hotspots compared to the 2009 data. A focus on the London Borough of Hounslow shows the changes that have been made (Figure 7.3 and Figure 7.4). The 2009 emission map does not include any methane hotspots, and the highest emissions are in the range between 50 and 80 tonnes/year/km^2 and are relatively ^{13}C enriched (orange squares in the isotopic map in Figure 7.3 b). New methane sources are indicated on the emission map based on 2012 data. The red square in Figure 7.4a corresponds to Mogden sewage works, whose methane emissions have been verified and isotopically characterised in this study (see Chapter 5.4). All the ^{13}C depleted areas in the 2012 isotopic map in Figure 7.4 b coincide with high emissions areas, as methane is thought to derive from solid waste disposal and water treatment works. The area at the NW side of Kew Gardens comprises old landfill sites (i.e. Green Dragon Lane Flats, Watermans Park and Old Thames Water Gas Works) that closed in 1960s (see maps-environment-agency.gov.uk), and the green square at south of the borough corresponds to Kempton Park water treatment works.

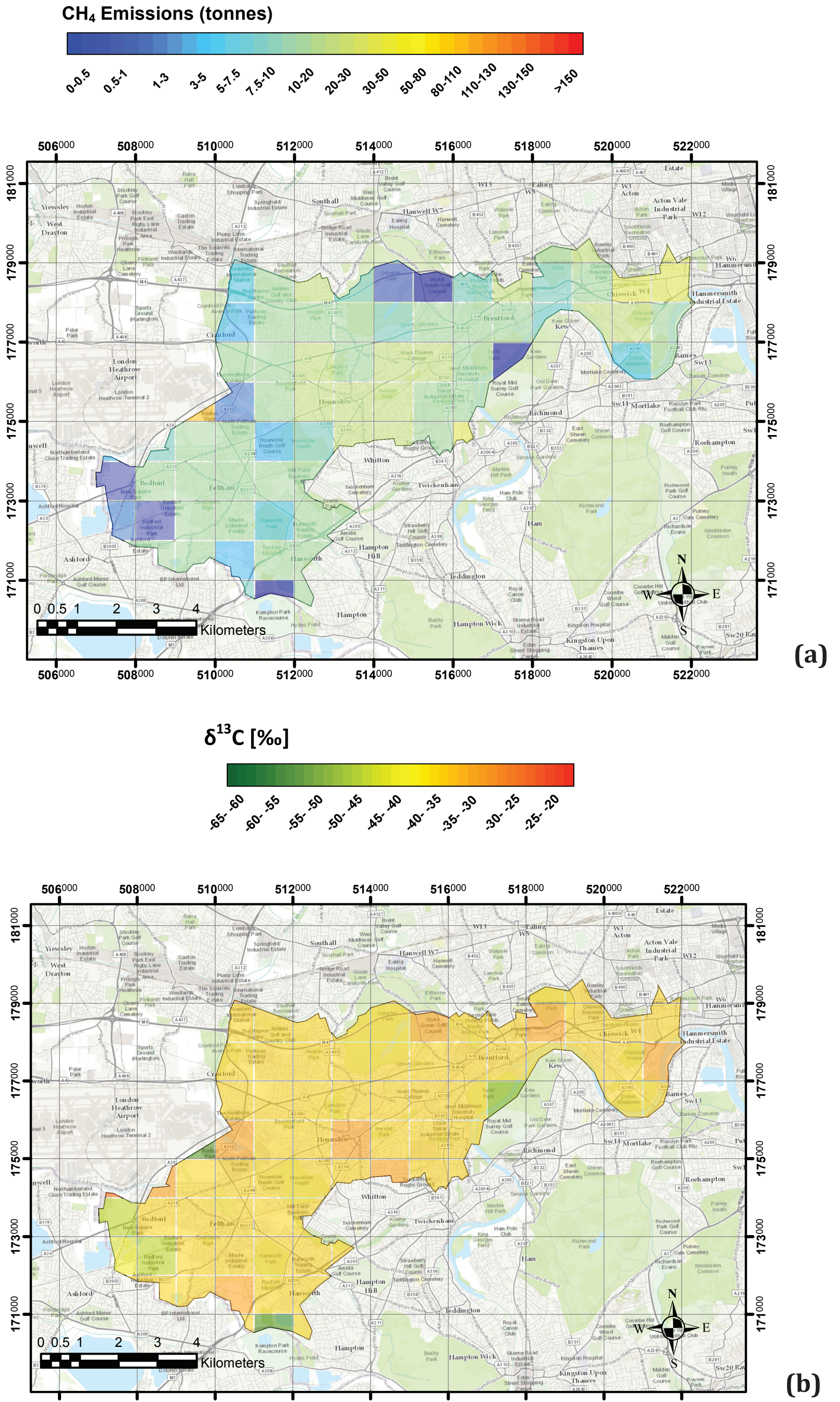

Figure 7.3 2009 emission (a) and isotopic (b) map for the Borough of Hounslow based on emission data from NAEI.

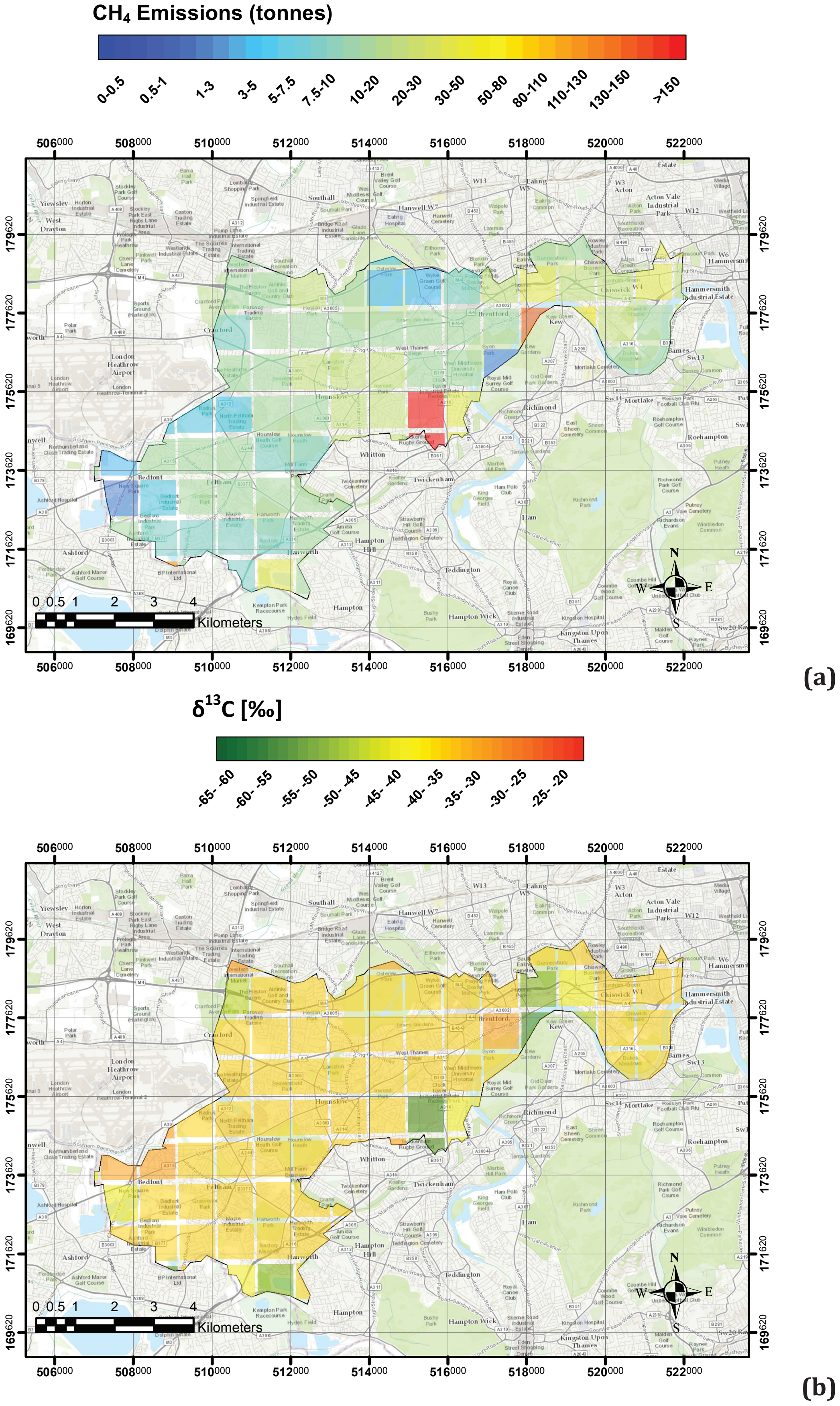

Figure 7.4 **2012 emission (a) and isotopic (b) map for the Borough of Hounslow based on emission data from NAEI.**

The latest inventories have been integrated with emissions from sewage works and old landfill sites that had been disregarded in the previous versions. Nevertheless, surveys carried out in July 2014 for a MSc project (Karim-zada, 2014) confirmed high methane emissions next to Modgen sewage works, but did not find methane plumes next to the other two hotspot areas. The map in Figure 7.5b shows the methane mole fraction excess above the background per km^2, calculated by surveying the borough of Hounslow with the mobile Picarro on 4 different days to give high spatial coverage, and averaging the differences between methane mole fractions measured for each km^2 and the background mole fraction as air entered the borough. Even though the two maps are not comparable in terms of emissions estimates, as no flux measurement system has been implemented in this study, the map based on measured methane mole fractions allows localisation of methane sources. The subsequent isotopic analysis of samples collected downwind of the observed methane plumes reveals the methane origin. Except for the area affected by emissions from Mogden sewage works and one old landfill site, only methane leaking from the natural gas distribution network has been detected across the borough. The 2012 inventory suggests that all old landfill sites that have been active at some time in the last 20-30 years are active methane sources, over-estimating emissions from the waste sector, whereas our measurements suggest natural gas leaks as the primary methane source in the boroughs surveyed.

The landfills that have closed in the last decade with active gas extraction emit very little methane and are therefore over-estimated in the inventory. The surveys for this study and in recent NPL reports (NPL 2011, 2013) suggest that the active cells of current landfills, prior to the waste being compacted and stable enough for insertion of the gas extraction system, are the main source of methane, and that these cells may be under-estimated in the emissions inventory.

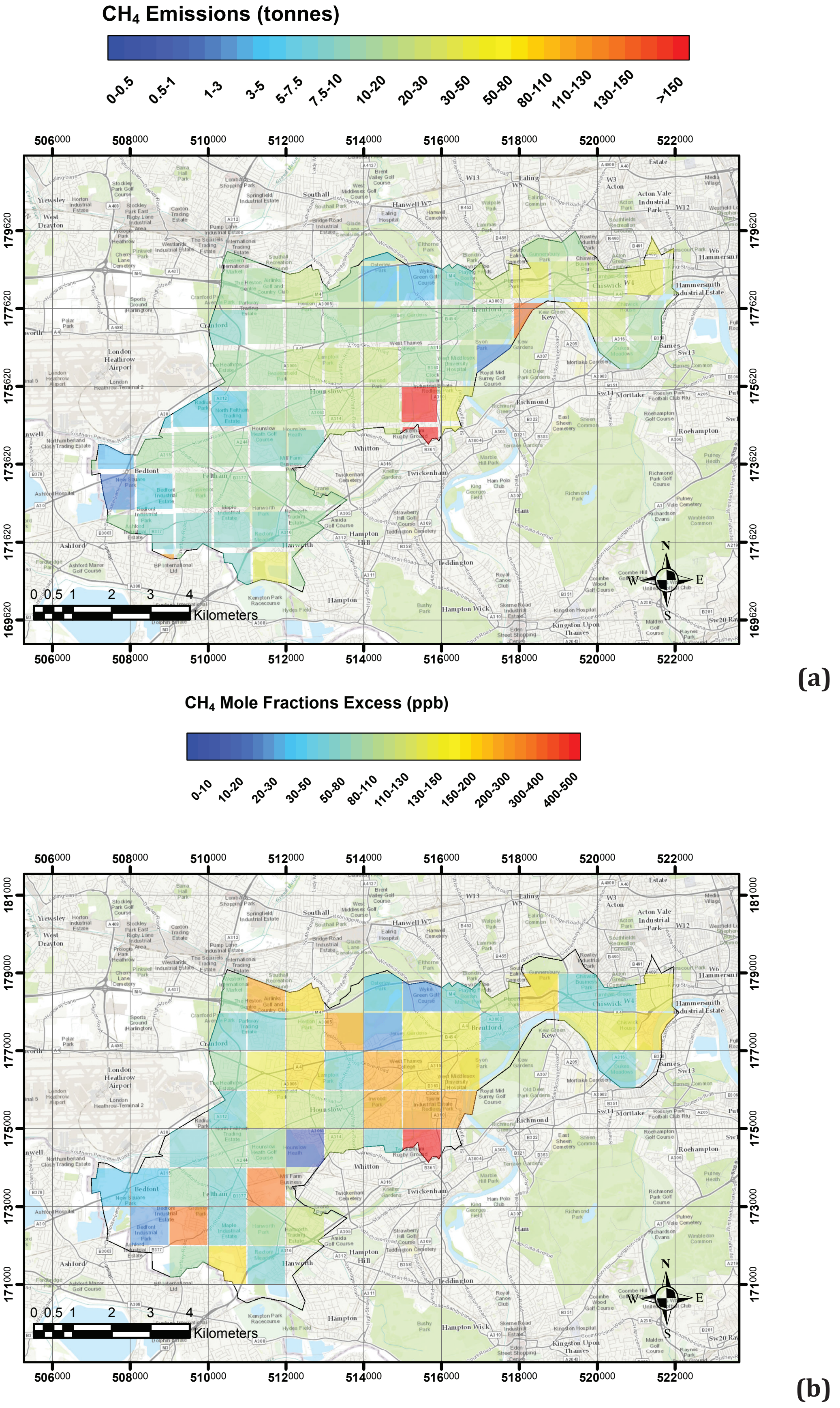

Figure 7.5 2012 inventory map (a) and map based on values of mole fraction excess relative to the methane baseline in ppb (b). Mole fractions data have been mapped on the coordinate grid used for 2009 inventory data.

7.2 UK Isotopic Time Series

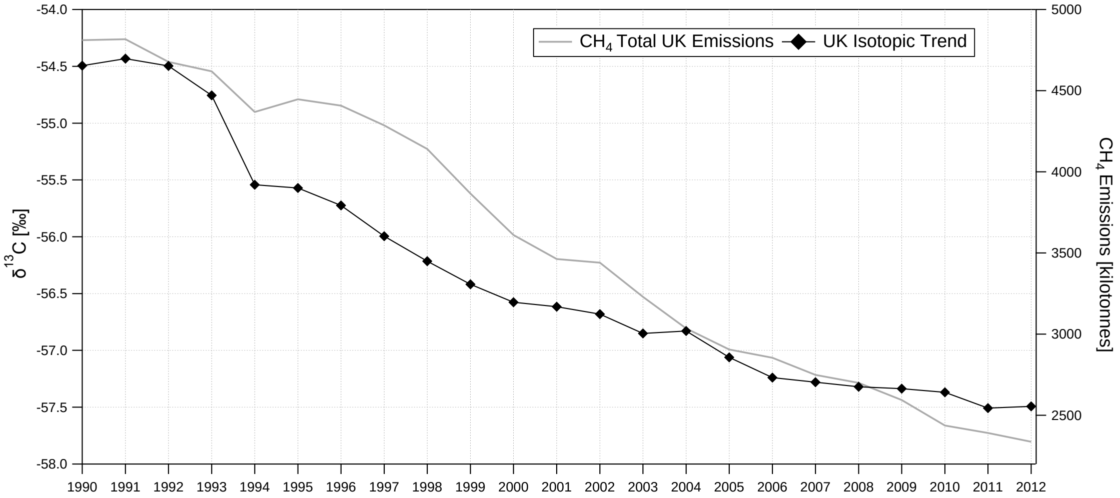

Figure 7.6 Temporal change of $\delta^{13}C\text{-}CH_4$ in the UK since 2002.

A weighted average of $\delta^{13}C\text{-}CH_4$ has been calculated for each year, using UK inventories provided by the NAEI website and typical isotopic values listed in Table 7.2, in order to evaluate the temporal change of $\delta^{13}C\text{-}CH_4$ signatures in the UK since 1990. A general trend towards lower values can be observed in Figure 7.6, which can be justified by an overall decrease of ^{13}C enriched methane sources, such as road transport, natural gas leaks, anthracite coal mining, together with the absence of a substantial reduction of methane emissions from the agricultural sector (see Chapter 2.6).

The attribution of refined $\delta^{13}C\text{-}CH_4$ values to updated inventories allows comparison between the calculated isotopic signature and the methane isotopic value measured in a specific region. The value of ≈-57.5 ‰ based on the latest UK inventories is in good agreement with the regional isotopic signatures of approximately -57 ‰ calculated by Keeling plot analysis in Dover and Bacton, which characterise air masses coming from Europe (see Chapter 6.3). The mean isotopic signature calculated for the London region using 1 km^2 emissions is -43 ‰ for the 2009 inventory and -39 ‰ for the 2012 inventory, due to a higher estimate of methane emissions from fossil fuel combustion and from the natural gas distribution system than the 2009 ones, and the redistribution of emissions from landfill sites in a less coarse spatial grid, removing the 5x5 km hotspots. The calculated isotopic signature of -39 ‰ is indeed more consistent with the value of

≈ -40 ‰ measured in central London during diurnal studies (see Chapter 6.7.1). These changes are typical of the revised back calculations for previous years that are made each time that the inventory is revised. Lowry et al. (2002) made similar calculations for the new 1997 inventory, which, using the natural gas (-34 ‰) and landfill (-52 ‰) signatures observed at that time, were -50.7 ‰ for the UK and -47.2 ‰ for London. The new 2012 inventory back-calculations for 1997 emissions and revised isotopic source signatures suggest that the UK source mix should have been -56.0 ‰ in 1997 (Figure 7.6). While this is partly due to the changing isotopic signatures of sources, due to better landfill practice and change of natural gas source supply, it also highlights the propagation of errors when trying to back-calculate emissions through time.

8

CONCLUSIONS

8.1 Reviewed δ^{13}C-CH4 values

The value of isotopic data (δ^{13}C-CH_4) in constraining the contributions of different methane sources in the mass balance of atmospheric methane at a global and regional scale has been asserted by several studies (Quay et al. 1991, Mikaloff Fletcher et al. 2004, Bousquet et al. 2006). However, in this project, stable isotope measurements have been employed for methane source apportionment aimed primarily at independently verifying UK emission inventories. For this purpose new δ^{13}C-CH_4 source signatures, with a correlated error, have been calculated.

The focus on a particular region, for instance SE England in this study, allowed isotopic ranges for methane sources available in literature to be narrowed down considerably. Within SE England, the isotopic signatures of emissions from specific source categories are coherent, with each source sector having a small range of signatures. Furthermore, there was no evidence of seasonal variability in the isotopic values, which makes the use of the revised isotopic values in future modelling work more feasible.

The source categories that have been isotopically characterised are summarised below.

Waste disposal and landfill (-58 ±3 ‰)

A δ^{13}C-CH_4 value of -52.5 ‰ has been estimated from past measurements of active landfill sites in the London Region (Lowry et al., 2001), highly different from the value calculated in this study, meaning that a periodic reappraisal of isotopic values from landfills is recommended. Landfill sites that predate gas extraction rely on the oxidation through the covering soil, and the biogas escaping is ^{13}C enriched due to the oxidation process occurring in the soil. Methane emissions from more recent landfills come from leakages in the gas extraction system, overcoming the oxidation through the soil cover and thus being more ^{13}C depleted.

Gas transmission and distribution (-36 ±2 ‰)

The isotopic value of the natural gas supply to SW London has changed from -34 ‰ over 1998-99 period to -36 ‰ since at least 2002. The new isotopic value calculated after measuring campaigns in Staines, Bacton and Southampton confirms that this figure can be applied to emissions from a much larger region of England.

Coal Mining (-30 ±3 ‰ for anthracite and -50 ±3 ‰ for bituminous coal)

This study is the first detailed isotopic characterisation of methane emissions from UK coal mines. Different isotopic values have been assigned to different coal rank, and a process of ^{13}C depletion caused by the incursion of meteoric water has been also suggested. The extremely wide range of δ^{13}C values of methane from coal suggested by Rice et al. (1993) (-80 ‰ to -17 ‰) has been significantly narrowed down and more specific values are provided. Therefore, regional atmospheric models that use isotopes to partition methane sources in the methane budget and need to use a specific isotopic value for the coal sector, can use the new revised isotopic signatures, which take into account both coal rank and type of mining (opencast or underground).

Wastewater handling (-53 ±3 ‰)

Mogden sewage treatment plant has been chosen as a case study for isotopic characterisation of this category. Four surveys have been carried out and three methane sources were identified and isotopically characterised: -50.7 ±1.1 ‰ for anaerobic digesters, -59.2 ±1.2 ‰ for secondary treatment and -48.1 ±1.5 ‰ for the power station. -53 ‰ represents the averaged value. This can be considered as one of the first comprehensive isotopic characterisations of methane emissions from sewage works. In fact, few δ^{13}C-CH$_4$ isotopic values characterising wastewater treatments are available in literature. Townsend-Small et al. (2012) sampled a sewage plant in Los Angeles from just above the surface of the treatment tanks, finding δ^{13}C-CH$_4$ values of -46.3 and -47.0 ‰, which are ^{13}C enriched relative to the isotopic values measured in this study. However, comparisons with other studies would require a better understanding of the technology employed in the treatment, due to the diverse methane sources involved in sewage works.

Enteric fermentation (-66 ±3 ‰)

The value of -66 ‰ has been calculated following two experiments, where methane emissions from Holstein Fresian cows and from rare breed cows were measured in a shed and open field respectively. The large isotopic range suggested by Levin et al. (1993) (from -45 to -75 ‰) has been considerably narrowed down, even though more experiments should be carried out to confirm the revised value for enteric fermentation in UK.

Road Transport (-12 ±4 ‰)

An averaged value of -11.7 ±4.3 ‰ resulted from the sampling of emissions from 10 cars of different age and fuel type. A wider range of vehicles would be required to allocate a more precise isotopic value to vehicle methane emissions.

8.2 Development of a New Methodology for the Isotopic Characterisation of Methane Sources

The main novelty of this study was the development of a new system for measurement and isotopic characterisation of methane plumes from source areas (Zazzeri et al. 2015). The mobile Picarro G2301 CRDS analyser was installed in a vehicle, together with an anemometer and a Hemisphere GPS receiver, to measure atmospheric methane mole fractions and their relative location. The subsequent $\delta^{13}C$-CH_4 isotopic analysis by CF-GC-IRMS of the samples collected when plumes were intercepted, followed by Keeling plot analysis, determined the overall isotopic signature of the methane released into the atmosphere from the whole site.

The isotopic precision of ±0.05 ‰ achieved in the atmospheric laboratory at RHUL allows precise isotopic signatures of source plumes to be detected at near background atmospheric mole fractions (50 ppb excess CH_4 for a 20 ‰ difference between source and background air isotopic signatures, 100 ppb for 10 ‰ difference, 200 ppb for 5 ‰). Therefore, broad emission plumes from methane sources that are not particularly active, such as opencast coal mines and very old landfill sites, could be isotopically characterised.

The advantage of high precision measurements has been proved in areas with multiple sources, such as urban environments, where leaks in the natural gas supply pipes can occur near landfill sites and sewage works. While surveying these sites with the Picarro mobile system, occasional leaks were often attributed to the main source detected in the area, until the isotopic analysis revealed a different methane origin, allowing the different sources encountered to be carefully distinguished. So far the mobile isotopic instruments developed by Picarro and Aerodyne can at best achieve precisions 5 times worse over 15-minute integration times that are unsuitable for mobile measurement, or closer to 20 times worse for short integration times necessary for mobile measurement (e.g. Phillips et al., 2013).

In conclusion, the new methodology developed allows isotopic characterisation of emission plumes of less than 1 ppm over background, and distinction of methane sources whose emissions affect concurrently the same area.

8.3 Validation of Methane Inventories

The revised isotopic values have been used to verify the allocation of methane sources suggested by national inventories. Isotopic maps developed by converting 1 km^2 emission estimates to isotopic values using the updated signatures, show whether emissions hotspots are related to biogenic methane (i.e. methane from agricultural and waste sector) or fossil fuel sources (i.e. gas leaks and coal mines). Surveys carried out in these studies, aiming at verifying the actual provenance of methane emissions, not always confirmed the methane source figure suggested by the inventories. Indeed, only very rarely and under suitable declining atmospheric pressure conditions methane plumes have been detected downwind of old landfill sites that are listed as current methane emitters. Conversely, high methane mole fractions have been measured in areas that are not counted as methane hotspots. When surveying urban areas in the London Region, most of methane peaks were associated with gas leaks, and their inclusion in emission inventories would alter drastically the methane emissions scenario.

The isotopic signal of the source mix in the central London area has been measured carrying out diurnal studies on the roof of the King's College, in central London. The measured isotopic signal has been compared with the weighted isotopic value calculated using emission inventories and the revised signatures. The measured and calculated values were highly consistent (≈ -39‰), and fugitive gas and combustion were recognised as the prevailing methane sources. However, during the diurnal studies in London I identified also an isotopic signal from a biogenic source that might correspond to the Thames River, which is not taken into account in emission inventories. So far, the possible contribution of the Thames to methane emissions has not being assessed in any study; if the results I obtained could be confirmed through further research, the river would be identified as a new methane source, with significant implications for methane emissions estimates.

Diurnal measurements of methane mole fractions in Egham provided further understanding of the source mix in the London region. As the measurement site is located in a semi-rural area WSW of central London, depending on the wind direction, both background and polluted air from London could be detected and isotopically characterised. The mean isotopic value of -44.6 ±4.9 ‰ measured for the London sector (45^o to 110^o) further confirms the predominance of fossil fuel sources in the regional source mix, although it suggests a higher contribution of ^{13}C depleted sources (i.e. landfill sites) compared to central London.

In summary, isotopic analysis allowed identification of methane sources and localisation of the hotspots suggested by methane inventories, and gave insights on the source proportion at regional scale. Therefore, only a “qualitative” validation of inventories has been achieved, since numbers comparable with the emission estimates in the inventories can be produced only through flux measurements or mole fraction measurements coupled with atmospheric inversion modelling. However, the verification carried out in this study showed how methane sources are often spatially misallocated and some of them are not included in the inventories.

8.4 Potential for Modelling Methane Fluxes

Even though modelling of methane fluxes is beyond the scope of this thesis, the mobile Picarro system could be integrated with a setup for measuring mole fractions at different heights and with a more accurate instrumentation for the analysis of wind parameters. By implementing these changes, data acquired during the surveys could be used in atmospheric dispersion modelling to calculate methane fluxes from source areas, providing emissions estimates for a quantitative validation of inventories.

Flux calculations would be an asset to this type of study and modelling based on measured data could yield emission estimates with high spatial resolution. However, these measurements are very difficult and time consuming (NPL 2011,2013), and will only give fluxes at a snapshot in time, unless multiple surveys can be carried out in different seasons and under different meteorological conditions and can also encompass measurements of the whole source plume. Techniques are starting to emerge for the flux measurement of point sources (e.g. pressurised gas leaks) that form small discrete plumes, which can be identified and measured on multiple occasions (e.g. (Day et al., 2015)), but so far the regional isotopic characterisation of sources offers the best way of up-scaling to a global verification of methane emissions.

BIBLIOGRAPHY

Adams, H., 1967, The Seams of the South Wales Coalfield: a monograph: London, Institution of Mining Engineers.

Alderton, D., Oxtoby, N., Brice, H., Grassineau, N., and Bevins, R., 2004, The link between fluids and rank variation in the South Wales Coalfield: evidence from fluid inclusions and stable isotopes: Geofluids, v. 4, p. 221-236.

Allan, W., Lowe, D., Gomez, A., Struthers, H., and Brailsford, G., 2005, Interannual variation of ^{13}C in tropospheric methane: Implications for a possible atomic chlorine sink in the marine boundary layer: Journal of Geophysical Research: Atmospheres (1984–2012), v. 110, no.D11.

Allan, W., Struthers, H., and Lowe, D., 2007, Methane carbon isotope effects caused by atomic chlorine in the marine boundary layer: Global model results compared with Southern Hemisphere measurements: Journal of Geophysical Research: Atmospheres (1984–2012), v. 112, no.D4.

Andreae, M.O., 1991, Biomass burning: its history, use, and distribution and its impact on environmental quality and global climate: Global biomass burning: Atmospheric, climatic and biospheric implications, edited by J. S. Levine, MIT Press, Cambridge, 3-21 p.

Bergamaschi, P., and Bousquet, P., 2008, Estimating sources and sinks of methane: An atmospheric view, Ecological Studies, Volume 203: Ecological Studies : Analysis and Synthesis, p. 113-133.

Bergamaschi, P., Lubina, C., Königstedt, R., Fischer, H., Veltkamp, A., and Zwaagstra, O., 1998, Stable isotopic signatures (δ^{13}C, δD) of methane from European landfill sites: Journal of Geophysical Research: Atmospheres (1984–2012), v. 103, p. 8251-8265.

Bilek, R., Tyler, S., Kurihara, M., and Yagi, K., 2001, Investigation of cattle methane production and emission over a 24-hour period using measurements of δ^{13}C and δD of emitted CH_4 and rumen water: Journal of Geophysical Research: Atmospheres (1984–2012), v. 106, p. 15405-15413.

Blunier, T., Chappellaz, J., Schwander, J., Stauffer, B., and Raynaud, D., 1995, Variations in atmospheric methane concentration during the Holocene epoch: Nature, v. 374, p. 46-49.

Bogner, J., and Spokas, K., 1993, Landfill CH_4: rates, fates, and role in global carbon cycle: Chemosphere, v. 26, p. 369-386.

Börjesson, G., Chanton, J., and Svensson, B.H., 2001, Methane oxidation in two Swedish landfill covers measured with carbon-13 to carbon-12 isotope ratios: Journal of environmental quality, v. 30, p. 369-376.

Bousquet, P., Ciais, P., Miller, J., Dlugokencky, E., Hauglustaine, D., Prigent, C., Van der Werf, G., Peylin, P., Brunke, E.-G., and Carouge, C., 2006a, Contribution of anthropogenic and natural sources to atmospheric methane variability: Nature, v. 443, p. 439-443.

Bousquet, P., Ciais, P., Miller, J.B., Dlugokencky, E.J., Hauglustaine, D.A., Prigent, C., Van der Werf, G.R., Peylin, P., Brunke, E.G., Carouge, C., Langenfelds, R.L., Lathiere, J., Papa, F., Ramonet, M., Schmidt, M., Steele, L.P., Tyler, S.C., and White, J., 2006b, Contribution of anthropogenic and natural sources to atmospheric methane variability: Nature, v. 443, p. 439-443.

Bowes, H.L., and Hornibrook, E.R., 2006, Emission of highly ^{13}C-depleted methane from an upland blanket mire: Geophysical Research Letters, v. 33, no.4.

Brenninkmeijer, C., Lowe, D., Manning, M., Sparks, R., and Velthoven, P.v., 1995, The ^{13}C, ^{14}C, and ^{18}O isotopic composition of CO, CH_4, and CO_2 in the higher southern latitudes lower stratosphere: Journal of Geophysical Research: Atmospheres (1984–2012), v. 100, p. 26163-26172.

British Geological Survey 2010, Mineral Planning Factsheet British Geological Survey, Natural Environment Research Council. https://www.bgs.ac.uk/mineralsuk/planning/mineralPlanningFactsheets.html

Chanton, J., Chaser, L., Glasser, P., and Siegel, D., 2004, Carbon and hydrogen isotopic effects in microbial methane from terrestrial environments, Stable isotopes and biosphere-atmosphere interactions, physiological ecology series, edited by L. B. Flanagan, J. R. Ehleringer and D. E. Pataki, chapter 6, Elsevier–Academic Press, p. 85-105.

Chanton, J., and Liptay, K., 2000, Seasonal variation in methane oxidation in a landfill cover soil as determined by an in situ stable isotope technique: Global Biogeochemical Cycles, v. 14, p. 51-60.

Chanton, J.P., 2005, The effect of gas transport on the isotope signature of methane in wetlands: Organic Geochemistry, v. 36, p. 753-768.

Chanton, J.P., Martens, C.S., Kelley, C.A., Crill, P.M., and Showers, W.J., 1992, Methane transport mechanisms and isotopic fractionation in emergent macrophytes of an Alaskan tundra lake: Journal of Geophysical Research: Atmospheres (1984–2012), v. 97, p. 16681-16688.

Chanton, J.P., Rutkowski, C.M., Schwartz, C.C., Ward, D.E., and Boring, L., 2000, Factors influencing the stable carbon isotopic signature of methane from combustion and biomass burning: Journal of Geophysical Research: Atmospheres (1984–2012), v. 105, p. 1867-1877.

Chappellaz, J., Blunier, T., Kints, S., Dällenbach, A., Barnola, J.M., Schwander, J., Raynaud, D., and Stauffer, B., 1997, Changes in the atmospheric CH_4 gradient between Greenland and Antarctica during the Holocene: Journal of Geophysical Research: Atmospheres (1984–2012), v. 102, p. 15987-15997.

Chen, Y.H., and Prinn, R.G., 2006, Estimation of atmospheric methane emissions between 1996 and 2001 using a three-dimensional global chemical transport model: Journal of Geophysical Research: Atmospheres (1984–2012), v. 111, no.D10.

Chidthaisong, A., Chin, K.-J., Valentine, D.L., and Tyler, S.C., 2002, A comparison of isotope fractionation of carbon and hydrogen from paddy field rice roots and soil bacterial enrichments during CO_2/H_2 methanogenesis: Geochimica et Cosmochimica Acta, v. 66, p. 983-995.

Christensen, T.R., Ekberg, A., Ström, L., Mastepanov, M., Panikov, N., Öquist, M., Svensson, B.H., Nykänen, H., Martikainen, P.J., and Oskarsson, H., 2003, Factors controlling large scale variations in methane emissions from wetlands: Geophysical Research Letters, v. 30, no.7.

Chung, H.M., Gormly, J., and Squires, R., 1988, Origin of gaseous hydrocarbons in subsurface environments: theoretical considerations of carbon isotope distribution: Chemical Geology, v. 71, p. 97-104.

Chung, H.M., and Sackett, W.M., 1979, Use of stable carbon isotope compositions of pyrolytically derived methane as maturity indices for carbonaceous materials: Geochimica et Cosmochimica Acta, v. 43, no.12.

Cicerone, R.J., and Oremland, R.S., 1988, Biogeochemical aspects of atmospheric methane: Global Biogeochemical Cycles, v. 2, p. 299-327.

Clayton, J., 1998, Geochemistry of coalbed gas–A review: International Journal of Coal Geology, v. 35, p. 159-173.

Coleman, D.D., Risatti, J.B., and Schoell, M., 1981, Fractionation of carbon and hydrogen isotopes by methane-oxidizing bacteria: Geochimica et Cosmochimica Acta, v. 45, p. 1033-1037.

Colombo U., G.F., Gonfiantini F., Gonfiantini R., Kneuper G., Teichmuller I., Teichmuller R. , 1970, Carbon isotope study on methane from German coal deposits.: Advances in Organic Geochemistry 1966 (eds G. D. HOBSON and G. C. SPEERS), p. 1-26.

Conrad, R., 1993, Mechanisms controlling methane emission from wetland rice fields, Biogeochemistry of Global Change, Springer, p. 317-335.

Conrad, R., 2009, The global methane cycle: recent advances in understanding the microbial processes involved: Environmental Microbiology Reports, v. 1, p. 285-292.

Creedy, D.P., 1991, An introduction to geological aspects of methane occurrence and control in British deep coal mines: Quarterly Journal of Engineering Geology, v. 24, p. 209-220.

Crutzen, P., 1973, A discussion of the chemistry of some minor constituents in the stratosphere and troposphere: Pure and Applied Geophysics, v. 106, p. 1385-1399.

Czepiel, P.M., Crill, P.M., and Harriss, R.C., 1993, Methane emissions from municipal wastewater treatment processes: Environmental Science & Technology, v. 27, p. 2472-2477.

Daelman, M.R., van Voorthuizen, E.M., van Dongen, U.G., Volcke, E.I., and van Loosdrecht, M.C., 2012, Methane emission during municipal wastewater treatment: Water Research, v. 46, p. 3657-3670.

Dai, J.X., Qi, H.F., Song, Y., and Guan, D.S., 1987, Composition, carbon isotope characteristics and the origin of coal-bed gases in China and their implication: Scientia Sinica Series B-Chemical Biological Agricultural Medical & Earth Sciences, v. 30, p. 1324-1337.

Day, S., Ong, C., Rodge, A., Etheridge, D., Hibberd, M., Gorsel, E.v., Spencer, D., Krummel, P., Zegelin, S., Fry, R., Dell'Amico, M., Sestak, S., Williams, D., Loh, Z., and Barrett, D., 2015, Characterisation of RegionalFluxes of Methane in the Surat Basin, Queensland - Phase 2: A pilot study to detect and quantify methane sources. CSIRO Report EP15369, p. 78.

Deines, P., 1980, The isotopic composition of reduced organic carbon: Handbook of environmental isotope geochemistry, p. 329-406.

Denman, K.L., 2008, Climate change, ocean processes and ocean iron fertilization: Marine Ecology Progress Series, v. 364, p. 219-225.

Dentener, F., Stevenson, D., Cofala, J., Mechler, R., Amann, M., Bergamaschi, P., Raes, F., and Derwent, R., 2005, The impact of air pollutant and methane emission controls on tropospheric ozone and radiative forcing: CTM calculations for the period 1990-2030: Atmospheric chemistry and physics, v. 5, p. 1731-1755.

Dickens, G.R., 2003, A methane trigger for rapid warming?: Science, v. 299, p. 1017-1017.

Dlugokencky, E., Masarie, K., Lang, P., and Tans, P., 1998, Continuing decline in the growth rate of the atmospheric methane burden: Nature, v. 393, p. 447-450.

Dlugokencky, E.J., Nisbet, E.G., Fisher, R., and Lowry, D., 2011, Global atmospheric methane: budget, changes and dangers: Philosophical Transactions of the Royal Society A: Mathematical, Physical and Engineering Sciences, v. 369, p. 2058-2072.

Dragosits, U., Mitchell, R., Tang, Y., and Sutton, M., 2013, 2013 Modelling and mapping UK emissions of ammonia, methane and nitrous oxide from agriculture, nature, waste disposal and other miscellaneous sources for 2011. Edinburgh, NERC/Centre for Ecology & Hydrology, 21pp. (CEH Project Number: C04531).

Drake, D., 1983, Working the Warwickshire Thick Coal, Improved Techniques for the Extraction of Primary Forms of Energy, Springer Netherlands, p. 156-156.

Draxler R.R. and Rolph G.D., 2015, HYSPLIT (HYbrid Single-Particle Lagrangian Integrated Trajectory) Model access via NOAA ARL READY Website (http://ready.arl.noaa.gov/HYSPLIT.php). NOAA Air Resources Laboratory, Silver Spring, MD.

Dwyer, E., Pinnock, S., Grégoire, J.-M., and Pereira, J., 2000, Global spatial and temporal distribution of vegetation fire as determined from satellite observations: International Journal of Remote Sensing, v. 21, p. 1289-1302.

EEA (European Environment Agency), 2014, Annual European Union greenhouse gas inventory 1990–2012 and inventory report 2014,Technical report No 9/2014, ISSN 1725-2237, p. 19.

Ehhalt, D., and Heidt, L., 1973, Vertical profiles of CH_4 in the troposphere and stratosphere: Journal of Geophysical Research, v. 78, p. 5265-5271.

Engeln, R., Berden, G., Peeters, R., and Meijer, G., 1998, Cavity enhanced absorption and cavity enhanced magnetic rotation spectroscopy: Review of Scientific Instruments, v. 69, p. 3763-3769.

Etheridge, D., Steele, L.P., Francey, R., and Langenfelds, R., 1998, Atmospheric methane between 1000 AD and present: Evidence of anthropogenic emissions and climatic variability: Journal of Geophysical Research: Atmospheres (1984–2012), v. 103, p. 15979-15993.

European Commission Joint Research Centre/Netherlands Environmental Assessment Agency, 2011, Emission Database for Global Atmospheric Research (EDGAR) (version 4.2) (2011); http://edgar.jrc.ec.europa.eu.

Ferretti, D.F., Miller, J., White, J., Etheridge, D., Lassey, K., Lowe, D., Meure, C.M., Dreier, M., Trudinger, C., and Van Ommen, T., 2005, Unexpected changes to the global methane budget over the past 2000 years: Science, v. 309, p. 1714-1717.

Fisher, R., Lowry, D., Wilkin, O., Sriskantharajah, S., and Nisbet, E.G., 2006, High-precision, automated stable isotope analysis of atmospheric methane and carbon dioxide using continuous-flow isotope-ratio mass spectrometry: Rapid Communications in Mass Spectrometry, v. 20, p. 200-208.

Fisher, R.E., 2006, Development and applications of continuos-flow gas chromatography isotope ratio mass spectrometry for atmospheric methane and carbon dioxide studies, PhD thesis, Univ. of Royal Holloway University of London.

Fuex, A., 1980, Experimental evidence against an appreciable isotopic fractionation of methane during migration: Physics and Chemistry of the Earth, v. 12, p. 725-732.

Fung, I., John, J., Lerner, J., Matthews, E., Prather, M., Steele, L., and Fraser, P., 1991, Three-dimensional model synthesis of the global methane cycle: Journal of Geophysical Research, v. 96, no.D7.

Golueke, C.G., 1958, Temperature effects on anaerobic digestion of raw sewage sludge: Sewage and Industrial Wastes, v.30, p. 1225-1232.

Hamilton, S., Golding, S., Baublys, K., and Esterle, J., 2014, Stable isotopic and molecular composition of desorbed coal seam gases from the Walloon Subgroup, eastern Surat Basin, Australia: International Journal of Coal Geology, v. 122, p. 21-36.

Happell, J.D., Chanton, J.P., and Showers, W.S., 1994, The influence of methane oxidation on the stable isotopic composition of methane emitted from Florida swamp forests: Geochimica et Cosmochimica Acta, v. 58, p. 4377-4388.

Happell, J.D., Chanton, J.P., Whiting, G.J., and Showers, W.J., 1993, Stable isotopes as tracers of methane dynamics in Everglades marshes with and without active populations of methane oxidizing bacteria: Journal of Geophysical Research: Atmospheres (1984–2012), v. 98, p. 14771-14782.

Hein, R., Crutzen, P.J., and Heimann, M., 1997, An inverse modeling approach to investigate the global atmospheric methane cycle: Global Biogeochemical Cycles, v. 11, p. 43-76.

Hill, A., 2001, The South Yorkshire Coalfield: A History and Development, Tempus Books, Gloucestershire.

Hitchman, S., Darling, W., and Williams, G., 1990, Stable isotope ratios in methane containing gases in the United Kingdom. Report of the British Geological Survey, Processes Research Group WE/89/30.

Hobbs, P.V., 2000, Introduction to atmospheric chemistry, Cambridge University Press, p. 72-74.

Hodson, E., Poulter, B., Zimmermann, N., Prigent, C., and Kaplan, J.O., 2011, The El Niño–Southern Oscillation and wetland methane interannual variability: Geophysical Research Letters, v. 38, no.8.

Holloway, S., Jones, N., Creedy, D., and Garner, K., 2005, Can new technologies be used to exploit the coal resources in the Yorkshire-Nottinghamshire coalfield?: Carboniferous Hydrocarbon Geology: The Southern North Sea Surrounding Areas, Occasional publications of the Yorkshire Geological Society, v.7, p. 195–208.

Hornibrook, E.R., Longstaffe, F.J., and Fyfe, W.S., 1997, Spatial distribution of microbial methane production pathways in temperate zone wetland soils: stable carbon and hydrogen isotope evidence: Geochimica et Cosmochimica Acta, v. 61, p. 745-753.

Hornibrook, E.R., Longstaffe, F.J., and Fyfe, W.S., 2000, Evolution of stable carbon isotope compositions for methane and carbon dioxide in freshwater wetlands and other anaerobic environments: Geochimica et Cosmochimica Acta, v. 64, p. 1013-1027.

IMC Group Consulting Limited, 2002, A review of the remaining reserves at deep mines for the Department of Trade and Industry.

Innocenti, F., Robinson, R.A., Gardiner, T.D., Finlayson, A.J., Connor, A., Lowry, D., and Fisher, R., 2013, Measurement Of Methane Emissions And Surface Methane Oxidation at Landfills: A Supplementary Survey:WR1125, NPL REPORT AS (RES) 104, p. 42.

Innocenti, F., Robinson, R.A., Gardiner, T.D., Tompkins, J., Smith, S., Lowry, D., and Fisher, R., 2011, Measurements of Methane Emissions and Surface Methane Oxidation at Landfills: WR1125, NPL REPORT AS 072, p. 89.

Intergovernmental Panel on Climate Change (IPCC) 2006, IPCC Guidelines for National Greenhouse Gas Inventories, prepared by the National Greenhouse Gas Inventories Programme.

Intergovernmental Panel on Climate Change (IPCC), 2006, 2006 IPCC guidelines for national greenhouse gas inventories: industrial processes and product use, Kanagawa, JP: Institute for Global Environmental Strategies.

Intergovernmental Panel on Climate Change (IPCC), 2007, The Physical Science Basis, Contribution of Working Group I to the Fourth Assessment Report of the Intergovernmental Panel on Climate Change, edited by S. Solomon et al., Cambridge Univ. Press, Cambridge, U. K.

Ioannis Tsagatakis, S.B., Neil Passant, Sally Cooke, 2013, UK Emission Mapping Methodology 2011, Ricardo-AEA/R/3376 ED57422104 Issue 1.

Isaksen, I.S.A., Granier, C., Myhre, G., Berntsen, T.K., Dalsoren, S.B., Gauss, M., Klimont, Z., Benestad, R., Bousquet, P., Collins, W., Cox, T., Eyring, V., Fowler, D., Fuzzi, S., Joeckel, P., Laj, P., Lohmann, U., Maione, M., Monks, P., Prevot, A.S.H., Raes, F., Richter, A., Rognerud, B., Schulz, M., Shindell, D., Stevenson, D.S., Storelvmo, T., Wang, W.C., van Weele, M., Wild, M., and Wuebbles, D., 2009, Atmospheric composition change: Climate-Chemistry interactions: Atmospheric Environment, v. 43, p. 5138-5192.

Ito, A., and Inatomi, M., 2012, Use of a process-based model for assessing the methane budgets of global terrestrial ecosystems and evaluation of uncertainty: Biogeosciences, v. 9, p. 759-773.

Johnson, K.A., and Johnson, D.E., 1995, Methane emissions from cattle: Journal of animal science, v. 73, p. 2483-2492.

Jones N S, H.S., Creedy D P, Garner K, Smith N J P, Browne, M.A.E. & Durucan S., 2004, UK Coal Resource for New Exploitation Technologies Final Report, British Geological Survey.

Karakurt, I., Aydin, G., and Aydiner, K., 2012, Sources and mitigation of methane emissions by sectors: A critical review: Renewable energy, v. 39, p. 40-48.

Karim-zada, T., 2014, Identification of methane sources in Hounslow Borough using mobile laser sepctroscopy and validation of methane inventories, Master thesis, Univ. of Royal Holloway University of London.

Keeling, C.D., 1958, The concentration and isotopic abundances of atmospheric carbon dioxide in rural areas: Geochimica et Cosmochimica Acta, v. 13, p. 322-334.

Kennett, J.P., Cannariato, K.G., Hendy, I.L., and Behl, R.J., 2000, Carbon isotopic evidence for methane hydrate instability during Quaternary interstadials: Science, v. 288, p. 128-133.

Keppler, F., Hamilton, J.T., Braß, M., and Röckmann, T., 2006, Methane emissions from terrestrial plants under aerobic conditions: Nature, v. 439, p. 187-191.

Kirschke, S., Bousquet, P., Ciais, P., Saunois, M., Canadell, J.G., Dlugokencky, E.J., Bergamaschi, P., Bergmann, D., Blake, D.R., and Bruhwiler, L., 2013, Three decades of global methane sources and sinks: Nature Geoscience, v. 6, p. 813-823.

Klevenhusen, F., Bernasconi, S.M., Kreuzer, M., and Soliva, C.R., 2010, Experimental validation of the Intergovernmental Panel on Climate Change default values for ruminant-derived methane and its carbon-isotope signature: Animal Production Science, v. 50, p. 159-167.

Kotthaus, S., and Grimmond, C., 2012, Identification of Micro-scale Anthropogenic CO_2, heat and moisture sources–Processing eddy covariance fluxes for a dense urban environment: Atmospheric Environment, v. 57, p. 301-316.

Kotthaus, S., and Grimmond, C., 2013, Energy exchange in a dense urban environment–Part II: Impact of spatial heterogeneity of the surface: Urban Climate, v. 10, p. 281-307.

Koven, C.D., Ringeval, B., Friedlingstein, P., Ciais, P., Cadule, P., Khvorostyanov, D., Krinner, G., and Tarnocai, C., 2011, Permafrost carbon-climate feedbacks accelerate global warming: Proceedings of the National Academy of Sciences, v. 108, p. 14769-14774.

Krüger, M., Frenzel, P., and Conrad, R., 2001, Microbial processes influencing methane emission from rice fields: Global Change Biology, v. 7, p. 49-63.

Kvenvolden, K.A., 2002, Methane hydrate in the global organic carbon cycle: Terra Nova, v. 14, p. 302-306.

Lassey, K., Etheridge, D., Lowe, D., Smith, A., and Ferretti, D., 2007, Centennial evolution of the atmospheric methane budget: what do the carbon isotopes tell us?: Atmospheric chemistry and physics, v. 7, p. 2119-2139.

Lassey, K.R., Allan, W., and Fletcher, S.E.M., 2011, Seasonal inter-relationships in atmospheric methane and companion delta C-13 values: effects of sinks and sources: Tellus Series B-Chemical and Physical Meteorology, v. 63, p. 287-301.

Lassey, K.R., Lowe, D.C., Brenninkmeijer, C.A., and Gomez, A.J., 1993, Atmospheric methane and its carbon isotopes in the southern hemisphere: Their time series and an instructive model: Chemosphere, v. 26, p. 95-109.

Lelieveld, J., Crutzen, P.J., and Dentener, F.J., 1998, Changing concentration, lifetime and climate forcing of atmospheric methane: Tellus B, v. 50, p. 128-150.

Lelieveld, J., Peters, W., Dentener, F., and Krol, M., 2002, Stability of tropospheric hydroxyl chemistry: Journal of Geophysical Research: Atmospheres (1984–2012), v. 107, p. ACH 17-1-ACH 17-11.

Leng, L., Zhang, T., Kleinman, L., and Zhu, W., 2007, Ordinary least square regression, orthogonal regression, geometric mean regression and their applications in aerosol science, Journal of Physics: Conference Series, Volume 78, IOP Publishing, p. 012084.

Levin, I., Bergamaschi, P., Dörr, H., and Trapp, D., 1993, Stable isotopic signature of methane from major sources in Germany: Chemosphere, v. 26, p. 161-177.

Levin, I., Glatzel-Mattheier, H., Marik, T., Cuntz, M., Schmidt, M., and Worthy, D.E., 1999, Verification of German methane emission inventories and their recent changes based on atmospheric observations: Journal of Geophysical Research: Atmospheres (1984–2012), v. 104, p. 3447-3456.

Levin, I., Naegler, T., Heinz, R., Osusko, D., Cuevas, E., Engel, A., Ilmberger, J., Langenfelds, R.L., Neininger, B., and Rohden, C.v., 2010, The global SF6 source inferred from long-term high precision atmospheric measurements and its comparison with emission inventories: Atmospheric chemistry and physics, v. 10, p. 2655-2662.

Levin, I., Veidt, C., Vaughn, B., Brailsford, G., Bromley, T., Heinz, R., Lowe, D., Miller, J., Poß, C., and White, J., 2012, No inter-hemispheric $\delta^{13}CH_4$ trend observed: Nature, v. 486, p. E3-E4.

Levine, J.S., 1999, The 1997 fires in Kalimantan and Sumatra, Indonesia: Gaseous and particulate emissions: Geophysical Research Letters, v. 26, p. 815-818.

Levy, H., 1971, Normal atmosphere: Large radical and formaldehyde concentrations predicted: Science, v. 173, p. 141-143.

Liptay, K., Chanton, J., Czepiel, P., and Mosher, B., 1998, Use of stable isotopes to determine methane oxidation in landfill cover soils: Journal of Geophysical Research: Atmospheres (1984–2012), v. 103, p. 8243-8250.

Lokhorst, A., 1997, NW European Gas Atlas, British Geological Survey (BGS), Bundesanstalt für Geowissenschaften und Rohstoffe (BGR), Danmarks og Grønlands Geologiske Undersøgelse (GEUS), Panstwowy Instytut Geologiczny (PGI), Nederlands Instituut voor Toegepaste Geowetenschappen TNO (NITG-TNO), European Union.

Lowe, D.C., Brenninkmeijer, C.A., Brailsford, G.W., Lassey, K.R., Gomez, A.J., and Nisbet, E., 1994, Concentration and ^{13}C records of atmospheric methane in New Zealand and Antarctica: Evidence for changes in methane sources: Journal of Geophysical Research: Atmospheres (1984–2012), v. 99, p. 16913-16925.

Lowry, D., Holmes, C.W., Nisbet, E.G., and Rata, N.D., 2002, Can EC and UK national methane emission inventories be verified using high precision stable isotope data? In Proceedings: Study of Environmental Change using Isotope Techniques, IAEA-CSP-13/P, IAEA, Vienna, p. 399-409.

Lowry, D., Holmes, C.W., Rata, N.D., O'Brien, P., and Nisbet, E.G., 2001, London methane emissions: Use of diurnal changes in concentration and $\delta^{13}C$ to identify urban sources and verify inventories: Journal of Geophysical Research: Atmospheres, v. 106, p. 7427-7448.

MacFarling Meure, C., Etheridge, D., Trudinger, C., Steele, P., Langenfelds, R., Van Ommen, T., Smith, A., and Elkins, J., 2006, Law Dome CO_2, CH_4 and N_2O ice core records extended to 2000 years BP: Geophysical Research Letters, v. 33, no.14.

MacLeay, I., Harris, K., and Annut, A., 2014, Digest of United Kingdom Energy Statistics 2014, UK Department of Energy and Climate Change.

McCarthy, M., Connell, P., and Boering, K., 2001, Isotopic fractionation of methane in the stratosphere and its effect on free tropospheric isotopic compositions: Geophysical Research Letters, v. 28, p. 3657-3660.

McEvoy F. M., M.D., Harrison D.J., Cameron D.G., Burke H.F., Spencer N.A., Evans D.J., Lott G.K., Hobbs S.F. and Highley D.E., 2006, Mineral Resource Information in Support of National, Regional and Local Planning: South Yorkshire (comprising Metropolitan Boroughs of Barnsley, Doncaster and Rotherham and City of Sheffield), British Geological Survey Commissioned Report.

Mikaloff Fletcher, S.E., Tans, P.P., Bruhwiler, L.M., Miller, J.B., and Heimann, M., 2004, CH_4 sources estimated from atmospheric observations of CH_4 and its $^{13}C/^{12}C$ isotopic ratios: 2. Inverse modeling of CH_4 fluxes from geographical regions: Global Biogeochemical Cycles, v. 18, no.4.

Milkov, A.V., 2005, Molecular and stable isotope compositions of natural gas hydrates: a revised global dataset and basic interpretations in the context of geological settings: Organic Geochemistry, v. 36, p. 681-702.

Miller, J.B., 2004, The carbon isotopic composition of atmospheric methane and its constraints on the global methane budget, Stable Isotopes and Biosphere-Atmosphere Interactions: Processes and Biological Controls, Elsevier Academic Press California, p. 288-306.

Mischler, J.A., Sowers, T., Alley, R., Battle, M., McConnell, J., Mitchell, L., Popp, T., Sofen, E., and Spencer, M., 2009, Carbon and hydrogen isotopic composition of methane over the last 1000 years: Global Biogeochemical Cycles, v. 23, no.4.

Mitchell, L.E., Brook, E.J., Sowers, T., McConnell, J., and Taylor, K., 2011, Multidecadal variability of atmospheric methane, 1000–1800 CE: Journal of Geophysical Research: Biogeosciences (2005–2012), v. 116, no.G2.

Molins, S., Mayer, K., Scheutz, C., and Kjeldsen, P., 2008, Transport and reaction processes affecting the attenuation of landfill gas in cover soils: Journal of environmental quality, v. 37, p. 459-468.

Montzka, S., Dlugokencky, E., and Butler, J., 2011, Non-CO_2 greenhouse gases and climate change: Nature, v. 476, p. 43-50.

Moriizumi, J., Nagamine, K., Iida, T., and Ikebe, Y., 1998, Carbon isotopic analysis of atmospheric methane in urban and suburban areas: fossil and non-fossil methane from local sources: Atmospheric Environment, v. 32, p. 2947-2955.

Myhre, G., Shine, K.P., Rädel, G., Gauss, M., Isaksen, I., Tang, Q., Prather, M., Williams, J., van Velthoven, P., and Dessens, O., 2011, Radiative forcing due to changes in ozone and methane caused by the transport sector: Atmospheric Environment, v. 45, p. 387-394.

Naik, V., Voulgarakis, A., Fiore, A.M., Horowitz, L., Lamarque, J.-F., Lin, M., Prather, M.J., Young, P., Bergmann, D., and Cameron-Smith, P., 2013, Preindustrial to present-day changes in tropospheric hydroxyl radical and methane lifetime from the Atmospheric Chemistry and Climate Model Intercomparison Project (ACCMIP): Atmospheric chemistry and physics, v. 13, p. 5277-5298.

Nakagawa, F., Tsunogai, U., Komatsu, D.D., Yamada, K., Yoshida, N., Moriizumi, J., Nagamine, K., Iida, T., and Ikebe, Y., 2005, Automobile exhaust as a source of ^{13}C- and D-enriched atmospheric methane in urban areas: Organic Geochemistry, v. 36, p. 727-738.

Nisbet, E.G., 2002, Have sudden large releases of methane from geological reservoirs occurred since the Last Glacial Maximum, and could such releases occur again?: Philosophical Transactions of the Royal Society of London. Series A: Mathematical, Physical and Engineering Sciences, v. 360, p. 581-607.

Nisbet, E.G., Dlugokencky, E.J., and Bousquet, P., 2014, Methane on the rise—again: Science, v. 343, p. 493-495.

Nisbet, R., Fisher, R., Nimmo, R., Bendall, D., Crill, P., Gallego-Sala, A., Hornibrook, E., López-Juez, E., Lowry, D., and Nisbet, E.G., 2009, Emission of methane from plants: Proceedings of the Royal Society of London B: Biological Sciences, v. 276, p. 1347-1354.

Oremland, R.S., 1988, Biogeochemistry of methanogenic bacteria, Biology of anaerobic microorganisms, John Wiley & Sons, New York, p. 641-705.

Papendick, S.L., Downs, K.R., Vo, K.D., Hamilton, S.K., Dawson, G.K., Golding, S.D., and Gilcrease, P.C., 2011, Biogenic methane potential for Surat Basin, Queensland coal seams: International Journal of Coal Geology, v. 88, p. 123-134.

Pataki, D.E., Bowling, D.R., and Ehleringer, J.R., 2003, Seasonal cycle of carbon dioxide and its isotopic composition in an urban atmosphere: Anthropogenic and biogenic effects: Journal of Geophysical Research-Atmospheres, v. 108, no.D23.

Phillips, N.G., Ackley, R., Crosson, E.R., Down, A., Hutyra, L.R., Brondfield, M., Karr, J.D., Zhao, K., and Jackson, R.B., 2013, Mapping urban pipeline leaks: Methane leaks across Boston: Environmental pollution, v. 173, p. 1-4.

Platt, U., Allan, W., and Lowe, D., 2004, Hemispheric average Cl atom concentration from $^{13}C/^{12}C$ ratios in atmospheric methane: Atmospheric chemistry and physics, v. 4, p. 2393-2399.

Prather, M.J., Holmes, C.D., and Hsu, J., 2012, Reactive greenhouse gas scenarios: Systematic exploration of uncertainties and the role of atmospheric chemistry: Geophysical Research Letters, v. 39, no.9.

Quay, P., Stutsman, J., Wilbur, D., Snover, A., Dlugokencky, E., and Brown, T., 1999, The isotopic composition of atmospheric methane: Global Biogeochemical Cycles, v. 13, p. 445-461.

Quay, P.D., King, S.L., Lansdown, J.M., and Wilbur, D.O., 1988, Isotopic composition of methane released from wetlands: implications for the increase in atmospheric methane: Global Biogeochem. Cycles, v. 2, p. 385-397.

Ramaswamy, V., Chanin, M.L., Angell, J., Barnett, J., Gaffen, D., Gelman, M., Keckhut, P., Koshelkov, Y., Labitzke, K., and Lin, J.J., 2001, Stratospheric temperature trends: Observations and model simulations: Reviews of Geophysics, v. 39, p. 71-122.

Reeburgh, W., 2003, Global methane biogeochemistry: Treatise on geochemistry, v. 4, p. 65-89.

Rice, D.D., 1993, Composition and origins of coalbed gas: Hydrocarbons from coal: AAPG Studies in Geology, v. 38, p. 159-184.

Rigby, M., Toumi, R., Fisher, R., Lowry, D., and Nisbet, E.G., 2008, First continuous measurements of CO_2 mixing ratio in central London using a compact diffusion probe: Atmospheric Environment, v. 42, p. 8943-8953.

Ringeval, B., Friedlingstein, P., Koven, C., Ciais, P., Noblet-Ducoudré, N.d., Decharme, B., and Cadule, P., 2011, Climate-CH_4 feedback from wetlands and its interaction with the climate-CO_2 feedback: Biogeosciences, v. 8, p. 2137-2157.

Rolph G.D., 2015, Real-time Environmental Applications and Display sYstem (READY) Website (http://ready.arl.noaa.gov). NOAA Air Resources Laboratory, Silver Spring, MD.

Sapart, C., Monteil, G., Prokopiou, M., van de Wal, R.S., Kaplan, J., Sperlich, P., Krumhardt, K., Van der Veen, C., Houweling, S., and Krol, M., 2012, Natural and anthropogenic variations in methane sources during the past two millennia: Nature, v. 490, p. 85-88.

Saueressig, G., Crowley, J.N., Bergamaschi, P., Brühl, C., Brenninkmeijer, C.A., and Fischer, H., 2001a, Carbon 13 and D kinetic isotope effects in the reactions of CH_4 with O (1 D) and OH: New laboratory measurements and their implications for the isotopic composition of stratospheric methane: Journal of Geophysical Research: Atmospheres (1984–2012), v. 106, p. 23127-23138.

Saueressig, G., Crowley, J.N., Bergamaschi, P., Brühl, C., Brenninkmeijer, C.A., and Fischer, H., 2001b, Carbon 13 and D kinetic isotope effects in the reactions of CH_4 with O(1D) and OH: New laboratory measurements and their implications for the isotopic composition of stratospheric methane: Journal of Geophysical Research: Atmospheres (1984–2012), v. 106, p. 23127-23138.

Scheutz, C., Kjeldsen, P., Bogner, J.E., De Visscher, A., Gebert, J., Hilger, H.A., Huber-Humer, M., and Spokas, K., 2009, Microbial methane oxidation processes and technologies for mitigation of landfill gas emissions: Waste Management & Research, v. 27, p. 409-455.

Schlegel, M.E., McIntosh, J.C., Bates, B.L., Kirk, M.F., and Martini, A.M., 2011, Comparison of fluid geochemistry and microbiology of multiple organic-rich reservoirs in the Illinois Basin, USA: evidence for controls on methanogenesis and microbial transport: Geochimica et Cosmochimica Acta, v. 75, p. 1903-1919.

Scott, A.R., 2002, Hydrogeologic factors affecting gas content distribution in coal beds: International Journal of Coal Geology, v. 50, p. 363-387.

Scott, A.R., Kaiser, W., and Ayers Jr, W.B., 1994, Thermogenic and secondary biogenic gases, San Juan Basin, Colorado and New Mexico-implications for coalbed gas producibility: AAPG bulletin, v. 78, p. 1186-1209.

Shakhova, N., Semiletov, I., Leifer, I., Salyuk, A., Rekant, P., and Kosmach, D., 2010a, Geochemical and geophysical evidence of methane release over the East Siberian Arctic Shelf: Journal of Geophysical Research: Oceans (1978–2012), v. 115, no.C8.

Shakhova, N., Semiletov, I., Salyuk, A., Yusupov, V., Kosmach, D., and Gustafsson, Ö., 2010b, Extensive methane venting to the atmosphere from sediments of the East Siberian Arctic Shelf: Science, v. 327, p. 1246-1250.

Shindell, D.T., Faluvegi, G., Bell, N., and Schmidt, G.A., 2005, An emissions-based view of climate forcing by methane and tropospheric ozone: Geophysical Research Letters, v. 32, no.4.

Shindell, D.T., Faluvegi, G., Koch, D.M., Schmidt, G.A., Unger, N., and Bauer, S.E., 2009, Improved Attribution of Climate Forcing to Emissions: Science, v. 326, p. 716-718.

Smith, J.W., Gould, K., and Rigby, D., 1981, The stable isotope geochemistry of Australian coals: Organic Geochemistry, v. 3, p. 111-131.

Smith, K., Dobbie, K., Ball, B., Bakken, L., Sitaula, B., Hansen, S., Brumme, R., Borken, W., Christensen, S., and Priemé, A., 2000, Oxidation of atmospheric methane in Northern European soils, comparison with other ecosystems, and uncertainties in the global terrestrial sink: Global Change Biology, v. 6, p. 791-803.

Snover, A.K., and Quay, P.D., 2000, Hydrogen and carbon kinetic isotope effects during soil uptake of atmospheric methane: Global Biogeochemical Cycles, v. 14, p. 25-39.

Sokal, R.R., and Rohlf, F.J., 1995, Biometry: the principals and practice of statistics in biological research: WH Freeman and Company, New York, p. 541-554.

Sowers, T., 2010, Atmospheric methane isotope records covering the Holocene period: Quaternary Science Reviews, v. 29, p. 213-221.

Spahni, R., Wania, R., Neef, L., Weele, M.v., Pison, I., Bousquet, P., Frankenberg, C., Foster, P., Joos, F., and Prentice, I., 2011, Constraining global methane emissions and uptake by ecosystems: Biogeosciences, v. 8, p. 1643-1665.

Stach, E., and Murchison, D.G., 1982, Stach's Textbook of coal petrology, Borntraeger, Stuttgart (1982), p. 33-54.

Stahl, W.J., 1977, Carbon and nitrogen isotopes in hydrocarbon research and exploration: Chemical Geology, v. 20, p. 121-149.

Stauffer, B., Fischer, G., Neftel, A., and Oeschger, H., 1985, Increase of atmospheric methane recorded in Antarctic ice core: Science, v. 229, p. 1386-1388.

Sternberg, L.O., Deniro, M.J., and Johnson, H.B., 1984, Isotope ratios of cellulose from plants having different photosyntetic pathways: Plant Physiology, v. 74, p. 557-561.

Stevens, C., and Wahlen, M., 2000, The isotopic composition of atmospheric methane and its sources, Atmospheric Methane:Its role in the Global Environment: New York, Springer, p. 25-41.

Stevens, C.M., and Engelkemeir, A., 1988, Stable carbon isotopic composition of methane from some natural and anthropogenic sources: Journal of Geophysical Research: Atmospheres (1984–2012), v. 93, p. 725-733.

Stevenson, D., Doherty, R., Sanderson, M., Johnson, C., Collins, B., and Derwent, D., 2005, Impacts of climate change and variability on tropospheric ozone and its precursors: Faraday discussions, v. 130, p. 41-57.

Teixeira, E.C., de Santana, E.R., Wiegand, F., and Fachel, J., 2009, Measurement of surface ozone and its precursors in an urban area in South Brazil: Atmospheric Environment, v. 43, p. 2213-2220.

Toerien, D., and Hattingh, W., 1969, Anaerobic digestion I. The microbiology of anaerobic digestion: Water Research, v. 3, p. 385-416.

Townsend-Small, A., Tyler, S.C., Pataki, D.E., Xu, X.M., and Christensen, L.E., 2012, Isotopic measurements of atmospheric methane in Los Angeles, California, USA: Influence of "fugitive" fossil fuel emissions: Journal of Geophysical Research-Atmospheres, v. 117, no.D7.

Tyler, S.C., Ajie, H.O., Rice, A.L., Cicerone, R.J., and Tuazon, E.C., 2000, Experimentally determined kinetic isotope effects in the reaction of CH_4 with Cl: Implications for atmospheric CH_4: Geophysical Research Letters, v. 27, p. 1715-1718.

Tyler, S.C., Crill, P.M., and Brailsford, G.W., 1994, $^{13}C^{12}C$ fractionation of methane during oxidation in a temperate forested soil: Geochimica et Cosmochimica Acta, v. 58, p. 1625-1633.

U.S. EPA, 2008, EPA's Report on the Environment (ROE). U.S. Environmental Protection Agency, Washington, D.C., EPA/600/R-07/045F (NTIS PB2008-112484).

U.S. EPA, 2010, Methane and nitrous oxide emissions from natural sources. United States Environmental Protection Agency (EPA) Report. Washington, DC. http://www.epa.gov/outreach/pdfs/Methane-and-Nitrous-Oxide-Emissions-From-NaturalSources.pdf.

U.S. EPA, 2011, Global anthropogenic non-CO_2 greenhouse gas emissions: 1990–2030, United States Environmental Protection Agency (EPA) Report. Washington, DC. http://www.epa.gov/climatechange/Downloads/EPAactivities/EPA_Global_NonCO2_Projections_Dec2012.pdf.

U.S. EPA, 2013, US Environmental Protection Agency, Global Mitigation of Non-CO_2 Greenhouse Gases: 2010–2030, USEPA, Washington, DC EPA-430-R-13-011.

Valentine, D.L., 2002, Biogeochemistry and microbial ecology of methane oxidation in anoxic environments: a review: Antonie van Leeuwenhoek, v. 81, p. 271-282.

van der Werf, G.R., Randerson, J.T., Collatz, G.J., and Giglio, L., 2003, Carbon emissions from fires in tropical and subtropical ecosystems: Global Change Biology, v. 9, p. 547-562.

Van Der Werf, G.R., Randerson, J.T., Giglio, L., Collatz, G., Mu, M., Kasibhatla, P.S., Morton, D.C., DeFries, R., Jin, Y.v., and van Leeuwen, T.T., 2010, Global fire emissions and the contribution of deforestation, savanna, forest, agricultural, and peat fires (1997–2009): Atmospheric chemistry and physics, v. 10, p. 11707-11735.

Vigano, I., Röckmann, T., Holzinger, R., Van Dijk, A., Keppler, F., Greule, M., Brand, W.A., Geilmann, H., and Van Weelden, H., 2009, The stable isotope signature of methane emitted from plant material under UV irradiation: Atmospheric Environment, v. 43, p. 5637-5646.

Vinogradova, A., Fedorova, E., Belikov, I., Ginzburg, A., Elansky, N., and Skorokhod, A., 2007, Temporal variations in carbon dioxide and methane concentrations under urban conditions: Izvestiya, Atmospheric and Oceanic Physics, v. 43, p. 599-611.

Voulgarakis, A., Naik, V., Lamarque, J.-F., Shindell, D.T., Young, P., Prather, M.J., Wild, O., Field, R., Bergmann, D., and Cameron-Smith, P., 2013, Analysis of present day and future OH and methane lifetime in the ACCMIP simulations: Atmospheric chemistry and physics, v. 13, p. 2563-2587.

Waldron, S., Fallick, A., and Hall, A., 1998, Comment on" Spatial distribution of microbial methane production pathways in temperate zone wetland soils: Stable carbon and hydrogen evidence" by ERC Hornibrook, FJ Longstaffe, and WS Fyfe: Geochimica et Cosmochimica Acta, v. 62, p. 369-372.

Weiss, R.F., Mühle, J., Salameh, P.K., and Harth, C.M., 2008, Nitrogen trifluoride in the global atmosphere: Geophysical Research Letters, v. 35, no. 20.

Westbrook, G.K., Thatcher, K.E., Rohling, E.J., Piotrowski, A.M., Pälike, H., Osborne, A.H., Nisbet, E.G., Minshull, T.A., Lanoisellé, M., and James, R.H., 2009, Escape of methane gas from the seabed along the West Spitsbergen continental margin: Geophysical Research Letters, v. 36, no.L15608.

Whiticar, M., and Schaefer, H., 2007, Constraining past global tropospheric methane budgets with carbon and hydrogen isotope ratios in ice: Philosophical Transactions of the Royal Society of London A: Mathematical, Physical and Engineering Sciences, v. 365, p. 1793-1828.

Whiticar, M.J., 1996, Stable isotope geochemistry of coals, humic kerogens and related natural gases: International Journal of Coal Geology, v. 32, p. 191-215.

Whiticar, M.J., 1999, Carbon and hydrogen isotope systematics of bacterial formation and oxidation of methane: Chemical Geology, v. 161, p. 291-314.

Whiticar, M.J., and Faber, E., 1986, Methane oxidation in sediment and water column environments - isotope evidence: Organic Geochemistry, v. 10, p. 759-768.

Widory, D., Proust, E., Bellenfant, G., and Bour, O., 2012, Assessing methane oxidation under landfill covers and its contribution to the above atmospheric CO_2 levels: The added value of the isotope ($\delta^{13}C$ and $\delta^{18}O$ CO_2; $\delta^{13}C$ and δD CH_4) approach: Waste management, v. 32, p. 1685-1692.

Williamson, I., 1967, Coal Mining Geology: Oxford University Press, p. 266.

Xu, L., Lin, X., Amen, J., Welding, K., and McDermitt, D., 2014, Impact of changes in barometric pressure on landfill methane emission: Global Biogeochemical Cycles, v. 28, p. 679-695.

Young, P., Archibald, A., Bowman, K., Lamarque, J.-F., Naik, V., Stevenson, D., Tilmes, S., Voulgarakis, A., Wild, O., and Bergmann, D., 2013, Pre-industrial to end 21st century projections of tropospheric ozone from the Atmospheric Chemistry and Climate Model Intercomparison Project (ACCMIP): Atmospheric chemistry and physics, v. 13, p. 2063-2090.

Zazzeri, G., Lowry, D., Fisher, R., France, J., Lanoisellé, M., and Nisbet, E., 2015, Plume mapping and isotopic characterisation of anthropogenic methane sources: Atmospheric Environment, v. 110, p. 151-162.

Zhang, T., and Krooss, B.M., 2001, Experimental investigation on the carbon isotope fractionation of methane during gas migration by diffusion through sedimentary rocks at elevated temperature and pressure: Geochimica et Cosmochimica Acta, v. 65, p. 2723-2742.

APPENDIX A

Use of ArcMap Software for Creating Emissions Maps and Mole Fractions Plots

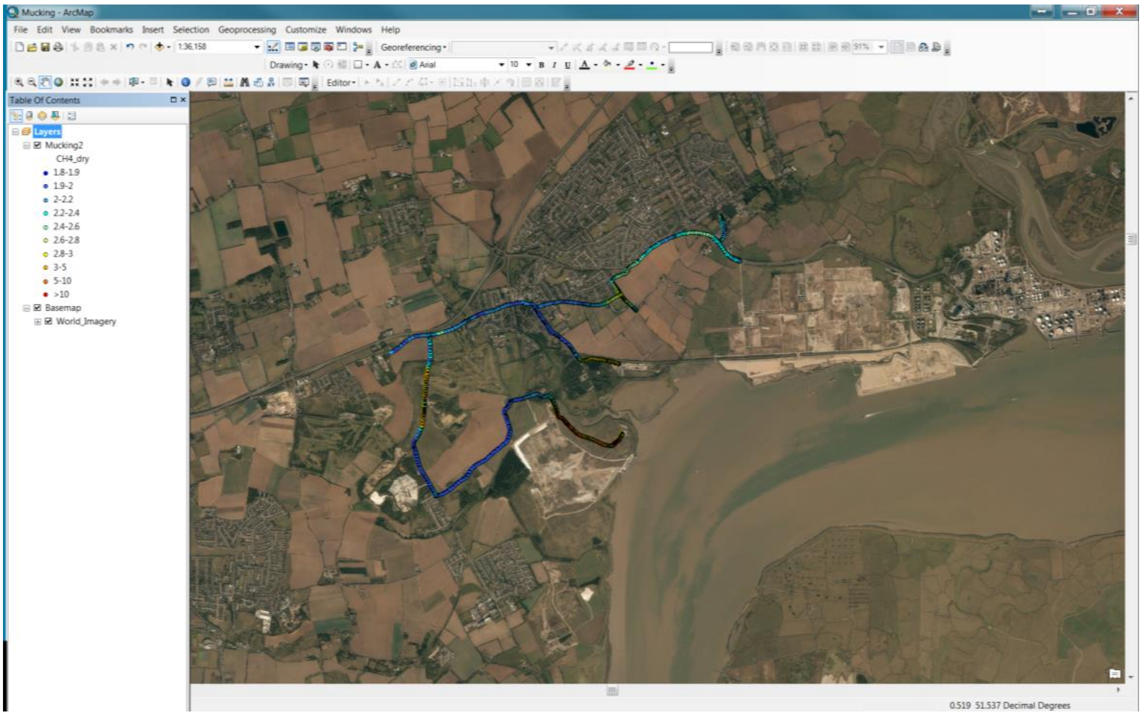

The ArcMap software is used to display georeferenced data and analyse map data. All the maps of surveys included in this thesis work were created with this software, using the row file (.dat file) produced by the Picarro analyser after each measurement campaign, which includes CO_2 and CH_4 mole fraction measurements with the associated gps coordinates.

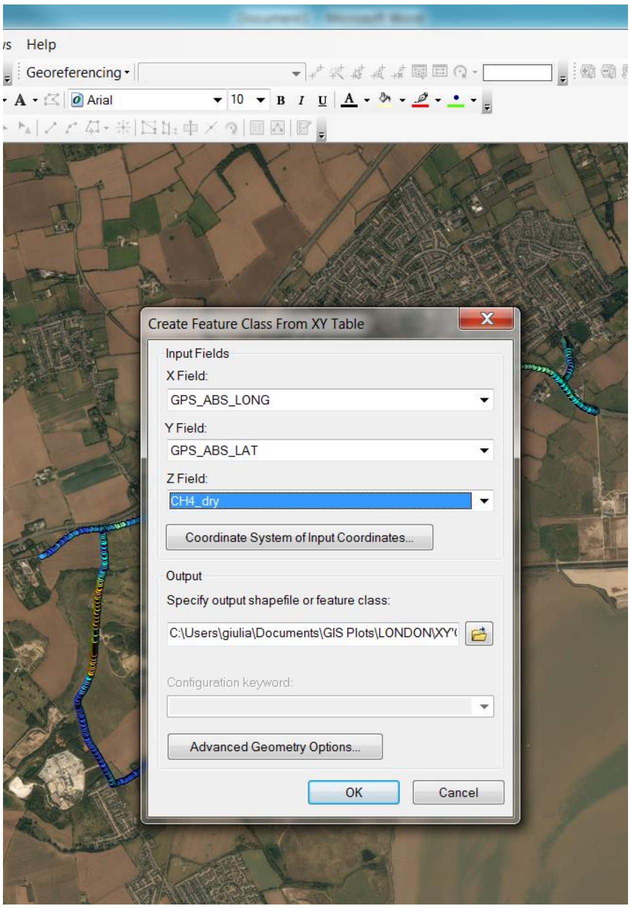

Create Feature Class From XY Table

Input Fields

X Field: GPS_ABS_LONG

Y Field: GPS_ABS_LAT

Z Field: CH4_dry

Output

Specify output shapefile or feature class: C:\Users\giulia\Documents\GIS Plots\LONDON\XY'(

Configuration keyword:

Data were organised in an excel file with 5 columns including date, CO_2, CH_4, latitude and longitude. The excel file was then converted in shape file (.shp) using the tool "create feature class from XY table" in ArcMap and specifying on the x-y-z field, longitude, latitude and CH_4 mole fractions respectively (on the *Catalog* window right click on the .xlsx file – *Create feature class From XY table*).

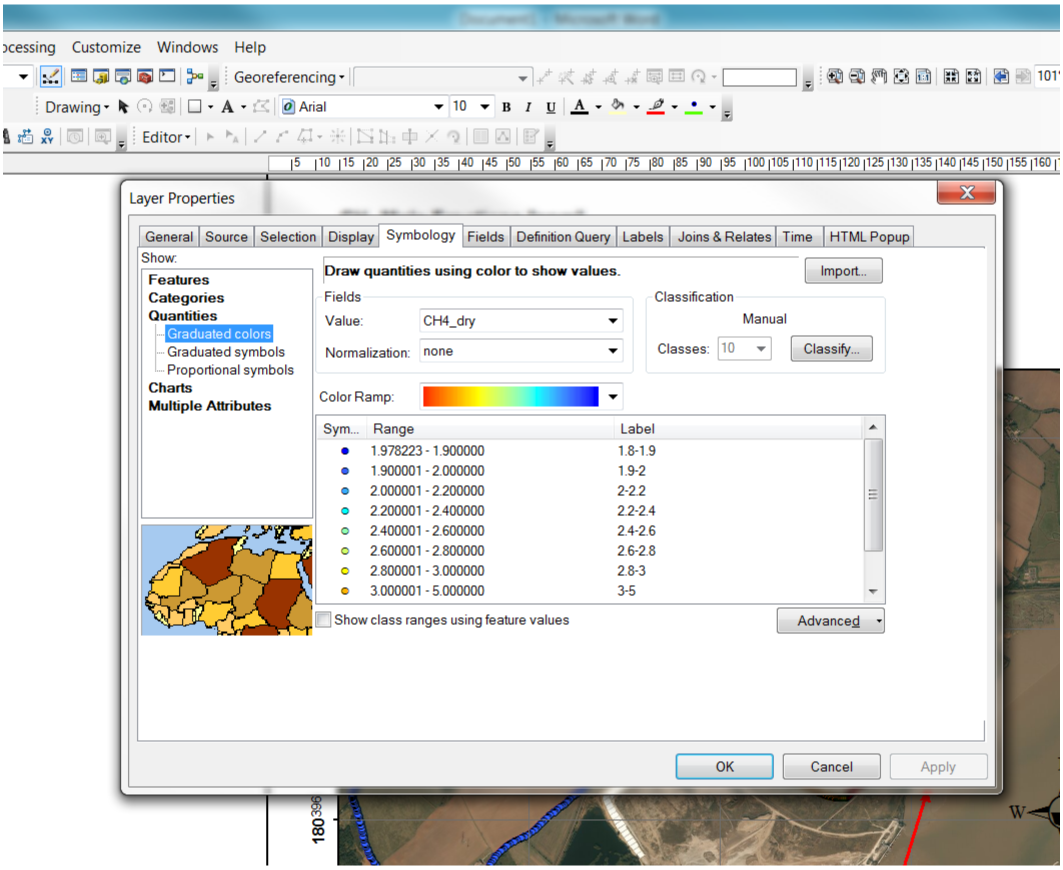

Layer Properties

Draw quantities using color to show values.

Fields

Value: CH4_dry

Normalization: none

Classification

Manual

Classes: 10

Sym...	Range	Label
●	1.978223 - 1.900000	1.8-1.9
●	1.900001 - 2.000000	1.9-2
●	2.000001 - 2.200000	2-2.2
●	2.200001 - 2.400000	2.2-2.4
●	2.400001 - 2.600000	2.4-2.6
●	2.600001 - 2.800000	2.6-2.8
●	2.800001 - 3.000000	2.8-3
●	3.000001 - 5.000000	3-5

☐ Show class ranges using feature values

Once the shape file is created and imported in the map window, it can be modified to show mole fraction ranges with different colours. In layer properties (right click on the selected layer on the *Table Of Content*) the data symbology can be changed by choosing *Quantities* on the *Symbology* tab, which allows several ranges of the value chosen (CH_4 in this case) to be displayed. ArcMap provides several predefined ramp colours and symbol shapes, so that the survey route and the mole fraction ranges can be properly visualised. ArcMap automatically selects the colour and number intervals, but these can be modified manually.

ArcMap 10.2 also provides base maps centred on the route, according to the coordinate system chosen for the data frame. Before the upgrade of the software, base maps were created by geo-referencing images and scanned maps.

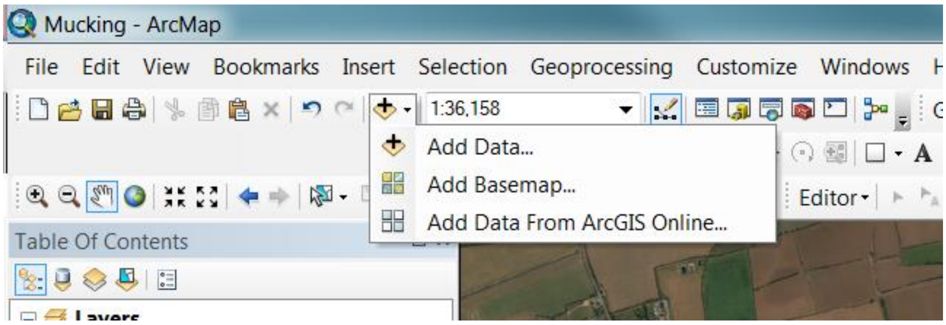

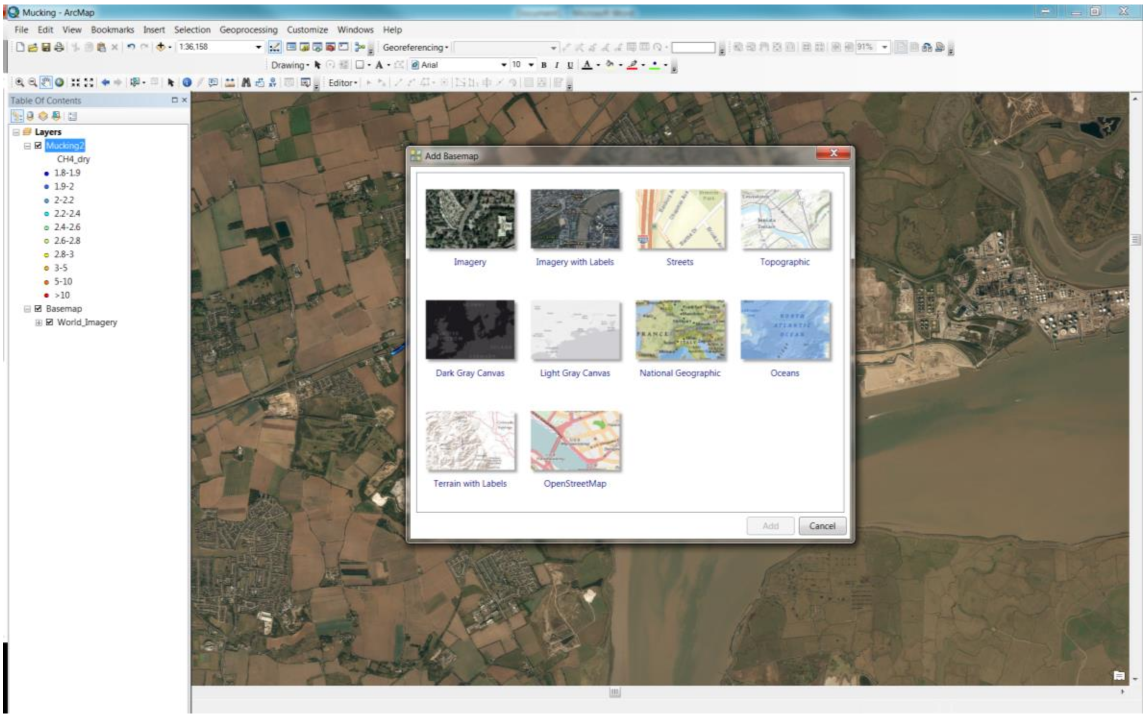

Data Frame Coordinate System

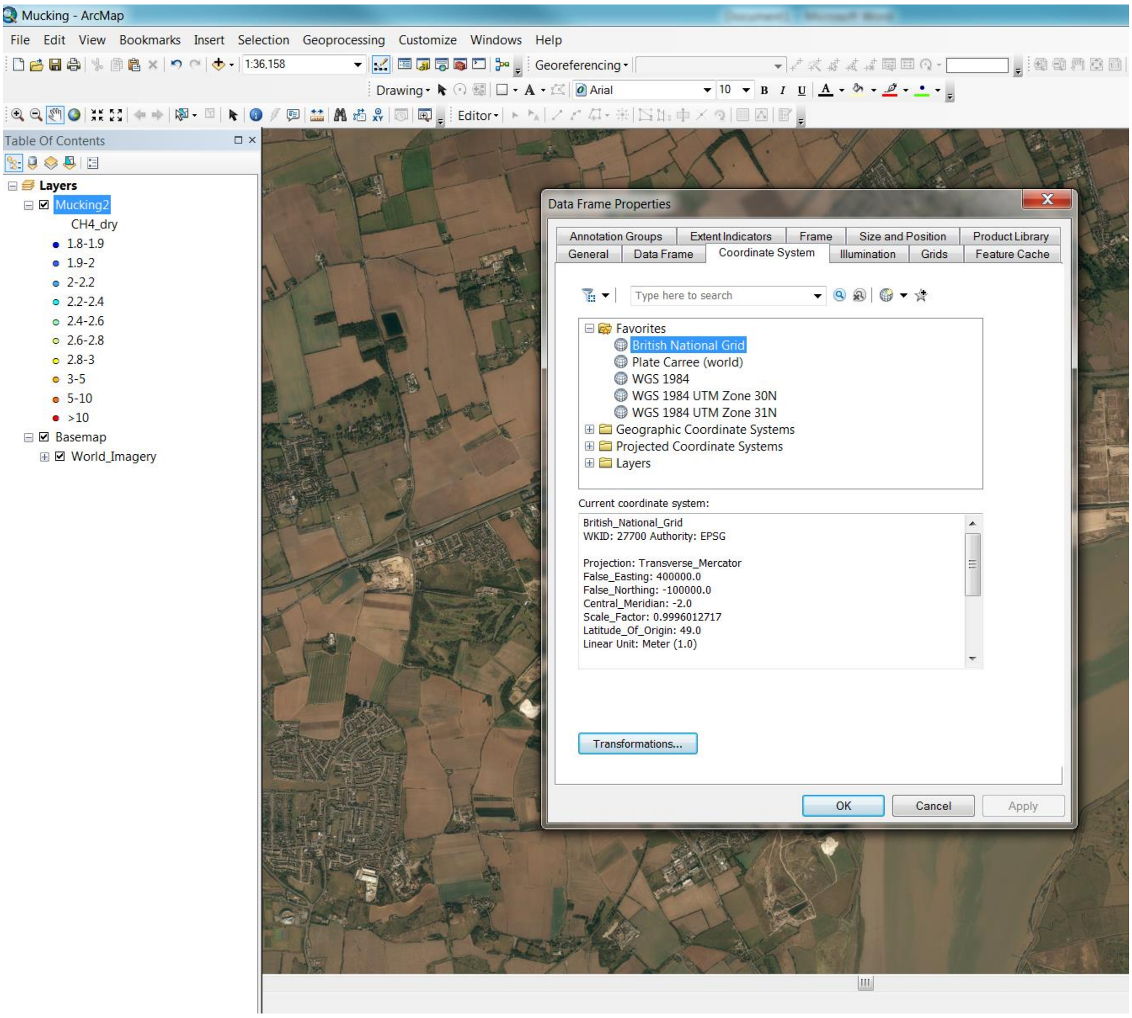

Current coordinate system:

```
British_National_Grid
WKID: 27700 Authority: EPSG

Projection: Transverse_Mercator
False_Easting: 400000.0
False_Northing: -100000.0
Central_Meridian: -2.0
Scale_Factor: 0.9996012717
Latitude_Of_Origin: 49.0
Linear Unit: Meter (1.0)
```

As all map objects are spatially georeferenced, the choice of the coordinates system is one of the first actions to follow before creating a map. The sequence herein shows the steps for the coordinate system selection:

Click on *View - Data Frame Properties - Coordinates Systems*.

The coordinate system used for the maps in this thesis work is the *British National Grid*.

The Layout Window

The layout window shows how the map is arranged on the page, and many objects, such as legend, north arrow, scale, can be added. The legend Wizard lets you choose the map layers to include in the legend, modify the font, the style and many other features. The map window can be zoomed or moved and, while all the objects in the map will remain in their geographical position, the objects added in the layout window will have a fixed position relative to the page.

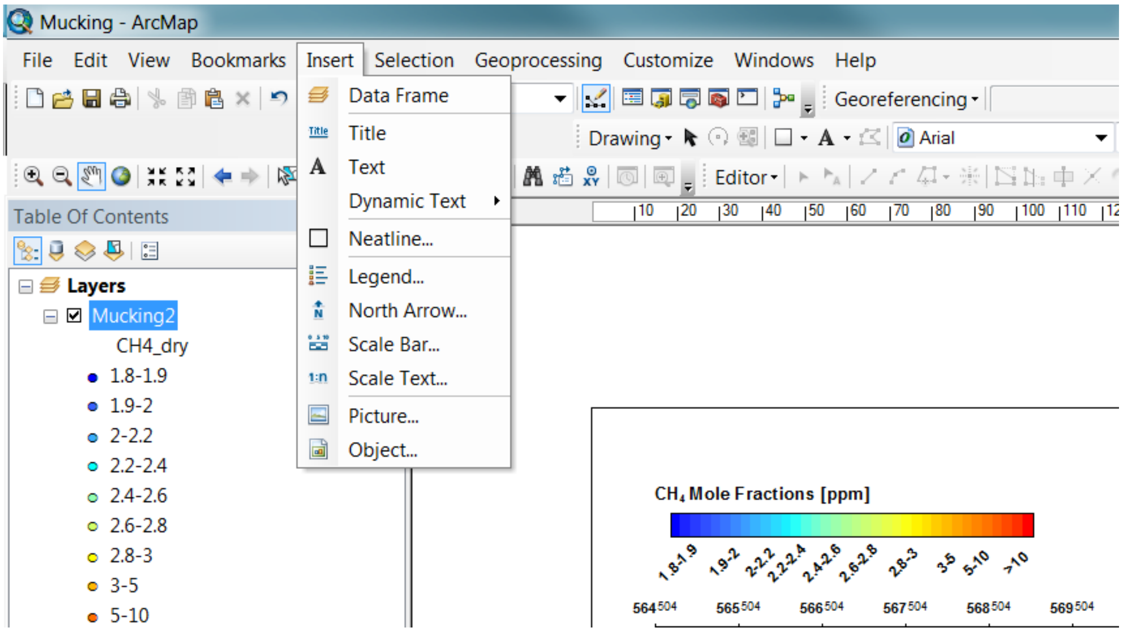

Adding Grids

In the layout window we can add also a customised grid based on the coordinate system chosen for the map.

Click on *View - Data frame Properties - Grids-New Grid*

There are three types of grids available in ArcMap: Graticule, Index Grid and Measured Grid. A Measured Grid allows the intervals to be set and it is appropriate for coordinate system such as the British National Grid one, which measures in meters. The grid labels can be customised by choosing the number format, the number of digits and the decimal places.

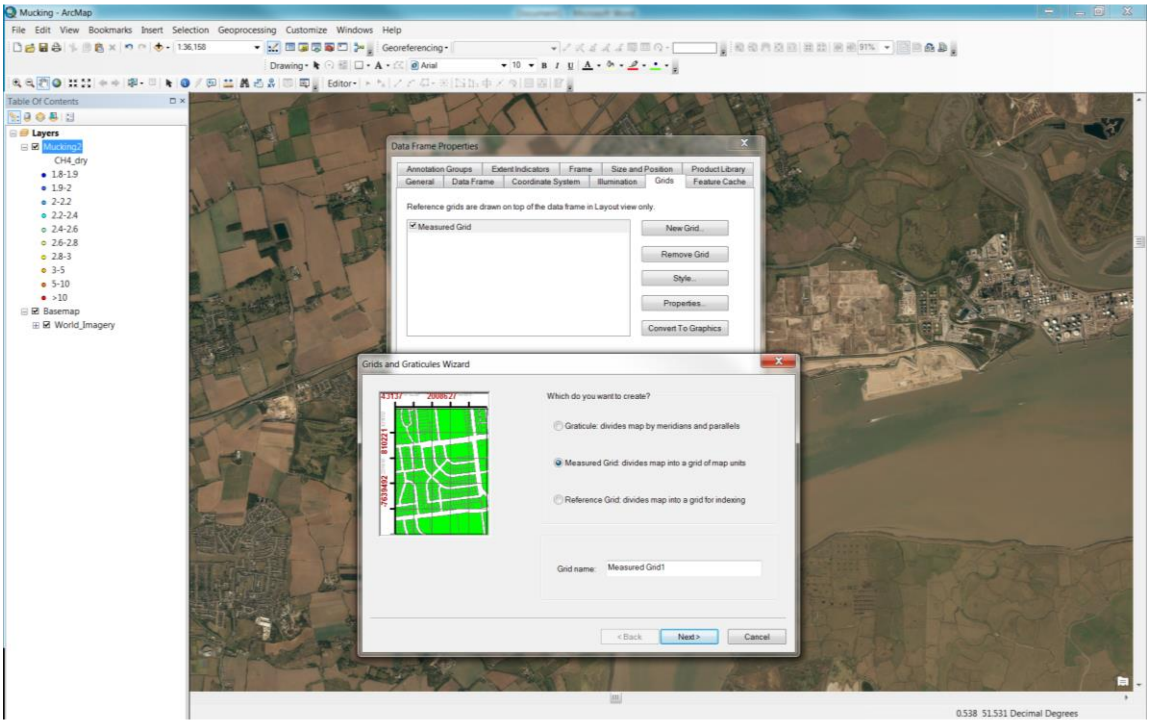

Data Frame Properties

Reference grids are drawn on top of the data frame in Layout view only.

☑ Measured Grid

Grids and Graticules Wizard

Which do you want to create?

○ Graticule: divides map by meridians and parallels

● Measured Grid: divides map into a grid of map units

○ Reference Grid: divides map into a grid for indexing

Grid name: Measured Grid1

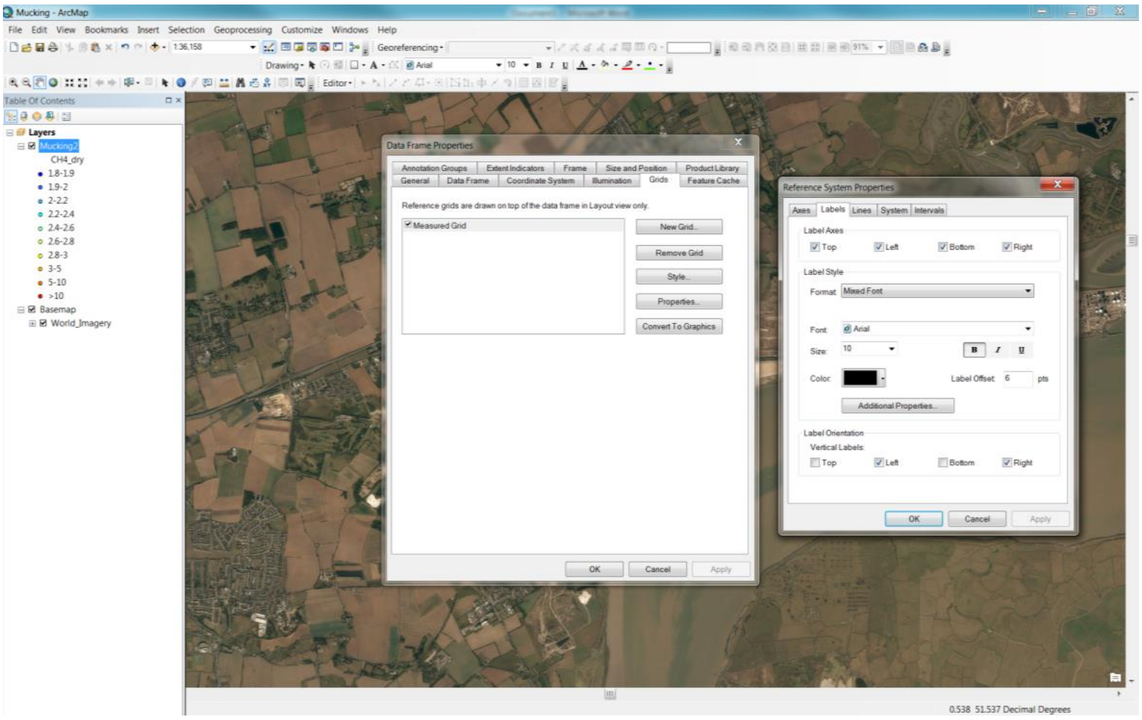

Data Frame Properties

Reference grids are drawn on top of the data frame in Layout view only.

☑ Measured Grid

Reference System Properties

Label Axes: ☑ Top ☑ Left ☑ Bottom ☑ Right

Label Style

Format: Mixed Font

Font: Arial

Size: 10

Label Offset: 6 pts

Label Orientation

Vertical Labels: ☐ Top ☑ Left ☐ Bottom ☑ Right

The maps created can be eventually exported (*File-Export Map*) to various image formats such as TIFF, JPEG, EMF or as PDF files.

APPENDIX B

CH_4 Mole Fractions and $\delta^{13}C$ Measured at RHUL during Diurnal Studies

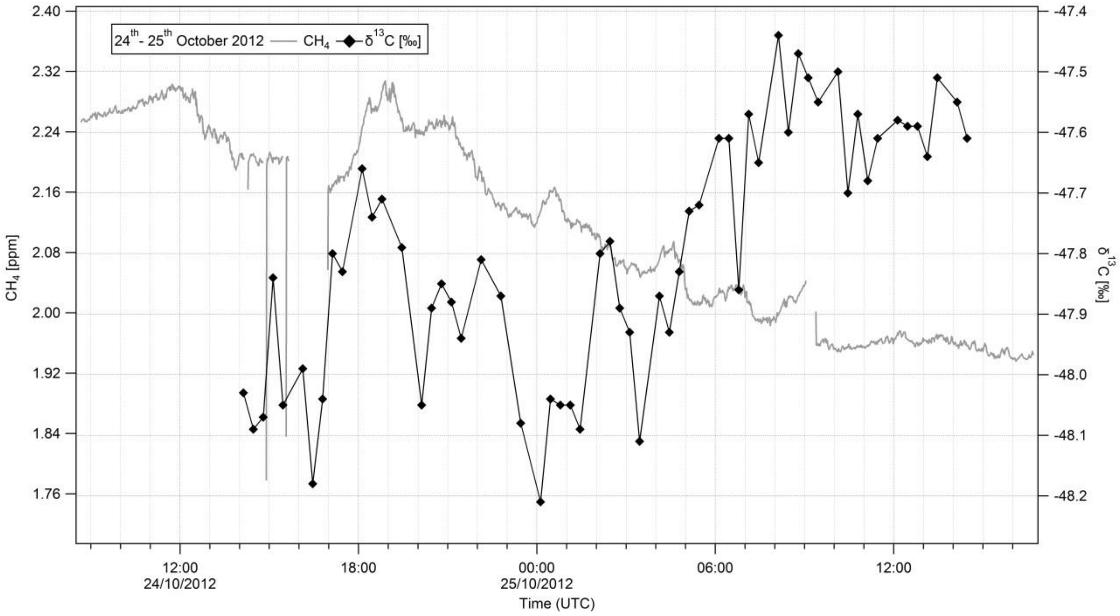

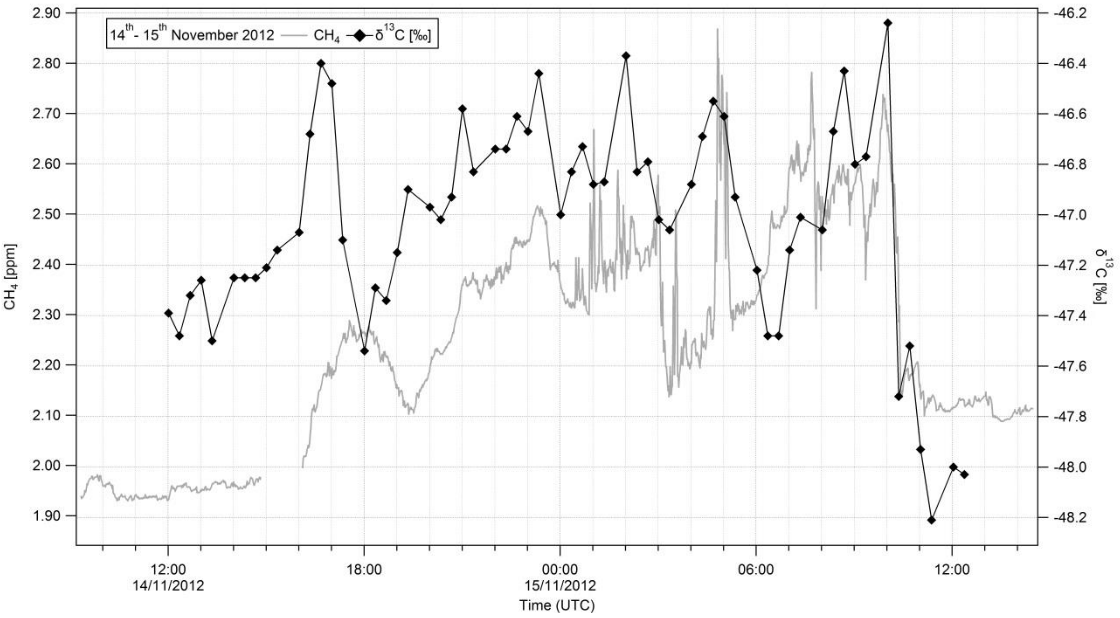

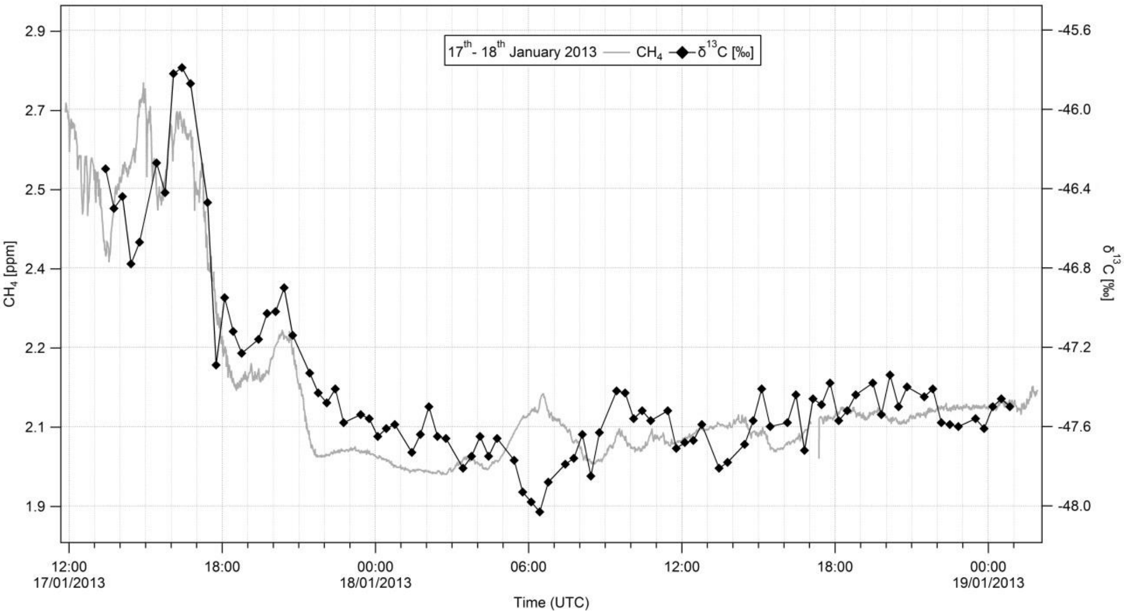
17th - 18th January 2013 — CH4 ◆ δ13C [‰]
CH4 [ppm]
2.9
2.7
2.5
2.4
2.2
2.1
1.9
δ13C [‰]
-45.6
-46.0
-46.4
-46.8
-47.2
-47.6
-48.0
12:00
17/01/2013
18:00
00:00
18/01/2013
06:00
12:00
18:00
00:00
19/01/2013
Time (UTC)

APPENDIX C

CH_4 and CO_2 Mole Fractions Complete Record at King's College

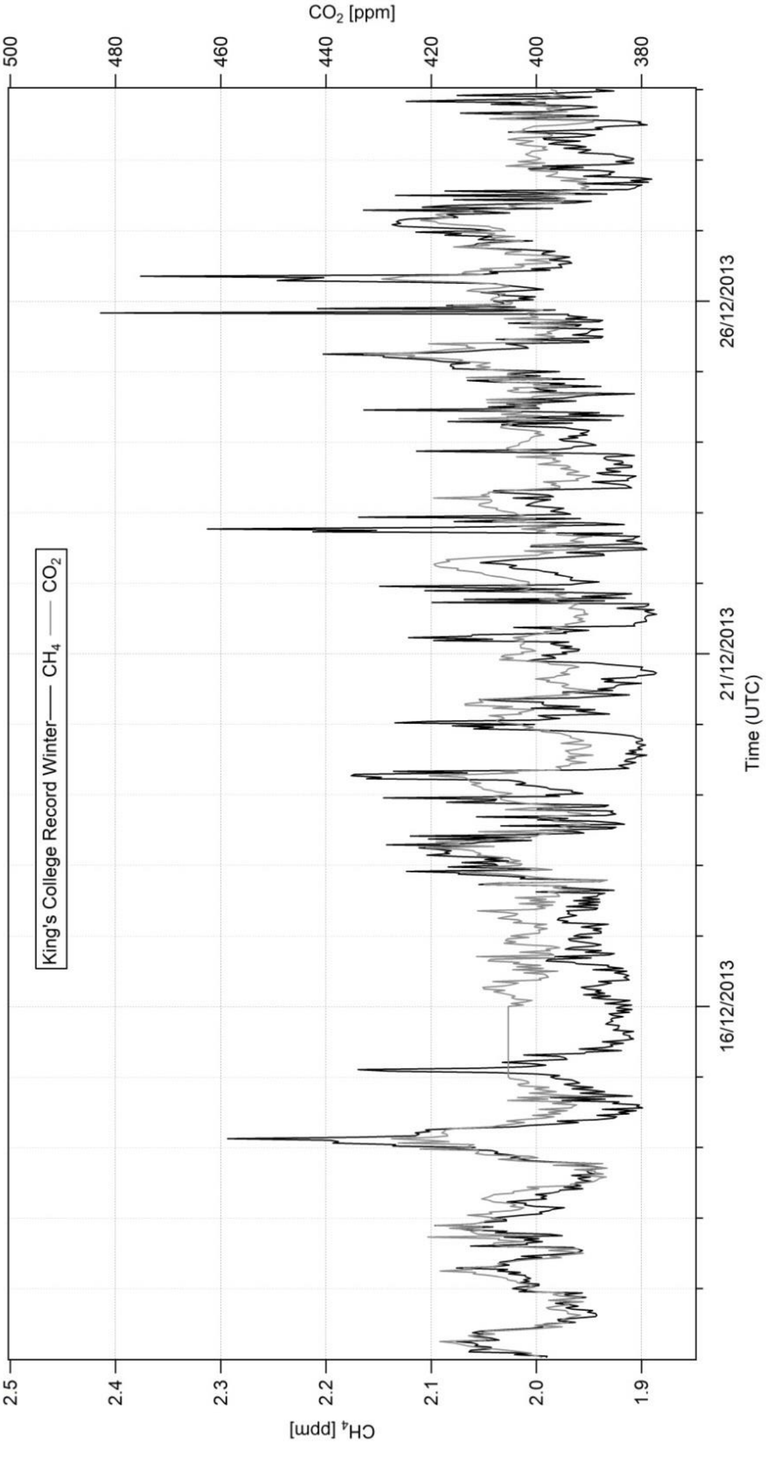

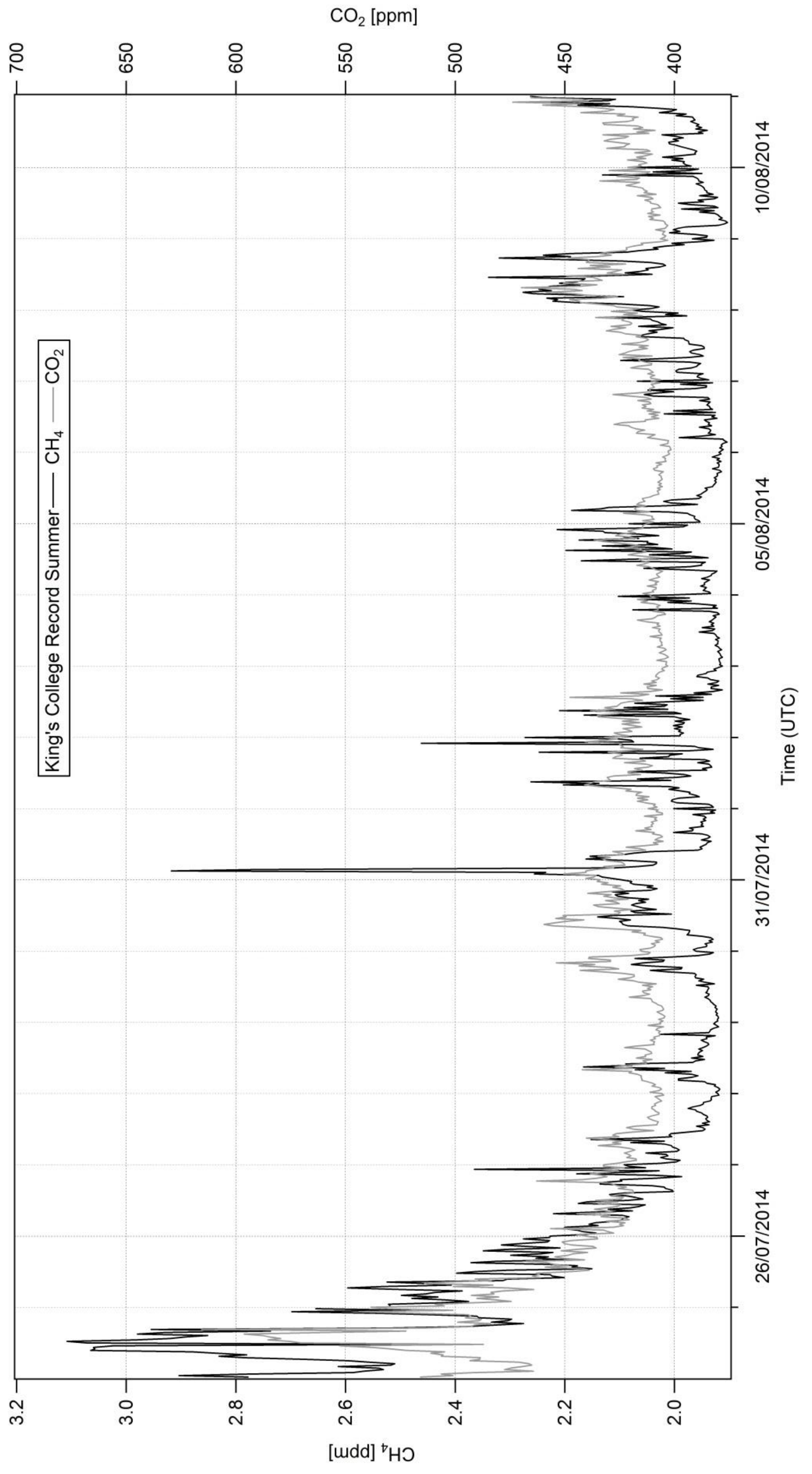
King's College Record Summer —— CH$_4$ —— CO$_2$
CO$_2$ [ppm]
700
650
600
550
500
450
400
CH$_4$ [ppm]
3.2
3.0
2.8
2.6
2.4
2.2
2.0
Time (UTC)
26/07/2014
31/07/2014
05/08/2014
10/08/2014

APPENDIX D

2009 Inventories for Runnymede and Hounslow Borough

Runnymede Borough 2009 Emissions Inventories

			Heating			**Gas**		**Cars**		**Waste**	**Cows**	**Bogs**	
X	Y	a01	a02	a03	a04	a05	a06	a07	a08	a09	a10	a11	pt
498500	172500	0	0.0847	0	0	0.797	0	0.0231	0.000963	0.0501	1.91	0.00593	0
499500	172500	0	0.25	0	0	0.481	0	0.0442	0.000812	0.0496	1.91	0.00627	0
500500	172500	0	0.0647	0	0	0	0	0.0469	0.000941	0.0255	0.47	0.0039	0
497500	171500	0	0.00702	0	0	0.191	0	0.00617	0.000506	0.0495	1.91	0.00665	0
498500	171500	0	0.204	0.00288	0	2.75	0	0.0321	0.00404	0.0502	1.91	0.00857	0
499500	171500	0	0.351	0.00299	0	9.12	0	0.0942	0.005	0.0516	1.91	0.017	0
500500	171500	0	0.308	0.00218	0	5.97	0	0.116	0.00668	0.0263	0.47	0.0165	0
501500	171500	0	0.536	0.323	0	9.77	0	0.72	0.0263	0.0277	0.47	0.0236	0
502500	171500	0	0.533	1.16	0	9.3	0	0.129	0.0958	0.0266	0.47	0.0281	0
497500	170500	0	0.00366	0	0	0.12	0	0.00803	0.000749	0.0498	1.91	0.00366	0
498500	170500	0	0.343	0	0	6.11	0	0.0486	0.00466	0.0506	1.91	0.0242	0
499500	170500	0	0.594	0.0961	0	9.12	0	0.152	0.00789	0.0513	1.91	0.0226	0
500500	170500	0	0.332	0.000416	0	8.79	0	0.0672	0.00694	0.0267	0.47	0.0214	0
501500	170500	0	0.136	0.00264	0	2.83	0	0.534	0.0063	0.0265	0.47	0.0132	0
502500	170500	0	0.496	0.00387	0	13.5	0	0.0939	0.0154	0.0273	0.47	0.0331	0
503500	170500	0	0.276	0.0055	0	8.84	0	0.0923	0.0123	0.0268	0.47	0.0243	0
497500	169500	0	0.0848	0.00217	0	0	0	0	0.0141	45	0.398	0.00587	0
498500	169500	0	0.126	0	0	0.0417	0	0.0559	0.000288	45	0.398	0.00765	0
499500	169500	0	0.0453	0	0	0.773	0	0.0152	0.000727	45	0.398	0.00771	0
500500	169500	0	0.0578	0	0	1.51	0	0.016	0.0035	45	0.873	0.00642	0

			Heating			**Gas**		**Cars**		**Waste**	**Cows**	**Bogs**	
X	Y	a01	a02	a03	a04	a05	a06	a07	a08	a09	a10	a11	pt
501500	169500	0	0.031	0	0	0.285	0	0.501	0.00103	45	0.873	0.00651	0
502500	169500	0	0.167	0.764	0.116	1.7	0	0.0192	0.117	45	0.873	0.00636	0.304
503500	169500	0	0.201	0.00995	0	6.28	0	0.0807	0.00685	45	0.873	0.0116	0
497500	168500	0	0.0476	0	0	0.352	0	0.0671	0.000233	45	0.398	0.0053	0
498500	168500	0	0.0738	0	0	1.87	0	0.0346	0.000569	45	0.398	0.00584	0
499500	168500	0	0.305	0	0	4.6	0	0.0194	0.00124	45	0.398	0.009	0
500500	168500	0	0.354	0.00503	0	5.63	0	0.0234	0.00725	45	0.873	0.0132	0
501500	168500	0	0.144	0.00174	0	3.57	0	0.54	0.00299	45	0.873	0.00573	0
502500	168500	0	0.118	0.0677	0	1.53	0	0.0397	0.115	45	0.873	0.00338	0
503500	168500	0	0.113	0.0414	0	0.014	0	0.0236	0.00671	45	0.873	0.00158	0
504500	168500	0	0.249	0.00386	0	0.361	0	0.0576	0.00564	45	0.873	0.00706	0
496500	167500	0	0.0859	0	0	1.14	0	0.0526	0.000575	45	0.398	0.00618	0
497500	167500	0	0.322	0	0	0.427	0	0.0157	0.000553	45	0.398	0.00486	0
498500	167500	0	0.137	0	0	1.09	0	0.00425	0.0011	45	0.398	0.00699	0
499500	167500	0	0.274	0.00195	0	7.83	0	0.0164	0.00414	45	0.398	0.0139	0
500500	167500	0	0.341	0.0254	0	2.47	0	0.368	0.0047	45	0.873	0.00928	0
501500	167500	0	0.119	0.00368	0	0.264	0	0.637	0.00482	45	0.873	0.00273	0
502500	167500	0	0.0608	0.00792	0	0.736	0	0.418	0.00241	45	0.873	0.00505	0
503500	167500	0	0.153	0.0102	0	4.57	0	0.257	0.0114	45	0.873	0.0147	0
504500	167500	0	0.169	0	0	1.62	0	0.171	0.00205	45	0.873	0.00884	0
497500	166500	0	0.00342	0	0	0.105	0	0	0.000672	45	0.398	0.00369	0
498500	166500	0	0.0338	0	0	0.322	0	0.175	0.000797	45	0.398	0.00584	0
499500	166500	0	0.0631	0	0	2.05	0	0.411	0.00088	45	0.398	0.0062	0.0762
500500	166500	0	0.00468	0	0	0.141	0	0.112	0.000717	45	0.873	0.00294	0
501500	166500	0	0.989	0.019	0	2.01	0	0.00657	0.00478	45	0.873	0.0063	0
502500	166500	0	0.0688	0.000317	0	0.583	0	0.534	0.00226	45	0.873	0.00388	0
503500	166500	0	0.435	0.0177	0	8.39	0	0.296	0.0223	45	0.873	0.0206	0
504500	166500	0	0.612	0.0732	0	13.6	0	0.148	0.0973	45	0.873	0.0307	0
505500	166500	0	0.202	0.0314	0	3.73	0	0.0529	0.0278	45	0.358	0.00936	0
498500	165500	0	0.0353	0.00768	0	0.484	0	0.303	0.00556	45	0.398	0.00298	0

			Heating			**Gas**		**Cars**		**Waste**	**Cows**	**Bogs**	
X	Y	a01	a02	a03	a04	a05	a06	a07	a08	a09	a10	a11	pt
499500	165500	0	0.0395	0.00672	0	0.346	0	0.0179	0.00505	45	0.398	0.00477	0
500500	165500	0	0.0569	0	0	0.365	0	0.014	0.000561	45	0.873	0.00465	0
501500	165500	0	0.0954	0.00105	0	0.162	0	0.017	0.00211	45	0.873	0.00451	0
502500	165500	0	0.534	0	0	2.39	0	0.0513	0.000952	45	0.873	0.00628	0
503500	165500	0.00031	0.245	0.0587	0	6.06	0	0.669	0.0231	45	0.873	0.0144	0
504500	165500	0	0.211	0.00429	0	5.72	0	0.17	0.00899	45	0.873	0.0217	0
505500	165500	0	0.828	0.0041	0	1.83	0	0.108	0.00469	45	0.358	0.00833	0
506500	165500	0	0.381	0	0	1.71	0	0.0439	0.00221	45	0.358	0.00814	0
499500	164500	0	0	0	0	0	0	0	0.000546	0.0545	0.736	0.00515	0
500500	164500	0	0.0275	0	0	0	0	0.00627	0.00035	0.0344	0.767	0.00656	0
501500	164500	0	0.0463	0.00405	0	0.319	0	0.00788	0.00437	0.0346	0.767	0.00702	0
502500	164500	0	0.148	0	0	1.02	0	0.126	0.00106	0.0352	0.767	0.00683	0
503500	164500	0	0.0614	0.00205	0	1.91	0	0.303	0.00272	0.0348	0.767	0.00979	0
504500	164500	0	0.634	0.00605	0	15.2	0	0.456	0.0155	0.0359	0.767	0.0393	0
505500	164500	0	0.611	0.552	0	14.6	0	0.118	0.0836	0.0383	0.147	0.0373	0
506500	164500	0	0.451	0.00614	0	4.13	0	0.109	0.00718	0.037	0.147	0.0146	0
500500	163500	0	0.00424	0.00522	0	0.0417	0	0.012	0.00169	0.0345	0.767	0.00565	0
501500	163500	0	0.0854	3.97E-05	0	2.06	0	0.0507	0.00113	0.0346	0.767	0.00864	0
502500	163500	0	0.398	0.00319	0	9.23	0	0.0923	0.00671	0.0357	0.767	0.0186	0
503500	163500	0	0.303	0.00134	0	8.74	0	0.0433	0.00451	0.036	0.767	0.0206	0
504500	163500	0	0.209	0.00289	0	6.25	0	0.591	0.00486	0.0349	0.767	0.0192	0
505500	163500	0	0.168	0.000274	0	3.64	0	0.07	0.00284	0.037	0.147	0.0112	0
501500	162500	0	0.0111	0	0	0.319	0	0.0413	0.000534	0.0342	0.767	0.00455	0
502500	162500	0	0.0492	0	0	0.681	0	0.0197	0.000668	0.0347	0.767	0.00771	0
503500	162500	0	0.117	0.000546	0	2.92	0	0.0236	0.00228	0.0352	0.767	0.0104	0
504500	162500	0	0.563	0.00355	0	10.5	0	0.0888	0.00993	0.0361	0.767	0.0277	0.0263
505500	162500	0	0.299	0.0699	0	8.49	0	0.627	0.0535	0.0381	0.147	0.0164	0
503500	161500	0	0.304	0.0234	0	9.66	0	0.094	0.00552	0.0358	0.767	0.0183	0

			Heating			Gas		Cars		Waste	Cows	Bogs	
X	Y	a01	a02	a03	a04	a05	a06	a07	a08	a09	a10	a11	pt
510500	178500	0	0.254	0.0265	0	5.9	0	0.653	0.0125	0.0227	0.12	0.0201	0
511500	178500	0	0.483	0.133	0	11.8	0	0.138	0.0756	0.023	0.12	0.0382	0
512500	178500	0	0.911	0.00946	0	24.9	0	0.136	0.0245	0.0239	0.12	0.0683	0
514500	178500	0	0.022	0	0	0.105	0	0.244	0.00129	0.0223	0.12	0.00319	0
515500	178500	0	0.00335	0	0	0.0277	0	0.285	0.00281	0.018	0.0864	0.00418	0
516500	178500	0	0.289	0.102	0	8.22	0	0.349	0.0401	0.0183	0.0864	0.0206	0
517500	178500	0	0.919	0.0932	0	27.1	0	0.572	0.0706	0.018	0.0864	0.0691	0
518500	178500	0	0.474	0.111	0	6.35	0	0.498	0.0589	0.0183	0.0864	0.0291	0
519500	178500	0	0.755	0.0664	0	14.9	0	0.629	0.0512	0.0184	0.0864	0.0388	0
520500	178500	0	1.23	0.0827	0	31.5	0	0.264	0.0725	0.00843	0.0236	0.0673	0
521500	178500	0	1.59	0.0733	0	42	0	0.504	0.0388	0.00839	0.0236	0.0784	0
510500	177500	0	0.163	0	0	4.27	0	0.266	0.00388	0.0226	0.12	0.0157	0
511500	177500	0	0.442	0.0035	0	12.1	0	0.391	0.0104	0.0237	0.12	0.0373	0
512500	177500	0	0.7	0.0101	0	18	0	0.379	0.0159	0.0237	0.12	0.0483	0
513500	177500	0	0.414	0.00562	0	11.5	0	0.173	0.0116	0.0227	0.12	0.0381	0
514500	177500	0	0.27	0	0	8.26	0	0.13	0.00299	0.0231	0.12	0.0145	0
515500	177500	0	0.457	0.000562	0	14	0	0.247	0.00551	0.019	0.0864	0.0225	0
516500	177500	0	0.608	0.0415	0	9.21	0	0.347	0.0555	0.018	0.0864	0.0238	0
517500	177500	0	0.797	0.116	0	13	0	0.249	0.108	0.018	0.0864	0.0394	0
519500	177500	0	1.03	0.0175	0	25.5	0	0.23	0.0272	0.0186	0.0864	0.0534	0
520500	177500	0	0.828	0.0178	0	23.5	0	0.395	0.0191	0.00954	0.0236	0.0482	0
521500	177500	0	0.538	1.08	0	11.3	0	0.309	0.137	0.00875	0.0236	0.0332	0
510500	176500	0	0.536	0.00781	0	15.6	0	0.311	0.202	0.023	0.12	0.0439	0
511500	176500	0	0.635	0.00447	0	18.6	0	0.354	0.198	0.0245	0.12	0.0551	0
512500	176500	0	0.83	0.000937	0	22.8	0	0.316	0.2	0.0237	0.12	0.0646	0
513500	176500	0	0.846	0.0131	0	16.7	0	0.278	0.0131	0.0235	0.12	0.0467	0
514500	176500	0	0.791	0.00236	0	22.5	0	0.214	0.0132	0.0245	0.12	0.0593	0
515500	176500	0	0.876	0.0894	0	21.8	0	0.203	0.0454	0.0199	0.0864	0.0522	0

			Heating			**Gas**		**Cars**		**Waste**	**Cows**	**Bogs**	
X	Y	a01	a02	a03	a04	a05	a06	a07	a08	a09	a10	a11	pt
516500	176500	0	0.677	0.00237	0	11.5	0	0.188	0.00845	0.0181	0.0864	0.034	0
517500	176500	0	0.00831	0	0	0.0417	0	0	0.00118	0.0178	0.0864	0.00601	0
520500	176500	0	0.18	0.000217	0	5.45	0	0.145	0.00433	0.00877	0.0236	0.0132	0
510500	175500	0	0.113	0.00899	0	1.62	0	0.372	0.193	0.0225	0.12	0.0062	0
511500	175500	0	0.561	0.741	0	14.7	0	0.0808	0.28	0.0236	0.12	0.0398	0
512500	175500	0	0.851	0.028	0	21.9	0	0.236	0.211	0.0233	0.12	0.0719	0
513500	175500	0	3.76	0.197	0	23.9	0	0.288	0.0977	0.0227	0.12	0.0586	0
514500	175500	0	0.954	0.0365	0	20.7	0	0.174	0.0284	0.0231	0.12	0.0578	0
515500	175500	0	0.464	0.0809	0	11.9	0	0.112	0.0687	0.0189	0.0864	0.0367	0
516500	175500	0	0.655	0.0348	0	16.6	0	0.205	0.0186	0.0182	0.0864	0.044	0
509500	174500	0	0.303	0	0	9.16	0	0.118	0.00501	0.0249	0.369	0.0236	0
510500	174500	0	0.512	0.0878	0	10.7	0	0.265	0.123	0.0252	0.0797	0.0263	0
511500	174500	0	0.21	0.0284	0	4.24	0	0.0957	0.0156	0.0248	0.0797	0.0143	0
512500	174500	0	0.242	0	0	7.19	0	0.0522	0.00602	0.0249	0.0797	0.0307	0
513500	174500	0	0.906	0.0169	0	27.8	0	0.245	0.0239	0.026	0.0797	0.0709	0
514500	174500	0	0.718	0.0218	0	22.3	0	0.128	0.0142	0.0259	0.0797	0.0558	1.46
515500	174500	0	0.479	0.0418	0	9.8	0	0.201	0.0225	0.0209	0.0201	0.0468	0
507500	173500	0	0.0305	0.00106	0	0.144	0	0.123	0.00428	0.0242	0.369	0.00506	0
508500	173500	0	0.603	0.000149	0	11.4	0	0.293	0.00617	0.0253	0.369	0.0277	0
509500	173500	0	0.618	0.0118	0	18.3	0	0.152	0.0307	0.0247	0.369	0.0526	0
510500	173500	0	0.774	0.0133	0	12.5	0	0.225	0.0246	0.0249	0.0797	0.0482	0
511500	173500	0	0.453	0.00115	0	13.6	0	0.148	0.0102	0.0251	0.0797	0.0367	0
508500	172500	0	0.185	0.0443	0	0.0417	0	0.0136	0.0315	0.0244	0.369	0.0047	0
509500	172500	0.568	0.33	0.0112	0	9.17	0	0.124	0.0185	0.0245	0.369	0.0387	0
510500	172500	0	0.799	0.21	0	14.4	0	0.165	0.145	0.0255	0.0797	0.0395	0
511500	172500	0	0.651	0.0119	0	6.38	0	0.16	0.0115	0.0248	0.0797	0.0207	0
512500	172500	0	0.574	0.101	0	16	0	0.365	0.0825	0.0256	0.0797	0.0487	0
509500	171500	0.00031	0.337	0.000922	0	9.56	0	0.11	0.00719	0.0253	0.369	0.0263	0
510500	171500	0	0.0945	0.613	0	2.18	0	0.0459	0.0623	0.0246	0.0797	0.0171	0
511500	171500	0	0.594	0.00248	0	11.3	0	0.464	0.00573	0.025	0.0797	0.0245	0

2012 UK inventories are provided on the NAEI website in a different format and are not separated by borough. The following table shows an example of the 2012 inventories dataset.

OBJECTID	Year	Met1km_ID	Latitude	Longitude	energyprod	domcom	indcom	indproc	offshore	roadtrans	othertrans	waste	agric	nature
					a01	a02	a03	a04	a05	a07	a08	a09	a10	a11
1	2012	1015	49.39516	-8.16816	0	0	0	0	0	0	5.03E-05	0	0	0
2	2012	1016	49.39516	-8.15408	0	0	0	0	0	0	5.03E-05	0	0	0
3	2012	1017	49.39516	-8.14	0	0	0	0	0	0	5.08E-05	0	0	0
4	2012	1018	49.39516	-8.12592	0	0	0	0	0	0	5.69E-05	0	0	0
5	2012	1019	49.39516	-8.11184	0	0	0	0	0	0	6.79E-05	0	0	0
6	2012	1020	49.39516	-8.09776	0	0	0	0	0	0	6.56E-05	0	0	0
7	2012	1021	49.39516	-8.08368	0	0	0	0	0	0	6.17E-05	0	0	0
8	2012	1022	49.39516	-8.0696	0	0	0	0	0	0	5.60E-05	0	0	0
9	2012	1023	49.39516	-8.05552	0	0	0	0	0	0	5.98E-05	0	0	0
10	2012	1024	49.39516	-8.04144	0	0	0	0	0	0	7.34E-05	0	0	0
11	2012	1025	49.39516	-8.02736	0	0	0	0	0	0	7.50E-05	0	0	0
12	2012	1026	49.39516	-8.01328	0	0	0	0	0	0	7.50E-05	0	0	0
13	2012	1027	49.39516	-7.9992	0	0	0	0	0	0	7.50E-05	0	0	0
14	2012	1028	49.39516	-7.98512	0	0	0	0	0	0	7.56E-05	0	0	0
15	2012	1029	49.39516	-7.97104	0	0	0	0	0	0	7.68E-05	0	0	0
16	2012	1030	49.39516	-7.95696	0	0	0	0	0	0	7.69E-05	0	0	0

Atmospheric Environment 110 (2015) 151–162

Contents lists available at ScienceDirect

Atmospheric Environment

journal homepage: www.elsevier.com/locate/atmosenv

Plume mapping and isotopic characterisation of anthropogenic methane sources

G. Zazzeri [a, *], D. Lowry [a], R.E. Fisher [a], J.L. France [b], M. Lanoisellé [a], E.G. Nisbet [a, *]

[a] Royal Holloway, University of London, United Kingdom
[b] University of East Anglia, United Kingdom

HIGHLIGHTS

- CH_4 source plumes were located by a mobile Picarro analyser.
- CH_4 plumes from landfill sites, coal mines and gas leaks were sampled.
- High precision isotopic analysis of air samples collected was carried out.
- CH_4 isotopic signatures were allocated to CH_4 sources in UK.
- The method provides an independent constraint to determine CH_4 sources contribution.

ARTICLE INFO

Article history:
Received 23 November 2014
Received in revised form
11 March 2015
Accepted 13 March 2015
Available online 14 March 2015

Keywords:
Plume mapping
Methane isotopes
Picarro mobile

ABSTRACT

Methane stable isotope analysis, coupled with mole fraction measurement, has been used to link isotopic signature to methane emissions from landfill sites, coal mines and gas leaks in the United Kingdom. A mobile Picarro G2301 CRDS (Cavity Ring-Down Spectroscopy) analyser was installed on a vehicle, together with an anemometer and GPS receiver, to measure atmospheric methane mole fractions and their relative location while driving at speeds up to 80 kph. In targeted areas, when the methane plume was intercepted, air samples were collected in Tedlar bags, for $\delta^{13}C-CH_4$ isotopic analysis by CF-GC-IRMS (Continuous Flow Gas Chromatography-Isotope Ratio Mass Spectrometry). This method provides high precision isotopic values, determining $\delta^{13}C-CH_4$ to ±0.05 per mil. The bulk signature of the methane plume into the atmosphere from the whole source area was obtained by Keeling plot analysis, and a $\delta^{13}C-CH_4$ signature, with the relative uncertainty, allocated to each methane source investigated. Both landfill and natural gas emissions in SE England have tightly constrained isotopic signatures. The averaged $\delta^{13}C-CH_4$ for landfill sites is -58 ± 3‰. The $\delta^{13}C-CH_4$ signature for gas leaks is also fairly constant around -36 ± 2‰, a value characteristic of homogenised North Sea supply. In contrast, signatures for coal mines in N. England and Wales fall in a range of -51.2 ± 0.3‰ to -30.9 ± 1.4‰, but can be tightly constrained by region. The study demonstrates that CRDS-based mobile methane measurement coupled with off-line high precision isotopic analysis of plume samples is an efficient way of characterising methane sources. It shows that isotopic measurements allow type identification, and possible location of previously unknown methane sources. In modelling studies this measurement provides an independent constraint to determine the contributions of different sources to the regional methane budget and in the verification of inventory source distribution.

1. Introduction

After a steady increase of atmospheric methane in the 1980's and a stabilisation of the global levels between 1999 and 2006, methane concentrations have risen again (Nisbet et al., 2014) with implications for related climate change (IPCC, 2013), but the source contribution to the renewed growth rate is still under debate (Kirschke et al., 2013). Globally, over 60% of total CH_4 emissions come from human activities, with 22% of emissions from the energy sector and 10% from the waste sector (Dlugokencky et al., 2011).

---

* Corresponding authors.
E-mail addresses: Giulia.Zazzeri.2011@live.rhul.ac.uk (G. Zazzeri), e.nisbet@es.rhul.ac.uk (E.G. Nisbet).

http://dx.doi.org/10.1016/j.atmosenv.2015.03.029
1352-2310/

Conurbations such as London emit methane through leaks in the natural gas network, losses from heating systems and other combustion sources, and landfill emissions, which are all highly responsive to achievable control measures. With stricter regulations for landfills and improved maintenance on the gas network, UK national inventories (Webb et al., 2014) suggest that methane emissions from the waste and natural gas sectors declined throughout the 1990–2012 period. Semi-rural areas around London also contribute. Agriculture is the dominant methane-emitting sector in the UK, accounting for 44% of total methane emissions in 2012 according to inventories. Emissions from coal mining decreased sharply with the decline of the industry after 1993 and accounted for only 3% of all methane emissions in 2012 (Webb et al., 2014).

Methane inventories are compiled from statistical databases (e.g. number of cows, volume of gas used, etc. multiplied by predefined emission factors). This “bottom-up” approach may produce precise but highly inaccurate estimates, since databases might be incomplete and not updated, and some emission factors can be poorly established and may differ greatly among countries. Therefore, although UK national inventories suggest that methane emissions for waste, gas transmission and coal mining sectors have decreased since 1990 (Webb et al., 2014), the reduction trend must be verified by independent measurements. Direct atmospheric (or “top-down”) verification of emission inventories has been carried out (Lowry et al., 2001).

In this study methane stable isotope analyses, coupled with mole fraction measurements, have been employed to assess proportionate contributions of the main methane sources in SE England. The source of specific methane emissions can be identified by analysing the methane isotopic composition, as different source types are characterised clearly by distinct ^{13}C signatures. Biogenic methane is ^{13}C depleted (δ^{13}C = −50 to −70‰), compared to pyrogenic methane derived from incomplete combustion (δ^{13}C = −15 to −30‰) and fossil methane of thermogenic origin (δ^{13}C ≈ −40‰) (e.g. Lassey et al., 2011). Thus, the proportion of each source category within a source mix can be estimated and the actual contribution of each methane source in the atmospheric methane budget constrained. Several studies attest the value of the isotopic analysis as a tool for categorising methane sources and in verifying inventories (Levin et al., 1999; Lowry et al., 2001; Fisher et al., 2006; Townsend-Small et al., 2012). For this purpose, ^{13}C signatures of the methane sources that are listed in the UK inventories need to be defined accurately.

Isotopic data ($\delta^{13}C_{CH4}$) are used in modelling to constrain the contributions of different methane sources in the mass balance of atmospheric methane at a global and regional scale (Quay et al., 1991; Mikaloff Fletcher et al., 2004; Bousquet et al., 2006). However, the input values vary from model to model and the errors on these values are very large at the global scale. Quay et al. (1991) report a $\delta^{13}C_{CH4}$ range between −46 and −56‰ for landfills. For coal, values of −35 and −37‰ are suggested, whereas the isotopic signature for natural gas is thought to vary from −40 to −44‰ (Mikaloff Fletcher et al., 2004; Bousquet et al., 2006; Monteil et al., 2011). Errors can be narrowed down considerably when the focus is on a regional scale, as this study will prove.

This study aims to identify areas of high anthropogenic methane mole fractions in the UK and link them to specific identifiable sources, using isotopic characterisation. While there have been many previous studies of ^{13}C in methane, most are based on small scale processes and few have been on UK sources (Stahl, 1977; Deines, 1980; Chung et al., 1988; Hitchman et al., 1990; Bergamaschi et al., 1998; Levin et al., 1999; Whiticar, 1999; Lowry et al., 2001; Klevenhusen et al., 2010). Lowry et al. (2001) studied isotopic characterisation of specific methane peaks measured during diurnal air campaigns at the Royal Holloway site, on the western fringe of London, showing that peaks are derived either from natural gas leaks (δ^{13}C −33‰ to −35‰) or waste treatment emissions (δ^{13}C −51‰ to −53‰). Nevertheless, the isotopic characteristics of sources may vary over time and season, such as for landfill sites, where the reliance on methane oxidation by topsoil and gas flaring has been largely replaced by gas extraction systems, and for natural gas because of different gas source provider countries. Therefore isotopic values need to be regularly reassessed.

Sampling campaigns were focused on the targeted sources. A mobile greenhouse gas analyser (see Section 2.3) was installed on board a vehicle to allow measurement of atmospheric methane mole fractions while driving. A similar setup has been tested already by other studies to measure methane emissions at large spatial scales (Farrell et al., 2013) and to map methane leaks from a gas network (Phillips et al., 2013; Eapi et al., 2014). This work validates the use of the instrumentation for locating methane-emitting areas, as a tool to direct the sample collection for calculating the bulk isotopic signature of the methane released into the atmosphere.

2. Methods

The isotopic composition of methane sources from a 100 m to km-scale spatial area, such as landfills and open-cut coal mines, needs to be evaluated by assessing integrated emissions from the whole source site. Measurements of methane mole fractions downwind and upwind of the site enable a qualitative estimate of the source in terms of its importance in the atmospheric methane budget. Once the location has been identified as a source of methane emissions, the methane isotopic analysis of air samples collected downwind across the source plume allows assignment of a specific δ^{13}C signature to the source in question.

Each source investigation required a dedicated sampling campaign. By utilising the mobile gas analyser, various potential source sites were investigated on the same day, driving on public roads around the target area and collecting samples whenever relatively high mole fractions were measured. The mobile gas analyser was also used to detect the locations of gas leaks in a similar way to Phillips et al. (2013). Methane plumes and spikes are easily measured, and the subsequent isotopic analysis of the air sampled reveals the origin of these ‘unexpected’ methane peaks of local origin.

2.1. Identification of methane sources

The National Atmospheric Emission Inventory (NAEI) website (http://naei.defra.gov.uk/) makes available total methane emissions per km^2 per year and is updated annually with some time delay. Emissions for 2009 for the London region and surrounding boroughs have been mapped using the ArcGIS software. The resulting emission map (Fig. 1), where each square represents one km^2, offers a picture of the methane emissions distribution in the London area and was used to focus measurement campaigns. Red squares represent high emission areas. These are sited mainly outside and on the margins of the London conurbation, whereas central London emissions are uniformly in the range of 50–100 tonnes/km^2/yr. Hotspots were located and identified as first targets for the measurement campaigns from the map. Their exploration allows the consistency of the emissions data to be verified and has uncovered many discrepancies.

2.2. Sampling locations

The 2013 and 2014 monitoring campaigns aimed to characterise

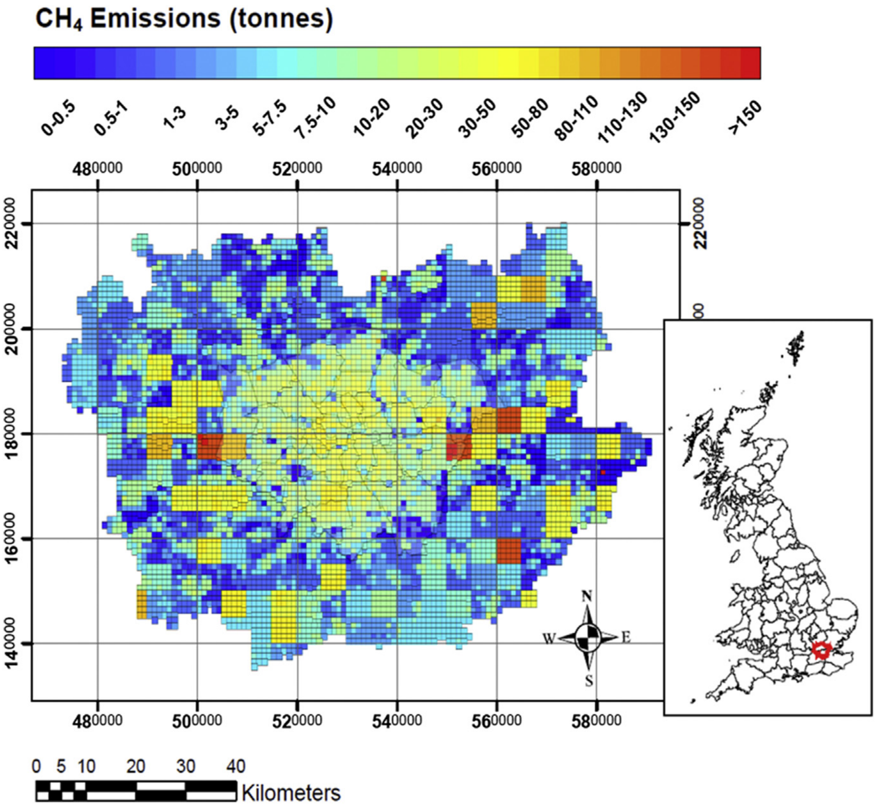

Fig. 1. London Region emission map derived from 1 km^2 methane emission data for 2009 from the NAEI website. Red squares represent high emission areas. These are sited mainly outside and on the margins of the London conurbation, whereas central London emissions are uniformly in the range of 50–100 tonnes/km^2/yr. (For interpretation of the references to colour in this figure legend, the reader is referred to the web version of this article.)

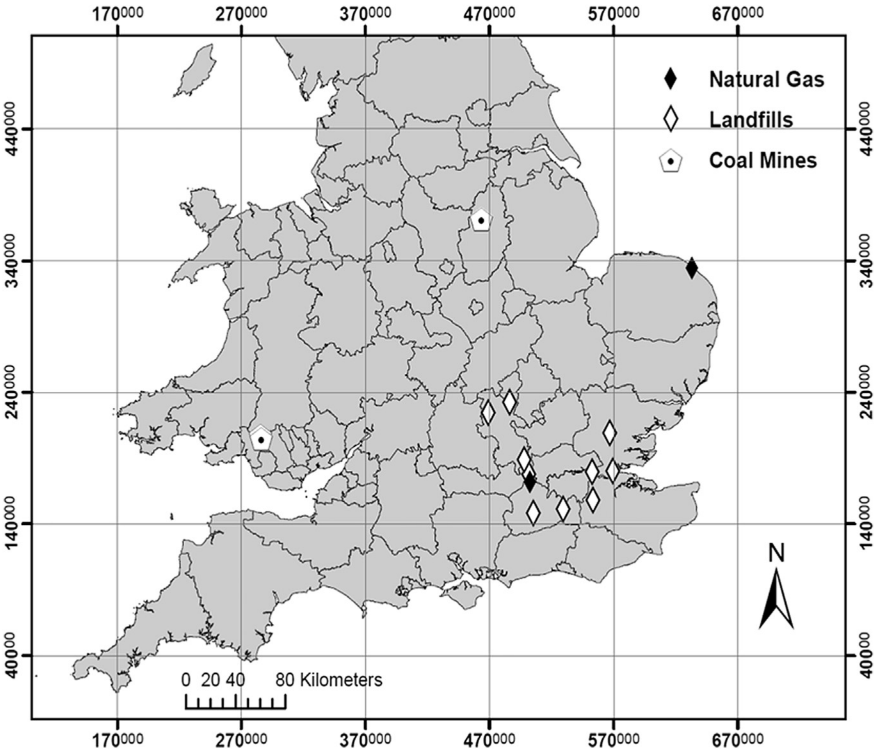

Fig. 2. Map of the sites surveyed for this study. White diamonds represent the landfill sites studied. Black diamonds indicate gas storage and distribution facilities. White pentagons represent coal mines.

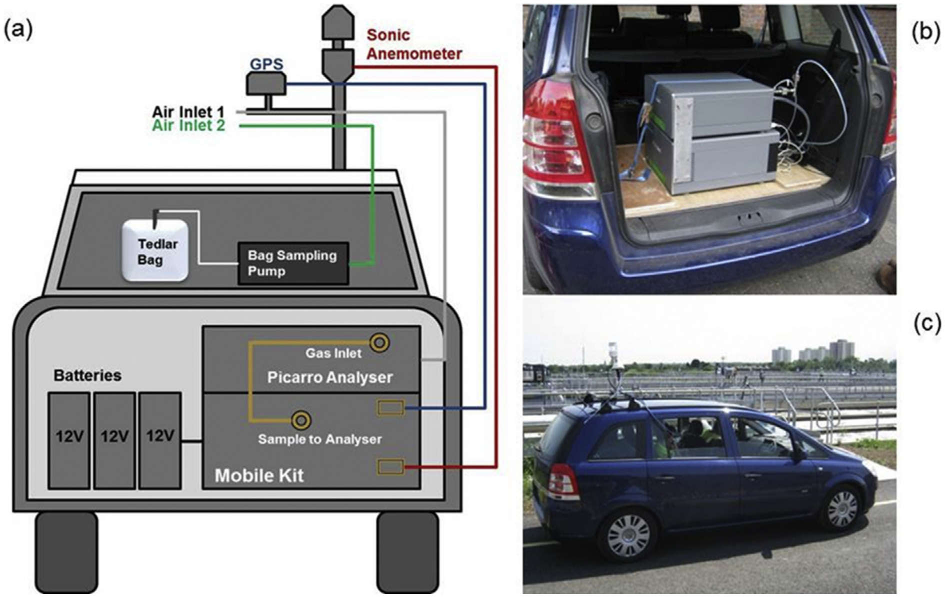

Fig. 3. a) Schematic set up of the RHUL Picarro mobile measurement system and all the physical connections b) Picarro Mobile c) vehicle used in the sampling campaigns.

isotopically the most important UK anthropogenic methane sources in terms of tonnes of methane emitted, with a focus on London conurbation and SE England. Landfills, coal mines and natural gas are the three source categories that have been assessed in this study (Fig. 2). All downwind plumes measured at these sources were at sub-regulatory levels.

The landfill sites studied are all located within 70 km of London, whereas the evaluation of the coal mining isotopic signature required an extension of the survey beyond the London area, to include South Yorkshire, Nottinghamshire, Warwickshire and South Wales. A more detailed study of the isotopic signatures from UK coal mines is in preparation. The isotopic signature of natural gas supplied to SE England has been identified by sampling methane plumes downwind of the gas storage and distribution facilities in Staines-upon-Thames and Bacton, on the Norfolk coast.

2.3. *Methodology and material*

2.3.1. *Picarro Mobile system*

The greenhouse gas monitoring system utilised in the monitoring campaigns consists of a mobile Picarro G2301 CRDS (Cavity Ring-Down Spectroscopy) analyser, which provides a new measurement of carbon dioxide (CO_2) and methane (CH_4) mole fractions in ppm and water vapour in % every 5s, with a rise and fall time between high and low concentrations that is 90% accurate in less than 3 s. The mobile module (A0941) consists of a pump, control systems for a Climatronics sonic anemometer and a Hemisphere GPS receiver. Two air inlets, plus the GPS and sonic anemometer are attached to a mast above the roof of the vehicle at 2.2 m above the ground. Three fully charged 12 V, 110 Ah lead-acid batteries allow the instrument to run for up to 9 h. The airline is

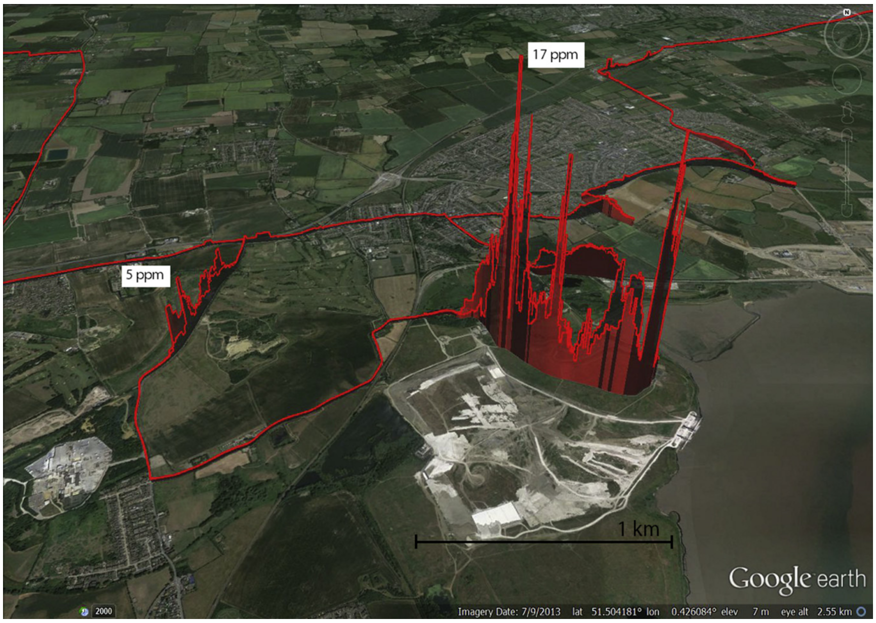

Fig. 4. Google Earth view of methane plumes detected around Mucking landfill location on 14th October 2013. The maximum mole fractions are labelled for each source plume measured.

Table 1
Landfill surveyed with the calculated $\delta^{13}C$ signature. Errors are calculated as 2 standard deviations. An averaged value of −58.0 ± 3.0 (2SD) ‰ was calculated.

Landfill	Current status	Sampling date	Number of samples collected	$\delta^{13}C$ signature (‰)
Albury	Active	Oct-13	4	−59.7 ± 1.1
Bletchley	Active	Mar-13	26	−58.8 ± 0.5
Calvert	Active	Mar-13	28	−58.5 ± 0.6
Colnbrook	Closed (2012)	Jul-13	6	−60.2 ± 1.4
Greatness Quarry	Active	Oct-13	8	−57.4 ± 0.5
Mucking	Closed (2011)	Oct-13	11	−56.1 ± 0.5
Redhill	Active	Oct-13	5	−59.6 ± 0.7
Roxwell	Active	Oct-13	5	−55.2 ± 0.6
Wapsey's wood	Active	Jul-13	5	−57.6 ± 0.7
		Apr-14	6	−57.3 ± 1.6

1/4″ outer diameter and 1.83 m length Nylon tube with the inlet end blocked and a series of 2 mm diameter holes drilled into the first 30 cm to allow ingress of air (air inlet 1 on Fig. 3) (Picarro, 2012). This is pumped to the mobile module through a 2 μm Swagelok filter, where the flow splits allowing approximately 300 cc/min to flow through the Picarro, and the rest of the air to vent. This greatly reduces the lag time between air entering the inlet and the measurement allowing successful surveying of small plumes at a vehicle speed of up to 50 km/h, and large plumes at up to 80 km/h on first pass. The second air inlet is another ¼" O.D. Nylon tube (air inlet 2 in Fig. 3a) connected to a battery operated diaphragm pump (KNF Neuberger) used to collect plume and background air samples for later isotopic analysis in the RHUL (Royal Holloway University of London) laboratory. The pump fills a 5L Tedlar air sample bag in 30 s.

The system is controlled by a laptop, so that continuous measurement of CO_2 and CH_4 mole fractions can be observed by the passenger during travel. Communication between the laptop and the Picarro mobile is by WiFi connection to a 3G or 4G system. Both CH_4 and CO_2 mole fractions can be displayed in real time on Google Earth, allowing the gas plumes to be geospatially visualised on site. The time delay between the instantaneous GPS location and the display of Picarro mole fractions has been calculated as approximately 7 s by measuring the time lag of the CO_2 peak arrival after blowing into the inlet tube.

The Picarro 2301 instrument was calibrated in the RHUL greenhouse gas laboratory before each survey against two National Oceanic and Atmospheric Administration (NOAA) calibrated air samples, with a resulting precision for CH_4 better than ±0.3 ppb at mole fractions ranging from 1840 to 1975 ppb and accuracies of better than ±1 ppb. A target gas has been analysed using the Picarro instrument while driving in order to test the stability of measurement during motion, with a precision of 0.3 ppb (1 σ) over 2 min of analysis.

The sites of interest were studied by driving downwind and visualising the mole fractions on Google Earth in real time. At some locations plumes could be bisected perpendicular to the wind direction, allowing the Gaussian shape to be mapped. Changes in wind direction and speed affect the plume dispersion; methane peaks might also change position and intensity from one pass to the next downwind of the same methane source. However, the current study is not aimed at calculating fluxes or accurately pinning down the location of small gas leaks, but at proportioning source inputs via the isotopic signatures of the sources. A strict accuracy of source position is also not required for large spatial sources such as landfills and open-cut coal mines where methane plumes can be easily transected.

Once the methane plume was identified, 5L Tedlar bags were filled as close to the plume centre as possible and at the edges of the plume. When the road traffic conditions allowed, air bags were collected along the plume transect by stopping the vehicle whenever above-background methane mole fractions were observed. When sampling was on a major road and the vehicle could not be stopped, and when the methane mole fraction was not steady during the sampling at a given point (due to a high variability of the wind direction or obstructions between the source and the road), samples were collected while driving, at a speed of 48 km/h (30 mph), giving an integrated sample over a distance of up to 400 m.

Fig. 4 demonstrates an example view of data as seen on Google Earth during sampling. The mole fraction data were re-plotted during post-analysis using ArcGIS software, utilising satellite images of the sites as base maps to give a clearer spatial representation of the data.

2.3.2. Sample analysis

The CH_4 mole fraction data representation along the route provided information on the actual plume extent, whereas the methane source characteristics were investigated by the isotopic analysis of the samples collected. CH_4 mole fractions of the air samples in Tedlar bags were measured independently in the laboratory with a Picarro G1301 CRDS analyser. Each sample was analysed for 3 min, with an average precision of ±0.5 ppb. The carbon isotopic ratio ($\delta^{13}C$) was measured in triplicate to high precision (+/− 0.05‰) by continuous flow gas chromatography isotope ratio mass spectrometry (CF GC-IRMS) (Fisher et al., 2006). This ratio is expressed in δ notation from the following equation:

$$\delta = (R_A/R_{std} - 1) \times 1000 \tag{1}$$

where R_A denotes the isotopic ratio in CO_2 derived by combustion of the methane sample ($^{13}C/^{12}C$) and R_{std} is the corresponding ratio in the CO_2 reference gas which is calibrated to the V-PDB scale for $\delta^{13}C$ using international standards. The isotopic ratio is expressed as per mil (‰).

2.3.3. Keeling plot approach

The signature of each methane source (or mixture of sources in an urban conurbation) was characterised using the Keeling plot method (Keeling, 1958). According to this approach, $\delta^{13}C$ values must be plotted against the inverse of mole fraction data to calculate the isotopic signature of the methane source responsible for the excess over background. Following the Keeling plot procedure, one isotopic signature (with calculated error to allow for some variability of source methane production pathways) was assigned to every methane source explored.

2.3.3.1. Keeling plot and the regression analysis. The atmospheric mixing ratio (mole fraction) of a gas ($\mathbf{c_a}$) in the lower boundary layer results from the combination of the background atmospheric mole fraction ($\mathbf{c_b}$) and the mole fraction of the gas added by the source ($\mathbf{c_s}$) (Pataki et al., 2003):

$$\boldsymbol{c_a} = \boldsymbol{c_b} + \boldsymbol{c_s} \tag{2}$$

By assuming the conservation of mass, the $\delta^{13}C$ signature of the source input to atmosphere can be calculated as follows:

$$\delta^{13}C_a = \boldsymbol{c_b}\left(\delta^{13}C_b - \delta^{13}C_s\right)\cdot 1\Big/\boldsymbol{c_a} + \delta^{13}C_s \tag{3}$$

$\delta^{13}C_a$ and $1/\mathbf{c_a}$ values are respectively the y and the x values of a best-fit line, whose intercept (at $1/\mathbf{c_a} = 0$) is the isotopic value at which the methane mole fraction tends to infinity. This is interpreted as the isotope signature of the methane source responsible for the excess over background.

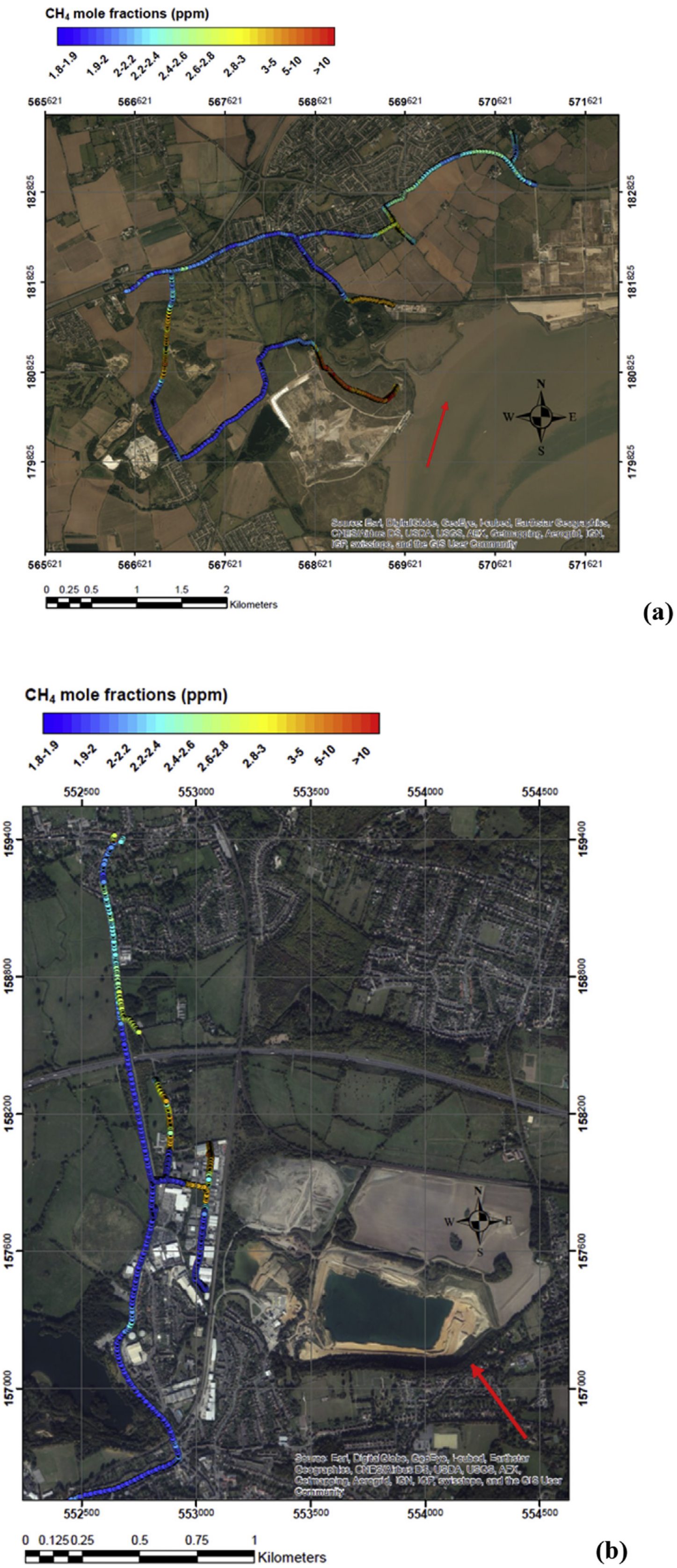

Fig. 5. ArcGIS plot of methane mole fractions in ppm recorded on 14th October 2013 around Mucking landfill site (a) and on 24th October 2013 around Greatness Quarry landfill site (b). The grid coordinates are displayed in the British National Coordinate System. The red arrow represents the wind direction. (For interpretation of the references to colour in this figure legend, the reader is referred to the web version of this article.)

A linear regression of data must be performed in order to compute the line slope and intercept. However, the estimate of the line parameters might be biased if an ordinary least squared (OLS) method is applied (as in many spreadsheets), which assumes errors are confined to the dependent variable (Leng et al., 2007). For our sources, both variables are measured with errors and another regression model must be implemented. Moreover, our measurements are affected by heteroscedasticity, where the error of a variable changes across the range of values of a second variable that predicts it (Berry and Feldman, 1985). Errors may increase as the value of the independent variable (1/[CH$_4$]) is decreasing, as higher mole fractions are measured with higher standard deviations. Although there are several fitting models that allow for errors in the independent variable (Sokal and Rohlf, 1995), e.g. orthogonal distance regression and geometric mean regression (recommended by Pataki et al (2003)), few models accommodate for heteroscedastic measurement errors. If a typical OLS approach, intended to minimize $\sum e_i^2$, is applied in case of heteroscedasticity, the calculation of the regression line would give greater emphasis to the extreme values (with greater errors), which are conversely less precise and, hence, contain less information.

Akritas and Bershady (1996) introduced the BCES estimators procedure (for Bivariate Correlated Errors and intrinsic Scatter). This statistical procedure, designed to overcome the heteroscedasticity case, accounts for correlated errors between the two variables and allows for the magnitude of measurement errors to be dependent on the measurements. These features make the BCES approach well suited for computing the slope and the intercept of the Keeling plot. Therefore the BCES regression program, available to download (http://www.astro.wisc.edu/~mab/archive/stats/stats.html), has been used to find the Keeling plot intercept with the relative uncertainty, and so the δ^{13}C value of the methane source. This technique results in a much more robust calculation of source signature but will only give very tightly constrained ‰ errors when the precision of both mole fraction and isotopic measurements are very high and the δ^{13}C of the source signature is homogenous across the plume (i.e. single source).

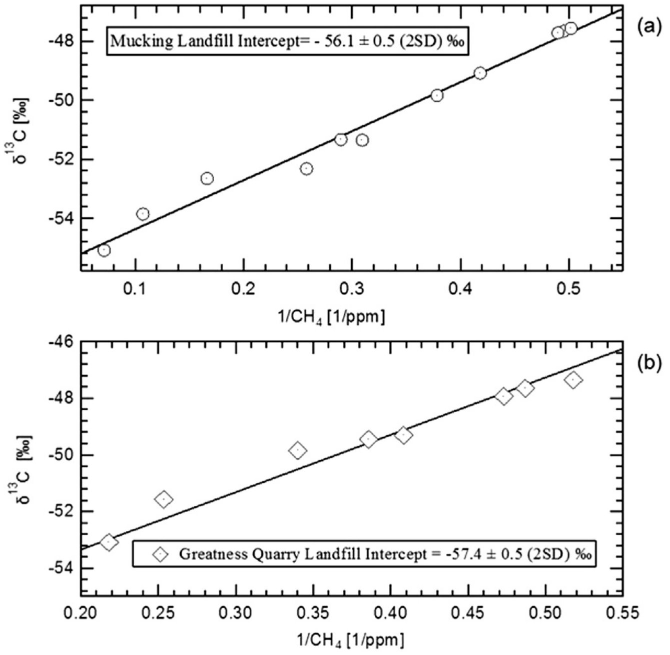

Fig. 6. Keeling plot based on the samples collected around Mucking landfill site (a) and around Greatness Quarry landfill site (b). Error bars are not shown as they are smaller than displayed symbols.

3. Results

3.1. Landfill sites

The widest plumes and highest recorded mole fractions of methane were from landfill sites, both still active and recently closed, as suggested by the UK national inventories. The excess methane over background recorded off site ranged from 0.1 ppm to 15 ppm.

Isotopic signatures observed for all the landfill studied (Table 1) span a range from −60.2 ± 1.4 to −55.2 ± 0.6‰, with an averaged value of −58.0 ± 3.0 (2SD) ‰. Wapsey's Wood was surveyed twice, in July and April, and the identified isotopic signature was consistent. The isotopic variability among sites depends upon several parameters such as waste composition, temperature and the level of methane oxidation performed by methanotrophic bacteria in the top-soil cover (Liptay et al., 1998).

The two landfill sites presented herein, Mucking and Greatness Quarry, were carefully surveyed thanks to the accessibility of public roads downwind of the sites, obtaining a wide range of mole fraction values for Keeling plot analysis.

Although it was closed in 2012, Mucking landfill (Fig. 5a) is still emitting a large amount of methane: the maximum mole fraction recorded in the measured part of the plume was approximately 17 ppm. With wind from the SSW it was possible to intersect the plume on 4 transects at different distances from the NNE side of the landfill and 11 samples were collected, covering a wide range of mole fractions, ideal for precise Keeling plot analysis.

The intercept of the Keeling plot based on all the samples collected in the vicinity of the landfill is −56.1 ± 0.5‰ (2SD) (Fig. 6a).

Greatness Quarry (Fig. 5b) is an active landfill site to the north of the town of Sevenoaks, which was surveyed on the 24th of October 2013. A methane plume was intercepted along the NW side of the landfill and 8 samples were collected for isotopic analysis. An averaged isotopic signature for the plume of −57.4 ± 0.5‰ (2SD) resulted from Keeling plot analysis of samples (Fig. 6b).

These two landfill sites, taken as representative examples of UK landfills, show a similar isotopic signature, although Mucking landfill was closed in 2012, while the Greatness Quarry is still active.

3.2. Coal mines

The collieries surveyed for this study are listed in Table 2, together with δ^{13}C signatures of the plumes sampled. Thoresby colliery in Nottinghamshire is one of the deep mines investigated for this study. It is one of the UK's largest coal mines but scheduled for closure in 2015. Mining is currently taking place at about 650 m underground. Although methane is drained off for 2.8 MWe electrical power generation (Holloway et al., 2005), mole fraction levels up to 4.6 ppm were observed in the downwind plume. As Fig. 7a shows, the methane plume was transected three times and 9 samples were collected. The resulting Keeling plot intercept is −51.2 ± 0.3‰ (2SD).

Table 2
Collieries discussed in the text and δ^{13}C signatures of methane plumes sampled. Errors in the^{13}C signature are calculated as 2 standard deviations.

Colliery	Current status	Sampling date	Number of samples collected	δ^{13}C signature (‰)
Thoresby	Active	Nov-13	9	−51.2 ± 0.3
Aberpergwm	Closed (2012)	Oct-13	4	−33.3 ± 1.8
Unity	Closed (2013)	Oct-13	3	−30.9 ± 1.4

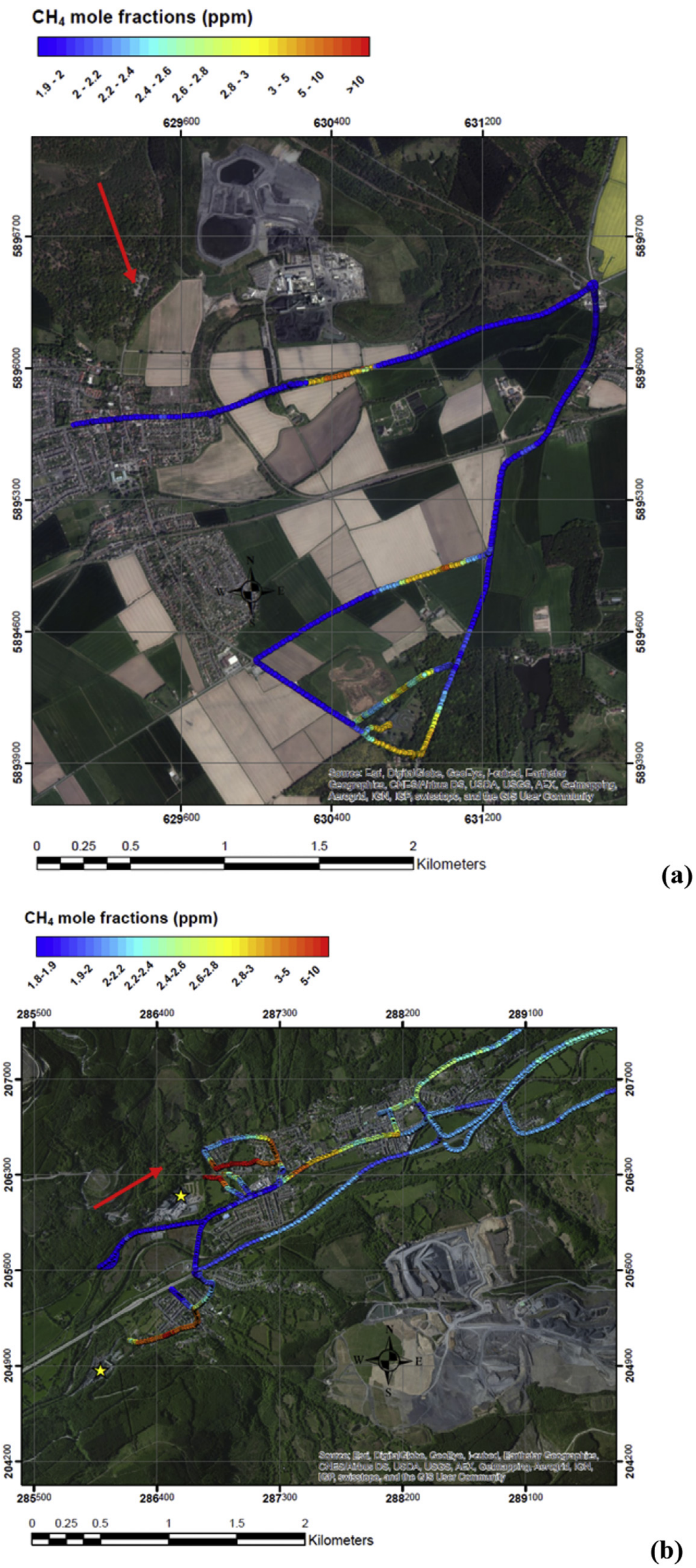

Source: Esri, DigitalGlobe, GeoEye, i-cubed, Earthstar Geographics, CNES/Airbus DS, USDA, USGS, AEX, Getmapping, Aerogrid, IGN, IGP, swisstopo, and the GIS User Community

Source: Esri, DigitalGlobe, GeoEye, i-cubed, Earthstar Geographics, CNES/Airbus DS, USDA, USGS, AEX, Getmapping, Aerogrid, IGN, IGP, swisstopo, and the GIS User Community

Fig. 7. ArcGIS plot of methane mole fractions in ppm recorded on 22nd November 2013 around Thoresby Colliery (a) and on 17th October 2013 around Aberpergwm and Unity deep mines in Wales (b). The grid coordinates are displayed in the British National Coordinate System. The red arrow represents the wind direction. Stars represent the coal mine locations. (For interpretation of the references to colour in this figure legend, the reader is referred to the web version of this article.)

Aberpergwm and Unity deep coal mines in Wales (Fig. 7b), which closed in December 2012 and in October 2013 respectively, were investigated on 17th October 2013. Mole fraction peaks of 6 ppm were observed downwind of both deep mines. The Keeling plots based on the samples collected near these deep mines give an isotopic source signature of −33.3 ± 1.8‰ for Aberpergwm and −30.9 ± 1.4‰ for the Unity colliery, both highly ^{13}C-enriched relative to Thoresby colliery (Fig. 8).

The coal exploited in Thoresby colliery, as in all deep English coal mines, is bituminous coal (Hill, 2001), whereas collieries in the north-west coalfield area of Wales exploit pure anthracite (Alderton et al., 2004). The characterisation of methane released from different coal types suggests a link between enrichment in the ^{13}C content of methane emitted to atmosphere with progression of coal rank as previously alluded to by Chung and Sackett (1979). This hypothesis will be tested by further study of coalfield composition for comparison with plumes sampled at other UK coal mines.

3.3. Natural gas signature

The gas installations surveyed and δ^{13}C signatures of the relative methane plumes sampled are shown in Table 3. Staines and Bacton (Fig. 2 for the location) have been chosen as sampling sites for assessing the isotopic signature of natural gas. A 1.2 km path was surveyed on the south (downwind side) of the Staines storage facility and 16 samples were collected for isotopic analysis with mole fractions ranging from 1.98 to 3.85 ppm. The Keeling plot for the whole transect (Fig. 11a) shows a constant origin for the methane of −36.3 ± 0.3‰ that is consistent with a dominantly thermogenic North Sea gas source (Lowry et al., 2001). It suggests that there are other leaks in the gas distribution system along with the storage tank ("gasometer") that is located in the middle of the transect (Fig. 9).

Table 3
Gas installations discussed in the text and δ^{13}C signatures of methane plumes sampled. Errors in the ^{13}C signature are calculated as 2 standard deviations.

Gas installation	Current status	Sampling date	Number of samples collected	δ^{13}C signature (‰)
Staines	Closed (2014)	Apr-14	16	−36.3 ± 0.3
Bacton	Active	Apr-14	14	−35.7 ± 1.2

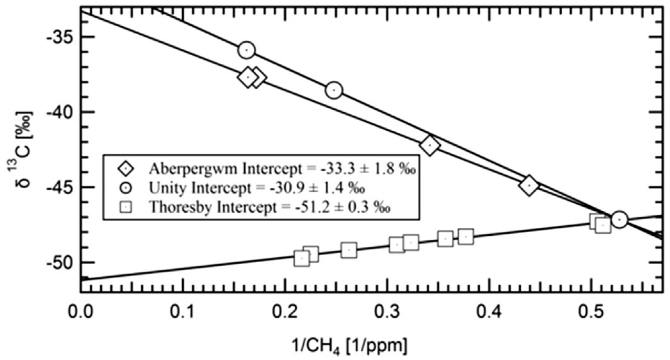

Fig. 8. Keeling plots based on samples collected downwind of two deep mines in Wales (Aberpergwm and Unity coal mines) on 17th October 2013 and the Thoresby Colliery on 22nd November 2013. Error bars are not shown as they are smaller than displayed symbols.

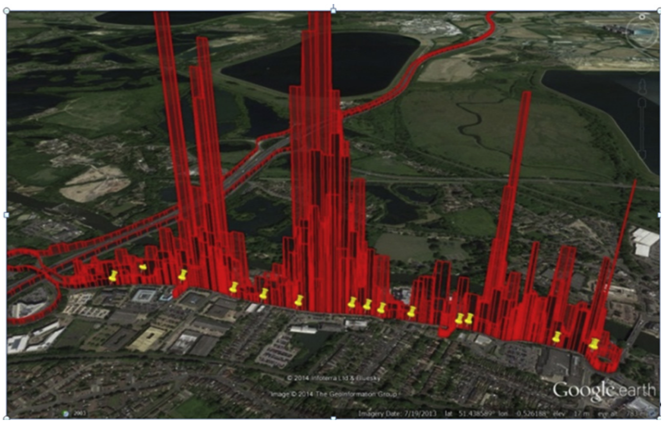

Fig. 9. Sample locations (yellow markers) and mole fraction peaks measured downwind of gas works in Staines (3 km ENE of RHUL) on 11th April 2014. 16 samples were collected for isotopic analysis, with mole fractions ranging from 1.98 to 3.85 ppm. (For interpretation of the references to colour in this figure legend, the reader is referred to the web version of this article.)

Mole fractions up to 24 ppm were recorded in the plume downwind of Bacton, where pipelines bring all southern and much northern North Sea Norwegian gas onshore, as well as gas from the interconnector pipeline to Belgium (Fig. 10). Nineteen air samples were collected for isotopic analysis. An isotopic signature of −35.7 ± 1.2‰ was observed (Fig. 11b), which is consistent with the isotopic value that has been ascribed to Staines gas works.

The intercept values of −36.3 ± 0.3‰ and −35.7 ± 1.2‰ are both in good agreement with the averaged value of −37.3 ± 0.9‰ (2SD) obtained by collecting monthly samples of natural gas in the geochemistry lab of the Earth Sciences Department at RHUL and measuring their isotopic signatures.

4. Discussion and conclusions

This study focuses on the isotopic characterisation of methane emission plumes from major UK anthropogenic methane sources. Landfill sites, coal mines and gas leaks have been surveyed and sampled using a mobile system based around the Picarro G2301 instrument. A δ^{13}C signature has been allocated to each methane source that has been investigated by the isotopic analysis of samples collected at each site. The δ^{13}C signatures for landfill sites span a range between −60.2 ± 1.4‰ (2SD) and - 55.2 ± 0.6‰ (2SD), whereas signatures for coal mines fall within a range of −51.2 ± 0.3‰ (2SD) to −30.9 ± 1.4‰ (2SD). The ^{13}C signature for gas leaks is found to be fairly constant at −36.4 ± 1.9‰ (2SD).

Detailed exploration of an area the size of a landfill or open-cut coal mine in its entire extent, measuring gas mole fractions, fluxes and isotopic signatures in order to estimate its contribution in terms of methane emissions, requires time consuming and labour-intensive procedures (e.g. flux chamber technique). Several previous studies have investigated isotopic signatures of methane emissions from landfills using flux chambers to capture methane fluxes from the soil and collect air samples (Liptay et al., 1998; Chanton and Liptay, 2000). In order to ensure a representative area is covered, many chambers need to be arranged across the site, often highlighting the large spatial variability of the ^{13}C signature measured. Isotopic signatures of landfill emissions from covered areas have been shown to differ from uncapped active tipping areas, due to the oxidation mediated by methanotrophic bacteria in the cover soil (Bergamaschi et al., 1998). Bergamaschi et al. (1998) obtained values highly enriched (−45.9 ± 8‰) in covered areas relative to those observed in uncovered areas (−55.1 ± 5.2‰).

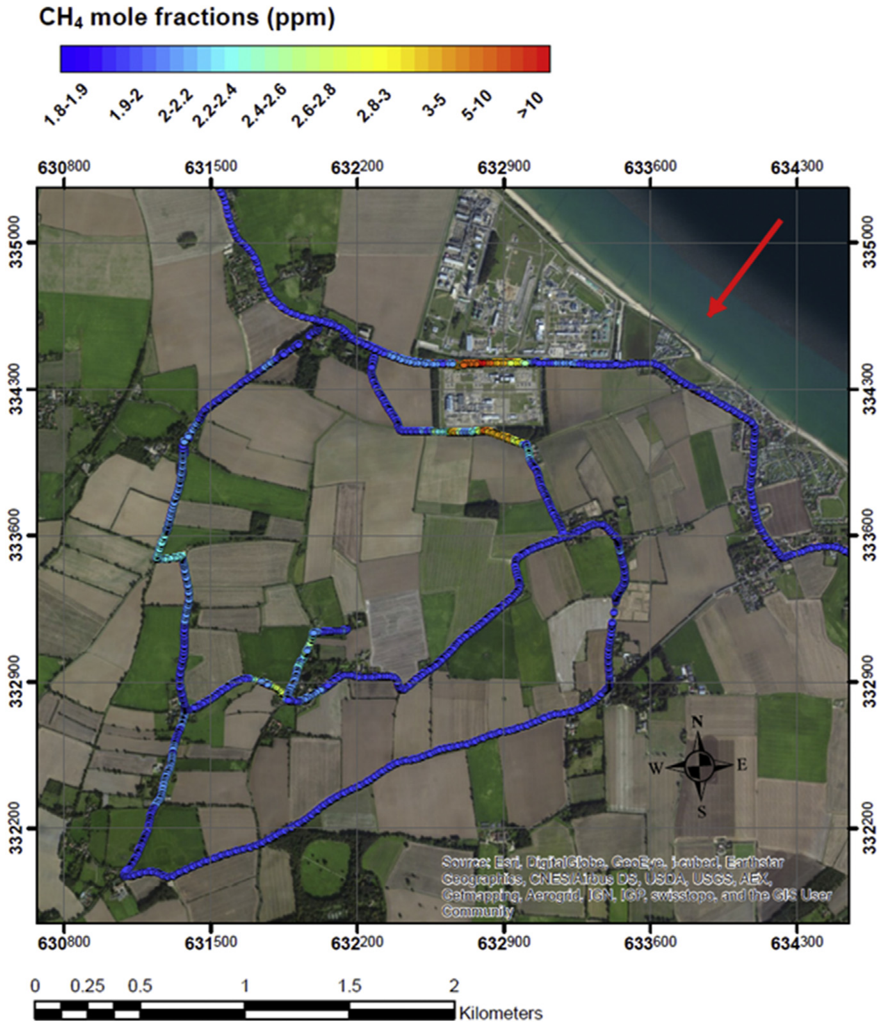

Fig. 10. ArcGIS plot of methane mole fractions in ppm recorded on 30th of April 2014 around Bacton gas terminals. The grid coordinates are displayed in the British National Coordinate System. The red arrow represents the wind direction. (For interpretation of the references to colour in this figure legend, the reader is referred to the web version of this article.)

When the methane plume downwind of a landfill is intercepted and analysed, the overall signature of the methane released into the atmosphere from the whole site can be estimated, which is the number needed at a minimum of regional level for atmospheric inversion models. The isotopic signatures of methane emissions from SE England landfills do not show great variability and a value of −58‰ could be safely used as model input for the whole of UK CH_4 emissions from active or recently closed landfills. Emissions from old landfills that predate gas extraction will likely account for a small proportion of emissions that are more enriched in $\delta^{13}C$ toward −50‰. As methane emissions from landfills can isotopically change over time, following enhanced landfill management schemes (e.g. gas extraction), systematic measurements of ^{13}C signatures of methane emissions need to be carried out in order to provide up-to-date and more representative values.

The isotopic range for coal is found to be relatively wide, compared to those assigned to landfill and natural gas emissions. Many factors are involved and might explain the variety of isotopic values measured, such as the depth of coal seams and coal rank. Preliminary results suggest a ^{13}C enrichment of methane with progression of rank, which needs to be confirmed with further sampling campaigns with the Picarro mobile system around other UK coal mines.

The $\delta^{13}C$ range for the natural gas source has been constrained to a value of −36‰, which represents the isotopic signature of the natural gas supplied to the whole of SE England. Natural gas samples from Holland and Italy were analysed at RHUL, giving values of −29.5 ± 0.1‰ (2SD) and −46.7 ± 0.1‰ (2SD) respectively. In the NW European Atlas report (Lokhorst, 1997), carbon isotope ratios between −33 and −36‰ for the Carboniferous reservoir gas in the North Sea and between −30 and −24‰ for the Rotliegend strata in the southern North Sea are indicated. The natural gas supply from western Siberia has been measured near source, and in St. Petersburg by the RHUL group and in Heidelberg by Levin et al. (1999) and is characterised by an isotopic signature of approximately −50‰. The isotopic value of the natural gas supply to SW London has changed little in recent years, being close to −34‰ over the 1998–99 period (Lowry et al., 2001) and close to −36‰ since at least 2002, and the new data show that this figure can be applied to emissions from a much larger region of England.

By using the Picarro mobile system, the survey of methane sources can be focused on a specific region or country, obtaining more precise isotopic values to be used in regional models. Furthermore, the isotopic precision of ± 0.05‰ achieved by CF GC-IRMS on collected samples is significantly better than current

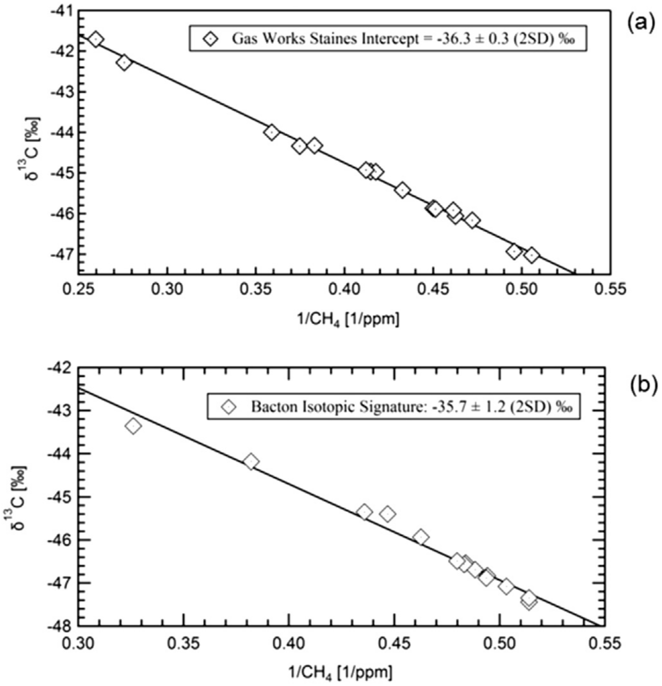

Fig. 11. Keeling plot based on samples collected downwind of gas works in Staines on 11th April 2014 (a) and downwind of gas terminals in Bacton on 30th April 2014 (b). Error bars are not shown as they are smaller than displayed symbols.

laser-based isotopic measurement systems, such as the CRDS analyser, which is within 1‰ for $\delta^{13}C$ of CH_4 (Phillips et al., 2013) operating under similar conditions of mobile measurement. This means that precise isotopic signatures of source plumes can be determined at near background atmospheric mole fractions (50 ppb excess CH_4 for a 20‰ difference between source and background air isotopic signatures, 100 ppb for 10‰ difference, 200 ppb for 5‰).

In areas with multiple sources, such as urban conurbations, where leaks in the natural gas supply pipes can occur near landfill sites and sewage works, high precision isotopic measurements allow different potential sources to be carefully distinguished. Due to the mixed nature of methane sources and their temporal variability, the evaluation of methane fluxes in urban environments involves numerous observations and measurement techniques, including the eddy covariance method (Gioli et al., 2012), techniques based on a mass balance approach (Zimnoch et al., 2010) and airborne measurements allowing a large surface footprint (O'Shea et al., 2014). The estimated methane fluxes are then linked to methane sources using inventory data. The high uncertainty affecting inventories is therefore propagated to the source partitioning, whereas isotopic measurements provide an independent constraint on source proportions.

To conclude, the Picarro mobile methane measurement system, coupled with the isotope analysis of sampled methane emissions by high precision CF GC-IRMS, is an efficient way of locating and precisely identifying methane emissions by source, since it enables a large spatial coverage and rapid location of downwind plumes in the survey of methane source areas. The instantaneous display of methane mole fractions during the survey allows the methane plume extent to be directly visualized and sample collection to be carefully directed. The technique can be further applied to detect small leaks from gas pipelines and fugitive emissions from alternative methane sources.

Therefore this system can be widely employed and has the potential to help in the reduction of methane emissions in a cost effective manner.

Acknowledgements

Giulia Zazzeri would like to thank Royal Holloway, University of London for provision of a Crossland scholarship and a contribution from the Department of Earth Sciences from 2011 to 2014. Thanks to WRG (now FCC environment) for access into 2 of the landfill sites included in this study, Chris Rella of Picarro Inc. for discussion of the mobile module measurement technique and Picarro Support for fault-finding.

References

Akritas, M.G., Bershady, M.A., 1996. Linear regression for astronomical data with measurement errors and intrinsic scatter. Astrophys. J. 470, 706–714.

Alderton, D., Oxtoby, N., Brice, H., Grassineau, N., Bevins, R., 2004. The link between fluids and rank variation in the South Wales Coalfield: evidence from fluid inclusions and stable isotopes. Geofluids 4, 221–236.

Bergamaschi, P., Lubina, C., Königstedt, R., Fischer, H., Veltkamp, A., Zwaagstra, O., 1998. Stable isotopic signatures ($\delta^{13}C$, δD) of methane from European landfill sites. J. Geophys. Res. Atmos. (1984–2012) 103, 8251–8265.

Berry, W.D., Feldman, S., 1985. Multiple Regression in Practice. Sage Publications, Newbury Park, CA, pp. 73–89.

Bousquet, P., Ciais, P., Miller, J., Dlugokencky, E., Hauglustaine, D., Prigent, C., Van der Werf, G., Peylin, P., Brunke, E.-G., Carouge, C., 2006. Contribution of anthropogenic and natural sources to atmospheric methane variability. Nature 443, 439–443.

Chanton, J., Liptay, K., 2000. Seasonal variation in methane oxidation in a landfill cover soil as determined by an in situ stable isotope technique. Glob. Biogeochem. Cycles 14, 51–60.

Chung, H.M., Sackett, W.M., 1979. Use of stable carbon isotope compositions of pyrolytically derived methane as maturity indices for carbonaceous materials. Geochim. Cosmochim. Acta 43.

Chung, H.M., Gormly, J., Squires, R., 1988. Origin of gaseous hydrocarbons in subsurface environments: theoretical considerations of carbon isotope distribution. Chem. Geol. 71, 97–104.

Deines, P., 1980. The isotopic composition of reduced organic carbon. In: Fritz, P., Fontes, J. Ch. (Eds.), Handbook of Environmental Isotope Geochemistry, Vol. I. Netherlands: Elsevier Sci. Publ, pp. 329–406.

Dlugokencky, E.J., Nisbet, E.G., Fisher, R., Lowry, D., 2011. Global atmospheric methane: budget, changes and dangers. Philos. Trans. R. Soc. A Math. Phys. Eng. Sci. 369, 2058–2072.

Eapi, G.R., Sabnis, M.S., Sattler, M.L., 2014. Mobile measurement of methane and hydrogen sulfide at natural Gas production site fence lines in the Texas Barnett Shale. J. Air & Waste Manag. Assoc. 64, 927–944.

Farrell, P., Culling, D., Leifer, I., 2013. Transcontinental methane measurements: part 1. A mobile surface platform for source investigations. Atmos. Environ. 74, 422–431.

Fisher, R., Lowry, D., Wilkin, O., Sriskantharajah, S., Nisbet, E.G., 2006. High-precision, automated stable isotope analysis of atmospheric methane and carbon dioxide using continuous-flow isotope-ratio mass spectrometry. Rapid Commun. Mass Spectrom. 20, 200–208.

Gioli, B., Toscano, P., Lugato, E., Matese, A., Miglietta, F., Zaldei, A., Vaccari, F., 2012. Methane and carbon dioxide fluxes and source partitioning in urban areas: the case study of Florence, Italy. Environ. Pollut. 164, 125–131.

Hill, A., 2001. The South Yorkshire Coalfield: a History and Development. Tempus Books, Gloucestershire.

Hitchman, S., Darling, W., Williams, G., 1990. Stable Isotope Ratios in Methane Containing Gases in the United Kingdom. Report of the British Geological Survey, Processes Research Group WE/89/30.

Holloway, S., Jones, N., Creedy, D., Garner, K., 2005. Can new technologies be used to exploit the coal resources in the Yorkshire-Nottinghamshire coalfield? In: Collinson, J.D., Evans, D.J., Holliday, D.W., Jones, N.S. (Eds.), Carboniferous Hydrocarbon Geology – The Southern North Sea and Surrounding Onshore Areas. Yorkshire Geological Society Occasional Publication, pp. 195–208. No. 7.

IPCC, 2013. Climate change 2013: the physical science basis. In: Working Group I Contribution to the Fifth Assessment Report of the Intergovernmental Panel on Climate Change, Summary for Policymakers, WMO/UNEP. Cambridge University Press.

Keeling, C.D., 1958. The concentration and isotopic abundances of atmospheric carbon dioxide in rural areas. Geochim. Cosmochim. Acta 13, 322–334.

Kirschke, S., Bousquet, P., Ciais, P., Saunois, M., Canadell, J.G., Dlugokencky, E.J., Bergamaschi, P., Bergmann, D., Blake, D.R., Bruhwiler, L., 2013. Three decades of global methane sources and sinks. Nat. Geosci. 6, 813–823.

Klevenhusen, F., Bernasconi, S.M., Kreuzer, M., Soliva, C.R., 2010. Experimental validation of the Intergovernmental Panel on Climate Change default values for ruminant-derived methane and its carbon-isotope signature. Anim. Prod. Sci. 50, 159–167.

Lassey, K.R., Allan, W., Fletcher, S.E.M., 2011. Seasonal inter-relationships in atmospheric methane and companion delta C-13 values: effects of sinks and sources. Tellus Ser. B Chem. Phys. Meteorol. 63, 287–301.

Leng, L., Zhang, T., Kleinman, L., Zhu, W., 2007. Ordinary least square regression, orthogonal regression, geometric mean regression and their applications in aerosol science. J. Phys. Conf. Ser. 78, 012084. IOP Publishing.

Levin, I., Glatzel-Mattheier, H., Marik, T., Cuntz, M., Schmidt, M., Worthy, D.E., 1999. Verification of German methane emission inventories and their recent changes based on atmospheric observations. J. Geophys. Res. Atmos. (1984–2012) 104, 3447–3456.

Liptay, K., Chanton, J., Czepiel, P., Mosher, B., 1998. Use of stable isotopes to determine methane oxidation in landfill cover soils. J. Geophys. Res. Atmos. (1984–2012) 103, 8243–8250.

Lokhorst, A., 1997. NW European Gas Atlas. British Geological Survey (BGS), Bundesanstalt für Geowissenschaften und Rohstoffe (BGR), Danmarks og Grønlands Geologiske Undersøgelse (GEUS), Panstwowy Instytut Geologiczny (PGI), Nederlands Instituut voor Toegepaste Geowetenschappen TNO (NITG-TNO), European Union.

Lowry, D., Holmes, C.W., Rata, N.D., O'Brien, P., Nisbet, E.G., 2001. London methane emissions: use of diurnal changes in concentration and $\delta^{13}C$ to identify urban sources and verify inventories. J. Geophys. Res. Atmos. 106, 7427–7448.

Mikaloff Fletcher, S.E., Tans, P.P., Bruhwiler, L.M., Miller, J.B., Heimann, M., 2004. CH_4 sources estimated from atmospheric observations of CH_4 and its $^{13}C/^{12}C$ isotopic ratios: 2. Inverse modeling of CH_4 fluxes from geographical regions. Glob. Biogeochem. Cycles 18, GB4004.

Monteil, G., Houweling, S., Dlugockenky, E., Maenhout, G., Vaughn, B., White, J., Rockmann, T., 2011. Interpreting methane variations in the past two decades using measurements of CH_4 mixing ratio and isotopic composition. Atmos. Chem. Phys. 11, 9141–9153.

http://naei.defra.gov.uk/.

Nisbet, E.G., Dlugokencky, E.J., Bousquet, P., 2014. Methane on the rise—again. Science 343, 493–495.

O'Shea, S.J., Allen, G., Fleming, Z.L., Bauguitte, S.J.B., Percival, C.J., Gallagher, M.W., Lee, J., Helfter, C., Nemitz, E., 2014. Area fluxes of carbon dioxide, methane, and carbon monoxide derived from airborne measurements around Greater London: a case study during summer 2012. J. Geophys. Res. Atmos. 119, 4940–4952.

Pataki, D.E., Bowling, D.R., Ehleringer, J.R., 2003. Seasonal cycle of carbon dioxide and its isotopic composition in an urban atmosphere: anthropogenic and biogenic effects. J. Geophys. Res. Atmos. 108, 4735.

Phillips, N.G., Ackley, R., Crosson, E.R., Down, A., Hutyra, L.R., Brondfield, M., Karr, J.D., Zhao, K., Jackson, R.B., 2013. Mapping urban pipeline leaks: methane leaks across Boston. Environ. Pollut. 173, 1–4.

Picarro, 2012. Picarro Mobile Kit User's Guide 40047 Revision B, p. 18.

Quay, P., King, S., Stutsman, J., Wilbur, D., Steele, L., Fung, I., Gammon, R., Brown, T., Farwell, G., Grootes, P., 1991. Carbon isotopic composition of atmospheric CH4: fossil and biomass burning source strengths. Glob. Biogeochem. Cycles 5, 25–47.

Sokal, R.R., Rohlf, F.J., 1995. Biometry: the Principals and Practice of Statistics in Biological Research. WH Freeman and Company, New York, pp. 541–554.

Stahl, W.J., 1977. Carbon and nitrogen isotopes in hydrocarbon research and exploration. Chem. Geol. 20, 121–149.

Townsend-Small, A., Tyler, S.C., Pataki, D.E., Xu, X.M., Christensen, L.E., 2012. Isotopic measurements of atmospheric methane in Los Angeles, California, USA: influence of “fugitive” fossil fuel emissions. J. Geophys. Res. Atmos. 117, D07308.

Webb, N., Broomfield, M., Brown, P., Buys, G., Cardenas, L., Murrells, T., Pang, Y., Passant, N., Thistlethwaite, G., Watterson, J., 2014. UK Greenhouse Gas Inventory, 1990 to 2012: Annual Report for Submission Under the Framework Convention on Climate Change. Harwell, Ricardo-AEA, p. 594.

Whiticar, M.J., 1999. Carbon and hydrogen isotope systematics of bacterial formation and oxidation of methane. Chem. Geol. 161, 291–314.

Zimnoch, M., Godlowska, J., Necki, J., Rozanski, K., 2010. Assessing surface fluxes of CO2 and CH4 in urban environment: a reconnaissance study in Krakow, Southern Poland. Tellus B 62, 573–580.